Detailed temporal modelling of carbon and water fluxes from pastures in New Zealand: Case study of an experimental dairy farm in the Waikato region

A thesis presented in partial fulfilment of the

Requirements for the degree of

Doctor of Philosophy

In

Soil Science

Massey University, Palmerston North, New Zealand

Nicolas Puche

2017

ABSTRACT

The terrestrial biosphere is an important pool of carbon, with its size governed by the opposing processes of CO_2 uptake through photosynthesis and release through respiration. It is therefore critically important to understand and reliably and accurately model these processes and predict changes in carbon exchange in response to key drivers. Pasture-based livestock production is particularly important for the New Zealand's economy but it is also a main contributor to NZ's greenhouse gas budget. My Ph.D. work used half-hourly eddy-covariance (EC) data, previously collected over 2 consecutive years from a grazed pasture in the Waikato region. The main aims of this study were to assess whether there was any bias in gap-filled eddy covariance measurements, to assess whether incomplete capture of cow respiration during grazing events could have led to biased observations, and to quantify the resulting difference on the net carbon budget of the farm. I approached the work by developing a new process-based model, CenW_HH, running at a half-hourly time step, to predict the energy and CO_2 exchange of grazed pastures. I implemented and evaluated different photosynthesis models and upscaling schemes and modelled the energy budget separately for the canopy, litter layer, and the soil. CenW_HH was then parameterised and validated with the available EC measurements. The paddocks surrounding the EC tower were rotationally grazed, which caused heterogeneities in respiratory pulses when grazing events were in the flux footprint and subsequent vegetation cover on the different paddocks. To deal with that heterogeneity, the model was run independently for each individual paddock and a footprint model was used to estimate resultant net fluxes at the EC tower. Modelled fluxes agreed well with half-hourly observed fluxes as seen by model efficiencies of 0.81 for net ecosystem productivity, 0.75 for gross primary production, 0.70 for ecosystem respiration, 0.87 for latent heat flux, 0.76 for sensible heat flux, 0.94 for net radiation, and 0.92 for soil temperature. CenW_HH was then used to test for any biases in gap-filled data for times without the presence of grazing animals, but identified no consistent systematic deviations. Eddy covariance measurements often failed to capture carbon losses due to cattle respiration, especially when measurements had to rely on gap-filled data. By replacing gap-filled NEP fluxes affected by grazing cattle by estimates generated by CenW_HH, the farm carbon budget was reduced by 31% and 113% (and turning from a positive into a slight negative balance) in 2008 and 2009, respectively.

ACKNOWLEDGEMENTS

Firstly, I would like to express my sincere gratitude to my advisor Doctor. Miko Kirschbaum for the continuous support during my Ph.D., for his patience, motivation and immense knowledge on many different topics and for the talks that we had. His feedbacks and guidance helped me at all steps of this research project and on the writing of the thesis and I could not imagine having done it without such a great supervisor.

My sincere thanks also go to Professor. Mike Hedley for his guidance and useful insights and suggestions. I am grateful that despite is busy schedule he was always able to meet me at short notice and for going through and making comments and suggestions that improved drafts of my thesis.

I also thank Associate Professor Marta Camps Arbestain for accepting to be one of my co-supervisor and for organising the “journal club” sessions in which most of the presentations and discussions where far away of my research project but widen my view on soil science in general.

I am thankful to my other co-supervisors, Professor Louis Schipper and Doctor Michael Dodd for being part of my Ph.D. advisory panel and for providing the data that were needed to accomplish this project.

I am grateful to the NZAGRC (New Zealand Agricultural Greenhouse Research Centre) for providing me the funding to complete my Ph.D. and to Landcare Research for accepting me to use their facilities; this was an awesome place to work with kind and brilliant persons.

A big thanks also goes to all friends and persons that encouraged me pursue my studies towards the completion of this thesis, without your encouragements this would have not been possible.

And last but not least, I would like to thanks my family and family in law for they support and understanding during all stages of my Ph.D. and specially my wife Justine which followed me abroad for 4 years, I am very grateful for your support during hard times, for your patience and for all the good time we had.

TABLE OF CONTENT

LIST OF ABBREVIATIONS

NH_4^+	Ammonium
NO_3^-	Nitrate
°C	Degree Celsius
A	Instantaneous single leaf photosynthesis
A/PPFD	Photosynthesis light response curves
A_c	Daily canopy net CO_2 assimilation rate
ADP	Adenosine Di-Phosphate
AGC	Automated gain control
ATP	Adenosine Tri-Phosphate
BL	Big-leaf upscaling scheme
C	Carbon
CH_4	Methane
CO_2	Carbon dioxide
EC	Eddy-covariance
ER	Ecosystem respiration
ET	Evapotranspiration
FvCB	Farquhar et al. (1980) photosynthesis model
G	Soil heat flux
GCM	Global climate models
GHG	Greenhouse gas
GPP	Gross primary production
H	Sensible heat flux
H_2O	Water
IPCC	Intergovernmental Panel for Climate Change
IRGA	Infrared gas analyser
LAI	Leaf area index
LE	Latent energy flux
LSM	Land surface model
LUC	Land use change
LUE	Light use efficiency
MBE	Mean bias error
N	Nitrogen
N_2O	Nitrous oxide
$NADP^+$	Nicotinamide Adenine Dinucleotide Phosphate
NADPH	Nicotinamide Adenine Dinucleotide Phosphate Hydrogen
NECB	Net ecosystem carbon balance
NEE	Net ecosystem exchange
NEP	Net ecosystem production
NOAA	National oceanic and atmospheric organisation
NPP	Net primary production
NRHC	Non-rectangular hyperbolic curve
NSE	Nash-Sutcliff criteria or model efficiency
NZ	New Zealand
OM	Organic matter
P	Phosphorus
P	Energy flux associated with photosynthesis
PFT	Plant functional type
PKE	Palm kernel expeller
PPFD	Photosynthetic photon flux density

ppm	Part per million
PR	Photorespiration
PS	Photosynthesis
r^2	Coefficient of determination
R_a	Autotrophic respiration
R_g	Growth respiration
R_h	Heterotrophic respiration
RH	Atmospheric relative humidity
RHC	Rectangular hyperbolic curve
R_m	Maintenance respiration
RMSE	Root mean squared error
R_n	Net radiation
RuBP	Ribulose 1.5-bisphosphate
SG 90	Shuttleworth and Gurney (1990) model
SOC	Soil organic carbon
SOM	Soil organic matter
SS	Sun/shade canopy integration scheme
SVA	Soil-vegetation-atmosphere
SVAT	Soil-vegetation-atmosphere-transfer model
SW 85	Shuttleworth and Wallace (1985) modelling scheme
Tac 86	Taconet et al. (1986) model
TPU	Triose phosphate utilisation
Tsoil	Soil temperature
VPD	Vapour pressure deficit
WUE	Water use efficiency
ΔS	Heat storage of the vegetation canopy

CHAPTER 1: INTRODUCTION AND RATIONAL OF THE STUDY

1.1 Climate change and global carbon cycle

The Earth's atmosphere contains an indispensable pool of gases that provide connectivity allowing the carbon and nitrogen cycles to function. In addition, the gases, like carbon dioxide (CO_2), nitrous oxide (N_2O), and methane (CH_4), absorb infrared radiation emitted from Earth's surface and re-emit this radiation component toward the surface instead of it being lost into space. This creates atmospheric warming known as the greenhouse gas (GHG) effect, which is essential to sustain the biosphere's temperature at a level favourable to sustain plant, animal, and human lives. The increase of anthropogenic emissions and concentrations of the GHGs CO_2, N_2O, and CH_4 in the atmosphere has a direct effect on the radiative budget of the Earth, which tends to stimulate the GHG effect, which in turn affects the whole climate and its pattern.

Even if GHGs are naturally present in the atmosphere, since the industrial revolution anthropogenic activities have greatly modified (increased) their concentration in the atmosphere. For example, the atmospheric concentration of carbon dioxide increased from 280 ppm 150 years ago to about 400 ppm in 2015 (Fig. 1.1c). Such a high concentration has not been experienced on Earth for millennia, and even if its effects on the climatic system are not yet fully understood, most climate experts agree that over the next century it could become a serious problem and a threat to our way of life.

Some effects directly related to the augmented concentration of GHGs in the atmosphere are already visible, such as the increase of the Earth surface temperature (Fig. 1.1a) or the rise of the sea level (Fig. 1.1b). Anthropogenic activities responsible for these global climate changes have been identified as fossil fuel utilisation, cement production, and gas flaring, which have drastically increased since the 1950s. Another source is linked to land use changes and land management practices (Fig. 1.1d).

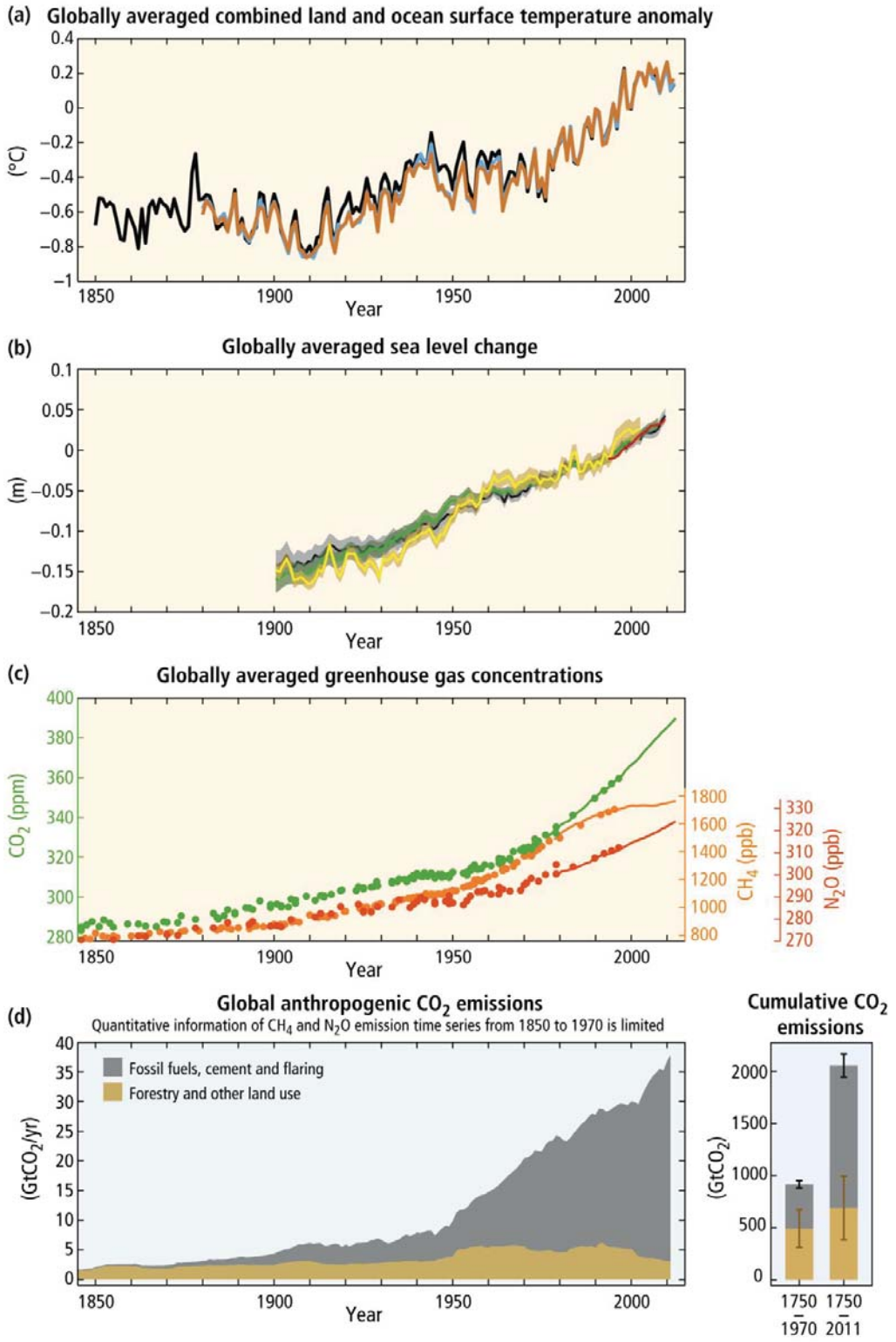

Figure 1.1: Graphic showing surface temperature change, sea level rise, global greenhouse gas concentrations in the atmosphere and anthropogenic carbon dioxide emissions since 1850. Extracted from IPCC (2014).

Over the past 150 years human activities have strongly modified CO_2 concentrations in the atmosphere, and in the global carbon cycle. The global carbon cycle can be seen as different reservoirs (the atmosphere, the terrestrial biosphere, the oceans that contain dissolved organic carbon and living and dead biota, the sediments, and the Earth's crust and mantle that interact with other components of the cycle through geological processes) of carbon interconnected by fluxes of exchange between them (Fig. 1.2).

Oceanic and terrestrial ecosystems, by acting as carbon sinks, have buffered the increase of GHGs in the atmosphere and as a consequence the rate and effects of climate change have been reduced. It has been estimated that they have absorbed about 60% of all the anthropogenic carbon released in the atmosphere by human activities (IPCC, 2007) through physical, chemical, and biological processes acting at different time scale.

In the early 1990s, carbon sequestration suddenly became a topic of interest in science, and politics. The various mechanisms that are responsible for the extraction of carbon dioxide from the atmosphere and its sequestration (in soils or oceans) for a greater period of time were seen to play a major role in global warming mitigation (Powlson et al., 2011).

Oceans contain 50 times more CO_2 than does the atmosphere and offer a huge surface of exchange with the atmosphere (70% of the Earth surface); however, increased dissolution of atmospheric CO_2 in water (oceans and lakes) leads to acidification, with many undesirable consequences (Smith et al., 2004). Terrestrial ecosystems are expected to be a better choice for long-term carbon storage. It was estimated that soils contain at least twice as much carbon as the atmosphere and three times as much as is present in vegetation (Kell, 2011).

Soils are key players in the process of storing (sequestering) carbon and in the recycling of organic compounds. The amount of carbon stored in soils result mostly from the balance between the input of dead plant material (leaf and root litter) and losses from decomposition and mineralization processes (heterotrophic respiration). When plants or animals die, the organic materials of which they are made are decomposed by soil microorganisms that feed on their

organic matter and respire back a portion of this carbon to the atmosphere; the remaining carbon, instead of being released as carbon dioxide, becomes part of the organic component of the soils for times varying from hours to millennia.

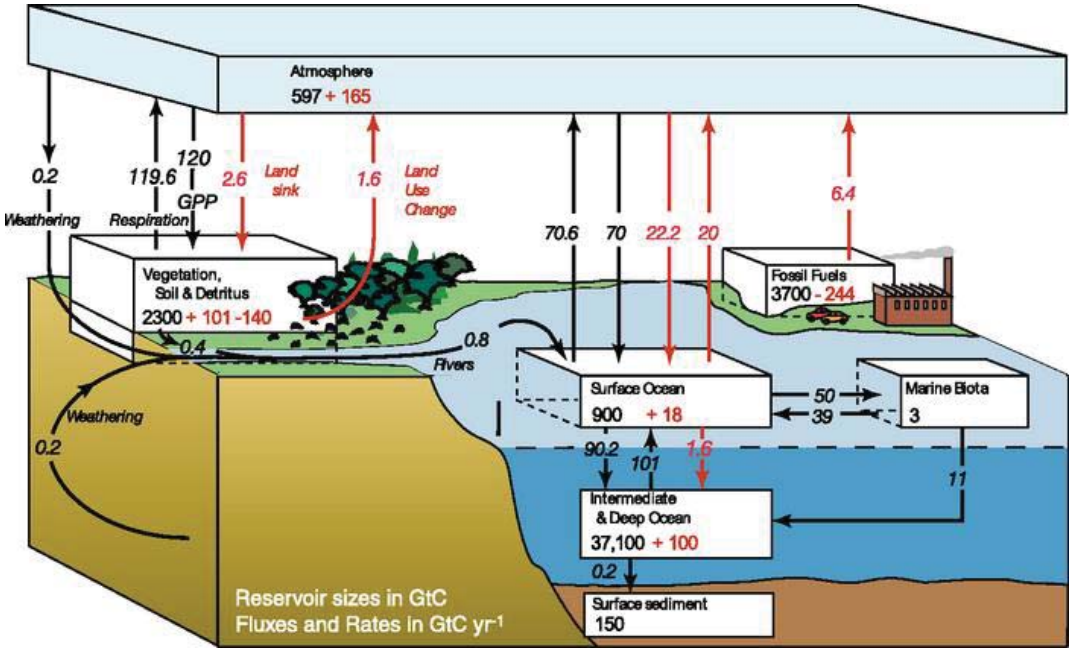

Figure 1.2: The global carbon cycle for the 1990s, showing the main annual fluxes in GtC yr^{-1}: pre-industrial 'natural' fluxes in black and 'anthropogenic' fluxes are in red. Extracted from IPCC (2007).

It is estimated that only around 1% of the carbon entering the soil will remain in stable fractions for a longer time. Most of the decomposition processes (i.e. soil respiration) happen in a layer of soil called the rhizosphere. This is the portion of soil in direct contact (a few mm) with plant roots and that contains the highest proportion of microbial decomposers (Killham, 1994).

1.2 Why do we want to store carbon in soil?

According to Le Quéré et al. (2014), fossil fuel burning, cement production, and gas flaring accounted for 92% and land use change (LUC) for 8% of the global anthropogenic CO_2 emissions in 2013. In fact, cumulative emissions for the period 1870–2013 show contributions of about 70% and 30% for fossil fuel combustion and LUC respectively.

Land-use change and soil degradation are major processes implied in the release of CO_2 into the atmosphere, and under the Kyoto Protocol most of the countries were committed to develop and implement new strategies and policies in order to reduce their emissions of GHGs. This can be achieved by developing and implementing agricultural and forestry management practices that favour the sequestration of carbon in the biomass and in the soil.

According to Fischer et al. (2007), the mitigation of GHGs emissions are actions taken in order to reduce the effects and/or the magnitude of climate change by limiting/reducing the amount of GHGs present in the atmosphere. This can be done by using techniques that enable the reduction of anthropogenic emissions or by increasing the capacities of carbon storage of natural sinks.

It is thought that carbon sequestration in terrestrial ecosystems is a possible way to mitigate the impacts of anthropogenic emissions of carbon dioxide in the atmosphere and the resulting climate warming of the Earth (Post et al., 2007; Rantakari et al., 2012; Minasny et al., 2017).

Carbon sequestration has been defined as the process of removing CO_2 from the atmosphere and storing it in pools with longer residence times. However, the size and distribution of these carbon sinks remain uncertain and it is understood that every ecosystem type has different behaviour as regards greenhouse gas emissions.

It has been demonstrated that over the last 8,000 years, agriculture has had a significant global impact on atmospheric GHG concentrations, and more particularly on carbon dioxide and methane (Salinger, 2007). Massive deforestation to convert native forests into arable lands has caused large disturbances in the global carbon cycle.

Carbon is present in the soil in complex association with mineral particles and it is the nature of this relationship that determines how long the carbon remains in the soil (Conant et al., 2011). Plant and soil organism residues enter the soil and are mixed with soil particles to form what is called soil organic matter (SOM), which is roughly made of 50% of carbon. Most of this organic matter is unprotected and mineralized within months but a portion can form aggregates

with soil particles and become physically or biochemically protected from microbial decomposition for decades to centuries (Conant et al., 2011).

Research on carbon sequestration in soil falls into three categories: 1) monitoring C stocks; 2) experimental manipulations; and 3) numerical simulations. The three research categories of soil carbon sequestration are of equal importance for a better understanding of the C storage capacities of ecosystems (Grace et al., 2006). Human activities, like climate change, land use change, and farming practices have a large effect on SOM dynamics and, in this context, the storage capacities of C in soils need further investigation (Post et al., 2007).

A better understanding of the impacts of human activities on greenhouse gas emissions from productive soils is the key point for mitigating the negative effects of global warming and climate change while continuing to provide enough food to meet the requirements of the Earth's increasing population.

Soils are expected to have a mitigation potential through enhanced C sequestration because most cultivated soils (especially under cropping systems) have lost carbon in the past and most terrestrial soils have not reached their maximum C content. It is expected that even a small C gain in all cultivated soils might have a significant effect on the atmospheric CO_2 concentration (Minasny et al., 2017).

Natural ecosystems, principally forests and grasslands, usually have large carbon stocks because of the relatively stable soil environment favourable to accumulation of organic matter below the ground with a lower turnover rate. In contrast, soils under cropping often hold a lower amount of carbon because of frequent cultivation and harvest, and are often considered as sources of carbon.

In general, agro-ecosystems are strongly impacted by management practices including, fertilisation, harvesting, grazing or ploughing (Conant et al., 2001; Conant et al., 2007). According to Liu et al. (2003), the conversion of lands from a native state to agricultural use leads to a 20–40% reduction in soil organic carbon storage, and it is expected that modifying management practices could

lead to the sequestration of carbon in the soil and, ultimately, to the reduction of a country's emissions.

The soil C balance of New Zealand's pastoral soils is poorly understood and early studies have demonstrated that following the conversion of scrub or low-producing pasture to improved pasture (mostly for the purpose of dairy farming), carbon tends to accumulate in the surface layers of the soil, and that after about 7–40 years (depending on soil types) a new equilibrium in the C content is reached (Jackman, 1964). It is generally accepted that soil C under established pasture in New Zealand was at near steady state (Tate et al., 2005). Surface soils from 43 sites were resampled after 30–50 years under pastoral farming and no systematic change in soil C was found (Tate et al., 1997).

However, Schipper et al. (2010) showed that the top metre of soils from 31 flat to gently rolling sites mostly under dairy farming around New Zealand had lost on average 1 t C ha^{-1} y^{-1} over the 13–40 years between samplings. The work of Schipper et al. (2010) also highlighted the contrasting behaviours of soils from flat pasture grazed by dry stock where the amount of carbon remained nearly constant and grazed lands in hill country where SOC tended to accumulate at an average rate of 500 kg C ha^{-1} y^{-1}. This study was unable to clearly identify the causes responsible for the contrasted carbon behaviours observed.

Schipper et al., 2014 extended the number of resampled sites to 148 and showed that carbon losses were restricted to Allophanic and Gley soils types under both dry stock and dairy pastures on flat land areas but no significant change in SOC stocks were identified for other soil types

1.3 Importance of agriculture in NZ's carbon budget

About 25% of the ice-free terrestrial surface of the planet is occupied by grazed grasslands (Steinfeld et al., 2006) and this land use is often seen as having a large potential for long-term carbon storage and an option to mitigate greenhouse gas emission from agriculture (Abberton et al., 2010).

Pasture occupies nearly 40% (10.7 million hectares) of the total New-Zealand land area and 16% (1.7 million hectares) of grassland are used for dairy farming. Recent intensification of pastoral agriculture has seen the number of dairy cows increase by 50% from about 2.40 million in 1990 to 4.78 million in 2013 (DairyNZ, 2014).

Unlike other developed countries, the largest source of GHG emissions in New Zealand is the agriculture sector, which represented 46.1% of the total emissions in 2012. These emissions are mostly methane, released by grazing animals through enteric fermentation and nitrous oxide released from agricultural soils (MfE, 2014).

New Zealand is the largest exporter of dairy products worldwide and its economy relies substantially on the dairy industry. In 2014 dairy farming contributed to 46% of NZ total primary industry export, which represents 37% of the earnings from merchandise exports (DairyNZ, 2014), making it more profitable than sheep, beef, and grain farming combined (MfE, 2015). Despite being highly important for its economy, dairy farming is also the main contributor to New Zealand's GHG budget (MfE, 2014) and atmospheric and water pollution (Thomas et al., 2005).

The majority of NZ pastoral systems are based on grass/legume mixed swards, and, thanks to mild climatic conditions, it is common practice for cattle to graze all year round in pastures. When pasture growth rates are insufficient to meet feed demand supplementary feeds such as maize and pasture silages, or imported palm kernel expeller (PKE) meal are provided for the herd.

1.4 The use of models to study SOC dynamics

In ecological studies, models are important to analyse whether the scenarios developed to provide a solution to a problem are likely to achieve their goals and long-term effects. Data collection is also a prime process that should be conducted to parameterise models and to test their accuracy. If a model is sufficiently able to reproduce the data collected today or the trends that were

experienced in the past, it can be used to test different scenarios, for example, to understand the effects of climate change on pasture productivity.

However, many natural processes are hard to simulate, or are not well understood. Because of this complexity, many existing models differ in their approaches and formulations (Adams et al., 2004) and they need to be updated following the improvement of our knowledge.

Ecosystem models exist in various forms, with different degrees of complexity, time steps, and behaviour of simulations, and follow different theories and algorithms (how the natural processes are transcribed into equations). These models are usually complex and use different coupled sub-models in order to simulate the different parts of the system being investigated.

Soil organic matter is a key indicator of the quality of soils (Six et al., 2004). From an economic perspective, a great deal of OM is usually linked to high plant productivity, and, from an environmental point of view, much OM relates to improved biodiversity and constitutes a large amount of stored carbon (Robert, 1997). The sequestration of carbon in soil is primarily driven by two processes: primary production (input) and decomposition (output). Measurements of the overall amount of C stored in an ecosystem by itself reveal little about the carbon behaviour and so modelling has been used as an effective way to analyse and predict the short- or long-term effects of land-management practices on the levels of C present in the soil.

Soil organic matter characterisation and turnover are very complex due to soil's intrinsic composition (more than 10,000 chemical compounds) and interactions with soil particles and micro-organisms, the modifications caused by climatic variables and human activities.

Models can be classified according to their formulation. At first it is possible to make the distinction between empirical and mechanistic modelling approaches. While 'empirical models' use empirical relationships between variables, 'mechanistic models' (process-oriented models) try to develop algorithms for and simulate detailed processes. This last category can be regarded as more representative because modellers try to simulate factors influencing the *in vivo*

mechanisms and the values used to parameterise their models are restricted by the realistic biophysical background present in the modelled processes. In contrast, while the values of the parameters employed in empirical models may describe relationships between variables obtained through observation and regression analysis, most of the time they do not correspond to biophysical processes with inputs, outputs or pools that were physically measureable. Process-oriented models are often seen to carry more information and to have more restricted behaviour than empirical models.

The second splitting of the model is into ‘deterministic models’, which have an initial condition, set parameters, and operate mechanistically within boundary conditions, as opposed to ‘stochastic models’, which allow the variation in inputs and the randomness of processes to be considered, and produce a range of outputs. At the beginning of ecosystem modelling (in the ’60s) most models were deterministic because computational resources were limited and adding probabilities consequently slowed down their runs. In the recent past, with the increase of computer power, more stochastic approaches have been developed in ecosystem modelling and are expected to generate more realism and accuracy in the representation and simulation of natural systems.

At a third level, a distinction can be made based on variable evolution with time. In static models, variables remain constants, while in dynamic models variables evolve with time. Within this last category, differentiation can be made regarding how variables evolved with time and models can be classified into continuous or discrete. In continuous models, variable evolution between simulation steps is smooth, in contrast to discrete models in which variables change by step and are usually limited to integer values.

Most ecosystem models are mechanistic or semi-mechanistic (partly mechanistic and partly empirical), dynamic because they are mainly used to study change over time, and deterministic and continuous because most changes in variables values are smooth over time.

In their review, Manzoni and Porporato (2009) highlighted the complexity of modelling the processes involved in the fluxes of C and N into and from the soil.

They reviewed and classified about 250 different models with different modelling approaches, time and spatial scales, and details in the modelled processes and complexity.

The internal structures of models used for the simulation of SOM dynamics are usually divided into four classes (Post et al., 2007):

(1) Process-oriented models (multi-compartments models)

(2) Organism-oriented models (food-web models)

(3) Cohort models (continuum in the SOM decomposition)

(4) Combination of classes (1) and (2)

Multi-compartment models describe organic matter turnover as the consequence of transformations between different compartments with different decomposability or biological quality. It is recognised that the different constituents of the SOM have different residence times, so most models discriminate between (a) an active pool, including fresh plant material and root exudates with residence times of approximately 1 year, (b) a slow pool, including SOC that is decomposed at intermediate rates, with residence times of between 1 and 1000 years, and (c) a passive (inert) pool, including SOC that, for physical reasons, has a residence time ranging between 1000 and 10000 years (Post et al., 2007).

One of the main problems of multi-compartment SOM models is the comparison of the C present in model compartments with measurable SOM fractions, or the difficulty of assigning measured SOM fractions according to residence times in model compartments. The carbon pools, and flows between them, are largely theoretical and were introduced to mimic the heterogeneity of SOM, but their existence has not been proved yet. Previous assumptions imply the use of empirical relationships in the core of these models. In order to make them more mechanistic, it has been argued that their pools should correspond to measurable SOM fractions that have a functional role in the soil (Post et al., 2007; Manzoni & Porporato, 2009).

CenW (Kirschbaum, 1999a, 1999b; Kirschbaum & Paul, 2002) is an ecosystem process-based model, running at a daily time step that simulates the carbon balance of a system over time (up to hundreds of years). The different modules combine the principal carbon, energy, nutrient, and water fluxes. The soil organic matter module was derived from the CENTURY model (Parton et al., 1987). Soil organic matter (soil carbon) is divided into three fractions with different residence times. CenW was originally designed to study forest ecosystems and has been tested over forest and grassland; however, its generic structure has allowed the necessary modifications to simulate carbon and nitrogen stocks and fluxes for various ecosystems (Kirschbaum et al., 2015). A more detailed description of the processes simulated and features of CenW are given in Chapters 3, 4, 5, and 6.

In order to monitor changes in soil carbon stocks by classical measurement techniques (soil sampling), the changes in SOM have to be in the order of several tonnes per hectare (tC ha^{-1}). As change is slow it often requires samples to be taken with a substantial interval of time between them. The long time interval makes it very challenging to attribute any observed changes in carbon stock to a particular change in farm management (Allen et al., 2010). Another option is to use eddy covariance measurements because they can detect very small changes in the net rate of CO_2 exchange between the soil and the atmosphere with a very high sampling rate (10–20 Hertz averaged to 30 minutes). Although this technique does not gives direct information on the soil carbon stocks at a given time, it is possible to observe trends (losses or gains) in C exchange and the source/sink status of the study site. With its high temporal resolution this technique makes it easier to relate particular management practices to the behaviour of carbon in the system. EC measurements are also very useful to parameterise/constrain mechanistic models and have been used in a range of modelling studies (Baldocchi & Wilson, 2001; Knorr & Kattge, 2005; Wang et al., 2007; Ingwersen et al., 2011; Verbeeck et al., 2011; El-Masri et al., 2013).

1.5 Research objectives

The principal objective of this research study was to develop a new modelling tool to study carbon dioxide and water fluxes over a research dairy farm (Scott Farm) in the Waikato region of New Zealand. The overall process of creating this new ecosystem model has been dictated by the fact that the fluxes measured by eddy covariance systems are highly influenced by the presence of grazing animals in the footprint of the tower (Kirschbaum et al., 2015; Felber et al., 2016) and that gaps in measurement are possibly non-randomly distributed but mostly occur under specific climatic conditions (rain events, fog, dew formation on the surface or stable atmospheric conditions) that could introduce bias in the dataset.

The new version of the model was developed from CenW 4.1, which runs with a daily time step and has been successfully applied by Kirschbaum et al. (2015) to this particular farming system. The main challenge for this PhD study has been to change the time step of the existing model by incorporating new procedures in the source code to make the time step consistent with the short measurement sampling interval (typically 30 minute for most EC datasets).

First, the literature was reviewed to find the most suitable description of carbon assimilation (Chapter 3) and surface water and energy budgets (Chapter 4). Suitable routines were then written in Delphi XE (Embarcadero, 2010). The carbon assimilation and surface water and energy budgets routines for simulating photosynthesis and water and energy fluxes were developed and tested as stand-alone sub-models before implementation in the complete model. Finally, the functioning of the model was tested with these new features and the model's accuracy and reliability compared with measurements made in the field. The new model was named CenW-HH. The comparison of CenW-HH model simulations with the field observations enabled an improved understanding of the influence of large, grazing animals (cows) on the observed CO_2 concentrations and allowed the correction of the resulting errors of not accounting for dairy cows respiration in the annual carbon balance of grazed pastures. CenW-HH was also used to fill gaps in data resulting from unsuitable

climatic conditions for eddy covariance measurement and to test whether there was bias in the dataset when those gaps were filled by a “traditional” gap-filling method.

1.6 Importance of the study

During this research project, a new modelling tool, CenW_HH, has been developed. This new model is based on the CenW model version 4.1, which has been already used and validated for forest and pasture ecosystems (Kirschbaum et al., 2015). The modifications that were made allow it to run at a sub-daily time step and have made it possible to use actual eddy-covariance measurements to parameterise and validate it. The model is process-based (mechanistic) and is able to simulate the short time response of photosynthesis, water, energy, and both heterotrophic and autotrophic respiration rates in response to management and changes in climatic conditions. The first focus was on the development, testing, and validation of the new version of the model (CenW_HH). In this study, the model has only been tested on one dairy farm but the structure of the model makes it usable on other dairy farms or other farming systems as long as enough information is available to be used as inputs (half hourly climate variables, farm management practices,…) and to parameterise and validate the runs.

The overall aim of the study was to compare half-hourly fluxes – principally net CO_2 flux (NEP) and water vapour flux (LE), observed by an eddy covariance system placed over an intensive dairy farm – with their modelled equivalents to identify the causes of the possible introduction of bias in the dataset and to quantify their effects on the annual carbon budget of the study site.

1.7 Thesis structure

Eddy covariance systems have been used worldwide to study carbon, water, and energy fluxes over a large range of biome types, with more sites being installed on grazed grasslands over the recent years to study soil carbon stocks behaviour. However, eddy covariance measurements of the emissions of CO_2

from grazed pastures cannot take place in wet and still conditions and are compromised during grazing events by cow respiration: both events create gaps in the observations. The aim of this thesis was to evaluate the quality of the eddy covariance technique applied to a grazed dairy pasture with the help of a detailed simulation model. Figure 1.3 shows the structure of the dissertation. Chapter 1 provides the general introduction and rationales of the study (see above) and is not represented on Figure 1.3. Chapter 2 introduces the theory and methods used to measure carbon, water, and sensible heat fluxes with eddy covariance systems above terrestrial ecosystems, and more attention is given to pastures as it is the main focus of the thesis and some insights on modelling. Chapter 3 describes some of the most used photosynthesis modelling schemes, with their comparisons at the leaf and canopy levels. This is to illustrate the changes made to the existing model to run it with a half-hourly time step and select the most appropriate photosynthesis algorithm to be used to complete the study. Chapter 4 describes new routines, also implemented in the newly developed version of CenW, that were chosen to simulate water and energy balances. In Chapter 5 the study site is described and information presented to run the model and evaluate its performances to simulate carbon, water, and energy fluxes measured by the eddy covariance system. The model predictions are compared with the observed data and tested for agreement during periods when climatic conditions were unsuitable for eddy covariance measurement and tries to identify systematic bias in the dataset. In Chapter 6, the model is used to study the effects of the presence of grazing cattle within the vicinity of the flux tower on systematic half-hourly measurements errors and on annual carbon balance of the dairy pasture. Finally, Chapter 7, the general conclusion, summarises the main findings of the previous chapters along with what could be possible directions for future researches.

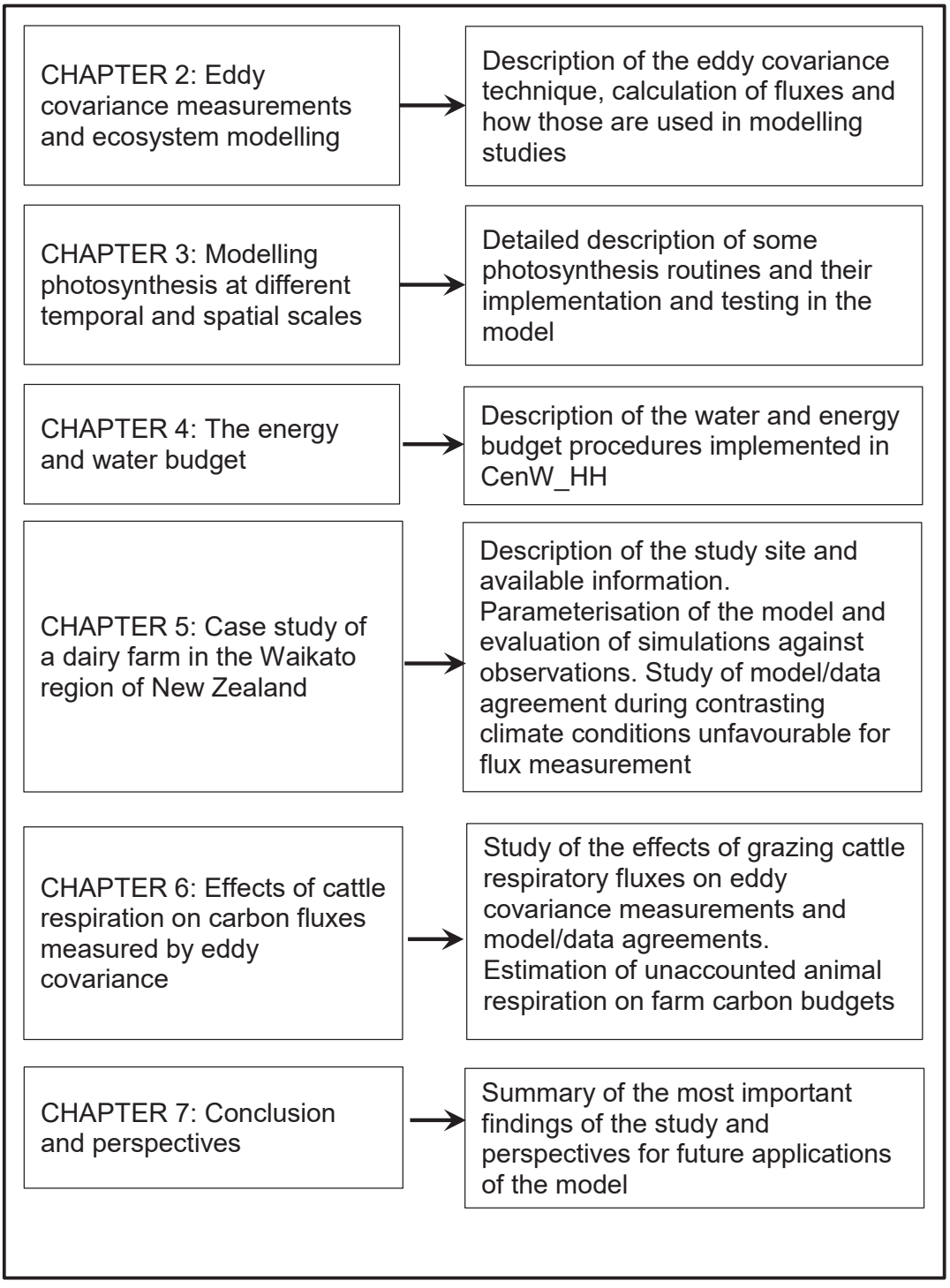

Figure 1.3: Layout of the thesis.

CHAPTER 2: EDDY COVARIANCE MEASUREMENTS AND ECOSYSTEM MODELLING

2.1 Introduction

This section gives a brief general description of the eddy covariance technique for measuring fluxes of CO_2, heat, and water over terrestrial ecosystems. The chapter provides only the information needed for required background understanding of the specific study site, the method for calculating fluxes and checking the quality of the data from the eddy-covariance (EC) tower, and the use of various correction factors applied to the raw measurements. This section thus summarises key information from several books and research papers that provide a more detailed and in-depth explanation of the various problems to be overcome to set up eddy-covariance equipment and derive useful and meaningful information about the behaviour and activity of the system under study (Burba, 2013; Aubinet et al., 2012).

According to Baldocchi (2003), the theory establishing the basis of the eddy covariance technique was first developed by Reynolds (1894), but it was not until the 1930s and the technological development of suitable instruments that the first study used the theory in a field campaign to measure momentum transfer. The second improvement of the technique came after World War II with the development of fast responding hot-wire anemometers, thermometers and digital computers (Swinbank, 1951). Measurements of CO_2 exchanges over vegetation started in the late 1960s and early 1970s with the flux-gradient method that was, however, still prone to large errors under some measurement conditions because of the lack of fast response anemometers and carbon dioxide sensors (Garratt, 1975).

It took another 10 years (to the 1980s), before the further technological developments of sonic anemoters and fast response (10 Hertz) open path infrared gas analysers allowed the development of studies of CO_2 fluxes over all sorts of vegetation types. However, a lack of reliability of the required sensors and data logger limitations restricted the use of EC systems to short measurement campaigns during the vegetation growing phase. In the early 1990s, instruments became even more reliable and consumed less energy, which enabled scientists to make continuous measurements all year round and

for multiple consecutive years. At this stage, the eddy covariance technique was used more intensively all around the world. Researchers were able to show that the technique has the potential to help answer a broad range of scientific questions at local, regional, and global scales. Regional networks started to emerge, e.g. AmeriFlux, AsiaFlux, CarboEurope, OzFlux, …, and FLUXNET, a global network of various regional networks. FLUXNET was started in 1997 with the aim of creating a global standardized database of flux measurements and producing annual and daily C budgets through the use of state-of-the-art gap filling and flux partitioning methods.

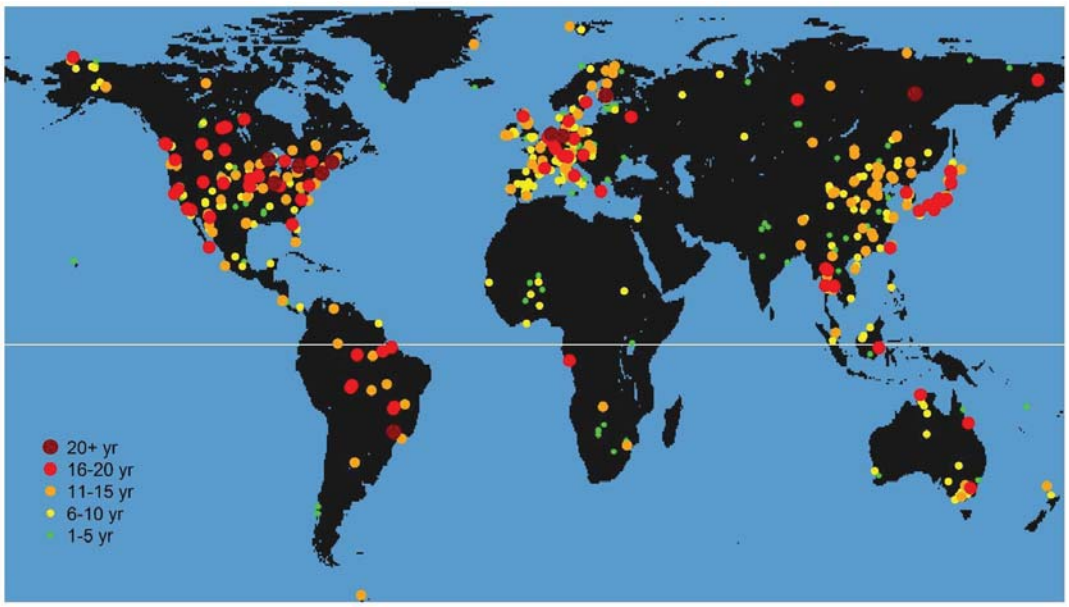

Figure 2.1: Locations of eddy covariance measurement sites included in the FLUXNET network. (http://fluxnet.fluxdata.org).

In 2015, there were 844 registered sites in the FLUXNET network (http://fluxnet.fluxdata.org/sites/historical-site-status), of which around 424 were actively taking core measurements of CO_2, water vapor, and energy fluxes. They have been employed over all sorts of vegetation and all around the world (Fig. 2.1), and some have been collecting data for more than 20 years. The FLUXNET database now contains more than 6,700 site years of eddy covariance measurements, with all sampling sites and datasets not yet included in this network.

The number of study sites using the EC technique increased rapidly all over the world since the middle of the 1990s (Fig. 2.2a). The first year-long study was conducted by Wofsy et al. (1993), during which net carbon dioxide measurements were taken over a central Massachusetts deciduous forest, starting in 1990 (Baldocchi, 2003). From the initial stage of the FLUXNET initiative, most of the sites were set above forest ecosystems, followed by grassland sites, which sharply increased in the mid-2000s, and a smaller number of cropland sites (Fig. 2.2b).

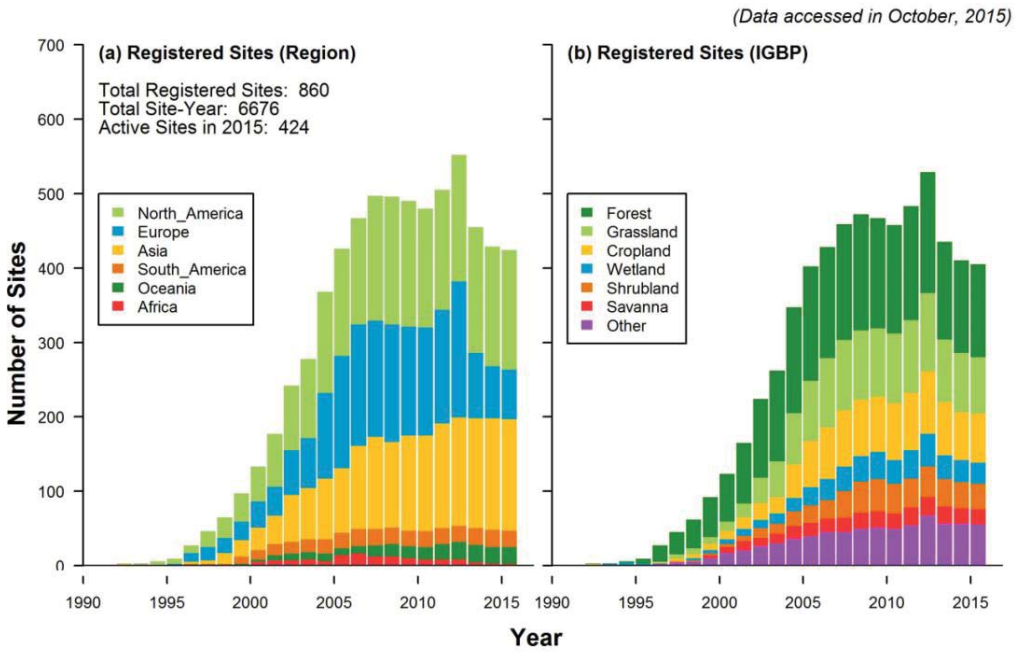

Figure 2.2: Summary of tower sites that are (a–b) registered in FLUXNET. “Registered sites” represent sites that have been registered in fluxdata.org, FLUXNET-ORNL, AmeriFlux, ICOS, AsiaFlux, OzFlux, or ChinaFlux. Sites are grouped by regions (a) and vegetation classification (b). Forest: ENF+DBF+EBF+MF, Grassland: GRA, Cropland: CRO+CVM, Wetland: WET, Shrub land: OSH+CSH, Savanna: SAV+WSA, Other: BSV+URB+WAT+SNO. (Figure from http://fluxnet.fluxdata.org).

Most of the datasets contain half-hourly averaged fluxes of carbon dioxide, water, heat, and the climatic variables observed during each measurement periods. This method has been widely used by ecologists as it allows direct and long-term measurements of the exchange rates of GHGs between the surface and the atmosphere without ongoing disturbances of the study area.

The EC technique is a complex but widely used method to measure fluxes over a wide variety of ecosystems and is based on the covariance between the vertical wind speed and the gas concentration at the measurement height (Burba, 2013; Aubinet et al., 2012). This method is now not only used for micrometeorology but is also applied in many other research and industrial fields such as climate science, GHGs exchange budgets over many different surfaces, agricultural sciences, hydrology, precision agriculture, geological carbon storage monitoring, industrial regulatory applications (Burba, 2013) or even oceanography (Berg et al., 2003; Koopmans and Berg, 2015). The technique is also used for the derivation, verification, and parameterisation of global climate models (GCM), complex biogeochemical and ecological models, and validation of remote sensing estimates from satellites or aircrafts.

2.2 Eddy covariance measurements

2.2.1 Theory of flux calculations

The air flow in the Earth's atmospheric boundary layer can be seen in the horizontal transport of numerous rotating eddies (turbulent vortices of various sizes). Each of these eddies has 3D components that can be measured at the level of the eddy covariance tower (Fig. 2.3). The turbulence from the lowest layers of the atmosphere is responsible of the transport of heat and various gases, such as CO_2 and water vapour (Kaimal and Finnigan, 1994).

The height of the tower above the surface is a critical parameter in the design of the experimental setting as the probability of having small eddies close to the surface is higher than it is further away from it. Under the same conditions, a higher tower measures fluxes originating from further afield, so covering a wider source area. While this is interesting because fluxes are averaged over a wider area, it also adds extra constraints on the site selection by requiring flux uniformity over that larger area (Aubinet et al., 2012).

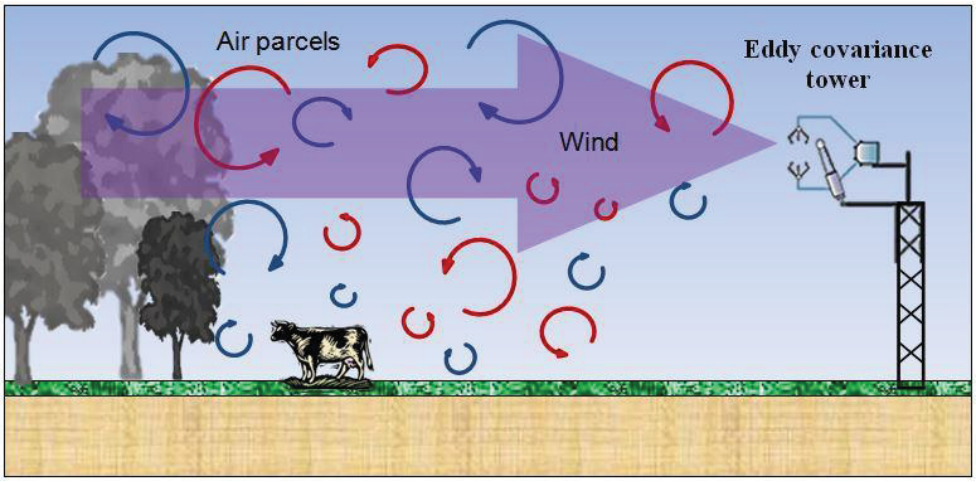

Figure 2.3: Schematic representation of the eddy covariance technique. The sensors are placed above the surface of interest on a tower, and the measured flux comes from an upwind area. The figure has been modified from Burba (2013).

A flux is by definition the transport of a scalar (matter or energy) per unit of surface (m) and time (s). In the case of eddy covariance technique, the flux of the considered gas is given by the covariance between its concentration and the vertical wind speed (Fig. 2.4).

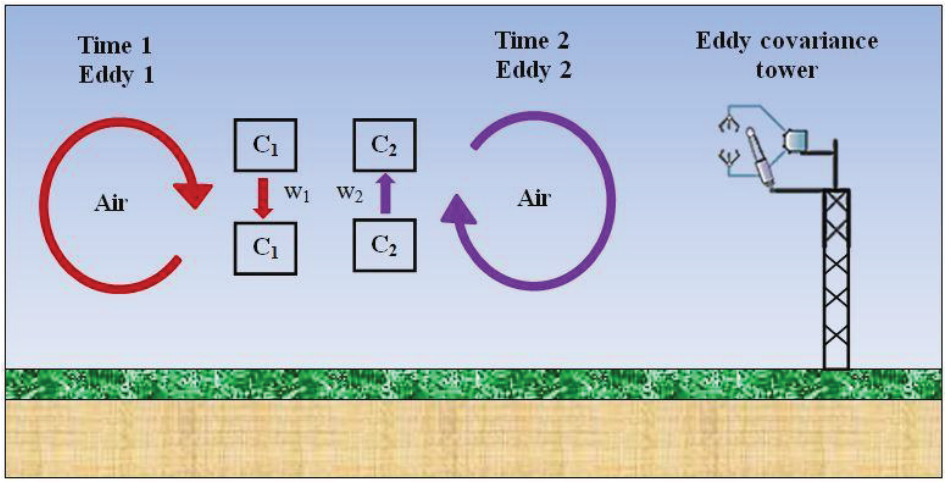

Figure 2.4: Theory of flux calculation with the eddy covariance technique (modified from Burba (2013)). At a given time (time 1), eddy 1 moves the air parcel c1 downward with the speed w1 and at the next instant (time 2), at the same point, eddy 2 moves the air parcel c2 upward with the speed w2. Each air parcel get its proper characteristics, e.g. gas concentration, temperature, humidity, etc., and the eddy covariance technique consists in sampling how many gas molecules go downward at time 1 and how many go upward at time 2.

At one moment (time 1), eddy number 1 moves air parcel c1 downward with the speed w1. At the next moment (time 2) at the same point, eddy number 2 moves air parcel c2 upward with speed w2. Each air parcel has its own characteristics, such as gas concentration, temperature, humidity, etc. If we can measure these characteristics and the speed of the vertical air movement, we can calculate the vertical upward or downward fluxes.

The basis of making measurements and interpreting them by the eddy covariance technique is the conservation equation (Baldocchi et al., 1988; Baldocchi, 2003; Finnigan et al., 2003; Aubinet et al., 2012) which can be applied to any scalar or vector quantity and which is given by:

$$\underbrace{\frac{\partial \rho_d\, \zeta}{\partial \mathrm{t}}}_{\mathrm{I}} + \underbrace{\vec{\nabla}(\vec{u}\rho_d\, \zeta)}_{\mathrm{II}} + \underbrace{K_\zeta \Delta(\rho_d\, \zeta)}_{\mathrm{III}} = \underbrace{S_\zeta}_{\mathrm{IV}} \tag{2.1}$$

where ζ represents the time series of the selected variable, ρ_d is the dry air density, K_ζ is the molecular diffusivity of the variable ζ, $\vec{u}$ is the wind speed vector, S_ζ is the strength of the source/sink term, and $\vec{\nabla}$ and Δ represent the divergence and Laplacian operators respectively.

Equation 2.1 is instantaneous and only applies to an infinitesimal volume of air (Aubinet et al., 2012). The rate of change of the quantity ζ (I) is caused by atmospheric transport (II), molecular diffusivity (III) or its production by a source or absorption by a sink. We are normally interested in the source or absorption of a quantity (IV), like CO_2 or water vapour, and it can be deduced from the sum of the other quantified terms (I–III).

To be applied to calculate fluxes of CO_2 or H_2O in the atmospheric boundary layer, the variable ζ in this equation need to be replaced by their respective mixing ratios and the variables have to be decomposed into their mean and fluctuating parts (Reynolds decomposition). As a result, Equation 2.1 becomes:

$$\overline{\rho_d}\,\overline{\frac{\partial \chi_s}{\partial \mathrm{t}}} + \overline{\rho_d \vec{u}}\,\vec{\nabla}(\overline{\chi_s}) + \vec{\nabla}\left(\overline{\rho_d \vec{u}'\,\chi_s{}'}\right) = \overline{S_s} \tag{2.2}$$

The source term $\overline{S_s}$ is the sum of the rate of change of the mixing ratio, advection caused by gradient of χ_s, and the divergences in eddy fluxes.

Application of the eddy covariance theory to estimate fluxes exchanges over ecosystems, Equation 2.2 needs to be integrated over a control volume as presented in Figure 2.5.

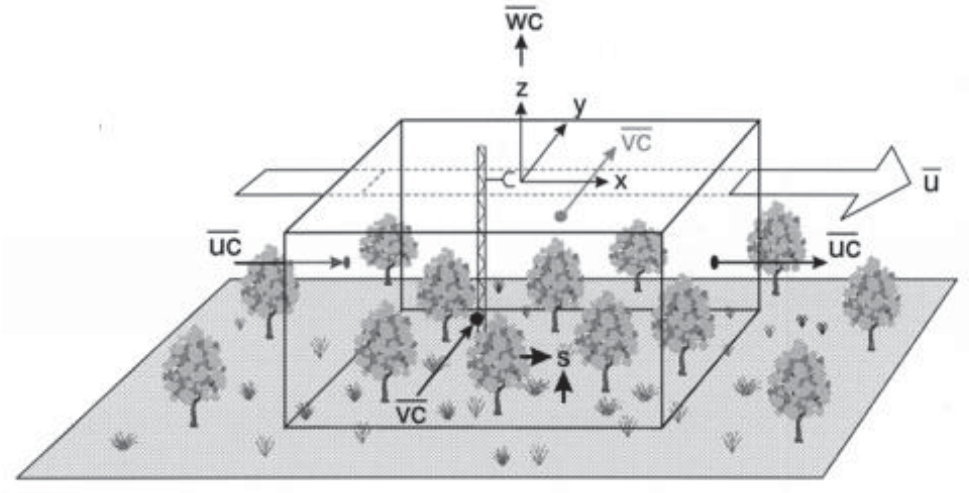

Figure 2.5: Schematic representation of the control volume used to integrate the mass conservation equation over a vegetated and homogeneous land surface area (from Finnigan et al., 2003).

Integration of Equation 2.2 and its simplifications are well described in Aubinet et al. (2012) and are not repeated in the following.

$$\underbrace{\int_0^{hm} \overline{\rho_d} \frac{\overline{\partial \chi_s}}{\partial t} dz}_{A} + \underbrace{\int_0^{hm} \overline{\rho_d w} \frac{\overline{\partial \chi_s}}{\partial t} dz}_{B_1} + \underbrace{\int_0^{hm} \left[\overline{\rho_d u} \frac{\Delta \overline{\chi_s}}{\Delta x} + \overline{\rho_d v} \frac{\Delta \overline{\chi_s}}{\Delta y}\right] dz}_{B_2} + \underbrace{\overline{\rho_d w' \chi_s'}}_{C} = \underbrace{Fs}_{D} \quad (2.3)$$

From Equation 2.3, one can see that the total flux (F_s) above a given surface consists of the sum of its four main components:

$$F_s = F_t + F_v + F_a + F_{sto} \quad (2.4)$$

With F_t, the vertical turbulent flux calculated from EC measurements (D), F_a is the flux of advection corresponding to the horizontal (B_2) or vertical (B_1) non-

turbulent flow (neglected if the measurement area qualifies with homogeneity theory), and F_{sto} is the storage term (A) of the scalar between the soil and the measurement height (h_m), which can be neglected if turbulences in the atmospheric boundary layer are sufficiently developed. Storage is also likely to play a more important role in forest than low-stature grassland systems principally due to the typically higher location of measurement towers in forest systems and the correspondingly larger volume of air within which gases can be stored.

Finally, the instantaneous turbulent vertical flux of a given scalar is expressed as the product of the vertical wind speed component (w) by the scalar (ρ) at the time t:

$$Fs(t) = w(t)\,\rho(t) \tag{2.5}$$

The time integration over a period of length T gives the averaged turbulent flux, which is calculated as the covariance between the vertical wind speed (w) and the considered scalar of interest (ρ). This is made by calculating the mean of the product of the fluctuations of w and ρ relative to their respective mean over the time period considered and using the Reynolds decomposition of time dependant variables:

$$F_s = \frac{1}{n}\sum_{t=1}^{t=n}\left((w(t) - \overline{w}) - (\rho(t) - \overline{\rho})\right) \tag{2.6}$$

The basic equation of the “eddy flux” calculation for the CO_2 flux in good measurement conditions is:

$$Fs = \overline{\rho_d w' \chi_s'} \tag{2.7}$$

From which it is possible to derive equations for the turbulent fluxes of sensible heat (Equation 2.8), latent heat (Equation 2.9) also called evapotranspiration and the flux of CO_2 (Equation 2.10).

$$\mathrm{H} = \rho_a c_p \overline{w'T'} \tag{2.8}$$

$$\mathrm{LE} = \rho_a L_v \overline{w'q'} \tag{2.9}$$

$$\mathrm{Fc} = \rho_a \overline{w's'} \tag{2.10}$$

Where ρ_a is air density, c_p the specific heat of the air, L_v the latent heat of vaporisation, and w', T', q', s' are the fluctuations of vertical wind speed, temperature, water vapour mixing ratio, and the mixing ratio of any other substance of interest, which in this case is CO_2.

Both the period of integration and the sampling rate are important for capturing high and low frequency signals in the turbulences (Burba, 2013). The sampling frequency should be at least 10 Hz (1 measurement every 100 ms).

Corrections factors have also to be applied to EC measurements to take account of fluctuations in pressure, temperature, and humidity as they could have effects on fluxes (Webb et al., 1980) but they will not be further described in this study.

By using this technique, it is possible to use a single-point measurement to get the spatial characteristics (from the surface area designated as the flux footprint) of the fluxes of H_2O, CO_2 and CH_4 and other gases from above soil and water surfaces, plant canopies, and urban or industrial areas. This could use mobile stations or a permanent installation as was used to obtain the data for the present study.

In the present work, the EC tower observations covered an overall footprint area of 26 individually managed small paddocks. To relate EC measurements to the growth and grazer respiration of specific paddocks, it was therefore necessary to relate fluxes observed at the tower to the activity on specific paddocks. EC data are measurements of fluxes that are representative from a surface source located in the upwind direction relative to the tower location and which is called the flux footprint. Several footprint models relying on different theories have been developed and reviewed by Vesala et al. (2008) and Schmid (2002):

- Analytical models
- Lagrangian-stochastic particle dispersion algorithms
- Large-eddy simulations

- Ensemble-averaged closure models

The last three categories of footprint models listed above are complex and more resource intensive than the first one. Vesala et al. (2008) and Schmid (2002) pointed out that analytical footprint models can give erroneous results if the assumptions made to derive them are violated during their application. Nevertheless, analytical footprint algorithms are the most widely used in eddy covariance applications as they can be easily implemented to filter and correct fluxes or to scale and validate models. Among them, the Kormann and Meixner (2001) model is one of the most widely used and the one that has been used in this study (for the Scott Farm site). The characteristics of the footprint are affected by measurement height, surface roughness, wind direction, and atmospheric thermal stability. Since these quantities are known or can be computed from the measurements taken every 30 minutes, the footprint area of fluxes can be calculated.

2.2.2 Experimental set up

Eddy-covariance measurements require two different fast responding sensors:

- A three dimensional sonic anemometer to measure the three space component (u, v and w) of the wind speed and the sonic temperature.
- An Infrared Gas Analyser (IRGA) to measure the molar concentration of a scalar present in the atmosphere.

These two sensors must be placed close to each other in order to minimise reading/screening errors in measurements as it is critically important to match eddies with the quantities being moved and that cannot be done unless measurement are made at the same time and space.

Two technologies of IRGA are available but, most of the time, an open-path IRGA is preferred because it has the advantage of making the measurements directly in the atmosphere close to the sonic anemometer, which makes it easier to synchronise the relevant measurements. It also has very low power consumption but this can lead to unreliable readings under certain meteorological conditions (e.g. rainfall or fog events). The alternative type is a

closed system that operates at a distance from the sampling point with air drawn in through pipes to the IRGA. This has the advantage of giving better and more stable readings under most climatic and turbulence conditions; however, it creates a delay between the quantities measured by the two sensors and an attenuation of the high frequency signal and measurements need to be corrected for that.

In addition to these two devices, some other conventional/slow response meteorological sensors are needed to make the required corrections to flux measurements, enable the use of gap filling algorithms, and be used to run models.

There is no one, single methodology to make EC measurements and different research groups use different data processing tools and experimental designs to answer specific questions (Burba, 2013).

2.2.3 What do we measure over land ecosystems?

The most common data available from an EC tower are 30-minute averaged net ecosystem exchange (NEE) and evapotranspiration (ET) that is the sum of surface evaporation and vegetation transpiration.

Atmospheric scientists typically use the convention of describing net ecosystem exchange with positive values when the flux goes from the ecosystem to the atmosphere (such as for respiration) and negative values for fluxes from the atmosphere to the ecosystem (such as for photosynthesis). Ecophysiologists, however, prefer the opposite convention and describe ecosystem uptake with positive values, often designated as the net ecosystem productivity (NEP). This terminology is used below, with positive values implying carbon uptake by the ecosystem. NEP is considered to be more appropriate for our study where we are ultimately interested in net changes in SOM so that, as for gross primary production (GPP), a positive sign is related to a carbon gain/accumulation in the studied system.

Figure 2.6 gives a schematic representation of the different components of the measured NEP. In the context of describing the different fluxes of carbon into and out of ecosystems, the uptake of carbon dioxide through the process of

photosynthesis is typically called GPP of an ecosystem (Ciais et al., 2010). Autotrophic respiration (R_a) corresponds to the consumption of photo-assimilates for the synthesis of new plant tissues and the maintenance of living ones. About fifty percent of photo-assimilates coming from photosynthesis is typically consumed and lost from the ecosystem in this process (Luyssaert et al., 2007b). The difference between the amounts of carbon fixed by photosynthesis and that lost by autotrophic respiration is called the net primary production (NPP).

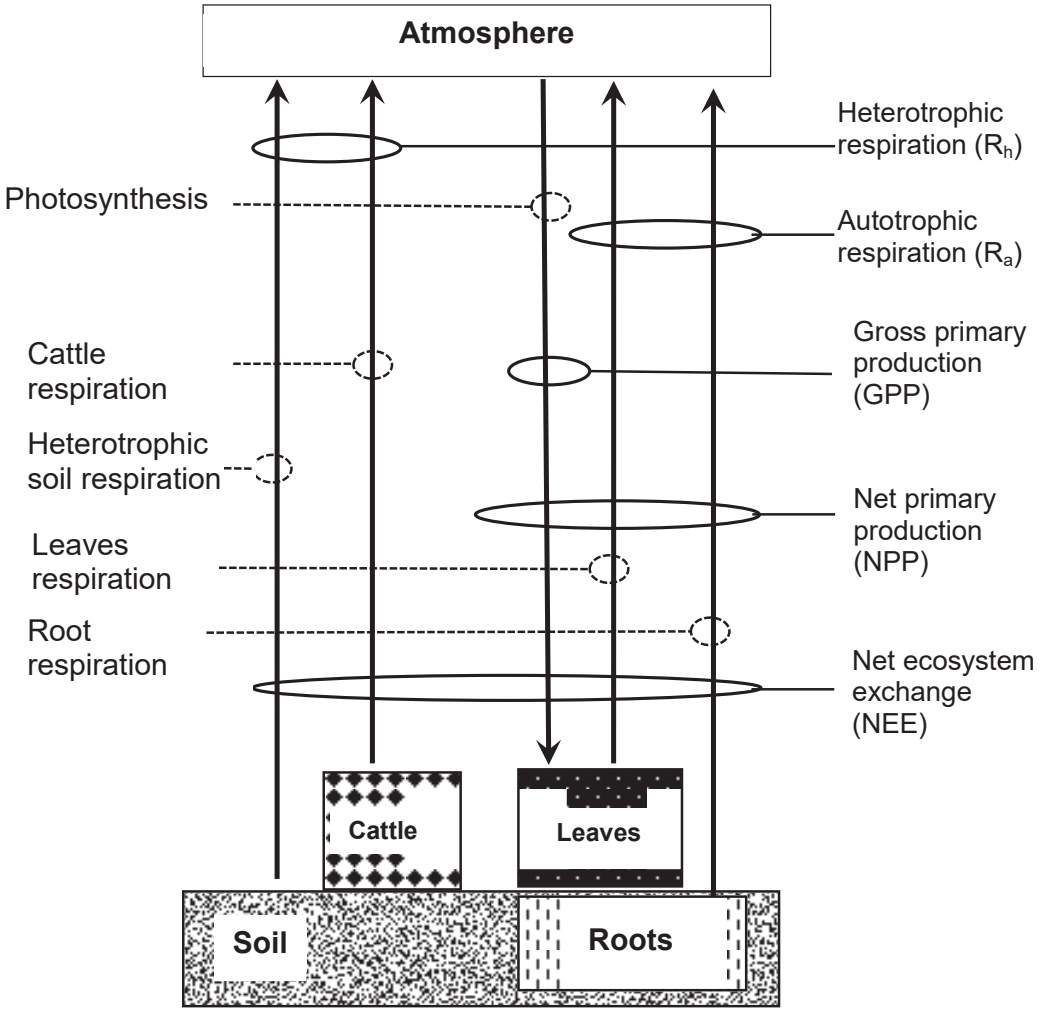

Figure 2.6: Diagram of the principal component of CO_2 fluxes over a dairy pasture, adapted from Gifford (2003) to take account of the respiration rate from grazing cattle.

The net ecosystem productivity is calculated (see Equation 2.11) as the difference between the gross primary production (GPP) and the total ecosystem respiration (ER):

$$\mathrm{NEP} = \mathrm{GPP} - \mathrm{ER} \quad (2.11)$$

Soil carbon content can change when there is an imbalance between C inputs (photosynthesis and feed imports) and C outputs (plant, soil and cattle respiration, product exports, methane emission, leaching, and erosion) (Amundson 2001). Measurements made using eddy covariance have the advantage that they continuously track small carbon fluxes at a high frequency and without interfering in the normal functioning of the system (Baldocchi, 2003).

From these measurements, CO_2-C budgets can be calculated on time scales ranging from hours to several years. Most of the other C fluxes can be quantified reasonably accurately from farm records (e.g. milk and meat production, and imported and exported supplementary feed). Losses of C in methane can be reasonably estimated as a fixed fraction of feed intake that can be obtained from the literature. Leaching and erosion losses must be specified for each study site. And by accounting for all carbon fluxes in or outgoing from the farm, a full carbon budget for pastoral systems can be quantified (Mudge et al., 2011; Rutledge et al., 2015; Hunt et al., 2016).

Micrometeorological (EC) techniques measure NEP and heat fluxes over land ecosystems, and it is important to note for the work presented in the following chapters of this study that GPP and ER cannot be directly measured but must be derived from a model based on a site NEP observations (Reichstein et al., 2005). The Reichstein et al. (2005) gap-filling and flux partitioning procedure is described in Chapter 5.2.2.

2.3 Uses of EC data with ecosystem models

Eddy covariance technique allows the collection of a large and continuous quantity of carbon, water, and energy flux data with no major disturbance of the ecosystem after the initial set up of the tower.

Measures of fluxes over land surfaces have been used in combination with models to serve two main objectives:

1) Derive direct relationships between ecosystem processes and meteorological drivers such as light use efficiency models (Yuan et al., 2007)
2) Optimise model parameters and validate model simulations (Medlyn et al., 2005; Santaren et al., 2007; Kirschbaum et al., 2015; Collalti et al., 2016)

In both cases, the information obtained through eddy covariance measurements helped either to derive accurate relationships or to greatly improve the simulations of ecosystem models.

Model/data agreement is affected by the quality of the measured fluxes (Kramer et al., 2002) as observations could potentially contain systematic and random errors (Wofsy et al., 1993; Aubinet et al., 2000; Wilson et al., 2002) as well as uncertainties in gap filled fluxes (Falge et al., 2001). Falge et al. (2001) studied the potential effect of errors related to eddy covariance flux measurements, and found that the processes included in the model also have to be representative of what happens in the studied ecosystem. For example, if the photosynthesis routine is not well implemented, and does not include some important limitation terms, the agreement between model output and data will be poor. This can easily happen in the field if parameter sets or equations are used that are not valid for the circumstances (Kramer et al., 2002; Ciais et al., 2013).

2.4 Description of the CenW 4.1 (daily) model

This section describes the simulation of some important processes in the CenW 4.1 model. It includes several processes except the carbon assimilation and energy budget procedures, which are each described in detail in subsequent dedicated sections. A very brief overview of the model has already been given in Chapter 1 of this thesis.

2.4.1 General overview of the model

The CenW (carbon, energy, nutrients, and water) model was first designed to study *Pinus radiata* plantations in Australia (Kirschbaum, 1999). The model is

mechanistic, runs with a daily time step, and combines important flows of carbon, nutrients (nitrogen and/or phosphorus), and water between the ecosystem and the external environment (Fig. 2.7). The initial sets of equations used in the model were published in Kirschbaum (1999) and Kirschbaum (2000). Additional routines were added to the model over the following years, and some of the original routines were modified. These modifications have continued up to the present day. For example, Kirschbaum and Paul (2002) modified the original formulation of the soil-organic matter module to incorporate new litter pools. They also modified the controls on nitrogen pools and fluxes and re-formulated the temperature and moisture modifiers of SOM decomposition rates. The latest changes made to the source code of CenW were done in the modelling study of the Scott farm study site, which is a grazed dairy pasture described in Chapter 5 of this thesis and which were reported in Kirschbaum et al. (2015)

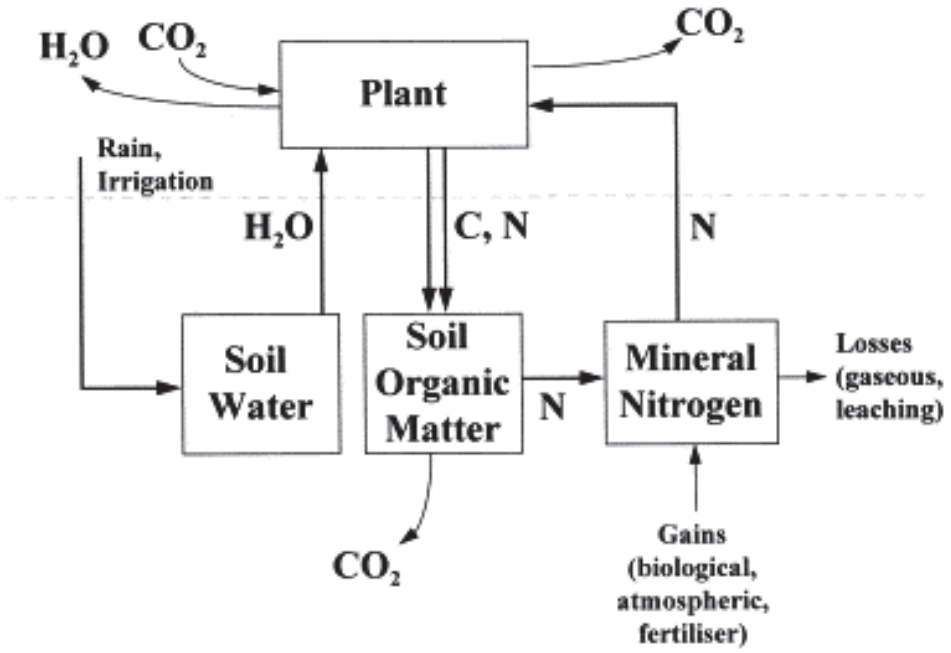

Figure 2.7: General overview of CenW showing the basic structure of the model (extracted from Kirschbaum, 1999).

The model is complex and can be used over several land use types such as forests (Kirschbaum et al., 2007; Kirschbaum and Watt, 2011) or grasslands (Kirschbaum et al., 2003; Kirschbaum et al., 2015). It can also incorporate diverse farming practice options as well as the possibility to modify climatic

background conditions on set dates. The current version of the daily model is CenW 4.1 and is available in a compiled form from http://www.kirschbaum.id.au/Welcome_Page.htm with a detailed description of the equations used in the model and its source code.

The following presents only details of selected procedures that are relevant for the present study.

2.4.2 Autotrophic and heterotrophic respiration

2.4.2.1 *Autotrophic respiration*

Autotrophic respiration (R_a) represents the respiration of previously fixed carbon by plants as part of their internal metabolism. It is generally accepted that only 30 to 50% of carbon fixed by photosynthesis is embedded by plants building the growth of new tissues, with the remainder lost as autotrophic respiration to maintain existing tissues, such as leaves, roots, stems and wood and to meet the metabolic requirements needed to grow new tissues (Luyssaert et al., 2007a; Litton et al., 2007).

In CenW, two options are available to simulate autotrophic respiration: 1) as a fixed fraction of the newly fixed carbon is respired; 2) with R_a calculated as the sum of growth (R_g) and maintenance respiration (R_m). The first option is more empirical and requires fewer parameters, while the second is more mechanistic as it splits respiration into its component processes that are differentially affected by external and internal factors.

Growth respiration can be interpreted as the amount of carbon consumed by the plant to build new tissues and is calculated as:

$$\mathrm{R_g} = f_{growth} \sum G_i \tag{2.12}$$

Where 'i' is a counter to refer to all the different plant organs, f_{growth} is an empirical term used to calculate the amount of C lost in growth respiration per unit of new growth, and G_i is the new carbon growth of the different plant organs.

In the latest version of the model, a new term was added to account for the reduction of the growth during periods of water limitation (see Kirschbaum et al., 2015, for details).

Maintenance respiration represents the amount of CO_2 produced in the maintenance of existing plant tissues and is given by Equation 2.13:

$$\mathrm{R_m} = f_{maint} f_{T,resp} R_b \sum N_i \tag{2.13}$$

where *'i'* is a counter to refer to all the different plant organs, $f_{maint}$is an empirical term that gives the daily respiration rate per unit of nitrogen at 25°C, $f_{T,resp}$ is the short-term temperature response that is calculated following Equation 2.14, R_b is the base rate of respiration, and N_i represents the nitrogen content of each plant component:

$$f_{T,resp} = exp\left[a + b\, T_{mean}\left(T_{max,resp} - T_{mean}\right)\right] \tag{2.14}$$

where T_{mean} is the daily mean temperature, $T_{max,resp}$ is the temperature for maximum respiration rate, 'a' is a term used to calculate the absolute rate of the function that is set to a value so that the function is normalised to '1' at 25 °C, and 'b' is a parameter used in combination with $T_{max,resp}$ to determine the temperature dependency of R_m.

In addition to the short-term effect of temperature given above, acclimation tends to occur in the longer term and can cause the temperature response of the respiration rate to become invariant with temperature (Gifford, 1995). To account for this modification of R_m, the base respiration rate (R_b) is modified according to Equation 2.15:

$$\frac{dR_b}{dt} = \frac{\frac{1}{f_{T,resp}} - R_b}{\tau_r} \tag{2.15}$$

where τ_r (days) is the time constant for the acclimation of the temperature response of the respiration rate.

2.4.2.2 *Heterotrophic respiration*

Decomposition of SOM releases CO_2 to the atmosphere as soil micro-organisms feed on soil organic matter. In CenW, heterotrophic respiration is modelled following the formulation of the CENTURY model from Parton et al. (1987) with further refinements described in Kirschbaum (1999) and Kirschbaum and Paul (2002). This soil organic carbon loss represents a flux that should be taken into account in the simulation of NEP and is an important factor controlling stocks of carbon in the soil.

Figure 2.8 shows a schematic representation of the carbon and nitrogen pools and flows as they are implemented in CenW 4.1. The model uses 4 litter pools for above-ground biomass (metabolic, structural, fine wood, and coarse wood), three for roots (metabolic, structural, and coarse wood) and three SOM pools (active, slow, and resistant), each with their own decomposition rate. CenW also uses a multilayer soil profile (users specify the number and depth of layers and their physical properties) so that the same scheme presented in Figure 2.8 is repeated for each soil layer.

For the simulation of pasture systems, not all these pools were used as some of them are only relevant for forest systems where there is woody material.

After the senescence of foliage or fine roots, the carbon from plant dead material is partitioned between the metabolic and structural pools based on the lignin:N ratio of the plant residues (Equation 2.16) according to Parton et al. (1987):

$$f_m = 0.85 - 0.018 \frac{N_r}{L_r} \tag{2.16}$$

Where f_m represents the fraction of fresh litter classified as metabolic litter and which is a linear function of the respective concentrations of lignin L_r and nitrogen N_r in the residue. The fraction classified as structural litter (f_s) is simply given by: $f_s=1-f_m$.

It is assumed that the structural litter pools have a slower decay rate than the metabolic ones. All lignin material from residues is transferred to the structural pool.

Microbial decomposition rates of all litter pools in the model are modified by multiplicative functions that take into account soil moisture and temperature:

$$D_l = k\, T_d W_d e^{-\delta L_s} \tag{2.17}$$

where D_l is the decomposition rate for litter pools, k is a basic rate constant, T_d and W_d are the temperature and moisture modifiers respectively, δ is a constant parameter (δ=5) and L_s is the lignin content of the structural litter pools (metabolic litter pools do not contain lignin and so the exponential term is not used for the metabolic litter pools).

As we see in Figure 2.8, the model has three soil organic matter pools. Metabolic litter is transferred only to the active pool, while structural litter goes in the active and slow pools. SOM pools also transfer a fraction of their carbon to other pools as they decompose, while another fraction is lost in respiration. The flows described above for carbon are also valid for nitrogen and are controlled by the calculated carbon fluxes and the C:N ratio of the originating pools or fresh litter materials (Kirschbaum and Paul, 2002).

Heterotrophic respiration is given by the sum of all the CO_2 losses from the decomposition of organic matter from all transitions and across all soil layers.

In grazed systems, however, the measured heterotrophic respiratory flux originates not only from the decomposition of soil organic matter, but cattle can also respire large amounts of CO_2 during each grazing event. The grazing routine implemented in CenW is described in the following (Section 2.4.3.2); it is assumed that 50% of the feed ingested by dairy cows is directly returned to the atmosphere through the animals' respiration and 5% as methane (Kirschbaum et al., 2015).

Also, a new 'dead foliage' pool was added in the latest version of the model (Kirschbaum et al., 2015). After leaves have died, they either directly fall onto the ground surface where they became part of the surface litter pool or they

remain standing, from where they decompose standing if the vegetation is wet or are transferred to the litter pool after some time or because of cattle trampling. Dead leaves account for interception of light and rainfall without being physiologically active, i.e. without contributing photosynthetic carbon gain, respiratory carbon loss or transpirational water loss.

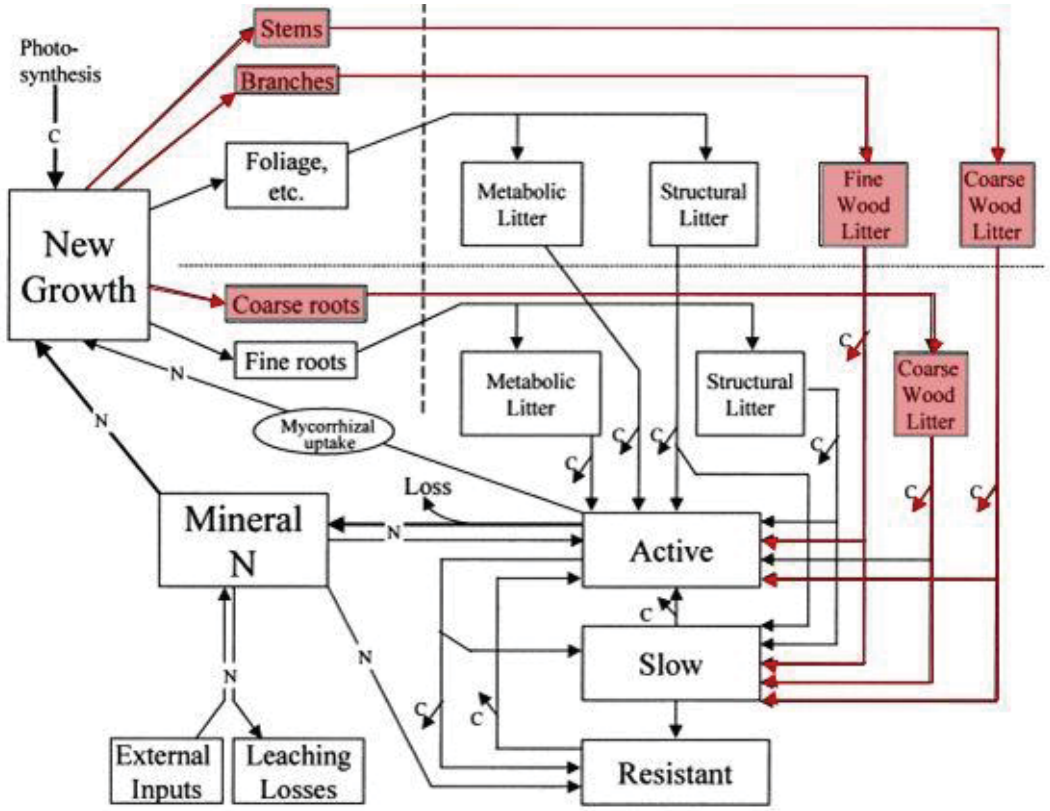

Figure 2.8: Schematic diagram of the pools and flows of carbon and nitrogen in CenW (adapted from Kirschbaum and Paul, 2002). Flows between pools involve transfers of both C and N. Transfers between pools are accompanied by respiratory losses of C indicated by short arrows not leading to other boxes. There are additional flows involving only N, indicated by 'N' on the arrows. These are flows to and from the pool of mineral N and direct mycorrhizal N uptake by plants. Red arrows and pools are present in the daily and half-hourly models but are not used for pastures systems.

The rate of change in the dead foliage pool ($^{dL_d}/_{dt}$) is given by:

$$\frac{dL_d}{dt} = f_d L_d + k_s f(T)\,(1 - l_f) L_d \quad \text{if foliage is wet} \tag{2.18}$$

$$\frac{dL_d}{dt} = f_d L_d \quad \text{if foliage is dry}$$

where L_d is the pool of dead foliage, f_d is the daily fraction of dead foliage returned to the surface, k_s is the decomposition rate constant for this pool, l_f is the fraction of lignin present in foliage and $f(T)$ is the same function that describes the temperature response of organic matter decomposition.

2.4.3 Farm management options included in the model

2.4.3.1 *Fertiliser applications*

Nitrogen fertiliser is widely used on dairy pastures in New Zealand to maintain grass and milk production at high levels. In the model, applied fertiliser is assumed not to enter the soil solution immediately, but rather to remain in a dry or solid form for some days. The driving variable of fertiliser release is the water content of the first layer of soil, and it is assumed that all applied fertiliser is deposited on top of the soil. When the soil is wet with a water content exceeding half the maximum water content of the first soil layer, fertiliser then gradually becomes available for plant uptake or leaching in mineral forms. The model makes no distinction between the nitrate (NO_3^-) and ammonium (NH_4^+) forms. The daily release rate of N fertiliser, given in kgN ha^{-1} d^{-1}, is controlled by a parameter in the model. Following fertiliser release, nitrogen is transferred into the mineral N pool (Fig. 2.8), from where it is available for plant uptake.

It is possible to specify the date of fertiliser applications, the amount applied during each application, and the percentage lost by volatilisation. Detailed and paddock-specific fertiliser application rates were not available for the study site. For the model runs made during this study, the same amounts and timings of N applications had to be specified for all the different paddocks.

2.4.3.2 *Grazing*

The grazing routines used in CenW 4.1 have been described in Kirschbaum et al. (2015). However, as it is an important feature of the model to simulate grazed grasslands, important key information is provided below.

Two options are available to take into account the effect of grazing cattle in the simulations:

1) Setting the timing and intensity of grazing events according to farm records
2) Using an automatic grazing routine

The first method can be used if information about grazing events has been recorded and is available to run the model (as it was for the runs at Scott Farm – see Kirschbaum et al., 2015). The second method can be used to run scenarios under changing conditions as users do not need to specify the timing of grazing events, and gazing frequency can be automatically adjusted to changing feed availability in response to change in any externally imposed conditions (Kirschbaum et al., 2017).

If method 1 is used during every grazing event specified by the user, the model assumes that cattle consumed a fixed proportion of above-ground biomass (Pal et al., 2012). This proportion is a model parameter that has been fixed to 55% both in Kirschbaum et al. (2015) and in this study. If grazing was spread over several consecutive days, amounts of feed ingested on individual days were adjusted to add to a total of 55% of foliage consumed over the consecutive days. We further assumed that if feed is ingested by dairy cows, 50% is lost through respiration (Zeeman et al., 2010), 5% is emitted as methane, 18% is exported as milk solids (Soussana et al., 2010), and 27% is returned to the paddocks as dung and urine. It was also assumed that cows neither gained nor lost weight so that weight changes by animals did not have to be included in the carbon budget of the paddocks.

The second method assumed the same partitioning of carbon during grazing events. However, instead of specifying the discreet timing of grazing events, users have to specify an upper above-ground biomass threshold that starts grazing and a lower threshold down to which level the animals graze the pasture.

In both methods to simulate grazing events in the model, the percentages used in the partitioning of the ingested carbon can be changed if needed. The values given in the text above were used in CenW 4.1 (Kirschbaum et al., 2015, 2017)

and were not changed for the half-hourly version of the model (CenW_HH) that was developed and used in this study.

Animals also received extra supplemental feed on the different paddocks, and excess available feed was sometimes removed in harvests. These extra gains and losses of carbon and nutrients were also specified, when appropriate, to complete a full site carbon budget.

CHAPTER 3: MODELING PHOTOSYNTHESIS AT DIFFERENT TEMPORAL AND SPATIAL SCALES

3.1 Introduction

To grow and support their metabolic activities, plants fix inorganic carbon (CO_2) from the atmosphere and transform it into sugars through biochemical reactions using solar irradiance as energy: the process of photosynthesis. At a global scale, photosynthesis is the principal flux of CO_2-C from the atmosphere to ecosystems that drives the growth of vegetation (primary carbon). The grazing or death of vegetation provides energy to macro-, meso- and micro-fauna and flora responsible for biochemical transformations of carbon compounds (secondary carbon) in the terrestrial environment

Accurate simulation of photosynthesis is a key process in the modelling of net greenhouse gas emissions, and, more particularly, CO_2 flux, because it is the main pathway of carbon from the atmosphere to the vegetation and ultimately to the soil (Dietze, 2014). Undecomposed primary or secondary carbon compounds in standing dead vegetation and soil provide a C pool that can be increased to mitigate the rise of atmospheric CO_2 concentrations. Carbon and water fluxes over agricultural lands are also strongly affected by vegetation cover, farming practices and climatic conditions. The need for accurate predictions of carbon assimilation rate in response to different plant growth, management, and climatic conditions has led to the development of photosynthesis models able to deal with all these important factors (Bernacchi et al., 2013).

Currently, CenW version 4.1 (Kirschbaum et al., 2015) is a daily time-step ecosystem model that incorporates modules for the simulation of gas exchange and growth of vegetation (photosynthesis, stomatal conductance, allocation), a SOM module derived from the CENTURY model (Parton et al., 1987), nutrient cycling of N and P, a multilayer soil water content (simple bucket) module, and farm management routines that include ploughing, fertiliser and irrigation application, and a grazing routine. The model has been widely tested on forests and to a lesser extent on pastures. However, recently the CenW model has been applied with success to a grazed pasture study site (Kirschbaum et al., 2015) at Scott Farm, Waikato, New Zealand.

The overall aim of this chapter is to present and test different leaf photosynthesis models and upscaling methods to the canopy level. Such detailed models and methods are required as sub-routines in ecosystem models if one wants to use half-hourly net ecosystem CO_2-C flux measured using eddy covariance techniques to validate or parameterise them or to make direct comparisons between modelled and observed fluxes.

The first part of the following study is dedicated to the description of leaf and canopy photosynthesis routines and the second part to the comparison of modelled and EC-derived GPP using the different models available that were implemented in CenW_HH, hereafter the name of the new version of the CenW model running at a half hourly time step developed in this thesis.

3.2 Description of some photosynthesis models

3.2.1 Modelling plant carbon assimilation rates

The accurate simulation of carbon assimilation rate is critical for studying the long-term behaviour of an ecosystem in response to climatic and plant-physiological conditions. The carbon assimilation procedure present in CenW 4.1 gives the daily canopy photosynthesis according to a set of integrated formulas. Strong assumptions were embedded in these formulas to allow calculation of nonlinear and coupled equations (Sands, 1995b), in which a non-rectangular hyperbolic curve was used to calculate the daily canopy carbon assimilation rate in response to solar radiation. A detailed description of the Sands (1995b) photosynthesis model is given in Section 3.2.2, and of light response curves using non-rectangular hyperbolic curve in Section 3.2.3.2.

In order to change the running time step of CenW to allow direct comparisons between modelled and measured carbon and water fluxes, different formulations of leaf photosynthesis models and canopy integration schemes have been tested. Data were collected half hourly with an eddy covariance system, over a dairy farm in the Waikato region of New Zealand (see Chapter 5 for the data/model comparison) for 2 years. Carbon assimilation is an important part of the model as it controls the amount of carbon fixed by the vegetation and

so its growth. This study of different leaf photosynthesis models and upscaling from the leaf level to the canopy scale was made with the overall aim of finding a good compromise between accuracy and complexity.

Over the years, several formulations with different complexity and time integration have been used to simulate reliable carbon assimilation rates. Detailed reviews and comparisons of various photosynthesis models with a complete description of some of the most-widely used ones have already been given elsewhere (Zheng et al., 2012; Bernacchi et al., 2013; Wang et al., 2015).

Zheng et al. (2012) used six popular leaf photosynthesis models, e.g. Non-rectangular hyperbolic model, Rectangular hyperbolic model, Bassman exponential model, Prado exponential model, Binomial regression model, and Rectangular hyperbolic correction model, and compared them against gas exchange measurements at the leaf and canopy scale by using a simple “big-leaf” integration scheme. They found that after independent parameterisation of light response curves (A/PPFD) of each leaf photosynthesis model, most of them were able to achieve good agreement with observations with. However, they found different values for parameters that should be thought to be equal between model formulation as they are linked to biophysical processes, like the maximum rate of photosynthesis (A_{max}).

Bernacchi et al. (2013) reviewed the development of the mechanistic photosynthesis model of Farquhar et al. (1980) at the leaf and canopy scale and highlighted the need for its proper parameterisation as most of the parameters are highly temperature dependent. They also highlighted that uncertainties in parameter values for different C_3 species could lead to significant error in the modelled rates of photosynthesis.

Wang et al. (2015) compared agreements of two photosynthesis models with eddy covariance measurements made over an alpine meadow in China. In their study, they used a simple, linear light use efficiency (LUE) model and the detailed biochemical leaf photosynthesis model from Farquhar et al. (1980) upscaled with a “big-leaf” scheme. They found that after individual parameterisation of both models on the same dataset, they were able to

reproduce observations accurately but with a better fit and predictive power for the more detailed mechanistic model from Farquhar et al. (1980).

As stated above, many different routines to simulate photosynthesis have been developed with different levels of complexity. The first model tested was the mechanistic biochemical model for leaves of C_3 plants that was proposed by Farquhar et al. (1980), hereafter called the FvCB model, from the initials of the authors of this study. This leaf photosynthesis model was chosen because it constitutes the basis of many ecosystem models and has been used in many modelling studies over the last 30 years. The FvCB model has been found to be a useful tool to study the changes in carbon assimilation rates over a wide range of climatic conditions and plant types (trees, crops, pastures). It was designed to give the steady-state CO_2 assimilation rate at the leaf level and its mechanistic basis made it also reliable in long-term studies, including the response to anthropogenically induced climate change (Solomon et al., 2007).

However, in order to make realistic runs the FvCB routine needs a large number of parameters to be set properly. Most of these parameters are species and/or site dependent and have to be calibrated against photosynthesis response curves to light, temperature and plant-physiological conditions. Response curves can be measured in the field with a portable infrared gas analyser or chambers (although these kinds of measurements were not available for the Scott farm study site) or by using parameters from the literature. Strong relationships can be found between the nitrogen content of leaves and their photosynthetic capacity (Evans, 1989; Kattge et al., 2009; Bernacchi et al., 2013; Walker et al., 2014), and several formulations have been used to simulate the response of photosynthetic capacity to leaf nitrogen content. In intensively managed dairy farms, substantial amounts of N fertiliser are applied to pastures to maximise plant growth with the overall aim to maintain or increase milk production and pastures were not expected to experience severe nutrient limitations over a long time period. Also CenW incorporate a detailed nitrogen cycling procedure (Chapter 2.4) that was used in the overall simulation of the pasture system.

Another modelling approach tested here was the use of non-rectangular hyperbolic (NRHC) or rectangular hyperbolic curves (RHC). These methods have been used in various previous studies, and it was assumed they could give an excellent phenomenological description of leaf photosynthesis (Hirose and Werger, 1987; Thornley and Cannell, 1997; Thornley, 1998, 2002; Johnson et al., 2010; Zheng et al., 2012) with fewer parameters than the FvCB model.

In order to assess the carbon assimilation rate at the canopy scale it is necessary to use integration or upscaling schemes like big leaf, sun/shade where contributions of sunlight and shaded leaves are simulated independently and summed to get the whole canopy carbon assimilation, or multilayer schemes. It is also possible to use integrated equations like the daily Sands model (Sands, 1995b) or the 30-minutes Thornley model (Thornley, 2002), which are described in detail in the following sections.

3.2.2 The daily canopy photosynthesis routine: Sands model

In CenW 4.1, daily canopy net CO_2 assimilation rate ($\mathrm{A_c}$) is calculated according to Sands (1995) by solving analytically the integral of Equation 3.1 by making constraining mathematical assumptions and simplifications listed below:

$$\mathrm{A_c} = \int A(x, y, z, t)dxdydzdt \tag{3.1}$$

where $\mathrm{A_c}$ is the daily canopy assimilation rate (mol m^{-2} d^{-1}), A represents the instantaneous single leaf photosynthesis (μmol m^{-2} s^{-1}), x, y and z are the coordinates of the leaf in the canopy, and t is the integration interval (day).

The 5 principal assumptions making these calculations possible are:

1) The single leaf light response is hyperbolic and the single leaf photosynthetic rate (A) is the solution of a non-rectangular hyperbolic curve (Equation 3.2):

$$\theta A^2 - (\alpha I_l + A_{max})A + \alpha I_l A_{max} = 0 \tag{3.2}$$

where I_l (μmol PAR m^{-2} s^{-1}) is the PPFD incident upon the leaf, A_{max} is the light saturated rate of photosynthesis, α is the quantum efficiency, and θ is a curvature parameter.

It is important to note that the three parameters ($A_{max}, \alpha, \text{and } \theta$) of the above equation (Equation 3.2) are not constant among C_3 plant species and are also modified through changes in environmental factors such as solar radiation, temperature, nutrient availability and soil and plant water status. It is through these variables that both instantaneous and daily canopy photosynthetic rates can be modified to respond to local conditions. Among them, solar radiation is certainly the most important variable because plants use this energy to assimilate CO_2 from the atmosphere and transform it into sugars. A_{max} is particularly sensitive to all the variables listed above while α and θ are generally not modified by microclimatic conditions or water stress but are rather kept constant among plant species.

2) The canopy is horizontally homogeneous but vertically heterogeneous. These assumptions allow the simplification of Equation 3.1 because the integral becomes independent of two spatial variables and integration is only needed over the depth of the canopy, which can be based on using the leaf area index accumulated from the top of the stand downwards (LAI_{cum}).

The radiation in the canopy is assumed to follow Beer's law. In this case, it is assumed that the PPFD incident upon an horizontal leaf surface at a depth L in the canopy is given by Equation 3.3:

$$I_l(\mathrm{L}) = \frac{k}{1-m} I_0 e^{-k_b LAI_{cum}} \tag{3.3}$$

where I_0 (μmol PAR m^{-2} s^{-1}) is the PPFD above the canopy, k_b is the extinction coefficient, *m* is the leaf transmission coefficient and LAI_{cum} is the cumulated leaf area index above the considered leaf.

3) A_{max} is proportional to the ratio of the local PPFD in the canopy and the full sun PPFD, which corresponds to the incident PPFD above the canopy without attenuation by the leaves in the canopy.

This is a mathematical consequence of an assumed optimal vertical distribution of leaf nitrogen concentration within the canopy. Optimal photosynthesis is achieved when leaf nitrogen is distributed vertically in such a way that A_{max} is proportional to local PPFD (Leuning et al., 1995; Sands, 1995a; dePury and Farquhar, 1997). The variables α and θ are independent of leaf N concentration or their position in the canopy (Sands, 1995a).

4) The incoming radiation (PPFD) above the canopy is described as a sinusoidal function of the time of day (Equation 3.4):

$$I_0(\mathrm{t}) = \begin{cases} \frac{\pi\, \mathrm{Q}}{2h}\gamma \sin\left(\frac{\pi t}{h}\right) & (0 \le t < h) \\ 0 & (h \le t \le 1\ day) \end{cases} \tag{3.4}$$

where Q (MJ m^{-2} d^{-1}) is the total daily irradiance above the canopy, h (s d^{-1}) is day length, γ (μmol PPFD MJ^{-1}) is used to convert total daily irradiance into PPFD and t is the time of day in seconds.

5) Photosynthetic parameters are assumed not to vary diurnally. This assumption is used even though it is known that A_{max} has a strong dependence on temperature and, consequently, it should vary with diurnal variations of temperature. The Sands model kept A_{max} constant to allow a computationally efficient modelling of daily photosynthesis with a single set of equations. To solve the integral (Equation 3.1), Sands made the approximation that this parameter does not vary diurnally but is modified by mean daily temperature.

By making these assumptions, Sands was able to derive a set of equations from which it is possible to compute daily canopy photosynthesis from single-leaf photosynthetic parameters and daily incident radiation (Equation 3.5):

$$A_c = A_{max} h g(q,\theta) \frac{1 - \exp(-k_b LAI_g)}{k_b} \tag{3.5}$$

where LAI_g is the total green leaf area index and *g(q,θ)* is a complex function that allows the assimilation rate to be calculated based on total daily radiation and single-leaf photosynthetic parameters, which is expressed as:

$$g(q,\theta) = \frac{g_r(q) f_1(\theta)}{1 + \left(\frac{g_r(q)}{g_b(q)} - 1\right) f_2(\theta)} \tag{3.6}$$

where f_1 and f_2 are empirical functions depending only on *θ*, g_r is a single leaf rectangular hyperbolic response curve, and g_b is a Blackman single leaf response curve.

$$\begin{aligned} f_1(\theta) &= 1 + a_1\theta(1-\theta) + b_1\theta^2(1-\theta)^2 \\ f_2(\theta) &= a_2\theta + b_2\theta^2 + (1 - a_2 - b_2)\theta^3 \end{aligned} \tag{3.7}$$

with $a_1 = 0.22$, $a_2 = -0.18$, $b_1 = 0.74$, $b_2 = 0.50$ are constants given in Sands (1995b).

$$g_r(q) = \frac{2\,b\,q}{\pi(b+q)} \tag{3.8}$$

where *b* is a parameter which is taken equal to 1.38 (Sands, 1995b):

$$g_b(q) = \begin{cases} \dfrac{2q}{\pi} & (q \le 1) \\ 1 + \dfrac{2}{\pi}\left(q - \sqrt{q^2 - 1} - \sin^{-1}\left(\dfrac{1}{q}\right)\right) & (1 \le q) \end{cases} \tag{3.9}$$

Sands (1995) used normalised radiation (q), which is derived according to Equation 3.10:

$$\mathrm{q} = \frac{\pi k \alpha Q \gamma}{2h(1-m)A_{max}} \tag{3.10}$$

with parameters as given above.

Sands (1995b) proposed to use a parabolic response to temperature derived from field observations:

$$A_{max}(T) = A_{opt}\left(1 - 0.5\left(\frac{T - T_{opt}}{t_{1/2}}\right)^2\right) \tag{3.11}$$

where A_{opt} is the rate of photosynthesis at optimum temperature, T is the daylight averaged temperature, T_{opt} is the temperature at which A_{max} is the maximum rate of photosynthesis, and $t_{1/2}$ is the change in temperature from T_{opt}, which reduces A_{max} to half the optimum.

In CenW (Kirschbaum, 1994), a more detailed and realistic parameterisation for the calculation of A_{max} is implemented that is related to the FvCB model formulations and thereby also includes the effect of changing CO_2 concentrations:

$$A_{max}(\mathrm{T}) = A_{\mathrm{Vj}}(\mathrm{T})\frac{C_i - \Gamma^*}{C_i + 2\Gamma^*} \tag{3.12}$$

where A_{Vj} is the rate of RuBP regeneration or photosynthesis with non-limiting CO_2 concentration, C_i is the intercellular CO_2 concentration, and Γ^* is the CO_2 compensation point without non-photorespiratory respiration. The temperature dependence of the maximum rate of photosynthesis is given by a hump function (Equation 3.13):

$$A_{Vj}(\mathrm{T}) = \begin{cases} 0 & T_{day} \le T_n \\ A_{\mathrm{opt}}\dfrac{T_{day} - T_n}{T_{opt1} - T_n} & T_n < T_{day} < T_{opt1} \\ A_{\mathrm{opt}} & T_{opt1} < T_{day} < T_{opt2} \\ A_{\mathrm{opt}}\dfrac{T_x - T_{day}}{T_x - T_{opt2}} & T_{opt2} < T_{day} < T_x \\ 0 & T_{day} \ge T_x \end{cases} \tag{3.13}$$

where T_n and T_x are the minimum and maximum temperatures that allow any photosynthesis to occur, T_{opt1} and T_{opt2} are lower and upper temperature

bounds that allow optimum photosynthetic rates, and T_{day} is mean daily temperature.

The optimum photosynthetic rate ($\mathrm{A_{opt}}$) depends on several limiting factors that are taken into account in the whole model (Equation 3.14):

$$A_{\mathrm{opt}} = A_x f_d N_{lim} W_{lim} \tag{3.14}$$

Where f_d is a temperature damage term, A_x is the highest photosynthetic rate for the considered species under optimum conditions, W_{lim} is a water-stress limitation parameter, and N_{lim} is a leaf nitrogen content limitation parameter.

In the model, it is assumed that plants can be damaged by either cold (frost) if minimum temperatures fall below a threshold value or by heat (scorch) if maximum temperatures increase above a threshold. These damages are counted cumulatively and parameters determine the temperature sensitivity of plants to frost and scorch damage and so, by how much photosynthesis rate is inhibited and the time needed for the vegetation to recover after the damage they experienced.

Because the photosynthetic capacity of leaves depends highly on their nitrogen content, the maximum rate of photosynthesis is achieved when there is no nitrogen shortage (N_{lim} = 1) and is reduced as the nitrogen content of leaves diminishes (Evans and Terashima, 1987; Evans, 1989; Verhoeven et al., 1997). These limitation terms are included in the simulations because they have an important role to play in reducing assimilation rates under some environmental stresses.

This procedure was described here because it is included in the daily version of the model (CenW version 4.1) and had to be modified to allow the new version of the model to run with a shorter time interval, identical to eddy covariance observations taken half-hourly. In the following, different instantaneous leaf photosynthesis routines and upscaling schemes at the canopy scale are described and tested.

3.2.3 Leaf photosynthesis modelling theory

3.2.3.1 *Description of the FvCB model*

In the early stages of photosynthesis research, researchers identified three metabolic pathways that regulate net leaf carbon dioxide fixation and which happen concurrently: photosynthesis, PS, which is the uptake of carbon from the atmosphere and photorespiration, PR, and non-photorespiratory respiratory losses that release carbon to the atmosphere. PS and PR are catalysed by the same enzyme in a competitive manner based on the relative concentrations of CO_2 and oxygen, and the relevant biochemical constants that are themselves strong functions of temperature (Farquhar et al., 1980; Von Caemmerer, 2000; Bernacchi et al., 2013). The stoichiometry of photorespiration means that for two oxygenation reactions of Rubisco only one molecule of CO_2 is released. The central equation of the model giving the carbon assimilation rate of a leaf (Equation 3.15) can therefore be written as:

$$A = V_c + 0.5V_o - R_d \tag{3.15}$$

where V_c (μmol CO_2 m^{-2} s^{-1}) is the rate of carboxylation by Rubisco, V_o (μmol O_2 m^{-2} s^{-1}) is the rate of oxygenation by Rubisco and R_d (μmol CO_2 m^{-2} s^{-1}) is the rate of day respiration.

Because the carboxylation and oxygenation reactions share the same active site on Rubisco, Equation 3.15 can be expressed as:

$$A = \left(1 - \frac{\Gamma^*}{C_i}\right) V_c - R_d \tag{3.16}$$

where C_i is the intercellular concentration of CO_2 (μmol mol^{-1}) and the term Γ^*(μmol mol^{-1}) is the photosynthetic CO_2 compensation point in the absence of non-photorespiratory respiration, which represents the concentration at which photosynthetic carbon uptake is equal to photorespiratory CO_2 release, or in other words, when the net rate of carbon assimilation equates to the rate of non-photorespiratory respiration.

For response curves, the intracellular CO_2 concentration is set to 270 ppm but in the overall CenW_HH model it is calculated iteratively to ensure the coupling of photosynthesis and water flux through stomatal conductance. At first C_i is set to a fixed value of 0.7 times the atmospheric CO_2 concentration (fixed at 380 ppm) then it is recalculated according to climatic conditions and plant stress factors until convergence is achieved (Collatz et al., 1991). Usually, less than five iterations are required to achieve convergence.

In Equation 3.16, the term $\frac{\Gamma^*}{C_i}$ represents a convenient simple form to express the relative catalytic activity of the competing oxygenation and carboxylation reactions at the active site of Rubisco determined by the combined effect of the relevant biochemical constants. Together, they determine the amount of CO_2 fixed by photosynthesis and that released by photo-respiration.

The carboxylation rate (V_c), in Equation 3.16, is limited by three different processes:

1) Rubisco (W_c): assimilation rate is limited by the kinetic properties of Rubisco, which generally occurs under high irradiance and high temperatures.
2) RuBP regeneration or transport of electrons across the electron transfer chain (W_j): limitation comes from the transport of electrons across the electron transfer chain and principally occurs at low radiation levels or low temperatures.
3) The rate of triose phosphate utilization (W_p): it results from a shortage of inorganic phosphorus, which leads to a reduction in the available ATP involved in the Calvin cycle and a decrease of the assimilation rate (Sharkey et al., 1986; Wullschleger, 1993). This limitation generally does not occur in cultivated lands as fertility is managed to prevent nutrient shortages. Moreover, it mainly plays a role under high radiation levels and generally only plays a small role compared with limitations by Rubisco kinetics or RuBP regeneration. This rate is often ignored in most ecosystem models because it is hard to differentiate TPU-limited from

RuBP-limited rates of C assimilation and only few studies published temperature functions (Harley et al., 1992; Bernacchi et al. 2013).

The FvCB model has been well described in literature (Farquhar et al. 1980; Collatz et al.1991; Von Caemmerer 2000; Bernacchi et al. 2013), and in the following only the main equations of the model are described. The FvCB model is implemented in both a standalone version, used to test the response curves of leaf photosynthesis to solar radiation, temperature, and intracellular carbon dioxide concentration, and in CenW_HH for the full simulation of the stand carbon assimilation rate and comparison with EC data.

Following the original model formulation, V_c is calculated as the minimum of these 3 processes (Equation 3.17):

$$V_c = \min\{W_j, W_c, W_p\} \tag{3.17}$$

The Rubisco limited rate of photosynthesis (W_c) is calculated according to a Michaelis-Menten response function (Equation 3.18) in which increasing the limiting substrate (CO_2), the amount of enzyme (Rubisco) or decreasing the concentration of the competitive inhibitor (O_2) can lead to higher reaction rates (Bernacchi et al., 2013):

$$W_c = V_{cmax} \times \frac{C_i - \Gamma^*}{C_i + K_c\left(1 + \frac{O_i}{K_o}\right)} \tag{3.18}$$

where V_{cmax} is the maximum rate of carboxylation by Rubisco (μmol CO_2 m^{-2} s^{-1}), K_c and K_o are Michaelis-Menten constants for CO_2 and oxygen, respectively, and O_i is the intercellular concentration of O_2 (mmol mol^{-1}).

The second limiting process (W_j, Equation 3.19) is related to the rate in which ATP (Adenosine Tri-Phosphate) and NADPH (Nicotinamide Adenine Dinucleotide Phosphate Hydrogen) are formed by light reactions from ADP (Adenosine Di-Phosphate) and $NADP^+$ (Nicotinamide Adenine Dinucleotide Phosphate) and is directly correlated to the rate of linear electron transport (J, Equation3.20). Here the formulation proposed by Medlyn et al. (2002a) is used:

$$W_j = \left(\frac{J}{4}\right) \times \left(\frac{C_i - \Gamma^*}{2 \times \Gamma^* \mp \mathrm{C_i}}\right) \tag{3.19}$$

where J is the rate of linear electron transport through the thylakoid membrane and the other terms are already defined above.

The rate of electron transport (J) is calculated from a non-rectangular hyperbolic function of photosynthetic photon flux density (I_l, µmol m^{-2} s^{-1}):

$$J = \frac{\propto I_l + J_{max} - \sqrt{(\propto I_l + J_{max})^2 - 4\theta \propto I_l J_{max}}}{2\theta} \tag{3.20}$$

where J_{max} is the maximum potential rate of electron transport, ∝ is the quantum yield of electron transport and θ a curvature parameter.

The third limitation process (W_p) was not included in the first publication of the model equations by Farquhar et al. (1980) but was later identified and included in the FvCB model (Kirschbaum and Farquhar, 1984; Sharkey et al., 1986). This limitation is related to the rate of RuBP (ribulose 1.5-bisphosphate) regeneration via triose phosphate utilisation (TPU):

$$W_p = \frac{3\ \mathrm{TPU}}{1 - \Gamma^*/\mathrm{C_i}} \tag{3.21}$$

where TPU is the rate of triose phosphate utilisation, which is calculated according to Equation 3.22, with specific parameters from Harley et al. (1992).

As the FvCB model is mechanistic, its parameterisation is critical to obtain reliable estimations of leaf carbon assimilation corresponding to various climatic and growth conditions. The two central parameters of the FvCB model, V_{cmax} and J_{max}, are highly sensitive to temperature and are known to be species dependent (Medlyn et al., 2002a). On the other hand, other parameters of the model also respond to temperature but because they are linked to intrinsic properties of Rubisco, it is commonly admitted that they would remain the same among species, which would reduce the number of parameters to be fitted.

Many temperature functions and parameter values have been developed over the years (Long et al., 1993; Bernacchi et al., 2001, 2003, 2009; Medlyn et al., 2002a, 2002b; Hikosaka et al., 2006) and the most commonly used are given below. Also, Medlyn et al. (2002a) highlighted that modellers should chose appropriate temperature response functions with their specific parameters values to model photosynthesis.

The temperature dependence of K_c, K_o, R_d, V_{cmax}, and TPU are most often described by Arrhenius functions (Equation 3.22):

$$k_T = k_{25} e^{\left(\frac{E_a(T-25)}{298\,R(T+273)}\right)} \tag{3.22}$$

Where k_{25} is the parameter value at 25°C and E_a is the activation energy (kJ mol^{-1}) that differs for the description of different parameters, R is the universal gas constant (8.314 J K^{-1} mol^{-1}), and T is the temperature in degree Celsius (°C).

The temperature dependence of J_{max} and sometimes V_{cmax} and TPU are given by a peaked equation (Equation 3.23), which is also used in this study following Medlyn et al. (2002a) who obtained good parameter fits by using this function, again with specific parameter values for each of the variables:

$$k_T = k_{25} e^{\left(\frac{E_a(T-25)}{298\,R\,(T+273)}\right)} \left(\frac{1 + e^{\left(\frac{298\,\Delta S - E_d}{298\,R}\right)}}{1 + e^{\left(\frac{\Delta S(T+273) - E_d}{R(T+273)}\right)}} \right) \tag{3.23}$$

where k_{25} is the value of the parameter at 25°C, E_a is the activation energy, ΔS is an entropy term (Medlyn et al., 2002a), and E_d represents the deactivation energy.

The temperature dependence of the parameters could also be given as a function of optimal temperature:

$$k_T = k_{\text{opt}} \frac{E_d e^{\left(\frac{E_a(T_k - T_{opt})}{T_k R T_{opt}}\right)}}{E_d - E_a\left(1 - e^{\left(\frac{E_d(T_k - T_{opt})}{T_k \, \mathrm{R} \, T_{opt}}\right)}\right)} \tag{3.24}$$

where k_{opt} is the parameter value at the optimum temperature, T_k is the temperature in Kelvin, ΔS and the optimal photosynthesis temperature (T_{opt}) are linked following the formulation from Medlyn et al. (2002a) as given in Equation 3.25:

$$T_{opt} = \frac{E_d}{\Delta S - R \; ln\left(\frac{E_a}{E_d - E_a}\right)} \tag{3.25}$$

The values of the different parameters used in the above equations for each of the different rates and constants are given in Table 3.2 with the exception of the temperature dependence of the CO_2 compensation point (Γ^*) which can be calculated following Bernacchi et al. (2001) as:

$$\Gamma^* = 42.75 \; e^{\left(\frac{37830 \; (T-25)}{298 \; R \; (T+273)}\right)} \tag{3.26}$$

As Γ^* describes an intrinsic enzymatic property of Rubisco, it is not expected to vary among C_3 plant species (Medlyn et al., 2002a).

Farquhar et al. (1980) formulated the relationship between the CO_2 compensation point (Γ^*) and Michaelis-Menten coefficients of Rubisco, K_c and K_o and the maximum oxygenation rate of Rubisco, V_{omax} as:

$$\Gamma^* = \frac{K_c V_{omax} O_i}{2 \; K_o V_{cmax}} \tag{3.27}$$

where V_{omax} = 0.21 V_{cmax}, is independent of temperature (Badger and Andrews, 1974). Illustrations of the temperatures' responses of Γ^* according to Equation 3.26 and 3.27 are given in Figure 3.1a, and of the resulting leaf photosynthesis rates in Figure 3.1b.

The two functions used to calculate the temperature dependence of the CO_2 compensation point show similar patterns, e.g. a sharp increase of Γ^* with temperature, but the equation from Bernacchi et al. (2001) also gives higher values than the Farquhar et al. (1980) formulation for the whole range of temperatures (Fig. 3.1 a). The effects of using one or other of the formulations for Γ^* on the leaf photosynthesis rate in response to temperature are given in Figure 3.1 b. Differences between the two formulations of $\Gamma^*$are present for the whole range of temperatures; however, the resulting leaf photosynthesis rates modelled with the FvCB model with the different compensation point formulations show marked differences only for a narrow range of temperature centred around the optimal photosynthesis temperature (25°C). These simulations were carried out with the set of parameters given in Table 3.2.

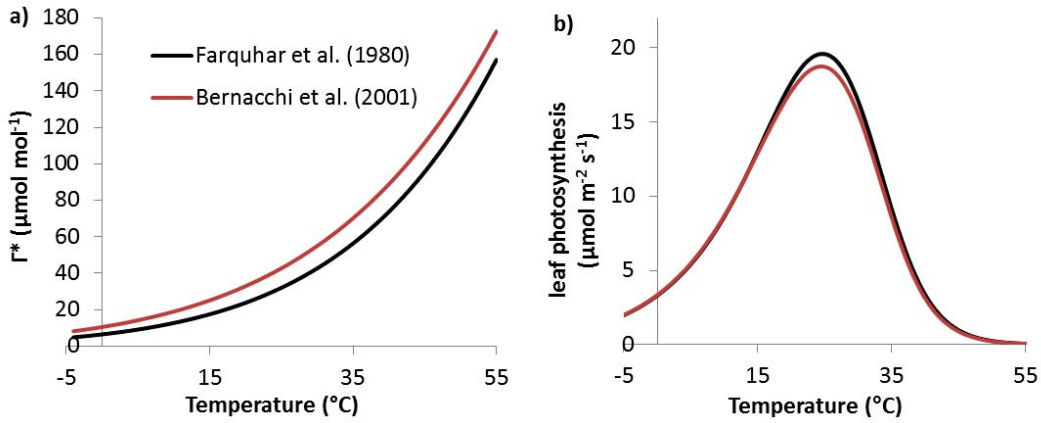

Figure 3.1: (a) Temperatures responses of Γ^* according to the formulations of Farquhar et al. (1980) and Bernacchi et al. (2001). (b) Temperature responses curves of the FvCB leaf photosynthesis model with the two formulations of Γ^*.

It is also possible to implement in the FvCB model the modifications proposed by Collatz et al. (1991) in order to smooth the transitions from one limiting rate of photosynthesis to another (Equation 3.28). This feature has been implemented and used in the standalone and in the new version of the CenW ecosystem model:

$$\begin{cases} \chi_1 {A_p}^2 - (W_c + W_j)A_p + W_c W_j = 0 \\ \chi_2 A^2 - (A_p + W_p)A + A_p W_p = 0 \end{cases} \quad (3.28)$$

where χ_1 and χ_2 are parameters used for the linking of the curves (Table 3.2); A_p is an intermediate rate of assimilation where A_p is co-limited by both W_c and W_j. A is the effective assimilation rate. These two quadratic equations are solved for their smaller roots to calculate assimilation rates.

Table 3.1: Summary of temperature dependence parameters for V_{cmax} and J_{max}. Calculations of the minimums, maximums, means and standard deviations (Std) are based on the values of the parameters given in Table 2 and 3 of Medlyn et al. (2002a) and Table 2 of Kattge and Knorr (2007) from which only data corresponding to herbaceous grasses (26 species) were used.

		Parameters	Min	Max	Mean	Std
(Medlyn et al., 2002a)	**V_{cmax}**	k_{25} (μmol m^{-2} s^{-1})	27.51	101.90	74.03	20.29
		E_a (kJ mol^{-1})	51.32	116.38	70.19	15.63
		E_d (kJ mol^{-1})	200	200	200	0
		T_{opt} (°C)	27.56	53.30	39.38	6.14
	J_{max}	k_{25} (μmol m^{-2} s^{-1})	44.83	217.88	122.16	39.68
		E_a (kJ mol^{-1})	34.83	108.45	55.61	23.42
		E_d (kJ mol^{-1})	113.77	200.00	187.52	26.69
		T_{opt} (°C)	19.2	38.48	32.71	5.36
(Kattge and Knorr, 2007)	**V_{cmax}**	k_{25} (μmol m^{-2} s^{-1})	38.3	205.20	123.47	57.78
		E_a (kJ mol^{-1})	45.37	172.84	74.27	25.04
		E_d (kJ mol^{-1})	200	200	200	0
		T_{opt} (°C)	29.4	41.90	33.00	3.01
	J_{max}	k_{25} (μmol m^{-2} s^{-1})	76.3	217.90	124.46	39.03
		E_a (kJ mol^{-1})	39.20	77.17	53.73	14.38
		E_d (kJ mol^{-1})	200	200	200	0
		T_{opt} (°C)	27.1	38.20	31.55	3.97

The FvCB model has been, and continues to be, widely used. However, any simulation results are strongly dependent on the quality of its parameterisation (Bernacchi et al., 2013). Because the response of photosynthesis to climatic conditions is non-linear, only a small variation in the values of the model parameters can lead to important changes in the shape of the response curves,

or may even lead to switches between one limiting processes and another (not shown here). This is especially true for the response of PS to temperature in which activation energies, optimal parameters values and their optimal temperatures are different between species and studies (Leuning, 1997; Medlyn et al., 2002a).

Medlyn et al. (2002a) derived and reported the values of the temperature dependence parameters for V_{cmax} and J_{max} of 17 deciduous and evergreen tree and 2 crop species and showed that a wide range of parameterisations were possible. A few years later, Kattge and Knorr (2007) extended the study of the temperature responses of the two central parameters of the FvCB model (V_{cmax} and J_{max}) to 36 species including herbaceous plants. These data are summarised in Table 3.1.

Table 3.1 reports the minimums, maximums, average, and standard deviations of the parameters used in the temperature responses of the two central parameters of the FvCB model derived in two studies including a wide range of herbaceous species. The first study (Medlyn et al., 2002a) used mostly woody species, but in the second, the temperature dependence of parameters of grasses (26 species) was reported. Overall, the range of all these parameters is wide, highlighting the importance of having site or at least species specific sets of parameters. In the following, the values of the parameters available in the literature (Wullschleger, 1993; Medlyn et al., 2002a; Bernacchi et al., 2013) are used for illustrative purposes.

Parameters reported in Table 3.2 were chosen to be within the range of parameter values found in the literature and which have been reported in Table 3.1 except for χ_1.and χ_2, which were directly taken from Collatz et al. (1991) and not modified.

Table 3.2: Parameters used in this study to test the FvCB leaf photosynthesis algorithm

Parameters	**Values**	**Units**

α	0.3	mol mol^{-1}
θ	0.9	-
V_{c25}	90	μmol m^{-2} s^{-1}
E_{a_Vc}	55.5	kJ mol^{-1}
E_{d_Vc}	200	kJ mol^{-1}
T_{opt_Vc}	30	°C
J_{25}	1.9 $_x$Vc25	μmol m^{-2} s^{-1}
E_{a_J}	45	kJ mol^{-1}
E_{d_J}	200	kJ mol^{-1}
T_{opt_J}	35	°C
TPU_{25}	10.5	μmol m^{-2} s^{-1}
E_{a_TPU}	63.1	kJ mol^{-1}
E_{d_TPU}	180.6	kJ mol^{-1}
T_{opt_TPU}	32	°C
K_{c25}	404.9	μmol mol^{-1}
E_{a_Kc}	79.430	kJ mol^{-1}
K_{o25}	278.4	mmol mol^{-1}
E_{a_Ko}	36.380	kJ mol^{-1}
χ_1	0.98	-
χ_2	0.95	-

Figure 3.2 shows the response curves of the three limiting processes discussed above and the resulting net carbon assimilation rate (PS rate) of a single leaf plotted in response to variations in intracellular CO_2 concentration (a), temperature (b), and photosynthetic photon flux density (c). These kinds of graphs are usually used to calibrate the model parameters based on leaf photosynthesis measurements, which were not available for our study site. Instead, a parameter set from the literature was used to check the basic set of equations for consistency with the graphs used in Bernacchi et al. (2013). Values of the parameters used to obtain the response curves plotted in Figure 3.2 are reported in Table 3.2.

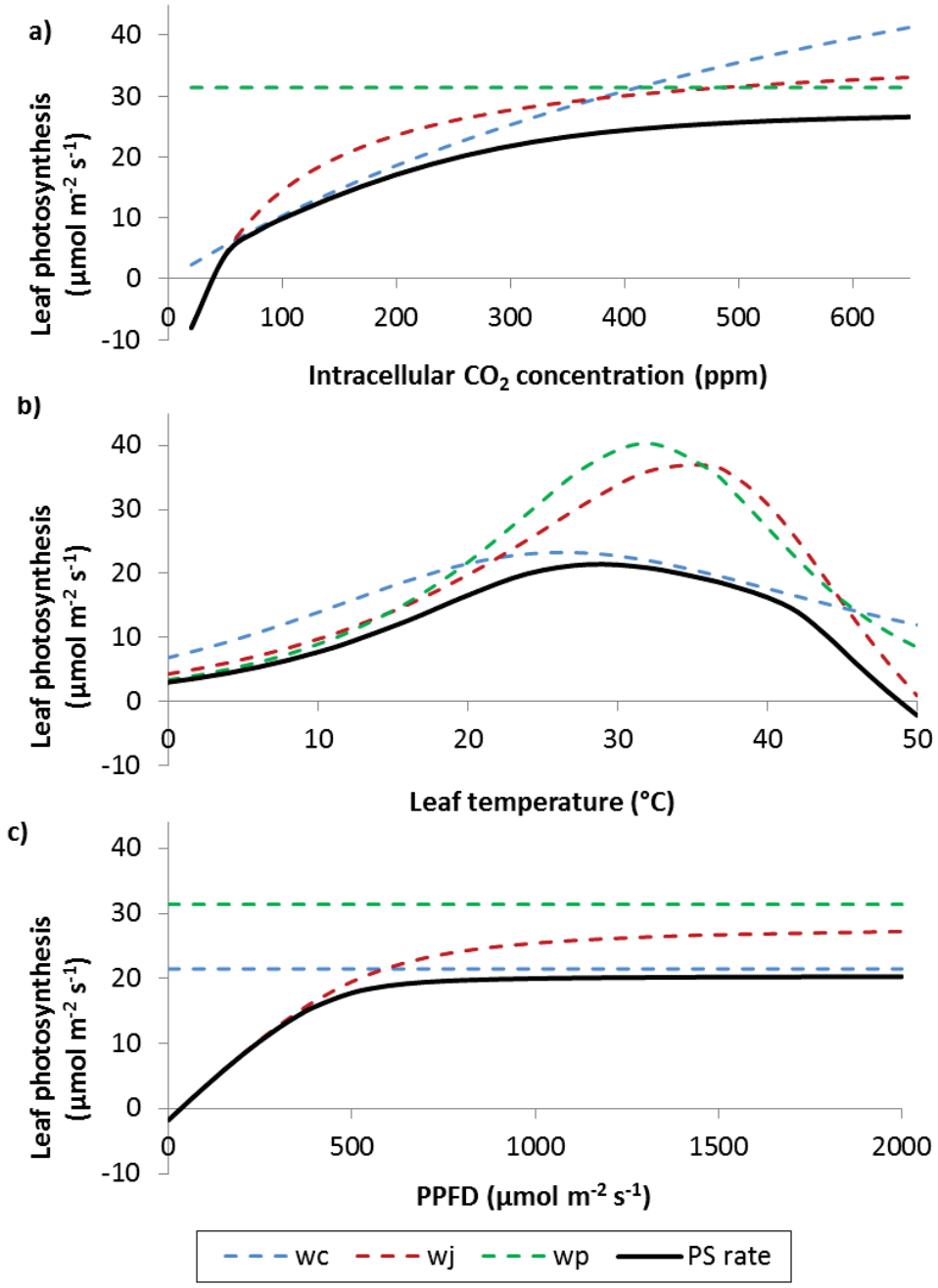

Figure 3.2: Responses curves of photosynthesis rates to intracellular CO_2 concentration (a), temperature (b) and photosynthetic photon flux density (c). The dashed lines represent the different limiting processes of carbon assimilation. W_j is the limitation due to the transport of electrons, W_c the Rubisco limited photosynthetic rate and W_p the triose phosphate utilization limitation. The resulting carbon assimilation rate is given by the minimum of the three processes and "PS rate" includes the smoothing transitions from one limiting process to the other of Collatz et al. (1991). When variables are not explicitly modified, temperature is set to 25°C, PPFD to 1500 µmol m^{-2} s^{-1} and C_i to 270 ppm.

An important aspect of photosynthesis modelling is the response of the carbon assimilation rate to solar radiation (PPFD). As Figure 3.2c shows, under low radiation, light reactions forming ATP and NADPH (w_j) are limiting PS. As leaves receive more radiation, the rate of carbon fixation increases linearly with the slope of this line being the quantum yield, which is a parameter representing the efficiency of sugars formation by plants in response to absorbed radiation. At higher irradiance, there is a switch between the RuBP-limited (w_j) and the Rubisco-limited (w_c) carbon assimilation rates where photosynthesis became light saturated and so does not respond to changes in radiation levels anymore.

Changes in modelled PS rates in response to temperature are plotted on Figure 3.2 b, according to the model parameterisation used here, at 0 degree Celsius, leaves continue to fix CO_2 at around 5 µmol m^{-2} s^{-1}. A temperature of 25 °C, corresponds to the optimal temperature for photosynthesis (the temperature where the C assimilation rate is maximal), and between 0-25 °C, the amount of fixed carbon dioxide, increases nearly steadily to reach its maximum value of 20 µmol m^{-2} s^{-1}. For temperatures above 25 °C, there is a slight decrease in photosynthesis up to 42 °C where the leaf carbon assimilation rate falls sharply.

An important aspect that is not included in the model is plant acclimation to its growing conditions (Bernacchi et al., 2013). A plant that grows at a given temperature will have a certain parameter set, but the same plant acclimated to another temperature will give a different temperature response curve and a different optimal temperature for maximum carbon assimilation rate (Kattge and Knorr, 2007; Smith and Dukes, 2013). This could potentially be problematic and limiting for the use of the FvCB model in this study because leaf gas exchange measurements are not available for Scott Farm to specifically parameterise the model.

Parameters used in model formulation vary among species, over time, space, and with nutrient regimes (Medlyn et al., 2002a; Wullschleger, 1993). This is especially true for parameters used to model the response of photosynthesis to temperature. Figure 3.2 shows that photosynthetic responses to climatic variables are non-linear, and limitations can readily change from one limiting process to another with changes in environmental variables. The sensitivity of

photosynthesis to the underlying parameters was assessed by changing the values of the parameters by +/- 10% one at a time and keeping all other parameters fixed to their baseline value (Liang et al., 2016), which are given in Table 3.2.

Figure 3.3 shows the results of the parameter sensitivity analysis for the FvCB leaf photosynthesis model. In this case, the change of 10% of the parameters is not realistic but informative of the model response to its parameters values. The optimal temperature for maximum photosynthesis is sensitive to most of the parameter used in the FvCB model (Fig. 3.3a), but the most sensitive parameters to affect this variable are those related to the temperature response function used the maximum rate of carboxylation (V_{c25}, E_{a_Vc}, E_{d_Vc}, T_{opt_Vc}) and those for the Michaelis-Menten parameter K_c (K_{c25} and E_{a_Kc}). The maximum rate of photosynthesis (Fig. 3.3b) responds strongly to variations of V_{c25} and the two Michaelis-Menten parameters (K_{c25} and K_{o25}). A change of 10% of the value of V_{c25} or K_{c25} results in a change of about 8% in the achievable maximum photosynthesis rate, with however an increase in V_{c25} causing an increase in A_{max} while an increase in K_{c25} causing a reduction of A_{max}. The slope of the light response of photosynthesis (Fig. 3.3c) is very sensitive to changes in α, θ and shows a weaker response to K_{c25}, K_{o25}, V_{c25} and J_{25}. Changes of 10% of the values of α and θ resulted in a modification of about 7% in the slope of the light response of PS but to only about 4% for K_{c25} and K_{o25} and less to 2% for V_{c25} and J_{25}.

Overall, while the FvCB leaf PS model is sensitive to all parameters, variables Topt, A_{max} and α are strongly affected by different parameters (Fig. 3.3). The most important parameters are α, θ, V_{c25}, K_{c25}, $K_{o25,}$ and T_{opt_Vc}.

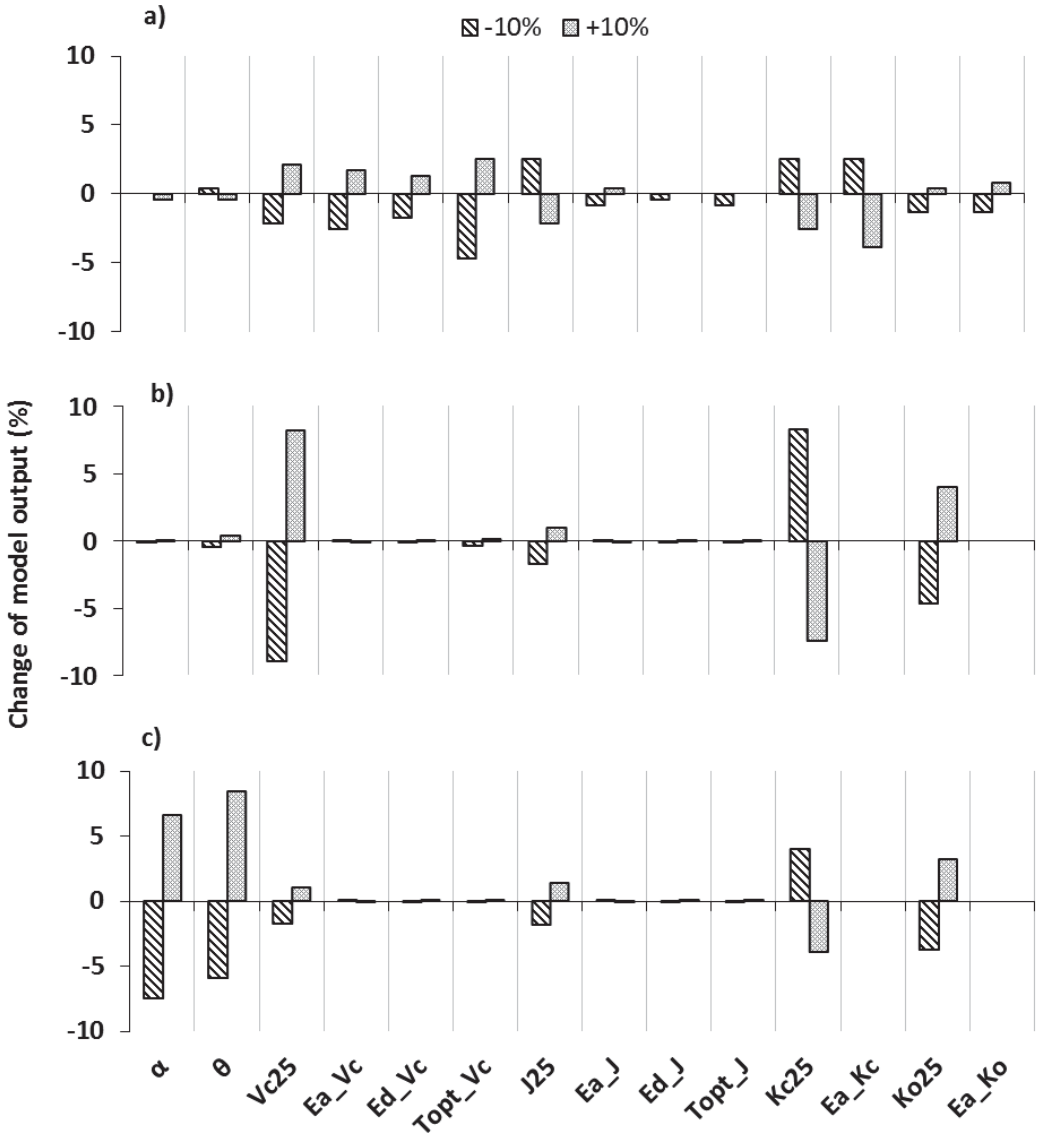

Figure 3.3: Sensitivity analysis of parameters of the leaf FvCB model for optimal temperature a), maximum photosynthesis rate b), and quantum yield which represents the slope of the light response curve c).

Parameter values appear to be very important for the simulation of photosynthesis with the FvCB model (Figs 3.2 and 3.3) at the leaf level and certainly at the stand scale with important implications for the modelling of GPP at Scott Farm and the overall performances of the model to reproduce eddy covariance observations.

3.2.3.2 *Non-Rectangular and Rectangular Hyperbolic response curves*

In contrast to the complex FvCB model, which describes photosynthesis largely mechanistically, the photosynthetic light-response curve can also be described phenomenologically with a simple rectangular (RHC) or non-rectangular hyperbolic curve (NRHC). This is not a mechanistic photosynthesis model, rather it describes the response of the leaf carbon assimilation rate to solar radiation. The general form of hyperbolic curves is given by Equation 3.29, which describes a NRHC, and which can be changed into a RHC simply by setting the parameter θ to zero:

$$\theta A^2 - (\propto I_l + A_{max})A + \propto I_l A_{max} = 0 \tag{3.29}$$

Equation 3.29 has three parameters: θ is a curvature parameter, which modifies the sharpness of the curve, A_{max} is the maximum rate of photosynthesis, and $\propto$ is the photosynthetic efficiency and represents the initial slope of the photosynthetic response curve to light.

This NRHC equation is the same type of equation used in the FvCB model to calculate W_j. Also, as with the FvCB model described before, it is accepted that parameters θ and $\propto$ are not constant between C_3 plant species and that they are not sensitive to climatic conditions. The parameter A_{max}, which represents the maximum rate of carbon assimilation, needs to be modified through species, climatic conditions, and leaf nitrogen concentration to make the rate of photosynthesis responsive to field conditions.

The results obtained with NRHC and RHC light response curves (Fig. 3.4) were considerably different when the same parameters are used in the two equations. For example, Figure 3.4 a shows the light response of the leaf photosynthesis rates calculated with NRHC (lines) and RHC (dashes) for different values of the maximum rate of photosynthesis (A_{max}). For the different values of A_{max}, the PS rate modelled by the RHC function is always lower than the ones from NRHC. This is also valid for the quantum efficiency (Fig. 3.4b) and the curvature parameter (Fig. 3.4c). By changing the values of the parameters between the functions it is possible to get very similar results (not

shown) but this also highlights the necessity to properly parameterise photosynthesis models when different functions are used to simulate this process. The shapes of the curves are very similar to those obtained with the FvCB model (Fig. 3.2c) and a more formal comparison of these two leaf photosynthesis model is given later in this chapter.

An increase in A_{max} does not affect the quantum efficiency (slope of the light response at low radiation levels) but has a strong effect on the light saturated rate of carbon assimilation, which corresponds to the horizontal plateau where increases in PPFD do not change PS (above 500 μmol m^{-2} s^{-1}) and have only a slight effect on the radiation level at which this plateau is reached (Fig. 3.4a).

The quantum efficiency (parameter α) affects the steepness of the light limited section of the light response curve and through it the amount of PPFD necessary to reach the light saturation (Fig. 3.4b). For α=0.08 μmol mol^{-1}, light saturation of PS is reached at a PPFD of about 700 μmol m^{-2} s^{-1}, when α is increased to 0.12 μmol mol^{-1} the plateau is reached for PPFD ≈500 μmol m^{-2} s^{-1} and if α=0.04 μmol mol^{-1} it would need 1200 μmol m^{-2} s^{-1} to reach light saturation.

The parameter θ influences the sharpness of the transition between the light limited section of the response curve and the light saturated section (Fig. 3.4c). As the value of θ diminishes, the transition between the segments of the light response curve become smoother and the levels of radiation needed to reach the plateau increase.

The fact that RHC has one less parameter reduced the scope for parameterising it to specific data sets. The curves plotted in Figure 3.4 also shows us that by varying only the 3 parameters of the NRHC, it is possible to describe a wide range of patterns based on variations in temperature, nitrogen content and water availability. More details are given later on these important limitation terms and their calculations.

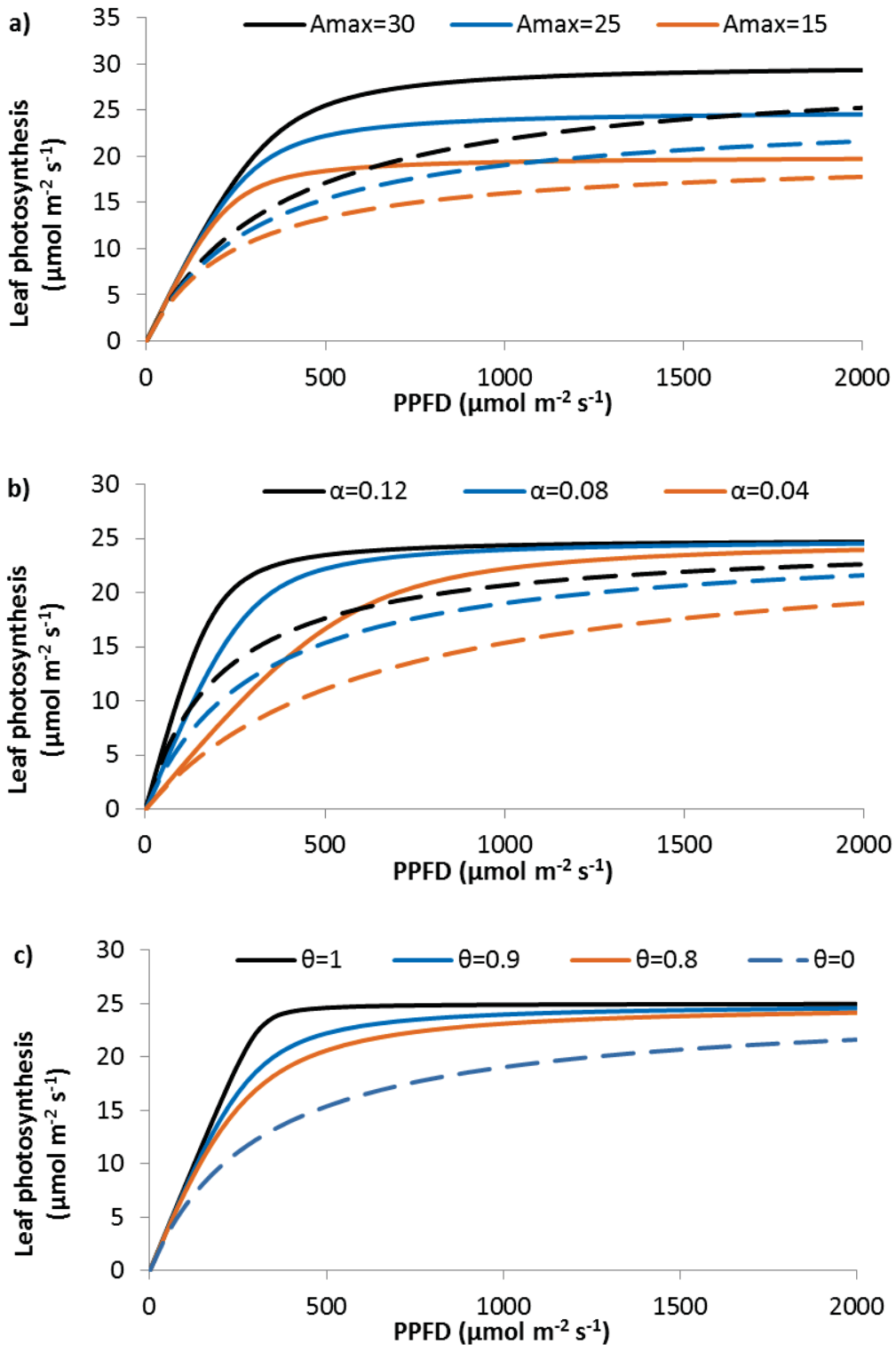

Figure 3.4: Response of Photosynthesis to light (PPFD) with different values of parameters. When parameters are not varying, their values are set to: α=0.08 µmol mol^{-1}, θ=0.9 for NRHC (solid lines) and 0 for RHC (dotted lines) and A_{max}=25 µmol m^{-2} s^{-1}.

As for the FvCB model, the temperature response of the parameter A_{max}, which is used in both the NRHC and RHC curves, is a critical aspect of the model, and temperatures functions are given below and plotted on Figure 3.5.

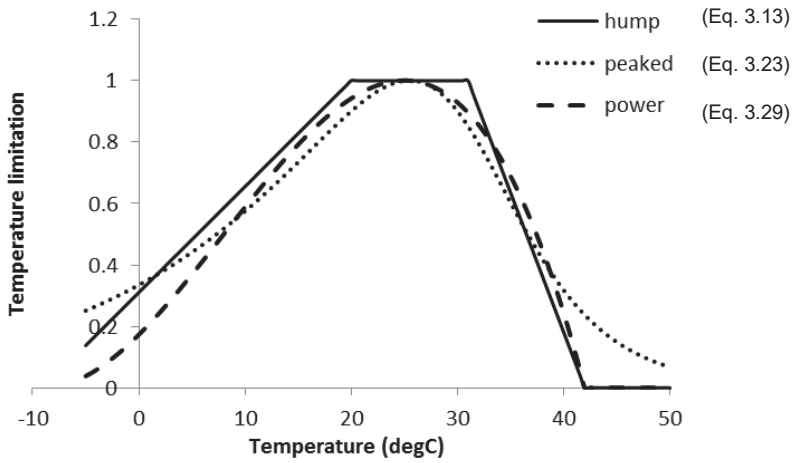

Figure 3.5: Three temperature limitation functions used in the Thornley photosynthesis routine hump function (line), power function (dash) and peaked function (dots). The parameters used are fitted to give similar results because they are species dependant.

The first function is a hump function similar to the one used in the daily Sands model (Equation 3.13) but with a different parameterisation to take account of the differences in time steps and the diurnal variability of temperature:

$$\mathrm{T_{lim}} = \left(\frac{\mathrm{T} - \mathrm{T_{min}}}{T_{opt} - T_{min}}\right)^2 \frac{T_{max} - T}{T_{max} - T_{opt}} \quad \text{if } \mathrm{T_{min}} < T < \mathrm{T_{max}}$$
$$\mathrm{T_{lim}} = 0 \quad \text{else} \tag{3.29}$$

The second was a power function (Equation 3.29) that comes from Johnson et al. (2010). The third equation corresponds to a peaked function, which is similar to the one used in the FvCB model to calculate the temperature response of the maximum rate of electron transport (Equation 3.23). Parameters of this last function also needed to be adjusted because the two models, e.g. NRHC and FvCB, do not simulate the same processes. The values of the parameters used in the inter-comparison of these temperature limitation functions (Fig. 3.5) are given in Table 3.3.

Table 3.3: Initial parameter set for the different temperature response functions tested in the Thornley leaf photosynthesis algorithm. The last three columns indicate in which functions parameters are used

Parameters	units	Definition	Values	Hump (Eq. 3.13)	Power (Eq. 3.29)	Peaked (Eq. 3.23)
T_{min}	°C	Minimum temperature	-9	✓	✓	
T_{max}	°C	Maximum temperature	42	✓	✓	
T_{opt1}	°C	Lower optimal temperature	20	✓	✓	✓
T_{op2}	°C	Upper optimal temperature	31	✓	✓	✓
E_a	KJ mol^{-1}	Activation energy of A_{max}	35			✓
E_d	KJ mol^{-1}	De-activation energy of A_{max}	175			✓

The three temperature limitation functions are very similar between 10 and 40°C (Fig. 3.5). The peaked function, with these specific parameters, does not limit photosynthesis as strongly as the two other functions for negative temperatures and temperatures above 40°C. The hump and power functions totally stop PS when the temperature reaches 42°C and the power function is also the most limiting for temperature below 10°C. As Figure 3.5 shows, the optimum temperature is set to 25.5°C for the peaked and power function and T_{lim}=1, e.g. there is no limitation, between 20 and 31°C for the hump function.

3.2.3.3 *Comparison of the FvCB and NRHC leaf photosynthesis models*

In the above sections, detailed descriptions of some of the most used leaf photosynthesis models (FvCB and NRHC) have been presented; in this section, a simple comparison of the FvCB and NRHC is made. One year of observed solar radiation and temperature at Scott Farm was used to drive the two models, no water or nitrogen limitations were applied, and simulations were done for a single horizontal leaf from the top of the canopy. For the FvCB model, parameters from Table 3.2 were used and parameters of the NRHC leaf photosynthesis were adjusted (Table 3.4) to achieve the best agreement possible between the two models. In the NRHC model, the temperature

limitation is modelled by the peaked function described above with parameters from Table 3.4.

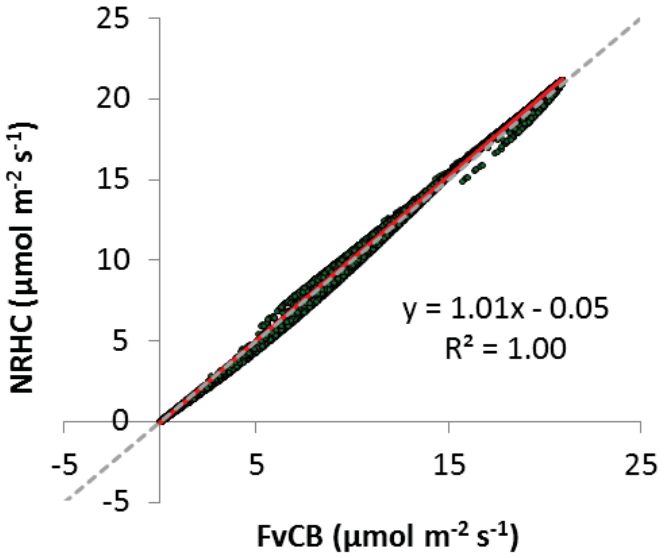

Figure 3.6: Scatter plot showing the comparison between the FvCB and NRHC leaf photosynthesis models. Simulations were done with the one years (2008) of climatic conditions observed at Scott Farm (17520 observations) for a leaf at the top of the canopy with no nitrogen or water limitations.

Figure 3.6 shows the agreement between the two leaf photosynthesis models. The dashed line is the 1:1 line, the red line is the linear regression equation of the scatter plot of the modelled photosynthesis rates, and dots are all the individual 30 minutes assimilation rates from the two models (17,520 points). The overall agreement between the FvCB and NRHC models is very good, as indicated by the linear regression equation, which has a slope very close to 1 (1.01),a very small intercept (0.05) and by the coefficient of determination (R^2) which is equal to 1.00.

It is important to note that 17,520 points are plotted on Figure 3.6 and that most of them are very close or superimposed to the 1:1 line and the small mismatches of a few µmol m^{-2} s^{-1} between the modelled carbon assimilation rates come from small discrepancies in the light responses and temperature limitations functions used in the two PS models.

Table 3.4: Parameters used in the NRHC leaf photosynthesis model for its comparison with the leaf FvCB model

Parameters	Units	Definition	Value
α	μmol mol^{-1}	Quantum efficiency	0.055
θ	-	Curvature parameter	0.95
Topt	°C	Optimal temperature	23
A_{max}	μmol m^{-2} s^{-1}	Maximum carbon assimilation under no limitation	21
Ea	KJ mol^{-1}	Activation energy of A_{max}	35
Ed	KJ mol^{-1}	De-activation energy of A_{max}	175

At the leaf level, the FvCB and NRHC photosynthesis models can model very similar carbon assimilation rates once parameters are adjusted (Fig. 3.6).

Now that we have seen that at the leaf level it was possible to get very similar carbon assimilation from different models, the next section focuses on upscaling schemes from the leaf to the canopy scale.

3.2.4 Spatial and temporal integration of photosynthesis

3.2.4.1 *Integration schemes*

Photosynthesis is not only important in terms of gas exchange but also for biomass growth, as plants need carbon to build new tissues and to maintain their metabolic activities. Mechanistic ecosystem models depend critically on the scaling of physiological processes at least to the canopy scale.

Over the years, scientists have developed theories aimed at upscaling processes from individual leaves to whole plant or population levels. Below only some of the most-widely used canopy integration schemes have been described. They have been implemented and tested in the half-hourly version of the CenW model (see Fig. 3.7). Several integration options are available in the literature, the most commonly of which are: big leaf, sun/shade, multilayers or

integrated models. The implementation and testing of these upscaling schemes has always been undertaken with the overall aim of finding a good compromise between simplicity and accuracy with an acceptable computing time of the complete model.

The big-leaf model assumes that the computation of canopy carbon assimilation rate and also other processes can be achieved by integrating the leaves' characteristics at the canopy scale to represent it as a single, horizontally extended leaf (Running and Coughlan, 1988; Running and Gower, 1991; Amthor, 1994).

The sun/shade model, which separates the canopy into its sunlit and shaded leaf portions, was developed to improve the big-leaf model (dePury and Farquhar, 1997; Leuning et al., 1998; Wang and Leuning, 1998). In this integration scheme, the total carbon assimilation of the stand is obtained by summing the PS rates calculated for each leaf class, e.g. sunlight and shaded fractions of leaves in the canopy.

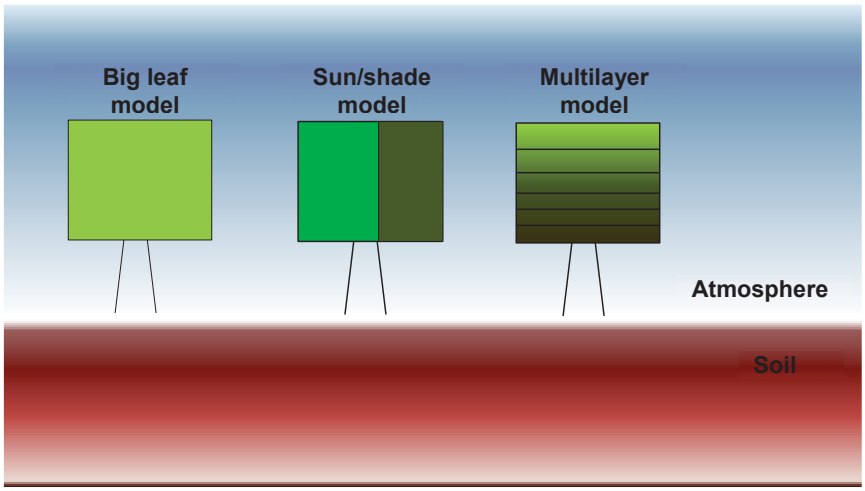

Figure 3.7: Schematic representation of the big leaf, sun/shade and multilayer models.

In the multilayer model, the rate of canopy photosynthesis is computed by summing the contributions of each canopy layer with modifications of the leaves' photosynthetic parameters and forcing variables down the canopy profile (Duncan et al., 1967; Caldwell et al., 1986).

More detailed descriptions of the different integration schemes used in this study are given in the following sections in order to understand the different formulations available in the literature that can be used in CenW_HH, and to identify which one gave the best results.

3.2.4.2 *Big leaf models*

As we have seen above, plant photosynthesis critically depends on solar radiation and canopy integration schemes need to be used to model the stand assimilation rate in response to climate and biological variables. The big-leaf model is the simplest form of integration scheme that has been tested in this study and instead of integration, some authors' recommended using the term "scaling" (dePury and Farquhar, 1997). The theory behind the big-leaf integration was developed after Farquhar (1989) showed that it was possible to describe the whole-leaf photosynthesis from the same kind of equation for individual chloroplasts across a leaf. Farquhar also showed that the distribution of photosynthetic capacity in the canopy is in proportion to the profile of absorbed solar radiation and that the shape of the response of photosynthesis to PPFD is identical in all layers of vegetation. These observations make it possible to treat the entire canopy as if it is only one single leaf.

According to dePury and Farquhar (1997), irradiance at a given depth in the canopy follows Beer's law and is calculated according to an exponential decay function from the top of the canopy by:

$$I(z) = I_0(1 - \rho_c)e^{-k_b LAI_{cum}} \tag{3.30}$$

Where LAI_{cum} is the cumulative LAI from the top of the canopy, I_0 represents the incident global solar radiation or PPFD above the vegetation layer, ρ_c is the canopy reflectance coefficient, and k_b is the extinction coefficient.

The radiation absorbed by the canopy is calculated as:

$$I = \frac{I_0(1 - \rho_c)(1 - e^{-k_b LAI_{tot}})}{k_b} \tag{3.31}$$

where I represents the radiation intercepted by the canopy and LAI_{tot} is the total leaf area index (m^2 m^{-2}).

The fraction of the incident radiation intercepted by the canopy depends strongly on the extinction coefficient over a wide range of leaf area indices. Only at very high leaf area index does radiation absorption become independent of the extinction coefficient as most incoming radiation is intercepted by leaves whatever the extinction coefficient. At very lower LAIs, however, light interception can be nearly proportional to the value of the extinction coefficient.

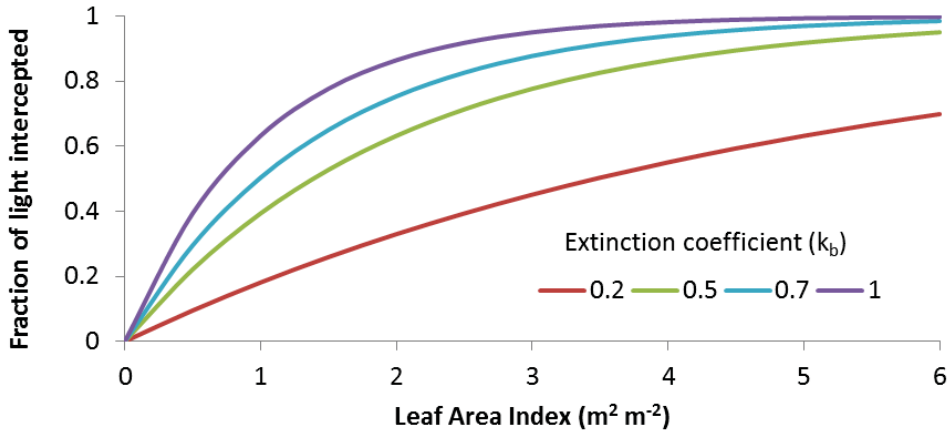

Figure 3.8: Variations in light interception fraction according to LAI and for some values of k_b within its typical range [0.2–1].

The extinction coefficient represents the efficiency of radiation interception by the canopy and depends on the interplay between the sun position and leaf angle distribution. Zhang et al. (2014), in a meta-analysis, reported values of extinction coefficients for real vegetation canopies of different PFTs (Plant Functional Types), ranging on average between 0.18 for lucerne and 0.98 for cauliflower crops, with a mean value of 0.5 for 17 grassland species. In principle, a high k_b indicates that much of the incident radiation is intercepted by leaves with only a small fraction of radiation passing through the canopy (Fig. 3.8) but it also depends of the amount of vegetation and diurnal variations of solar radiation and sun/earth geometry. The extinction coefficient can be calculated according to Equation 3.32 following the formulation of Sellers et al. (1996) and Campbell and Norman (1998) and is the function of the canopy leaf angle distribution and solar position at any given time:

$$k_b = \frac{G(\alpha_{leaf}, \psi_{sun})}{\cos \theta_{sun}} \tag{3.32}$$

where $\alpha_{leaf}$is the leaf inclination angle, θ_{sun} is the solar zenith angle, and $G(\alpha_{leaf}, \psi_{sun})$ is a function of canopy leaf angle distribution χ_L and solar elevation angle ψ_{sun}, which is given according to Sellers et al. (1996) as:

$$G(\alpha_{leaf}, \psi_{sun}) = \varphi_1 + \varphi_2 sin\, \psi_{sun} \tag{3.33}$$

with

$$\varphi_1 = 0.5 - 0.633\, \chi_L - 0.33\, \chi_L^2$$

$$\varphi_2 = 0.877\, (1 - 2\, \varphi_1)$$

In this case, χ_L represents a parameter calculated according to a function characterising the leaf angle distribution and some values have been tabulated for the most common leaves distributions. For a random/spherical distribution of the leaves orientation $\chi_L = 0$, and +1 and –1 for horizontal and vertical leaves respectively. However, Sellers et al. (1996) advocate use of Equation 3.33 with $-0.4 < \chi_L < 0.6$ if enough information on the structure of the leaves arrangements in the canopy is available or else to set the parameter$\chi_L = 0$, which corresponds to a spherical or random distribution of leaves and gives $G(\alpha_{leaf}, \psi_{sun}) = 0.5$ independent of solar position in the sky.

Figure 3.9a shows the response of the radiation extinction coefficient to solar elevation angle for 7 different leaves angle distributions. An important feature shown on this graph is that when the sun elevation angle is less than 35° (e.g. when the sun is close to the horizon), it is possible to get values of k_b greater than 1, especially for erectophile canopies. This is because the extinction of light is measured vertically down the canopy profile and horizontal foliage intercepts more radiation in this configuration and this effect becomes stronger as beam elevation decreases. There is also a switch at about 35° where the least efficient radiation absorbers turn into the most efficient ones and at this specific sun elevation all distributions have the same value of K_b (e.g. K_b=1). For the steepest solar elevation (at solar noon) in our case ψ_{sun}=80°, planophile

canopies absorb more radiation than erectophile ones and the values of k_b range between 1.02 and 0.27 for these two extreme distribution, respectively, and equal 0.5 for a spherical distribution of leaves.

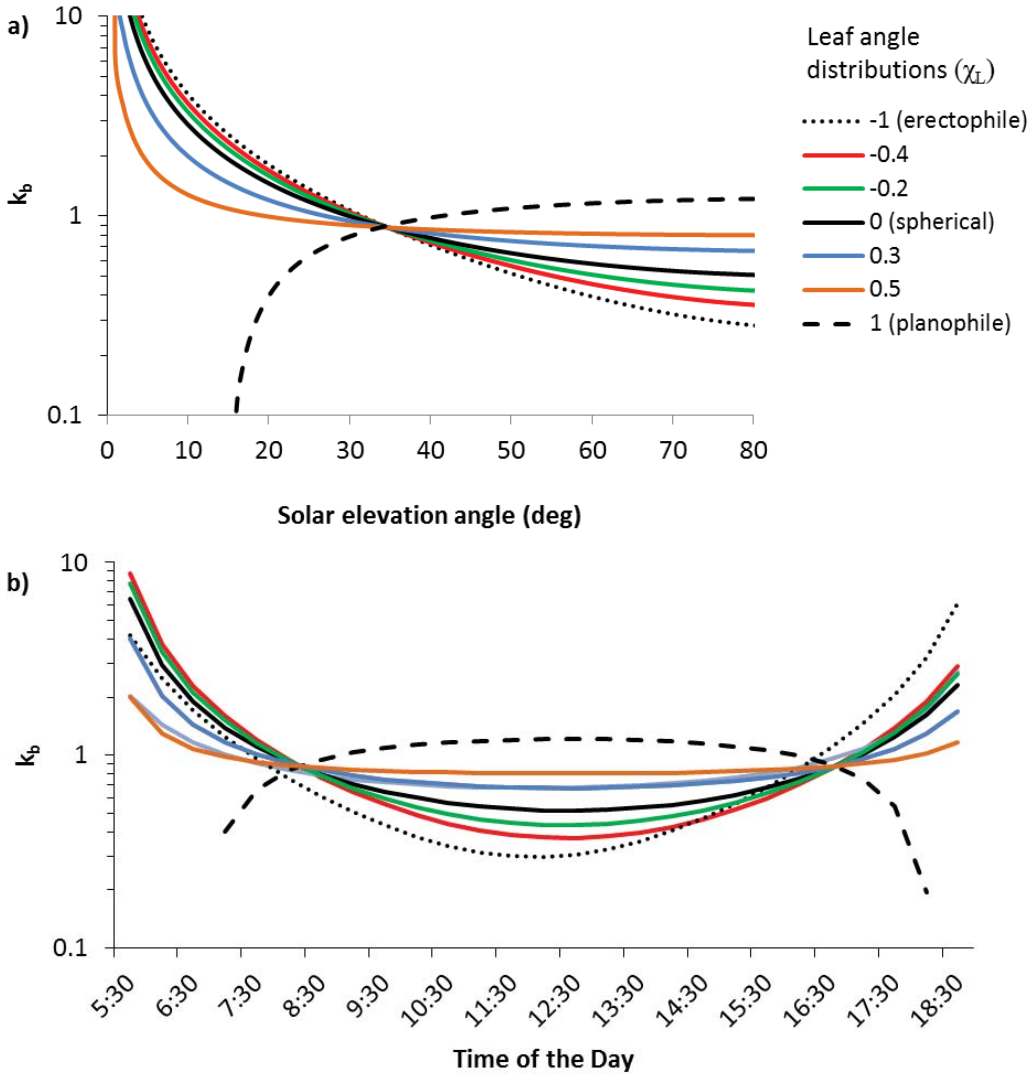

Figure 3.9: a) Relationship between the extinction coefficient (K_b) and the solar elevation angle (ψ_{sun}) for 7 leaf angle distributions (χ_L). b) Diurnal variations of the extinction coefficient for different leaf angle distributions. Graph is made for Scott Farm location on the 01/01/2008.

Figure 3.9b shows the simulated diurnal variations for 7 distributions of leaves, of the extinction coefficient (K_b) for which, in this particular example, the daily variation has been plotted for one typical summer day at the Scott Farm location. Calculations of solar/earth geometry variables were performed after the implementation in the model of the equations used by the NOAA solar

geometry calculator (www.esrl.noaa.gov/gmd/grad/solcalc/calcdetails.html). For all leaf angle distributions, the extinction coefficient reaches its minimum at solar noon, e.g. when the sun elevation angle is at a maximum. Also, at noon, K_b is lower for planar distributions than for vertical leaves because in the first case, more radiation is intercepted by the canopy when sun beams are vertical (perpendicular to the leaves). It is also noticeable that closer to sunset and sunrise, K_b diminishes earlier for erectophile distributions, as in this configuration vertical leaves intercept more radiation when beams are coming from a direction closer to the horizon, i.e. when the sun is lower in the sky.

The calculation of the light extinction coefficient depends on solar elevation angles and so time of day is important for the simulation of the canopy carbon assimilation rate as it is directly related to the amount of solar radiation absorbed by the vegetation which drives photosynthesis.

In the big-leaf upscaling scheme, the canopy photosynthesis rate (A_c) could be calculated by using either the FvCB or the NRHC leaf photosynthesis models, which were described in the previous sections. In addition to the canopy absorbed irradiance (Equation 3.31), it is also necessary to calculate the total canopy nitrogen content associated with photosynthesis (N_c) as:

$$\mathrm{N_c} = \int_0^{LAI_{tot}} N_l \, dL = LAI_{tot}(N_0 - N_b)\left(\frac{1-\exp(-k_n)}{k_n}\right) \tag{3.34}$$

where N_0 is the leaf nitrogen content of a leaf at the top of the vegetation canopy, N_b is the leaf nitrogen concentration not related to photosynthesis, and k_n is the leaf nitrogen allocation coefficient set to 0.71 in this study.

It is important to note that, as outlined in dePury & Farquhar (1997), for the big-leaf model to be used, it is necessary to assume that the photosynthetic capacities of leaves are optimally distributed to maximise photosynthesis, which in turn, assumes proportionality between absorbed solar radiation and photosynthetic capacity profiles. Also, because reallocation of nitrogen and photosynthetic capacity take several days to weeks but variations of absorbed solar radiation in the canopy are instantaneous, it is impossible for the stand

assimilation to be optimal at any given time. This is also the reason why in Equations 3.30 and 3.34 two different extinction coefficients are used.

The canopy photosynthetic capacity (V_c), which is the maximum rate of carboxylation at the canopy scale, or the canopy maximum rate of photosynthesis (A_{cm}) for the FvCB and NRHC models respectively, are then calculated from the canopy nitrogen concentration (N_c) as:

$$\mathrm{V_c} = \alpha_{FvCB} N_c \qquad (3.35)$$

$$\mathrm{A_{cm}} = \alpha_{NRHC} N_c$$

where α_{FvCB} and α_{NRHC} are parameters linking nitrogen content and photosynthetic capacity and maximum rate of photosynthesis in the FvCB and NRHC models, respectively.

Upscaled parameters are then directly passed to the chosen leaf photosynthesis model from which the canopy carbon assimilation is then directly modelled (dePury and Farquhar, 1997).

Figure 3.10 shows the diurnal variations of the big-leaf up-scaled canopy carbon assimilation rates modelled from FvCB and NRHC leaf photosynthesis models for a clear sky day a) and a cloudy day b). Overall, the two-leaf photosynthesis up-scaled at the stand scale from the use of the big-leaf scheme gives very similar rates of carbon fixation throughout these two climatically contrasting days. This is consistent with the comparison at the leaf scale, which has been presented above and shows that it is possible to use one or other of the leaf photosynthesis models, after their proper parameterisation and achieve close agreement in canopy photosynthesis rates.

It has been shown that this kind of integration can cause large discrepancies between measured and simulated fluxes (dePury and Farquhar, 1997; Chen et al., 1999). It was also found that aggregating canopy characteristics into one single leaf might lead to either an overestimation or an underestimation of the carbon assimilation rates, particularly on cloudy days when most of the solar radiation absorbed by the canopy correspond to diffuse radiation. Lloyd et al. (1995) showed that parameters used in the big-leaf upscaling scheme are not

representative of measurable physical or biological quantities but have to be fitted for the model to give accurate CO_2 assimilation rates at the stand level. However, calculations are simple and for daily or longer running steps or for spatial modelling studies, this model can give good approximations with few calculations and therefore, an efficient model running time.

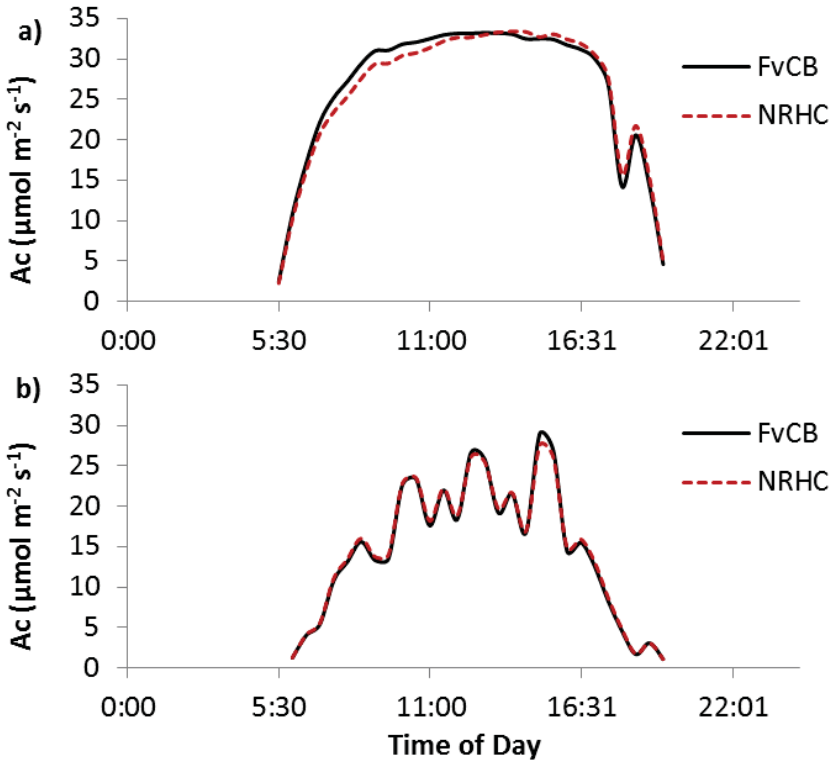

Figure 3.10: Diurnal variations of the canopy carbon assimilation rates modelled with the big-leaf integration scheme and the FvCB (black) and NRHC (red) leaf photosynthesis models. Graphs are made for Scott Farm location and observed climatic conditions for the 01/01/2008 a) and the 08/01/2008 b).

3.2.4.3 *Sun/shade models*

The sun/shade model (dePury and Farquhar, 1997) is a modification of the big-leaf model in which canopy is divided in two classes of leaves according to their light status. This kind of integration is expected to give better results than the simple big-leaf model while still having an efficient calculation time (Bodin and Franklin, 2012; dePury and Farquhar, 1997). Calculations of the canopy carbon assimilation rates are made by separating contributions of the sunlit fraction of

leaves receiving direct beam radiation (direct incoming solar radiation) and the shaded fraction which receives diffuse radiation.

The improvement of this method compared with the simple big-leaf model is related to the fact that to calculate the overall canopy assimilation rate, the characteristics driving the light-related parameters of photosynthesis can take different values for each class of leaves and gave a better approximation of the photosynthesis rate, which is calculated from non-linear responses functions. It is assumed that the photosynthetic capacities of the leaves making the two classes (sunlit and shaded) do not vary diurnally but that the proportions of sunlit and shaded leaves and the radiation levels vary. The sunlit fraction of the canopy, which corresponds to all the leaves exposed to direct solar radiation, is calculated as:

$$L_{sun} = \frac{1 - e^{-k_b LAI_{tot}}}{k_b} \tag{3.36}$$

where k_b is the light extinction coefficient and LAI_{tot} is the total leaf area index ($m^2\ m^{-2}$).

The shaded fraction of the canopy is simply given as the difference between the total leaf area index and the sunlit fraction of the vegetation layer as $L_{shade}=LAI_{tot}-L_{sun}$. That makes it possible to calculate the irradiance absorbed by shaded and sunlit fractions of leaves constituting the canopy.

The extinction coefficient for beam radiation is calculated as in the big-leaf model, and varies with the time of the day through diurnal changes in the solar elevation angle. Changes in the extinction coefficient also change the ratio of sunlit and shaded leaves over the course of the day (Fig. 3.6).

As the sun gets higher in the sky, the ratio of sunlit and shaded leaves changes (Fig. 3.11). At sunset and sunrise the contribution of the shaded part of the canopy is more important than the sunlit contribution. And around solar noon (when the sun is at its apogee), the opposite trend is simulated, with more leaves directly exposed to solar radiation.

Leaf Area Index (LAI) and leaf angle distribution also play an important role in the partitioning of canopy in its sunlit and shaded fractions (Fig. 3.12).

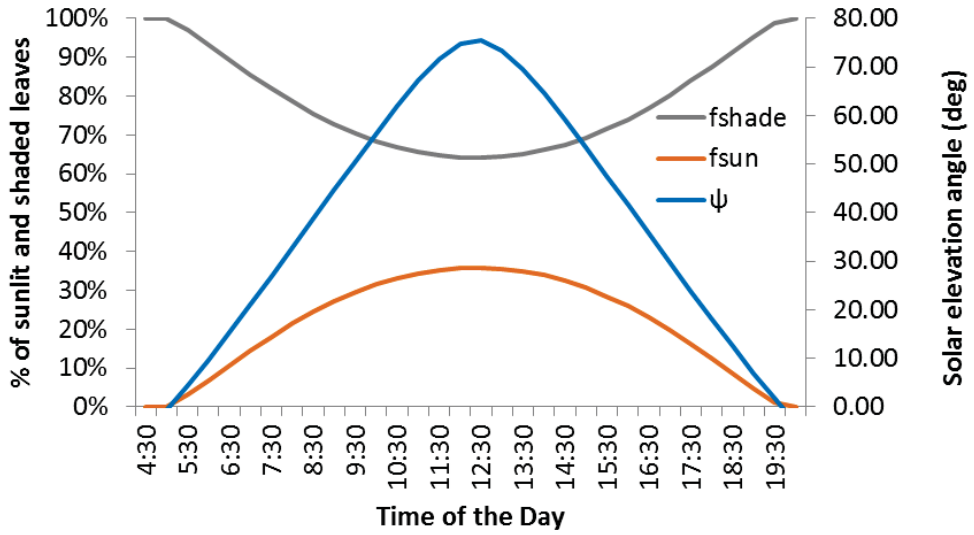

Figure 3.11: Diurnal variation of solar elevation and percentages of sunlit (f_{sun}) and shaded (f_{shade}) leaves of the canopy. Graph was made for the 01/01/2008 with Scott Farm coordinates, a leaf area index of 5 m^2 m^{-2} and a spherical distribution of leaves angle ($\chi_L = \mathbf{0}$).

Figure 3.12 shows that the percentages of leaves present in each of the leaf classes (sunlit and shaded) for all the distributions follow the same trends in response to LAI, i.e. an increase of the sunlit fraction of the canopy as the leaf area index increases. Because simulations were done for noon time, the percentage of sunlit leaves is more important for horizontal leaves than for spherical and vertical distributions whatever the amount of vegetation, so only spherical leaf distribution will be commented on below, as the same conclusions also apply to other distributions.

The main insight of the sun/shade upscaling scheme is that both leaf categories can be treated independently (dePury and Farquhar, 1997). The radiation intercepted by each class, which is very important for calculating the photosynthesis response, is updated at each time step, based on the amount of vegetation, the distribution of leaf angles, and the position of the sun in the sky.

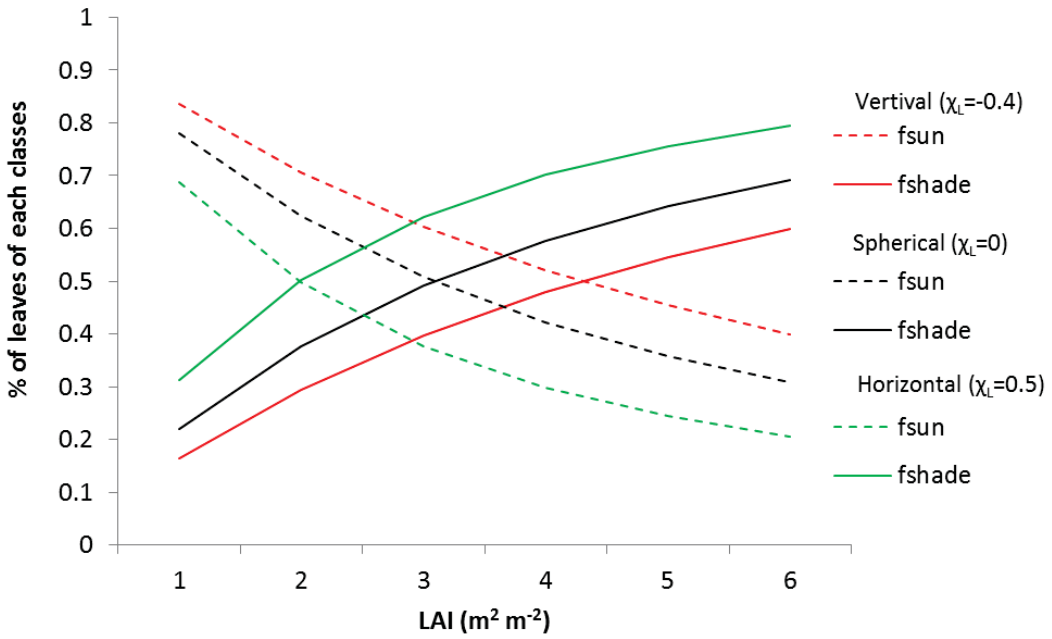

Figure 3.12: Variations of the percentages of sunlit and shaded leaves classes simulated at noon for three different leaf angle distributions (spherical, horizontal, and vertical) according to leaf area index.

The irradiance absorbed by the sunlit leaves is made as the sum of direct-beam, diffuse and scattered-beam components, while shaded leaves receive diffuse and scattered-beam radiation (dePury and Farquhar, 1997):

$$I_0 = I_{d0} + I_{b0} \tag{3.37}$$

where I_0 is the solar radiation of a horizontal plane above the canopy, I_{d0} and I_{b0} are the diffuse and direct irradiance respectively, and all are given in units of photosynthetic photon flux density (μmol m^{-2} s^{-1}).

The direct and diffuse radiation levels are calculated as:

$$I_{d0} = f_{sun} I_0 \tag{3.38}$$

$$I_{b0} = (1 - f_{sun})\, I_0$$

where f_{sun} represents the fraction of total radiation that is received as direct radiation. It can vary between 0 and 1 when there is only diffuse radiation or only direct radiation being absorbed.

The fractions of direct and diffuse radiation change diurnally, seasonally, and with daily weather patterns, such as cloud cover. To determine the value of f_{sun}, it is, therefore, necessary to account for the effect of solar angle as well as cloud cover. In practice, the solar position calculator is used to determine how much radiation can potentially reach the top of the canopy. Then, it is possible to determine the cloudless factor (clf) as:

$$clf = 1.35\,\frac{SR_{mes}}{SR_{sim}} - 0.35 \tag{3.39}$$

where clf represents the cloudless factor, SR_{mes} and SR_{sim} are measured and simulated short wave solar radiation and are given in W m^{-2}, respectively.

From the cloudless factor it is possible to calculate the fraction of direct radiation as:

$$\begin{cases} f_{sun} = 0.1 & if \quad clf < 0.3 \\ f_{sun} = 0.85 & if \quad clf > 0.7 \\ f_{sun} = 1.875\,clf - 0.4625 & else \end{cases} \tag{3.40}$$

If the cloudless factor is less than 0.3 this implies a totally overcast sky and only 10 % of the radiation is direct, if clf is greater than 0.7 we have a totally clear sky with only 15 % of diffuse radiation and a linear relationship between these two thresholds.

Following the formulation of dePury and Farquhar (1997), the total irradiance absorbed by the canopy (I_c) equals the sum of the irradiance absorbed by the sunlit (I_{csun}) and shaded (I_{cshd}) parts of the canopy:

$$I_c = (1-\rho_{cb})I_{b0}(1-\exp(-k'_b LAI_{tot})) + (1-\rho_{cd})I_{d0}(1 - \exp(-k'_d LAI_{tot})) \tag{3.41}$$

where $\rho_{cb} = 0.029$ is the canopy reflection coefficient, $k'_b$the direct and scattered direct PPFD extinction coefficient, $\rho_{cd} = 0.036$ the canopy reflection coefficient for diffuse PPFD, and $k'_d = 0.719$ the diffuse and scattered diffuse PPFD extinction coefficient. Parameters values given above are species dependent

and to illustrate this section, specific values from dePury and Farquhar (1997) for a wheat stand are used.

The total irradiance absorbed by the sunlit fraction of the canopy is given as:

$$I_{csun} = I_{b0}(1-\sigma)\left(1-\exp\left(-k_b\ LAI_{tot}\right)\right) + I_{d0}(1-\rho_{cd})\left(1-\exp\left(-(k'_d+k_b\ )LAI_{tot}\right)\right)\frac{k'_d}{k'_d+k_b} + I_{b0}(1-\rho_{cb})\left(1-\exp\left(-(k'_b+k_b\ )LAI_{tot}\right)\right)\frac{k'_b}{k'_b+k_b} - (1-\sigma)\frac{\left(1-\exp\left(-2k_b\ LAI_{tot}\right)\right)}{2} \quad (3.42)$$

where $\sigma = 0.15$ is the leaf scattering coefficient for PPFD.

Finally, the total irradiance absorbed by the shaded fraction of the canopy is simply given as the difference between I_c and I_{csun}.

As expected, when there are no clouds (clear sky conditions), most of the radiation arriving at the top of the canopy is in the form of direct beam (I_{b0}) and only a small fraction of diffuse radiation (I_{d0}) is present because the atmospheric scattering is small under clear sky conditions. The largest part of irradiance absorbed by the canopy is absorbed by sunlit leaves (Fig. 3.13a), whereas on an overcast day, radiation above the vegetation is mostly made of diffuse light (Fig. 3.13b). The radiation level (I_0) at the top of the vegetation for the overcast day is about half that observed for the clear sky day. For the 01/01/2008 (clear sky conditions), the sunlit fraction of leaves absorbs most of the radiation (I_{csun}) and only a small fraction is used by the shaded leaves (I_{cshade}). In contrast, on the 08/08/2008 (overcast conditions) the amounts of radiation absorbed by each leaf classes are much closer.

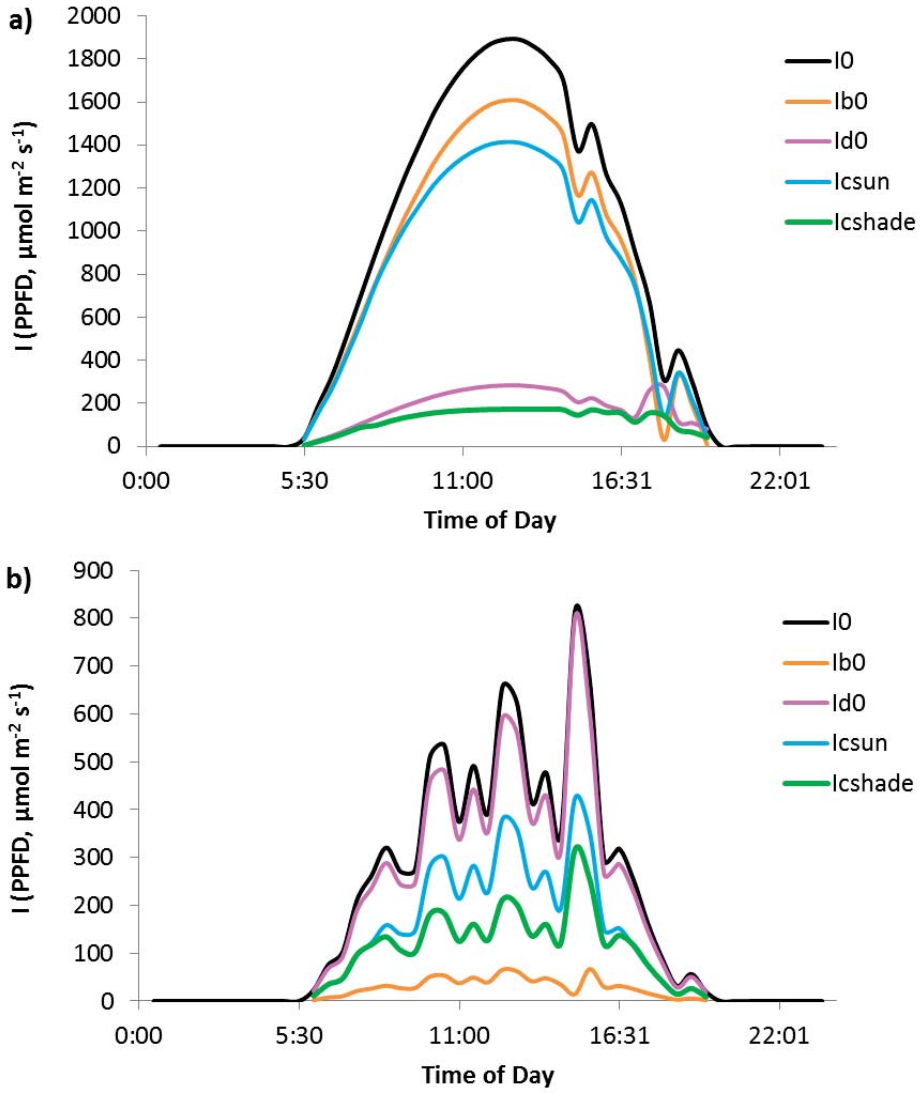

Figure 3.13: Diurnal variations of above canopy measured PPFD (I_0), direct (beam) and diffuse radiation above the vegetation, total irradiance absorbed by the sunlit fraction (I_{csun}) and for the shaded fraction (I_{cshade}) of the canopy for a) a clear sky day (01/01/2008) and b) an overcast day (08/01/2008). Simulations were performed for two days close in time to minimise the differences in solar radiation caused by changes in the earth/sun geometry.

By using this integration scheme (sun/shade), it is possible to account for the effects of the different incoming radiation levels on the two leaf classes, which also have different photosynthetic capacities through differences in the distribution of nitrogen concentration in the sunlit and shaded fractions of the vegetation canopy. The total stand photosynthesis (A_c) is then calculated by summing the carbon assimilation rates of the two leaf classes as:

$$A_c = A_{csun} + A_{cshd} - R_c \quad (3.43)$$

where A_{csun} and A_{cshd} are the rates of photosynthesis modelled for the sunlit and shaded fractions of the stand, respectively and R_c is the respiration of the canopy.

It is possible to use either the detailed FvCB leaf photosynthesis model (dePury and Farquhar, 1997; Dai et al., 2004) or the simpler NRHC light response curves (Thornley, 2002) with this integration scheme by using the calculated absorbed radiation and photosynthetic capacities for the two fractions in the leaf photosynthesis models.

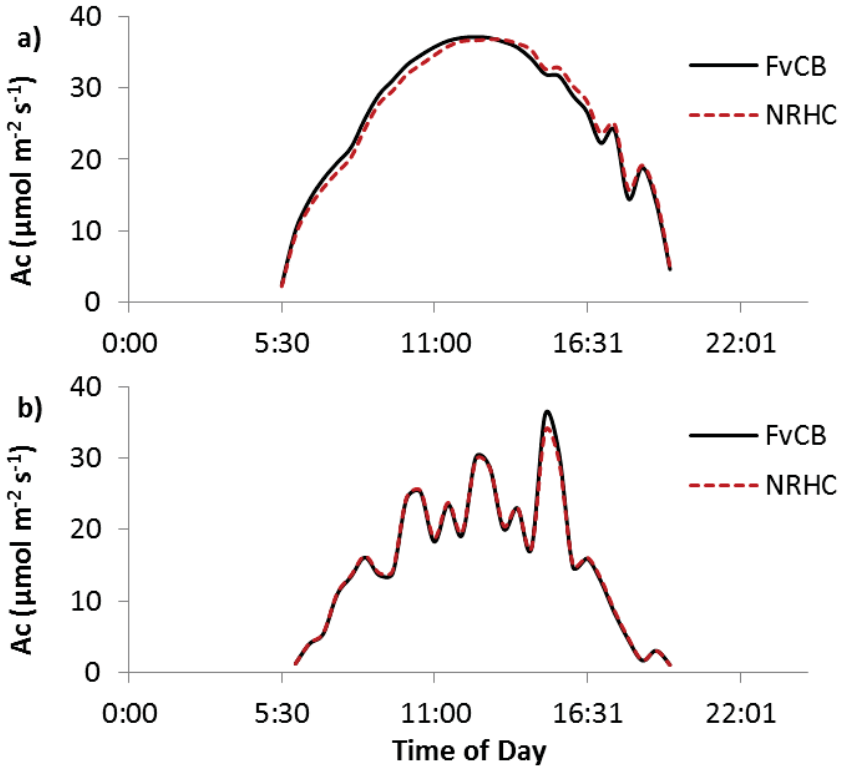

Figure 3.14: Diurnal variations of the canopy carbon assimilation rates modelled with the sun/shade integration scheme and the FvCB (black) and NRHC (red) leaf photosynthesis models. Graphs are made for Scott Farm location and observed climatic conditions for the 01/01/2008 a) and the 08/01/2008 b).

In the previous section, the use of the big-leaf upscaling scheme with either the FvCB or NRHC leaf PS models has shown that the results were highly analogous. Here again, as Figure 3.14 shows, using one or other of the leaf

photosynthesis models with the sun/shade integration scheme provides very similar canopy carbon assimilation rates. Ac rates plotted on Figure 3.14 are calculated from Equation 3.43 in which A_{csun} and A_{cshd} are calculated according to the decomposition of solar radiation absorbed by the sunlit and shaded fraction of the canopy for the 2 days of interest (Fig. 3.13). Both the FvCB and the NRHC leaf photosynthesis models agree well for clear sky a) and cloudy b) days, and respond to changes in climatic conditions. When clouds reduce the amount of solar radiation incoming upon leaves, the photosynthetic assimilation is also reduced. Having nearly identical carbon assimilation rates at the leaf level with these two different PS models is an important feature for the rest of the study as either of them can be used to get almost the same amount of carbon fixation.

3.2.4.4 ***Multilayer FvCB and NRHC models***

Multilayer integration scheme for the upscaling of leaf photosynthesis at the vegetation canopy scale would be the most realistic approach, but it was not practical to implement it in CenW_HH (see below). This integration scheme was not included in the rest of the study and only a brief description is given in this section because even if it was not used, it is an interesting option that has been increasingly used in modelling studies with the increase of computational power (Clark et al., 2011; Bonan et al., 2012).

Canopy multi-layers models divide the vegetation cover into a given number of layers or into a specified LAI thickness. Their main advantage is that they can deal more accurately with non-linear responses of photosynthesis to physiological and physical drivers.

The multilayer scheme is usually seen as the most accurate and reliable and is often used as reference in model inter-comparisons (Goudriaan, 1986; Reynolds et al., 1992; dePury and Farquhar, 1997). However, this scheme is more complex than the previous ones and the simulated processes cannot be ultimately simulated more accurately, especially if the canopy layers are not small enough and if the driving parameters and variables are not used properly or given enough detail within the simulation framework. Also, the running time of

the model is substantially increased because the assimilation rate of each layer of the canopy needs to be simulated independently. In this kind of spatial (vertical) integration, only half-hourly, or smaller time steps are commonly used as the responses of photosynthesis to meteorological variables (principally light and temperature) are non-linear and the parameters are adjusted to take account of the leaf conditions at a given point in the canopy and at a given time.

The vertical discretisation of the canopy is usually done by making layers of vegetation with the same LAI, with either the number of vegetation layers or the amount of LAI in each layer being fixed. The principal factors that influence the rate of photosynthesis between layers are:

- Light decay in the canopy (usually following an exponential light decay function).
- Sunlit and shaded leaves. It is possible to couple these two integration schemes, in this case, as in each layer there is a portion of sun leaves and shaded leaves (Clark et al., 2011).
- Nitrogen distribution within the canopy layers is related to photosynthetic enzyme concentrations. Generally, carbon assimilation rate can be maximised if photosynthetic enzyme concentrations follow the radiation interception curve.
- Calculation of the photosynthesis for different leaf angle classes for each layer of the canopy for very detailed models (Anten and Hirose, 2003; Dufrene et al., 2005).

The choice of not using this scheme has been motivated principally by the fact that the running time was an important consideration and constraint because of the large number of simulations needed to parameterise the model. dePury and Farquhar (1997) have also shown that the simpler sun/shade model they developed, and which has been described above, is as accurate as multilayer models.

3.2.4.5 *Thornley model*

The development of this model is based, like the daily Sands model, on four key assumptions to allow the integration of the model equations over the whole canopy:

1) The canopy is horizontally uniform.
2) The light down the canopy follows an exponential decay curve (Equation 3.3).
3) The leaf photosynthetic response to light is given by a non-rectangular hyperbola (NRHC, Equation 3.2).
4) The parameter A_{max} is proportional to the ratio of the local PPFD in the canopy and the full sun PPFD.

As described in previous sections, the partitioning of the total canopy photosynthesis into its sunlit and shaded fractions is useful as it allows the values of the parameters to change for each component independently, is computationally efficient and gives important differences compared with a model that does not make this distinction. These differences are mainly due to the non-linearity of the response of leaf photosynthesis to its light environment. A difference exists between the sun/shade integration presented above and the one used in the model presented by Thornley: in the equations presented in Section 3.2.4.3 the radiation absorption takes into account the scattering effect on diffuse and direct irradiance, while the Thornley model does not take this effect into account.

A complete and detailed derivation of the equations of this model is given in Thornley (2002) and in the following, only the final derived equations have been reported.

The contribution of the sunlit leaves to the total rate of canopy assimilation is given by Equation 3.44:

$$P_{sun} = \frac{1}{2k_b\theta}\left\{p_{so}(1 - e^{-k_b LAI_{tot}}) + \frac{p_{dpo}}{2}(1 - e^{-2k_b LAI_{tot}}) - \left[\frac{(2c+b)\sqrt{R_1}}{4c} - \frac{(2ce^{-k_b LAI_{tot}})\sqrt{R_{gnd}}}{4c} + \frac{\Delta}{8c\sqrt{c}} ln\left(\frac{2\sqrt{cR_1} + 2c + b}{2\sqrt{cR_{gnd}} + 2ce^{-k_b LAI_{tot}} + b}\right)\right]\right\} \quad (3.44)$$

where P_{sun} is the carbon assimilation rate of the sunlit part of the canopy, k_b and θ are the light extinction coefficient and curvature parameter, respectively and other terms are calculus intermediates described below.

The component for shaded leaves is given by Equation 3.45:

$$P_{shade} = \frac{1}{2k_b\theta}\left(1 - e^{-k_b LAI_{tot}} - \frac{1 - e^{-2k_b LAI_{tot}}}{2}\right)\left[p_{do} + p_{maxo} - \sqrt{(p_{do} + p_{maxo})^2 - 4\theta p_{do} p_{maxo}}\right] \quad (3.45)$$

where P_{shade} is the carbon assimilation rate of the shaded part of the canopy, and p_{max0} is the maximum carbon assimilation rate under no limitation.

The different terms in the two previous equations are given by:

$$\begin{cases} p_{so} = \dfrac{\alpha k_b I_{suno}}{1 - \mathrm{T}} \\ p_{do} = \dfrac{\alpha k_b I_{difo}}{1 - \mathrm{T}} \\ p_{dpo} = \dfrac{\alpha k_b I_{difo}}{1 - \mathrm{T}} + p_{maxo} \end{cases} \quad (3.46)$$

where α is the quantum yield of electron transport and corresponds to the slope of the photosynthesis light response curve, I_{sun0} and I_{dif0} are the direct incoming solar radiation and diffuse radiation at the top of the vegetation layer, respectively, and T is the leaf transmittance parameter fixed to 0.1, which is a typical value for ryegrass leaves (Thornley, 2002).

And:

$$\begin{cases} a = {p_{so}}^2 \\ b = p_{so}(p_{dpo} - 2\theta p_{maxo}) \\ c = {p_{dpo}}^2 - 4\theta p_{do} p_{maxo} \\ R_1 = a + b + c \\ R_{gnd} = a + be^{-k_b LAI_{tot}} + ce^{-2k_b LAI_{tot}} \\ \Delta = 4ac - b^2 \end{cases} \quad (3.47)$$

Parameters of the model allowing the carbon assimilation rate of the vegetation canopy to change areα, θ, and p_{max0}, which are similar than those of the NHRC photosynthesis routine.

This model is particularly interesting because it makes the link between the very detailed biochemical FvCB model and the model developed by Sands (1995b) to calculate canopy daily photosynthesis. The running time of the model using already integrated equations over the canopy is faster than a multilayer model and sun/shade models. The Thornley model was designed to be nearly as accurate as more detailed multilayer models and to give better results than big-leaf models (Thornley, 2002).

Here again the response curve of leaf photosynthesis to radiation is not plotted because the Thornley (2002) procedure uses a non-rectangular hyperbolic function to simulate the carbon assimilation rate in response to irradiance, which has been described in Section 3.2.3.2. In the original model description, no temperature function was prescribed and so the three options described above, i.e. hump (Equation 3.13), peaked (Equation 3.23), and power (Equation 3.29) functions, were introduced in the model.

3.2.4.6 ***Comparison of the big-leaf and sun/shade integration schemes***

In this section, only the standalone versions of the PS models and upscaling schemes were used, and no limitation terms and a constant vegetation biomass (LAI=4) were used to make the simulations. These strong assumptions make it impossible to compare these modelled fluxes with observations, as limitations and changes in biomass have an important role in regulating the fixation of carbon dioxide.

Figure 3.15 shows the inter-comparisons of the canopy carbon assimilation rates modelled by using the two tested up-scaling schemes described above, big-leaf and sun/shade, with the FvCB a) or NRHC b) leaf photosynthesis models. Leaf PS models were run with the same parameters when either the big-leaf or the sun/shade canopy integration schemes are used.

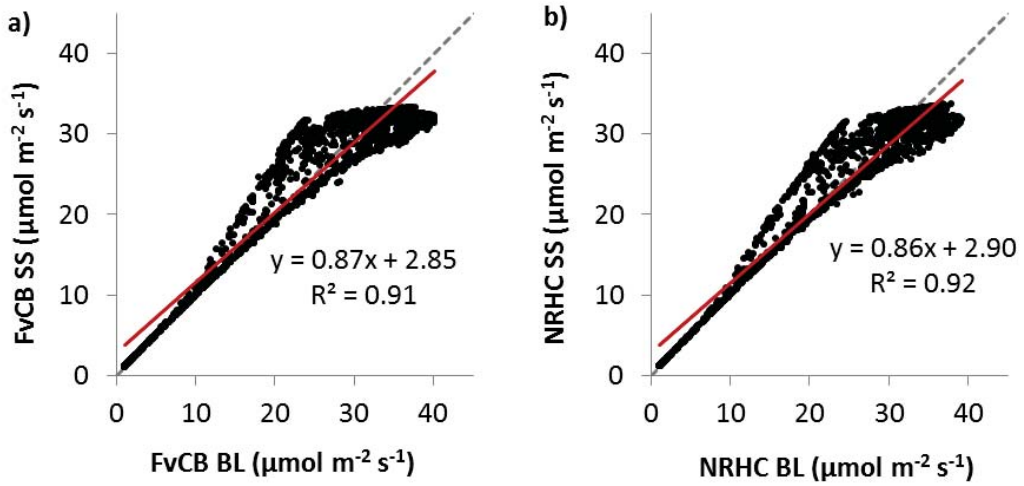

Figure 3.15: Scatter plots for the comparison of the big-leaf (BL) and sun/shade (SS) canopy integration schemes when the FvCB a) or the NRHC b) leaf photosynthesis models are used. Graphs were obtained from the responses of PS models to one year (2008) of climatic conditions observed at Scott Farm (17 520 observations).

The two graphs displayed in Figure 3.15 show very similar patterns, BL and SS schemes agree well for photosynthesis rates below 10 µmol m^{-2} s^{-1} that were achieved for low radiation levels. Divergence occurs at higher photosynthesis rates, especially for cloudy days where the solar radiation is mostly diffuse radiation. Under those climatic conditions, leaf photosynthesis models with the sun/shade integration modelled higher carbon assimilation rates than the PS models with the big-leaf integration (Fig. 3.15a and b). Another feature highlighted in these graphs is that with the big-leaf scheme it is possible to reach higher canopy photosynthesis rates than with the sun/shade scheme: 42 µmol m^{-2} s^{-1} and 32 µmol m^{-2} s^{-1} for the two schemes, respectively. This is caused by the inadequacy of the assumptions needed in the big-leaf model to solve the integral of leaf photosynthesis over the canopy, principally the proportionality between photosynthetic capacity and radiation levels in the

canopy, the optimality of the nitrogen distribution that is assumed to follow light decay in the canopy and the non-linear of photosynthesis to light intensity.

3.2.5 Limitation factors affecting the maximum rate of photosynthesis as implemented in CenW_HH

3.2.5.1 *Nutrients*

Nitrogen and phosphorus are the key nutrients for plants because they are both necessary in cellular functions and growth metabolism, and plants use them in large quantities to sustain their needs. In natural ecosystems, these two elements are often limiting factors of plant growth (Crous et al., 2015). Plants grow by absorbing nutrients from the soil but their ability to extract nutrients depends on the amount of nutrients present in the soil and on the nature of the soil (the combination of sand, silt, clay, and organic matter). Soil texture and acidity (pH) further determine the extent to which nutrients are available for plant uptake.

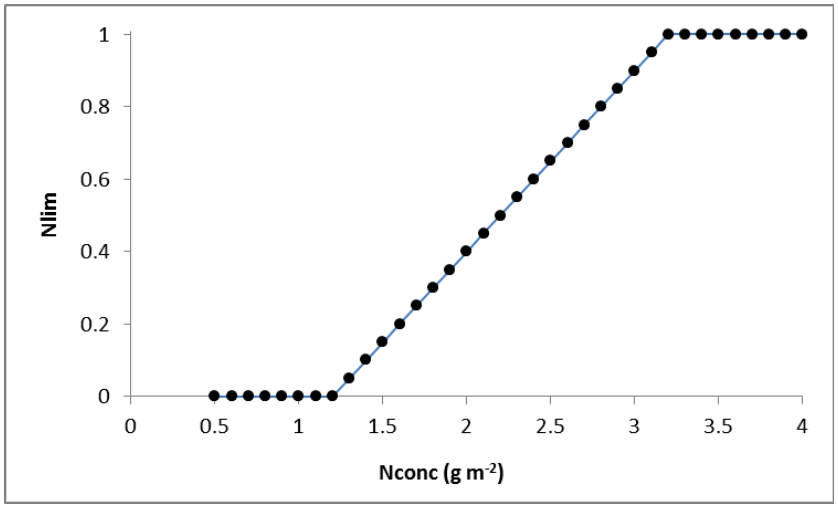

Figure 3.16: Nitrogen limitation expressed as a function of leaves' nitrogen concentration.

In our system, which consists of a heavily managed dairy pasture, it was assumed that nutrient levels were monitored to maximise pasture productivity by minimising nutrient limitations. Fertiliser applications therefore followed the best practices that farmers can use to maximise pasture production while limiting environmental damages. Phosphorus (P) cycling was not included in this study as it is very unlikely that plants will experience strong P-limitation on

Scott Farm (Mudge et al., 2011). However, as carbon and nitrogen are very closely linked and impact the whole model, nitrogen cycling was used in simulations, but in this chapter, where the focus is on the modelling of photosynthesis, only its direct effect on CO_2 assimilation is discussed and no details are given on the modelling of the nitrogen cycle. This is described in Kirschbaum and Paul (2002).

In the daily Sands model, which is used in the original version of CenW, various limitations are described through multiplicative factors, including a nitrogen limitation factor, N_{lim} that varies between 1, when N is not limiting, and 0, when the N concentration in leaves is too low to sustain any photosynthesis (Equation 3.48 and Fig. 3.16). The same limitation term was used in the different half-hourly photosynthesis models tested in this study to limit A_{max}, the maximum carbon assimilation rate or the maximum rate of carboxylation (V_{cmax}) for the FvCB model:

$$\begin{gathered} IF\ N_{conc} < N_0\ then\ N_{lim} = 0 \\ Else\ if\ N_{conc} < N_{crit}\ then\ N_{lim} = \frac{N_{conc} - N_0}{N_{crit} - N_0} \\ Else\ N_{lim} = 1 \end{gathered} \tag{3.48}$$

where N_{conc} is the nitrogen concentration of the leaves, N_0 represent a calibrated parameter that represents the nitrogen content below which no photosynthesis occurs, and N_{crit} is the critical N that marks the saturation level of N in plants leaves.

3.2.5.2 ***Temperature***

In addition to the direct effect of temperature on photosynthetic capacity through enzymatic kinematics modification (as described below), the CenW model also accounts for the limitation/reduction of the carbon assimilation rate caused by extreme temperature damage on leaves. Both cold and hot temperatures can potentially damage leaves. In practice, two threshold parameters are used to set these lower and upper boundaries and then calculate how damage will reduce the carbon assimilation rate. The temperature damage term varies

between 0 for extreme damages to the plants and totally stops photosynthesis to 1 when plants do not experience any temperature damage.

Calculations are made daily, even when the model is run at a half-hourly time step. At first the procedure assesses by how many degrees the minimum and maximum temperatures are beyond the set thresholds, and for each degree that exceeds the set thresholds, one damage unit is added to the cumulative count of damage units that determine the extent of photosynthesis reduction by multiplying the total amount of accumulated damage units by a sensitivity term. There is also the possibility for the plants to repair these damages over time, which is done by reducing the damage units by the daily repair rate.

This limitation term is applied to the maximum rate of photosynthesis with no limitation (A_{max}) for the Thornley and NRHC models, as in the original version of CenW with the Sands model, and to the maximum rate of carboxylation (V_{cmax}) for the FvCB model.

3.2.5.3 ***Water***

In the model, the water limitation term (WaterLimit) is related to root distribution and the water content of different soil layers. Water limitation is taken into account in the photosynthesis module in two ways. One limitation comes through the response of stomatal conductance to water stress. The water limitation variable (WaterLimit) is used to modify the parameter of the stomatal conductance model. In this study, the routine proposed by Ball et al. (1987), hereafter called the BB-model (Equation 3.49), was used because it has been successful in several studies (Kim and Lieth, 2003):

$$g_s = g_0 + \frac{1.6\, mAn_l RH}{C_s} \tag{3.49}$$

where g_s is the stomatal conductance to water vapour (mmol H_2O m^{-2} s^{-1}), g_0 is the residual stomatal conductance, the factor 1.6 is used to account for the difference in the molecular diffusion of CO_2 and H_2O, An_l is the leaf net carbon assimilation rate (μmol CO_2 m^{-2} s^{-1}), RH is the relative humidity at the leaf

surface, C_s the carbon dioxide concentration at the leaf surface (ppm), and m is a parameter that gives the slope of the relationship between g_s and $An_l\, RH/C_s$.

For well-watered plants, the slope of the BB stomatal conductance model (parameter m) is given as a species-dependent constant. In the model, we allow this parameter to vary in response to water stress to describe stomatal closure during drought conditions to prevent leaves drying out. If stomatal closure precedes reductions in photosynthetic capacity during times of developing water stress, it also conveys increased water use efficiency (WUE), the ratio of carbon gain to water loss.

A linear relationship between a stressed (m_{min}) and non-stressed (m_{max}) values of m and the water limitation term is used (Equation 3.50):

$$m = \mathrm{m}_{\min} + (\mathrm{m}_{\max} - \mathrm{m}_{\min}) * WaterLimit \tag{3.50}$$

where $\mathrm{m}_{\min}$ and $\mathrm{m}_{\max}$ are two parameters used to describe photosynthetic responses under well-watered and water-limited conditions.

The time response of plants' leaves to close their stomata in response to changes in solar radiation is not constant between species and also depends of the rate of change in radiation levels (Will and Teskey, 1999). An increase of PPFD from 200 to 800 μmol m^{-2} s^{-1}, imposed an equilibration time (time for stomatal conductance to reach equilibrium) of 3 minutes for *Fagus grandifolia*, 20 minutes for *Liriodendron tulipifera*, 12 minutes for *Acer rubrum* and *Quercus rubra* (Woods and Turner, 1971), and also 20 minutes for *Pinus taeda* (Whitehead and Teskey, 1995). Whitehead and Teskey (1995) also reported that stomata respond faster to a decrease than to an increase in irradiance.

It was therefore assumed that over the 30-minute time step of the model simulations, leaves have enough time to adjust to new measured climate conditions, and that stomatal conductance and leaf temperatures could be modelled to have reached a new pseudo equilibrium.

Severe water stress levels can also decrease the maximum rate of carbon assimilation by increasing the mesophyll resistance and by reducing the RuBP

carboxylase activity in water-stressed leaves (Kaiser, 1987). This second limitation term (WaterLimitPS) was used to apply further reduction to photosynthetic capacity when water stress developed (Equation 3.51).

$$WaterLimPS = 1 - Redux \;\; if\; WaterLimit \leq MinWStress$$
$$WaterLimPS = 1 \quad if\; WaterLimit \geq MaxWStress \tag{3.51}$$
$$else\; WaterLimPS = \frac{num}{MaxWStress - MinWStress}$$

where

$$num = (Redux * WaterLimit + (1 - Redux) * MaxWStress - MinWStress) \tag{3.52}$$

where $MinWStress$ and $MaxWStress$ are the lower and upper limits of the water limitation and $Redux$ is the reduction rate of the leaves photosynthetic capacity under extreme water limitation.

3.2.6 Efficiencies of the different photosynthesis routines to simulate GPP once incorporated in the ecosystem model.

The selected procedures discussed above are used to represent the same physical process, i.e. photosynthesis. The procedures use different respective response curves and include different processes, even if they also share similarities in the representation of some processes. These differences lead to some dissimilarities in respective simulated photosynthesis rates under certain forcing conditions.

On one hand, the biochemical model of Farquhar et al. (1980) is very detailed and contains much information on the real process of carbon assimilation by plants. However, the model contains a large number of parameters for which some values are very variable among species and cannot be easily or confidently derived unless measurements of leaf photosynthesis response curves made in situ are available. On the other hand, the NRHC or RHC and Thornley formulations are simpler and require fewer parameters to run, but they do not include all the identified processes that regulate leaf carbon assimilation.

The new version of CenW (running at a half-hourly time step) will have to run over long periods of time to study changes in soil organic carbon stocks under different farm management or climate regimes. Under those conditions, it is very important to have both a fast running time and accurate simulations of carbon fluxes, particularly carbon fixation through photosynthesis and plant allocation to soil carbon inputs.

The previous sections focussed on the different formulations of leaf photosynthesis and their integration at the canopy scale. Now that the basic set of equations for carbon assimilation sub-models have been selected and have been tested for their responses to climatic variables, it becomes possible to compare the models' performances under field conditions. This involves comparison with measured photosynthetic rates under measured climatic conditions and farm management practices.

In this part of the study, a model inter-comparison and validation against EC-derived GPP was carried out to determine if the different rates of photosynthesis simulated by these methods are equivalent and which rate gives the best results compared with data.

To achieve this goal, the comparison was made with the different photosynthesis routines included in the complete ecosystem model, and simulations were compared with observations of photosynthesis and evapotranspiration, because in CenW_HH, photosynthesis and evapotranspiration are tightly linked through stomatal conductance.

In order to see how the different photosynthesis modelling routines perform, CenW_HH has been parameterised for each of the routines to get the best possible goodness of fit based on net ecosystem productivity (NEP) and evapotranspiration (LE). Then, for this chapter, which is on photosynthesis modelling, model efficiencies between measured and simulated gross primary production (GPP) and evapotranspiration (LE) were calculated with the Nash-Sutcliff criteria (Equation 3.53) and results are given in Table 3.4:

$$NSE = 1 - \frac{\sum_{i=1}^{N}(O_i - S_i)^2}{\sum_{i=1}^{N}(O_i - \bar{O})^2} \tag{3.53}$$

where O_i represents an observed variable measured at a given time (i), S_i is the corresponding modelled variable, and $\bar{O}$ is used for the average of all observations.

NSE can range from $-\infty$ to 1. An efficiency of 1 (NSE = 1) corresponds to a perfect match between modelled and observed data. An efficiency of 0 (NSE = 0) indicates that the model predictions are as accurate as the mean of the observed data, whereas an efficiency less than zero (NSE < 0) occurs when the observed mean is a better predictor than the model, in other words, when the residual variance that is described by the numerator of Equation 3.53 is larger than variance of the data (given by the denominator of Equation 3.53). Essentially, the closer the model efficiency is to 1, the more accurate the model is. Also, NSE is sensitive to extreme values and might yield sub-optimal results when the dataset contains large outliers in it.

Overall, model data agreements for GPP and LE were good for all the photosynthetic implementation tested, as indicated by high model efficiencies above 0.8. For gross primary production, the highest model efficiency of 0.89 indicated that the best model/data agreement could be achieved by the Thornley routine (Thornley, 2002), followed by both the non-rectangular hyperbola (NRH) and FvCB routines with sun/shade (SS) integration (0.87), then by NRH BL (non-rectangular hyperbola with big leaf integration) with an efficiency of 0.83 and finally by FvCB BL with a NSE of 0.81.

Models performances evaluated for latent heat showed similar patterns as for GPP. Best performance was achieved with the Thornley routine, with a model efficiency of 0.85. Again, as for GPP, both leaf photosynthesis routines tested in this study with a sun/shade upscaling scheme managed to model LE with the same accuracy as indicated by equal model efficiencies of 0.84. The NRH and FvCB leaf photosynthesis algorithms up-scaled at the canopy level by using the big-leaf (BL) integration scheme had the poorest model/data agreements.

All canopy photosynthesis routines were tested with the same energy and water budget procedures, which are described in Chapter 4, the only differences between them being differences in stomatal conductance. In CenW_HH, the

canopy stomatal conductance is calculated inside the photosynthesis routines and then passed to the energy and water budgeting procedure to principally model LE.

Table 3.5: Comparison of the performances of different models of photosynthesis and integration schemes after model parameterisation. The values given in the table are model efficiencies (NSE) calculated following the Nash-Sutcliffe criteria for day-time gross primary production (LE) and latent heat flux (LE) for Scott Farm over the two years of study

	Thornley	NRH BL	NRH SS	FvCB BL	FvCB SS
GPP ($\mu molCO_2\ m^{-2}\ s^{-1}$)	0.89	0.83	0.87	0.81	0.87
LE ($W\ m^{-2}$)	0.85	0.81	0.84	0.83	0.84

Figure 3.17 shows two Taylor diagrams (Taylor, 2001) for gross primary production a) and for evapotranspiration b). According to Taylor (2001), these plots graphically summarise how well a model can reproduce observations and they are particularly useful for comparing the performance of multiple models relative to observations. Model/data agreements are quantified by their Pearson correlation coefficient, their centred root mean square error and their standard deviations which are a measure of the amplitude of their variations.

By using this kind of diagram, it is possible to summarise three different statistics related to the agreement of modelled and observed variables in a two dimensional space. Inferring the performances of several models can be done directly from the plot of the Taylor diagram because:

- the best agreeing models/observations will lie nearest to the point marked "observed" on the x-axis (high correlation and low RMSE)
- the closer the models are to the dashed black arc, the more their standard deviation is correct and variations are accounted for.

b)

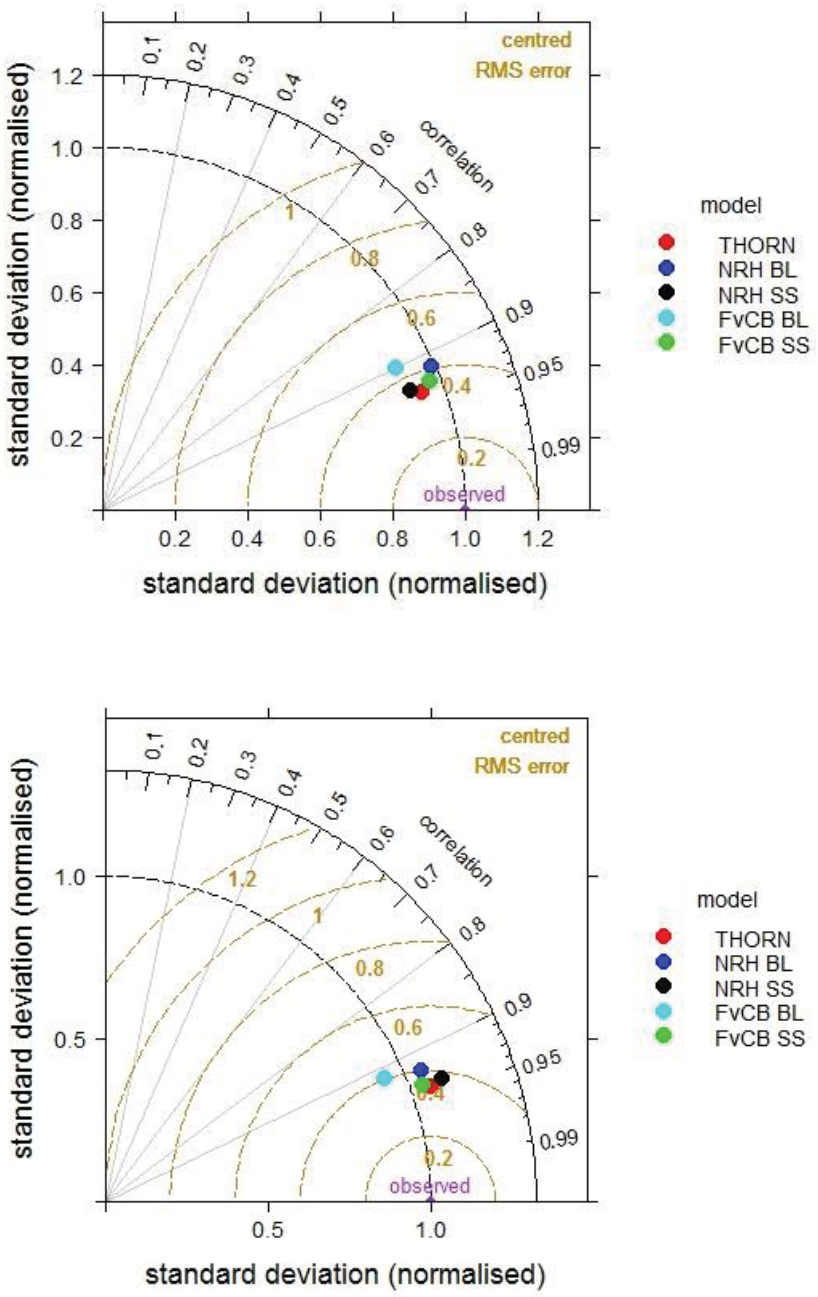

Figure 3.17: Normalized Taylor diagrams of gross primary production a) and latent heat fluxes b) observed and modelled by CenW_HH for Scott farm. Each coloured point represents the results from the model/data comparison with CenW_HH running one or the other of the photosynthesis routines (see text for description). Normalization is made by dividing both the RMS error and the standard deviation of the simulations by the standard deviation of the observations so that the "observed" point is plotted at unit distance from the origin along the x-axis.

We can see in the two diagrams of Figure 3.17 that all points, which individually represent the comparison of observations with their modelled counterparts using the different photosynthesis routine in CenW_HH (given in legend), are grouped in the same area of the plots. This would indicate that GPP and LE are reasonably well modelled with all the carbon assimilation procedures used in the model. However, on both graphs (Fig. 3.17a and b), the CenW_HH model with the Thornley photosynthesis routine (red dots) performed slightly better than the other photosynthesis algorithms that were implemented and tested. RMSE is minimal and correlation is maximal for both GPP and LE.

FvCB and NRH with sun/shade integration were very close to Thornley and to each other with approximately the same RMSE and correlation, which were just slightly better for the FvCB algorithm as it was closer to the dashed arc on both graphs. Slightly worse model performances were achieved with the use of the big-leaf integration scheme and both NRH and FvCB carbon assimilation routines. Even if model performances with the big-leaf up-scaling scheme are not as good as for the Thornley or sun/shade models, they are good enough for the models to give plausible results, as indicated by the good models performances reported in Figure 3.17 and the closeness of all points of the graph.

Figure 3.18 shows the comparisons of modelled data with CenW_HH and the Thornley photosynthesis routine, and EC-derived GPP a) and latent heat flux b). The dashed lines are the 1:1 lines, which indicate perfect agreement between the modelled and observed variables, and the red lines are linear least square regression lines with calculated slopes of 1.00 for gross primary production and 0.89 for latent heat fluxes (Fig. 3.18). This indicates that on average, GPP is well modelled with no systematic error but that LE tends to be overestimated by 11% by CenW_HH. The model efficiency (NSE) indicates that the model could explain 89% of the variations in observed carbon and water fluxes.

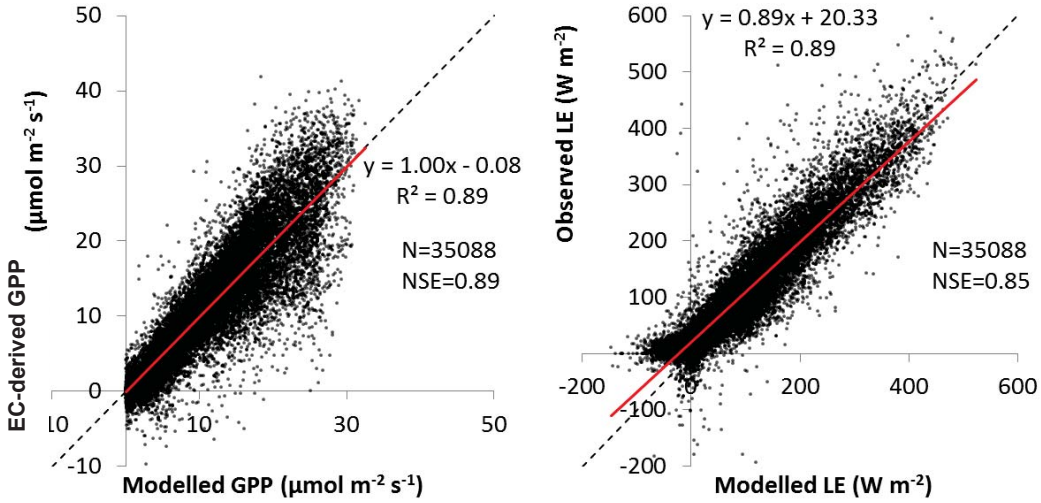

Figure 3.18: Comparisons of modelled and observed GPP a) and LE b). Modelled variables are from CenW_HH with the Thornley photosynthesis routine.

Overall, as CenW_HH with the Thornley photosynthesis algorithm shows the best agreement with observed GPP and LE (Table 3.4, Fig. 3.17a and b, and Fig. 3.18), it was chosen to be used in the rest of the study.

3.2.7 Summary and Conclusions

Throughout this section, different models of photosynthesis and integration schemes were used within the CenW model to be run at a half-hourly time step. Each version of the model was run with the same climatic conditions and farm management practices and re-parametrised with the best fit possible between observations and simulations. The completely modified version of the model was used to include the various feedbacks and limitations from other procedures in a comparison of modelled and observed carbon and water fluxes.

It is concluded that both models simulate photosynthesis at a half hourly time steps with similar results. However, they are not fully equivalent, and even if the FvCB is more mechanistic than the NRHC, it is also more difficult to parameterise as the parameters are very sensitive to temperature, and it is also more difficult to integrate over the canopy. The different formulations of the temperature responses functions and the fact that the FvCB uses different formulation for the different limiting processes led to substantial differences in the modelled carbon assimilations rates.

The overall findings were that the complete model (CenW_HH) with the new carbon assimilation procedure worked well. Perfect agreement between the different photosynthetic implementations was not expected as the different formulations used different formulations of the same processes and includes or excluded certain other processes. However, there were no major discrepancies between the different versions of the model with different photosynthesis modelling algorithms.

At the leaf level, all the photosynthesis routines tested here simulated similar leaf photosynthesis rates after adjusting their respective parameters. This was observed even though they used very different equations of very different complexity, ranging from the very detailed biochemical FvCB photosynthesis model to the much simpler NRH curve. Integration from the leaf to the vegetation canopy was achieved by using either a simple big-leaf scheme or a two-leaf (sun/shade) scheme and it is this step of upscaling the carbon assimilation rate that proved to be the cause of most of the discrepancies between photosynthesis routines, even after their proper and independent parameterisation.

Finally, as a result from all the comparisons made throughout this chapter, the Thornley (Thornley, 2002) algorithm was chosen to be used in all the following chapters of this study as it gave the best performances in the GPP.

CHAPTER 4: THE ENERGY AND WATER BUDGETS

4.1 Introduction

The transfer of water and energy between the atmosphere and the earth's surface occurs continuously. Globally, climate and weather patterns are driven by the energy received by the surface as solar and atmospheric longwave radiation. This energy can be stored by the land and oceans, be returned to the atmosphere where it contributes to warm the air, or be used to evaporate water. All these energy transfers are important fluxes for the global mean energy budget of the Earth's surface. Solar radiation varies in time (seasonally and daily), reflecting the relative positions of the sun and earth and also the atmospheric turbidity and cloudiness.

There are five ways for the surface to dissipate the energy received from the sun:

1) by reflection of some of the incoming solar radiation back to the atmosphere (quantified by surface albedo)
2) by emission of longwave radiation
3) by heat transfer through conduction (contact)
4) by convection (movement of air)
5) by vaporisation of liquid water (latent heat flux).

Over land, the turbulent mixing of air is responsible for the transport of heat (sensible heat) and moisture (latent heat) away from the surfaces, which leads to the resulting microclimatic conditions that are observed locally. As wind blows over land surfaces, ground, trees, grasses, buildings, and other objects, it causes turbulences in the atmospheric boundary layer. Air movement (wind) can be seen as the horizontal transport of rotating eddies, each with its own temperature, humidity, and momentum, and which transport heat and water in both directions between the surface and the atmosphere.

Energy, water, and carbon fluxes between the soil, the vegetation, and the atmosphere are interconnected and complex. Land surface models (LSMs) and soil-vegetation-atmosphere-transfer (SVAT) models with different complexity levels, spatial and temporal scales and with different physical theories or

representation of processes were developed to study these energy and mass fluxes over different surfaces and types of vegetation (Anderson et al., 2000; Gentine et al., 2007; Ingwersen et al., 2011).

The mathematical relationships describing energy and water budgets presented in this chapter describe the most important land surface processes encountered on grazed pastures of New Zealand. Once implemented in CenW_HH, which is the newly developed half-hourly version of the CenW model, the model couples vegetation dynamics with heat and water transfers for the soil and vegetation separately.

The first part of this chapter consists of a detailed description of the modelling scheme implemented in CenW_HH, followed by a report of how the system of equations is solved to ensure the closure of the energy budgets of the different parts of the system as soil and vegetation are treated individually to obtain energy balance. Finally, some typical patterns of soil temperatures over depth and time are shown, as temperature is both a measurable indicator and a key driver of the energy budget over time and under diverse conditions.

4.2 Modelling water and energy budgets for terrestrial ecosystems

The general expression of the energy balance at the soil-vegetation-atmosphere interface is usually written as:

$$R_n = H + LE + G + \Delta S + P \tag{4.1}$$

where R_n is the net radiation, H is the sensible heat flux, LE is the latent heat flux, G is the soil heat flux, ΔS is the heat storage of the vegetation canopy, and P is the energy flux associated with photosynthesis.

By convention, net radiation is assigned a positive number when directed towards the surface, the latent energy flux and sensible heat flux are positive towards the atmosphere, and the soil heat flux is positive towards the soil. The heat storage of the canopy (ΔS) and the energy flux associated with

photosynthesis (P) are usually omitted from the energy balance calculations because they are very small compared with the other terms, even on a half-hourly basis. The simplified equation becomes:

$$Rn = H + LE + G \tag{4.2}$$

where all fluxes are expressed in W m^{-2}.

Process-based ecosystem models that simulate the exchanges of water, energy, and mass between soil, plant, and atmosphere are used in a wide range of applications, and their complexity (like photosynthesis- integration from a single leaf to the canopy) varies from the big-leaf scheme that is a simple bulk-canopy model (Friend, 1995; Monteith, 1965), the two-sources (soil and canopy) in which the contributions from the soil and from the vegetation are simulated separately (Shuttleworth and Wallace, 1985; Shuttleworth and Gurney, 1990), to detailed multi-layer process modelling of soil-vegetation-atmosphere interactions (Baldocchi and Wilson, 2001). The choice was made to use the two-source scheme proposed by (Shuttleworth and Wallace, 1985; Shuttleworth and Gurney, 1990), which is described below with some modifications to the original set of equations. In the Shuttleworth and Wallace (1985) modelling scheme, hereafter called SW85, temperatures and humidities of the soil and vegetation layers are different. Two-sources models, like the SW85 models, were originally developed for sparse vegetation covers with a large contrast between the temperatures of the soil and vegetation, but they can also be considered as a general case of most systems where a layer of vegetation overlays the bare soil.

A multilayer soil temperature and water content profile is implemented instead of the original “force-restore” scheme (Bhumralkar, 1975; Noilhan and Planton, 1989), in which the soil is divided into two layers, e.g. 1) a soil surface layer that exchanges with the atmosphere and where there is no water uptake by roots; and 2) a deep soil layer that is usually larger, contains the root system, and buffers exchanges of the top soil layer with the atmosphere. Having two layers allows calculation of water extraction by deep soil roots, calculation of the soil

heat flux from a two temperature gradient, giving a better representation of water and heat exchanges between the two soil compartments.

A soil surface litter layer has also been added because it has been proven to improve simulations of energy and carbon fluxes in forest ecosystems (Wilson et al., 2012). In grassland ecosystems, litter does not usually represent a large pool of carbon, but to retain the generic properties of the CenW ecosystem model, these new equations were used so that CenW could continue to function adequately for different vegetation types even if in this study only a pasture system has been modelled.

4.2.1 Double source energy budget model

The model presented by Shuttleworth and Wallace (1985) was designed to simulate the energy and water budget of the surface by separating the contributions of the soil and of the vegetation layer with subscripts s and c, respectively. The model simulates the different processes analogous to an electric circuit where the fluxes of latent and sensible heat of each component of the system are expressed as a difference of potential between two nodes of the scheme (temperature or water vapour) divided by a resistance term (Fig. 4.1).

The net radiation available above the canopy is partitioned between the soil and the canopy such as in Equation 4.3:

$$RN = RNs + RNc \tag{4.3}$$

A new litter compartment in the soil energy budget routine has also been added to the original formulation proposed by Shuttleworth and Wallace (1985) and Shuttleworth and Gurney (1990). The original version of the Shuttleworth and Wallace (1985) scheme has been used in several modelling studies in which most of the processes and fluxes at the soil-vegetation-atmosphere interface were integrated and well modelled (LoSeen et al., 1997; Anderson et al., 2000; Cammalleri et al., 2010). These studies also used the original version of the routine. They did not include the effect of a litter layer in the partitioning of energy or water as well as how it affected soil temperature and evaporation

rates, which is however important in some biomes and, as Wilson et al. (2012) showed in a forest modelling study, improved model performances when included.

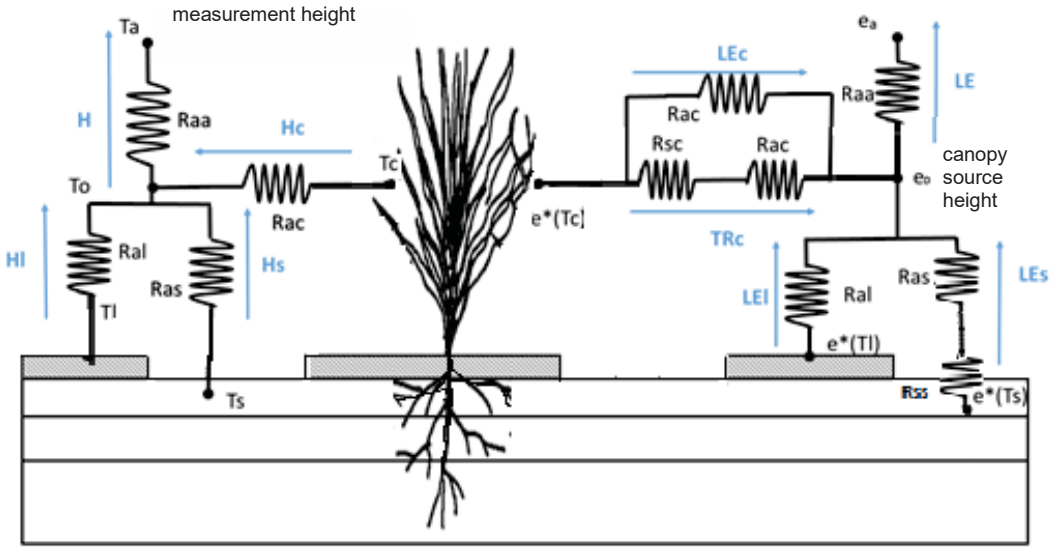

Figure 4.1: Diagram showing the double source modelling scheme for the simulation of the heat and water budgets at the earth-atmosphere interface. The model has been modified from Shuttleworth and Wallace (1985) with the inclusion in the scheme of a litter layer (grey) and a multilayer soil profile. The left hand side shows the transfer scheme for the sensible heat fluxes (H) from the different components of the system; the right hand side shows the transfer scheme for the latent heat fluxes (LE). **Key**: H, Hc, Hs, and Hl are the sensible heat fluxes for the system, crop, soil, and litter layer, respectively; LE, LEc, Les, and LEl are the latent heat fluxes for the system, crop, soil, and litter layer, respectively; Ta, Tc, Ts, Tl, and To are the temperatures for the measurement height, crop, soil, litter layer, and canopy source height, respectively; e_a and e_o are the vapour pressure at the measurement height and canopy source height, respectively; $e^*(Tc)$, $e^*(Ts)$, and $e^*(Tl)$ are the saturated vapour pressure at temperatures for the crop, soil, and litter layer, respectively; r_{aa} is the aerodynamic resistance between the canopy source height and the measurement height; r_{ac} is the bulk boundary layer resistance; r_{as} is the aerodynamic resistance between the soil and the canopy source height; r_{al} is the aerodynamic resistance between the litter layer and the canopy source height; r_{sc} and r_{ss} are the canopy and soil surface resistances, respectively;

The daily CenW model included a surface litter layer formed through plant litter fall. The calculated proportion of soil covered by litter could add a source of evaporative flux when wet but prevent evaporation from the soil beneath. Even though the amount of litter present on the soil surface in pasture systems is not

very important, we chose to also include it in the half hourly water and energy budget.

First, since a litter layer was included in the simulation of water fluxes in the daily version of CenW, it was also included in the half-hourly version to maintain comparability between the versions. Second, if the newly developed version of the model should be applied to a system where the amount of litter is important, as in forest ecosystems, it should allow ready application of the model with no major changes needed for the energy budget procedure.

While only a few studies have been conducted to understand how residues affect water, CO_2, and energy exchanges below the vegetation layer, their inclusion in the ALEX model improved model simulations of these fluxes (Wilson et al., 2012).

Radiative transfers are not represented in Figure 4.1. However, they are very important terms for the proper modelling of water and energy exchanges in the soil-vegetation atmosphere continuum and equations used in CenW_HH are given in Section 4.2.2. In the model, it is assumed that the vegetation layer is semi-transparent and placed above the soil layer, which is opaque.

The energy budget is written separately for the soil (Equation 4.4), the vegetation layer (Equation 4.5), and the litter layer (Equation 4.6) that was added to the original model formulation.

$$RNs - LEs - Hs - G = 0 \tag{4.4}$$

$$RNc - LEc - Hc = 0 \tag{4.5}$$

$$RNl - LEl - Hl = 0 \tag{4.6}$$

Solving these three simultaneous equations requires the correct calculation of their various constituent fluxes that depend on biotic and abiotic conditions.

The three equations above represent the energy partitioning between the different processes occurring in the various compartments of the system. As indicated, the energy budgets of the three system components are closed. At equilibrium temperature, the net radiation gain of any layer must be balanced by

energy losses from latent energy, with positive or negative heat transfer adding to the energy balance. Because the canopy and litter layers have very little thermal capacities, heat storage in those layers were ignored in the half-hourly calculations presented here, but the soil with its much larger heat capacity can substantially add to the overall energy balance through storage or release of heat.

Equation 4.4 and Equation 4.5 came from the original formulation of the double source model as proposed by Shuttleworth and Wallace (1985). Equation 4.6 has been added to take account of the energy balance of the surface litter pool that had been shown to improve the partitioning of surface energy fluxes of forests (Wilson et al., 2012) and crops (Farahani and Ahuja, 1996; Odhiambo and Irmak, 2011). According to the formulations of the energy budgets of the different components of the system, it is assumed that vegetation and litter layers have no heat storage terms and equations are solved iteratively. As seen above, the vegetation and litter layer energy budgets rely on the stationarity assumption, i.e. net radiation equals the sum of sensible and latent heat fluxes.

The original model proposed by Shuttleworth and Wallace (1985) only included a two-layer soil model for the calculation of the soil temperatures and water content called the “force restore modelling scheme”. In CenW_HH, the soil can be modelled with up to 20 layers. Their depths and properties are user specified so that soil water content and the temperature profiles can be modelled separately for each layer. Above-ground vegetation has also been partitioned into its live (LAI_{green}) and dead (LAI_{dry}) components. This partitioning led to better simulations of the different terms of the energy budget because the dead parts of the vegetation keep on intercepting solar radiation but do not contribute to transpiration and photosynthesis fluxes.

The application of the Shuttleworth and Wallace (1985) modelling approach requires a large number of parameters, and its practical application could be hindered by the lack of mechanistic and accurate formulation of the different resistances terms (Odhiambo and Irmak, 2011). However, this scheme has been successfully used in several modelling studies of evapotranspiration over agricultural land covers and has given good estimates of water fluxes (Farahani

and Bausch, 1995; Brisson et al., 1998; Anadranistakis et al., 2000; Lund and Soegaard, 2003; Kato et al., 2004). In the following sections, the key equations used to develop CenW_HH are described.

4.2.2 Net radiation

Development of the vegetation stands rely heavily on the interception of radiation from the sun, and it is diurnal changes in solar radiation levels that drive the diurnal changes of photosynthesis, evapotranspiration, and latent heat fluxes exchanged between the surface and the atmosphere. The total solar radiation reaching the surface can be sub-divided into its direct beam and diffuse components.

The canopy prevents solar radiation reaching the soil surface according to a shielding factor (σ_{fs}) expressed by Deardorff (1978) or Taconet et al. (1986), as given by Equation 4.7 for direct beam solar radiation and Equation 4.8 for diffuse and long-wave radiation:

$$\sigma_{fs} = 1 - \mathrm{e}^{-\mathrm{k}_b \,\mathrm{LAI}} \tag{4.7}$$

$$\sigma_{fl} = 1 - \mathrm{e}^{-\mathrm{k}_\mathrm{l} \,\mathrm{LAI}} \tag{4.8}$$

where LAI (m^2 m^{-2}) is the total leaf area index of the stand given by the sum of LAI_{green} and LAI_{dry}, k_b is the extinction coefficient for direct beam solar radiation that is simulated according to solar position in the sky and leaf angle distribution (see Chapter 3), and k_l is the extinction coefficient for diffuse and long wave radiation that value is fixed to 0.75 (Cammalleri et al., 2010b). Extinction coefficients for direct and diffuse radiation are different mainly because diffuse radiation is anisotropic, meaning it comes equally from all directions.

The general expression of net radiation at the SVA interface is expressed according to the electromagnetic wavelengths (Equation 4.9) and represents the radiative budget of the surface and the available energy responsible for conductive and convective fluxes.

$$RN = R_{SW\downarrow} - R_{SW\uparrow} + R_{LW\downarrow} - R_{LW\uparrow} \tag{4.9}$$

where subscript SW and LW are used to differentiate shortwave and longwave radiations respectively and ↓ and ↑ arrows indicate the direction of propagation of the radiation components. These terms correspond to:

$R_{SW\downarrow} = R_S$ is the global incident solar radiation (4.10)

$R_{SW\uparrow} = \alpha_{surf} R_S$ represents the reflected global solar radiation

$R_{LW\downarrow} = \epsilon_a \sigma T_a^4$ represents the incident atmospheric radiation

$R_{LW\uparrow} = \left(1 - \epsilon_{surf}\right)\epsilon_a \sigma T_a^4 + \epsilon_{surf} \sigma T_{surf}^4$ is the reflected atmospheric radiation and the intrinsic radiation from the surface

where R_s is the incoming solar radiation (W m^{-2}) and is an input of the model, α_{surf} is the surface albedo, ε_a and ε_{surf} are the emissivities of the air and the surface respectively, σ is the Stephan-Boltzmann constant (5.6705 10^{-8} W m^{-2} K^{-4}), and T_a and T_{surf} are the air and surface temperatures in Kelvin.

For a vegetated surface, usually constituting two imbricated layers, net radiation terms at the interface between the surface and the atmosphere can be computed according to the formulation proposed by Campbell and Norman (1998) according to Equations 4.11 and 4.12 for the soil and the vegetation respectively, for these equations no litter layer is used in their derivation.

At the soil level, the net radiation is calculated according to Campbell and Norman (1998) as:

$$RN_s = (1 - \alpha_s)\left(1 - \sigma_f\right)R_s + \left(1 - \sigma_{fl}\right)\epsilon_a \sigma T_a^4 + \sigma_{fl}\epsilon_c \sigma T_c^4 - \epsilon_s \sigma T_s^4 \tag{4.11}$$

And for the vegetation canopy:

$$RN_c = (1 - \alpha_c)R_s\sigma_{fs} + \sigma_{fl}(\epsilon_a\sigma T_a^4 + \epsilon_s\sigma T_s^4 - 2\epsilon_c\sigma T_c^4) \quad (4.12)$$

where α_s and α_c are the soil and vegetation albedos that are model parameters, σ_{fs} is the shielding factor for solar radiation, σ_{fl} is the shielding factor for long wave and diffuse radiations, ε_i are the emissivities of the different constituents of the system differentiated by their subscripts, a is used for the air, s for the soil and c for the vegetation canopy, and T_i are the various components' temperatures in Kelvin.

These equations have been modified to incorporate the litter layer in the energy partitioning. It has been done by partitioning the radiation in the fraction absorbed by the soil and by the litter by calculating the fraction of soil covered by dead plant material hereafter called f_{litt} and modifying equations from Campbell and Norman (1998) as:

$$RN_c = (1 - \alpha_c)R_s\sigma_f + \sigma_{fl}[R_{atm} + \epsilon_s\sigma T_s^4(1 - f_{litt}) - 2\epsilon_c\sigma T_c^4 + \epsilon_l\sigma T_l^4 f_{litt}] \quad (4.13)$$

$$RN_s = (1 - f_{litt})\left[(1 - \alpha_s)(1 - \sigma_f)R_s + (1 - \sigma_{fl})R_{atm} + \sigma_{fl}\epsilon_c\sigma T_c^4 - \epsilon_s\sigma T_s^4\right] + \epsilon_l\sigma T_l^4 f_{litt} \quad (4.14)$$

And the net radiation at the litter layer level is given by:

$$RN_l = \left[(1 - \alpha_l)(1 - \sigma_f)R_s + (1 - \sigma_{fl})R_{atm} + \sigma_{fl}\epsilon_c\sigma T_c^4 + \epsilon_l\sigma T_l^4\right]f_{litt} - \epsilon_s\sigma T_s^4(1 - f_{litt}) \quad (4.15)$$

where α_c, α_s, and α_l are the albedos of the vegetation, the soil, and the litter layer, ε_c and ε_s are defined above, and ϵ_l is the emissivity of the residue (litter layer), and R_{atm} represents the long wave radiation of the atmosphere which is calculated according to the Equation 4.16.

$$R_{atm} = \varepsilon_{sky}\sigma {T_a}^4 \quad (4.16)$$

where ε_{sky} represent the emissivity of the atmosphere and is the function of the emissivity of the clear sky and of a cloudiness factor.

The emissivity of the atmosphere is given by:

$$\varepsilon_{sky} = (clf + (1 - clf))\varepsilon_{clear} \quad (4.18)$$

where clf is the cloudiness factor that is defined as the ratio of modelled and measured solar radiation.

The clear sky emissivity is calculated for each time step of the model according to the empirical formula proposed by Brutsaert (1984), as described in the study of Herrero and Polo (2012), according to air temperature and water vapor pressure at saturation at measurement height and for which uncertainty is within ±5% (Kustas et al., 1989):

$$\varepsilon_{clear} = 1.24\left(\frac{e_a}{T_a}\right)^{1/7} \quad (4.17)$$

where e_a is the absolute humidity of the air at the measurement height.

4.2.3 Sensible heat flux

The sensible heat flux (H) corresponds to the process by which heat energy is transferred from the Earth's surface to the atmosphere by conduction and convection. For example, when energy is received by a substance or object that resulted in a change of its temperature, this change in temperature is called the sensible heat flux.

Total sensible heat flux is the sum of the contributions of the vegetation, litter and of the bare soil (Equation 4.19) such as it is calculated at different levels according to the nodes as shown on Figure 4.1:

$$H = H_s + H_c + H_l = \rho c_p \frac{(T_0 - T_a)}{r_{aa}} \quad (4.19)$$

where H is the sensible heat flux above the vegetation layer and is the sum of the contribution of the soil (H_s), canopy (H_c), and the litter layer (H_l). These three fluxes are calculated according to Equation 4.20, 4.21, and 4.22, respectively. And T_0 is the temperature at the canopy source height (see below), ρ is the air

density (1.2 kg m^{-3}), and c_p is the specific heat capacity of air at constant pressure (1012 J kg^{-1} K^{-1}).

The three components of the total sensible flux are calculated as:

$$H_s = \rho c_p \frac{(T_s - T_0)}{r_{as}} \tag{4.20}$$

$$H_c = \rho c_p \frac{(T_c - T_0)}{r_{ac}} \tag{4.21}$$

$$H_l = \rho c_p \frac{(T_l - T_0)}{r_{al}} \tag{4.22}$$

where T_0 is the temperature of the air at the mean canopy source height, r_{as} is the aerodynamic resistance between the ground surface and the source height within the canopy (Section 4.2.6.2), r_{ac} is the bulk boundary layer resistance to heat and water vapour in the canopy (Section 4.2.6.1), and r_{al} is the aerodynamic resistance between the litter layer and the source height within the canopy (Section 4.2.6.2).

The sensible heat flux is directly proportional to the difference in temperature between the air at a reference height (T_0) and the temperature of the studied surface (T_s, T_c or T_l), and inversely proportional to a resistance term (r_{as}, r_{ac} or r_{al}).

The surface is gaining energy (H<0) when its temperature is colder than the temperature of the air at the reference height (T_0) and is losing energy (H>0) when its temperature is warmer. The sensible heat flux increases as the temperature difference increases but is mediated by the resistance terms. As the resistance term increases, H becomes smaller for a given temperature difference.

4.2.4 Latent heat flux

The latent heat is by definition the amount of energy that needs to be applied to change the state of a substance from liquid to gas (vaporisation) or solid to liquid (liquefaction) or directly from solid to gas (sublimation). In the context of

this study, the latent heat flux is basically the heat dissipation by evaporation of water, when the flux goes from the surface of interest toward the atmosphere. It can also play a role in condensation of dew at night, e.g. when the latent heat flux is reversed and goes from the atmosphere to the surface

As for sensible heat fluxes, the total latent heat flux (or evapotranspiration) is calculated by summing the contributions of the vegetation canopy (LE_c), which is made of the sum of the evaporation contribution from the wet fraction of leaves and the transpiration from the dry parts, the soil surface layers (LE_s), and the litter layer (LE_l) fluxes:

$$LE = LE_s + LE_c + LE_l = \frac{\rho c_p}{\gamma} \frac{(e_0 - e_a)}{r_{aa}} \tag{4.23}$$

where ρ and c_p have been described above, γ is the psychrometric constant (0.66 mbar K^{-1}), e_0 is the vapour pressure at the canopy source height (Equation 4.30), and e_a is the actual vapour pressure of the air at the reference height above the canopy and is given by Equation 4.24:

$$e_a = e^*(T_a) \frac{RH}{100} \tag{4.24}$$

where T_a is the air temperature measured at reference height above the vegetation layer and RH is the atmospheric relative humidity measured at the same level.

$$e^*(T_{surf}) = 0.6108 \; e^{\left(\frac{17.27\, T_{surf}}{T_{surf}+273.15}\right)} \tag{4.25}$$

where $e^*(T_{surf})$ is the saturated vapour pressure at surface temperature in kPa and T_{surf} is the surface temperature (°C).

The different components of the latent heat flux (evapotranspiration) can be written as:

$$LE_s = \frac{\rho c_p}{\gamma} \frac{(e^*(T_s) - e_0)}{r_{as} + r_{ss}} \tag{4.26}$$

$$LE_c = LE_{cw} + LE_{cd} = \frac{\rho c_p}{\gamma} \left[\delta \frac{(e^*(T_c) - e_0)}{r_{ac}} + (1 - \delta) \frac{(e^*(T_c) - e_0)}{r_{ac} + r_{sc}} \right] \tag{4.27}$$

$$LE_l = \frac{\rho c_p}{\gamma} \frac{(e^*(T_l) - e_0)}{r_{al}} \tag{4.28}$$

where LE_{cw} represents the evaporation of water intercepted by leaves and LE_{cd} the transpiration of water through the stomata, δ is the fraction of the canopy covered by water, $e^*(T_c)$, $e^*(T_s)$, and $e^*(T_l)$ are the saturated vapour pressures at vegetation, soil, and litter temperatures, respectively, calculated according to Equation 4.25, r_{ss} is the soil surface resistance (Equation 4.62), and r_{sc} is the bulk stomatal conductance of the canopy (Equation 4.55).

Evapotranspiration corresponds to the process of vaporisation of liquid water and so involves transfers of mass and energy. The evaporation of a small amount of water requires a substantial amount of energy for the phase change to occur. Evapotranspiration combines evaporation, which is the process where liquid water is transformed into vapour, and transpiration, which is a process of water loss from plants through stomata. The vapour pressure deficit (VPD) between the surface and the air is the principal driver of both evaporation and transpiration fluxes, which are controlled by resistances. As the surface resistances increase as the surfaces dry, a well-watered site usually has a higher latent heat flux than a drier site under similar climatic conditions.

Evaporation only occurs when a surface is wet and exposed to a drier air, and ceases when the surface is dry or the air is saturated with water vapour. Transpiration is controlled by the same physical drivers, but is also controlled by stomatal conductance (opening of stomata present on leaves). It is assumed that when the surfaces of leaves are totally covered by water, the transpiration rate is zero.

When the values calculated for $e^*(T_c)$, $e^*(T_s)$ or $e^*(T_l)$ are lower than e_0, conditions are favourable for the formation of dew on the respective surfaces. Under these circumstances, it is assumed that dew is deposited on the whole surface and the extra amounts of water from dewfall add to water stored in the different parts of the ecosystem. In the general description of the Shuttleworth and Wallace (1985) model, it is necessary to calculate the temperature and vapour pressure at the canopy reference height. Calculations were done by applying the Millman's theorem (or parallel generator theorem), in analogy with an electric circuit, to the schematic representing the double-source energy balance model (Fig. 4.1). In an electrical analogy, temperatures or the saturated vapour pressures would represent currents in the different branches of the scheme and fluxes would be potential differences (voltages) between two nodes.

Equations 4.29 and 4.30 describe the original model without a litter layer (Shuttleworth and Wallace, 1985; Shuttleworth and Gurney, 1990; LoSeen et al., 1997):

$$T_0 = \frac{r_{aa}r_{as}T_c + r_{aa}r_{ac}T_s + r_{ac}r_{as}T_a}{r_{aa}r_{as} + r_{aa}r_{ac} + r_{ac}r_{as}} \tag{4.29}$$

and

$$e_0 = \frac{r_{aa}(r_{as}+r_{ss})e^*(T_c) + r_{aa}(r_{ac}+r_{sc})e^*(T_s) + (r_{ac}+r_{sc})(r_{as}+r_{ss})e_a}{(r_{ac}+r_{sc})(r_{as}+r_{ss}) + r_{aa}(r_{ac}+r_{sc}+r_{as}+r_{ss})} \tag{4.30}$$

This was extended by introducing a litter layer (subscript $_l$). From the schematic presented in Figure 4.1 and the application of the Millman's theorem the new equations became:

$$T_0 = \frac{r_{aa} r_{al} (r_{as} T_c + r_{ac} T_s) + r_{ac} r_{as} (r_{al} T_a + r_{aa} T_l)}{r_{aa} r_{al} (r_{as} + r_{ac}) + r_{ac} r_{as} (r_{aa} + r_{al})} \quad (4.31)$$

$$e_0 = \frac{num}{den} \quad (4.32)$$

with:

$$num = r_{aa} r_{al} [(r_{as} + r_{ss})\, e^*(T_c) + (r_{ac} + r_{sc}) e^*(T_s)] + (r_{ac} + r_{sc})(r_{as} + r_{ss})(r_{al} e_a + r_{aa}\, e^*(T_l))$$

$$den = (r_{ac} + r_{sc})(r_{as} + r_{ss})(r_{aa} + r_{al}) + r_{aa} r_{al} (r_{ac} + r_{sc} + r_{as} + r_{ss})$$

All resistances have already been described in the above sections. The node in the system corresponding to the canopy source height is purely conceptual and has no actual location or equivalent in a real vegetation canopy. However, this node is an important feature of the model as it helps the understanding of the system and simplifies fluxes calculations and partitioning between the soil and the vegetation.

4.2.5 Soil heat flux

The soil heat flux is a process of heat conduction that results from a temperature gradient and the thermal conductivity of the surface. Heat flux usually moves energy into the soil during the day, with a near equal energy flux out of the soil during the subsequent night. A small imbalance may remain that leads to longer-term seasonal soil warming or cooling.

As said in the previous paragraphs, the Shuttleworth and Wallace (1985) model formulation used the force-restore scheme to simulate soil water and energy fluxes. In Shuttleworth and Wallace (1985), the soil surface heat flux (G) is calculated according to Equation 4.33, which was also used by Mo and Liu (2001) and Cammalleri et al. (2010) among others:

$$G = k_1 \frac{T_s - T_{g1}}{z_{g1}} \tag{4.33}$$

where k_1 is the thermal conductivity of the first surface layer, and T_{g1} the temperature of the first soil layer corresponding to a depth z_{g1}.

The daily version of the model (CenW 4.1) already uses a multilayer soil model that gave satisfactory results and a good representation of the different processes controlling water movements (Kirschbaum et al., 2015) and is also important for soil organic carbon dynamics.

The procedure to calculate soil heat flux and soil temperature profile in CenW_HH uses the same multi-layer structure of the daily version but explicitly calculates the temperature at each soil depth. At first the thermal capacities, conductivities, and diffusivities of the different soil layers are calculated at the beginning of each half-hourly simulation periods and for each soil layer based on their specific texture, organic matter and water contents. Then the maximum time step required to solve the partial derivative equation is calculated based on the previously calculated thermal properties. In the next step, the soil heat flux between the different soils layers is calculated according to Equation 4.35, in which the horizontal fluxes are neglected:

$$G = k_T \frac{\partial T}{\partial z} \tag{4.35}$$

where k_T is the soil thermal conductivity (W K^{-1} m^{-2}) and $\frac{\partial T}{\partial z}$ is the gradient of temperature down the soil profile. Temperatures of the different soil layers are then adjusted according to Equation 4.36:

$$c_s \frac{\partial T}{\partial t} = \frac{\partial G}{\partial z} \tag{4.36}$$

where c_s is the soil heat capacity expressed in J m^{-3} K^{-1}, $\frac{\partial T}{\partial t}$ is the change in temperature with time, and $\frac{\partial G}{\partial z}$ is the change in soil heat flux with depth.

All the calculation steps are repeated until the end of the 30-minute period, with adjustment of the soil thermal properties, water content, and temperatures as well as all the fluxes and resistance terms used in the modelling scheme.

4.2.6 Resistances formulations

As shown in the Figure 4.1, the Shuttleworth and Wallace (1985) model involves the calculation of five resistances (see below) to compute the fluxes. These resistances are particularly important because they regulate the different modelled fluxes between the different constituents of the ecosystem.

4.2.6.1 *Resistance r_{ac}*

The resistance r_{ac} represents the bulk boundary layer resistance of the vegetative elements in the canopy (Shuttleworth and Gurney, 1990) and, like all other resistances involved in the modelling scheme presented here, is given in s m^{-1}. This resistance is a function of LAI and wind speed. In the following of this section different formulation are presented and compared.

- Norman et al. (1995) parameterised the canopy boundary layer resistance as:

$$r_{ac} = \frac{C'}{LAI}\left(\frac{s}{U_{d_0+z_{om}}}\right)^{1/2} \tag{4.37}$$

where C' is a constant set equal to 90 $s^{1/2}$ m^{-1} (Norman et al., 1995), s is the characteristic dimension of the leaves, and $U_{d_0+z_{om}}$ is the wind velocity at a height of $d_0 + z_{om}$ obtained by extrapolation of the exponential wind profile inside of the canopy (Equation 4.38) following the formulation of Lafleur and Rousse (1990).

$$U_{(z)} = u_a \, exp\left[-n_{(LAI)}\left(1 - \frac{z}{h}\right)\right] \tag{4.38}$$

- Shuttleworth and Gurney (1990); LoSeen et al. (1997):

This formulation assumes that the energy exchanges only occur by molecular diffusion through a laminar layer around the leaves and is derived from the formulation previously derived by Choudhury and Monteith (1988) given in Equation 4.37 but it assumes an identical decay rate of wind speed and eddy diffusivity in the canopy (Shuttleworth and Gurney, 1990).

$$r_{ac} = \frac{100\alpha'}{2LAI}\sqrt{\frac{s}{U_{d_0+z_{om}}}}\frac{1}{(1-\exp(-\alpha'/2))} \tag{4.38}$$

where α' is the wind speed attenuation constant within the canopy that is dimensionless and taken as 2.5.

- Choudhury and Monteith (1988)

$$r_{ac} = \frac{\alpha'}{4\alpha_2 LAI}\sqrt{\frac{s}{U_{d_0+z_{om}}}}\frac{1}{(1-\exp(-\alpha'/2))} \tag{4.39}$$

where α_2 is a constant coefficient.

In fact, Equations 4.38 and 4.39 are equal when the values of the parameters involved in each of them are selected adequately, e.g. $\alpha_2 = 0.005$.

- Taconet et al. (1986)

$$r_{ac} = \frac{1}{28}u_{ac}\frac{\beta LAI}{p_d} \tag{4.40}$$

where β is a parameter used to take into account the contribution of vegetation components other than foliage to the calculation of aerodynamic resistance (1.1), u_{ac} is the wind speed at the top of the vegetation layer and could be calculated according to a logarithm (Equation 4.41) or a power (Equation 4.42) as:

$$u_{ac} = \frac{u*}{0.4}\, ln\left[\frac{h - displ}{z_0}\right] \tag{4.41}$$

where $u*$ (m s^{-1}) is the friction velocity which is calculated according to Equation 4.43, h is the vegetation height, $displ$ the zero plane displacement height, and z_0 is the roughness length of the canopy (m) the last 2 parameters are calculated from the vegetation height according to Monteith (1973) as: $displ$=0.63h and z_0=0.13h.

$$u_{ac} = u_a \left(\frac{h}{z_{ref}}\right)^{0.46} \tag{4.42}$$

where z_{ref} is the reference height which is taken as the measurement height above the vegetation

$$u* = \frac{K\, ua}{\ln\left(\frac{z_{ref} - displ}{z_0}\right)} \tag{4.43}$$

and pd (Equation 4.40) is an empirical shelter factor for momentum transfer which is given by:

$$pd = \begin{cases} 2 & if\ LAI < 2 \\ LAI/2 + 1 & if\ LAI \geq 2 \end{cases} \tag{4.44}$$

Figure 4.2 shows the responses of the resistance r_{ac} to wind speed a) and to LAI b). Only two formulations have been plotted because the equations proposed by Choudhury and Monteith (1988), Shuttleworth and Gurney (1990) and Norman et al. (1995) give very similar results and are referred to SG 90 on Figure 4.2.

These two formulations give different values for the resistance r_{ac}, especially for very low amounts of vegetation (LAI<0.5) and for wind velocity below 0.5 m s^{-1}. However, the shapes of the curves show similar patterns with high values of r_{ac} found for low wind speed and amount of vegetation, with a sharp decrease

observed as these two variables increase, followed by a plateau where resistance values decrease only slightly.

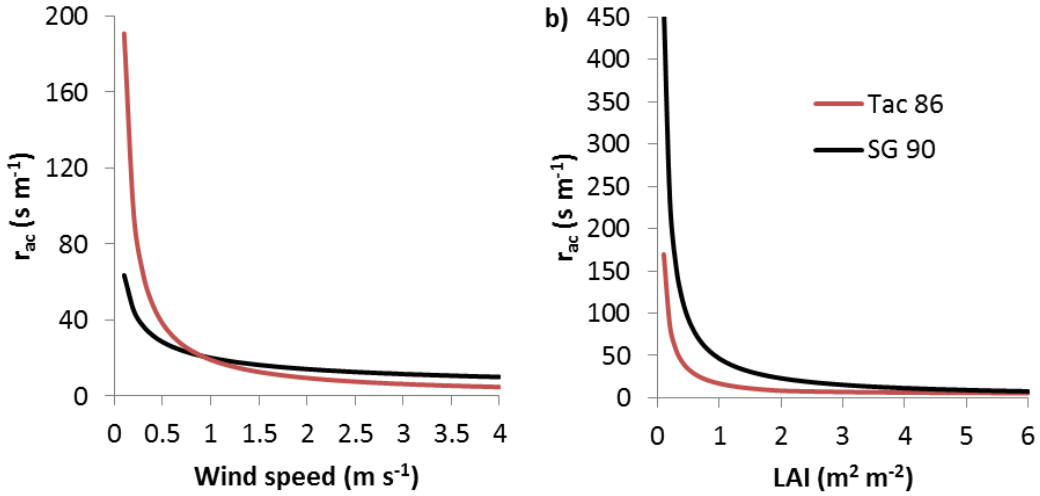

Figure 4.2: Responses of the bulk boundary layer resistance of the vegetative elements in the canopy (r_{ac}) to wind speed (a) and to leaf area index (b). The black line (SG 90) corresponds to the formulation of Shuttleworth and Gurney (1990) and the red line (Tac 86) to the equation proposed by Taconet et al. (1986). When LAI and wind speed are not varying, constant values of 4 m^2 m^{-2} and 3 m s^{-1} are used.

The two contrasting formulations of the aerodynamic canopy resistances proposed by Taconet et al. (1986) and Shuttleworth and Gurney (1990) have been tested in the model (CenW_HH). As the best model/data agreements were achieved with the Shuttleworth and Gurney (1990) equation (tests not shown here), this formulation was chosen to be used in CenW_HH and in the rest of this study. This resistance term also appeared to be particularly important in the calculation of the total latent energy of the system as it is used to regulate exchanges between the vegetation layer and the atmosphere (Fig. 4.1).

Demarty et al. (2002) tested and compared several alternatives for the formulation of aerodynamic resistances and found good agreement between all of them for the modelling of resistances and fluxes above the surface with, however, some discrepancies in the partitioning of the overall fluxes between the contribution of the vegetation and the soil.

4.2.6.2 ***Resistance r_{as} and r_{al}***

r_{as} corresponds to the aerodynamic resistance between the ground surface and the canopy source height and could be expressed according to different formulations, which overall should give very similar results (Demarty et al., 2002). For the modelling of the resistance r_{as}, the choice was made to use the expression as it was originally given in Shuttleworth and Gurney (1990), which is calculated as:

$$r_{as} = \frac{h \exp(\alpha)}{\alpha K_h}\left[exp\left(-\frac{\alpha z_0{}'}{h}\right) - exp\left(-\frac{\alpha(z_0 + d)}{h}\right)\right] \quad (4.45)$$

where α is a constant set to 2.5, h is the vegetation height, and K_h is the eddy diffusion coefficient that is given by:

$$K_h = K u^*(h - d) \quad (4.46)$$

In the description of the model, Shuttleworth and Gurney (1990) derived Equation 4.45 by integrating the eddy diffusion coefficient (Equation 4.46), which is assumed to decrease exponentially through the depth of the canopy, between the soil surface (height=0) and $z_0 + d$, which in this case is set to an height of 0.76 multiplied by the vegetation height (h).

The formulation of Shuttleworth and Gurney (1990) for the calculation of the aerodynamic resistance between the soil and the canopy reference height was preferred in this study because as Demarty et al. (2002) showed, the different formulations available in the literature gave very similar results.

The aerodynamic resistance over the litter layer (r_{al}) uses the formulation of Cammalleri et al. (2010) which corresponds to Equation 4.49.

$$r_{al} = \frac{1}{a' + b' u_s} \quad (4.49)$$

where u_s is the wind speed just above the soil surface that is calculated according to the attenuation of the wind velocity down the canopy profile as

given by Equation 4.37, and a' and b' are coefficients that could be parameterised.

In this study, the value of the parameters a' and b' are taken as 0.0035 and 0.011 respectively, according to Wilson et al. (2012), and were not reparameterised.

4.2.6.3 ***Resistance r_{sc}***

In the original energy budget model formulation, the bulk canopy stomatal resistance (r_{sc}) is calculated following the Jarvis (1976) approach as the product of a minimum stomatal resistance (r_{smin}) and time variant factors which are always ≥1. These modifiers simulate the response of stomatal resistance to climatic conditions that, according to Noilhan and Planton (1989), are f_1 for solar radiation (RS), f_2 for the water stress experienced by plants, f_3 for water vapour deficit of the atmosphere, and f_4 for a temperature stress factor.

$$r_{sc} = \frac{r_{smin}}{LAI} f_1(RS) f_2(SWC) f_3(e^*(T_a) - e_a) f_4(T_c - T_a) \tag{4.50}$$

and,

$$f_1(RS) = \frac{1+f}{f + \frac{r_{smin}}{r_{smax}}}, \ \ where \ \ f = 0.0055 \frac{2RS}{LAI} \tag{4.51}$$

$$f_2(SWC) = \begin{cases} 1 & when \quad SWC > w_{fc} \\ \dfrac{w_{fc} - w_{wp}}{SWC - w_{wp}} & when \quad w_{fc} \geq SWC \geq w_{wp} \\ \infty & when \quad SWC < w_{wp} \end{cases} \tag{4.52}$$

$$f_3(e^*(T_a) - e_a) = \frac{1}{1 - D_p(e^*(T_a) - e_a)} \tag{4.53}$$

$$f_4(T_c - T_a) = \frac{1}{1 - D_T(T_c - T_a)^2} \tag{4.54}$$

This formulation has been implemented in CenW_HH but has not been used in the rest of the study; however, an option in the user interface allows easy

selection and use of this stomatal conductance simulation option. Instead, stomatal resistance was calculated based on the formulation proposed by Ball et al. (1987) that links stomatal conductance to net photosynthesis (A_n), CO_2 concentration at the leaf surface (C_s) and relative humidity (RH). Leaf stomatal conductance is given by Equation 4.55:

$$gs_l = m\, A_n \frac{RH}{C_s} + g_0 \tag{4.55}$$

where m is the slope of the relationship between g_{sl} and $An\ \frac{RH}{C_s}$, which represent the stomatal sensitivity factor (Harley et al., 1992), and g_0 is the residual stomatal conductance (when A_n approaches zero) and is expected to remain constant. In contrast, the parameter m is expected to vary in response to the amount of soil water available for plant uptake (water stress). The model deals with it by varying m linearly between two extreme values as water stress develops (Equation 4.56).

$$m = m_2 + (m_1 - m_2)\, WaterLimit \tag{4.56}$$

where m_2 and m_1 are the parameters for stressed and unstressed plants, respectively, and $WaterLimit$ is the water limitation experienced by plants that is recalculated at every time step and depends on soil water contents in the different soil layers and on root distribution with depth.

It is important to note that leaf stomatal conductance is iteratively coupled to the photosynthesis routine as described in the section that describes the leaf photosynthesis modelling and its upscaling to the canopy scale (Chapter 3).

The upscaling of leaf stomatal conductance follows the studies of Ding et al. (2014) and Zhang et al. (2011) with use of leaf area index.

4.2.6.4 ***Resistance r_{ss}***

The soil surface resistance (r_{ss}) represents an empirical term that is intended to account for the resistance of evaporation through soil pores at the soil surface and to the directly overlaying air. When the upper-most soil layer is completely

wet, soil surface resistance is minimal. According to Sellers et al. (1996), many studies found it necessary to include this resistance term in models in order to prevent excessive evaporation rates from the soil surface.

Different formulations are available because in many studies the authors have derived their own relationships, which in most cases take into account the soil texture, moisture content, and thickness of the soil layers. Some formulations found in the literature are given below and showed very different behaviour when plotted in response to soil water content when the empirical parameters were not adjusted (not shown). In the following equations, W_{sat} represents the soil water content at saturation (%), the first relationship was proposed by Fen Shu (1982):

$$r_{ss} = 3.5\left(\frac{W_{sat}}{SWC}\right)^{2.3} + 33.5 \tag{4.57}$$

Camillo and Gurney (1986) derived a linear equation to represent the response of the soil surface resistance to soil moisture content according to Equation 4.58.

$$r_{ss} = 4140(W_{sat} - SWC) - 805 \tag{4.58}$$

where W_{sat} is the relative soil water content at saturation and SWC the relative soil water content observed at any given time in the top soil layer.

In the formulation proposed by Kondo et al. (1990), the soil surface texture and physical properties had a strong effect on the value of the parameters (Equation 4.60).

$$r_{ss} = \frac{a(W_{sat} - SWC)^b}{0.229\ 10^{-4}\ \left(\frac{T_s}{273.15}\right)^{1.75}} \tag{4.59}$$

where a and b are parameters which depend of soil properties. Kondo et al. (1990) reported the parameter values for sandy soils of a = 8.32 $\cdot$ 10^5 and b = 16.6, and a = 2.16 $\cdot$ 10^2 and b = 10 for loamy soils, respectively.

The formulation proposed by Vandegriend and Owe (1994), unlike all other formulations presented in this section, does not use the water content at saturation but rather the residual soil water content, which corresponds to the remaining water at very high extraction pressure, above the wilting point extraction pressure. In this case, r_{ss} is expressed as:

$$r_{ss} = 10e^{0.3563(W_{res}-SWC)} \tag{4.60}$$

where W_{res} is the residual soil water content of the top soil layer.

In the study of Randall et al. (1996), another formulation was also used according to Sellers et al. (1996), which is given by Equation 4.61.

$$r_{ss} = \max\left[23.6\,;\,694 - 1500\left(\frac{SWC}{W_{sat}}\right)\right] \tag{4.61}$$

Sellers et al. (1992) also derived a relationship between the soil water content and the soil surface resistance used to limit the evaporative fluxes from the top soil layers to be used in the SiB2 model (Equation 35 a in Sellers et al. (1992)):

$$r_{ss} = \exp\left[A - B\left(\frac{SWC}{W_{sat}}\right)\right] \tag{4.62}$$

For the purpose of this study, the formulation proposed by Sellers et al. (1992) has been used in the model, and parameters A and B from Equation 4.62 were adjusted. After CenW_HH parameterisation, the values that gave the best fit of the model compared with observations were, in this study, A=8.3 and B=3.85, which are very similar to values used in other studies. Sellers et al. (1992) reported values of 8.2 and 4.3 for A and B respectively, Kustas et al. (1998) used A=8.4 and B=5.9 for simulating water fluxes of a semi-arid watershed in Arizona, and Mo and Liu (2001) used the same values as Sellers et al. (1992).

Overall, the different Equations gave similar relationships between the soil surface resistance and soil water content (Fig. 4.3). The trends of these curves show that, as expected, the value of the soil surface resistance diminishes as the soil water content increases. This is expected because as the soil gets

dryer, the amount of water in the soil pores spaces is reduced and so the resistance should increase to reduce the amount of water that is lost through soil evaporation.

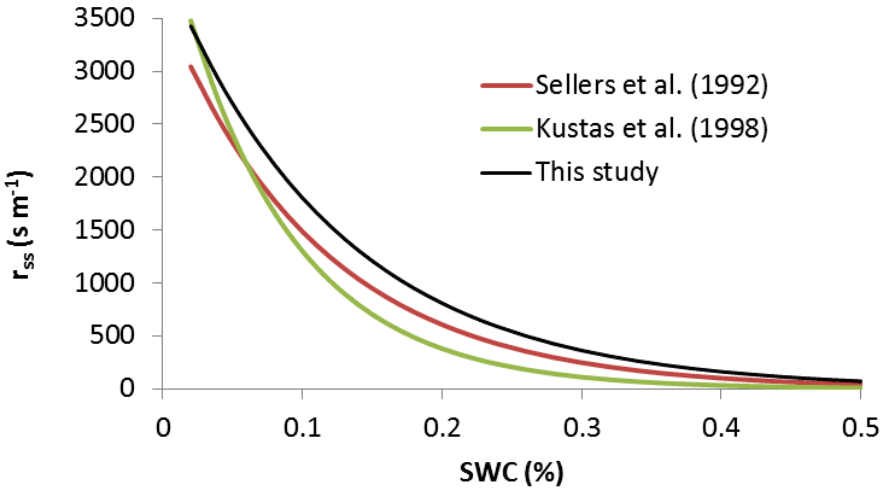

Figure 4.3: Soil surface resistance (r_{ss}) response to top soil water content (SWC). The relationship is given according to Equation 4.62.

4.2.6.5 ***Resistance r_{aa}***

In this study two methods for the calculation of the aerodynamic resistance between the canopy source height and the atmosphere just above the vegetation layer (see Fig. 4.1) have been tested and can be used in CenW_HH:

- The first one, proposed by Mahrt and Ek (1984), has been used in the modelling study of LoSeen et al. (1997) and takes into account the effects of atmospheric stability on the value of the resistance:

$$r_{aa} = \frac{1}{C_q \, u_a} \tag{4.63}$$

where u_a is the wind speed at the measurement height and C_q an exchange coefficient that depends on atmospheric stability based on the stability criteria given by the value of the Richardson number (Ri , Equation 4.64):

$$Ri = \frac{g(T_a - T_s)(z_{ref} - displ)}{{u_a}^2} \tag{4.64}$$

where g is the acceleration due to gravity (9.81 m s^{-2}), T_a is air temperature at the measurement height z_{ref}, u_a is wind velocity at z_{ref} (m), T_s is the soil surface temperature, and displ (m) is the zero plane displacement height for the canopy.

For stable atmospheric conditions (Ri > 0), the exchange coefficient C_q is given according to Equation 4.65:

$$C_q = \left[\frac{K}{\ln\left(\frac{z_{ref} - displ + z_0}{z_0}\right)}\right]^2 \frac{1}{(1 + 15\,Ri)(1 + 5Ri)^{0.5}} \tag{4.65}$$

where z_0 is the roughness length of the canopy (m) and K represents the von Karman's constant (0.4).

In the case of unstable conditions (Ri < 0), C_q is calculated by Equation 4.66.

$$C_q = \left[\frac{k}{\ln\left(\frac{z_{ref} - displ + z_0}{z_0}\right)}\right]^2 \left(1 - \frac{15\,Ri}{1 + C(-Ri)^{0.5}}\right) \tag{4.66}$$

with C given as:

$$C = \frac{75k^2\left(\frac{z_{ref} - displ + z_0}{z_0}\right)^{0.5}}{\left[\ln\left(\frac{z_{ref} - displ + z_0}{z_0}\right)\right]^2} \tag{4.67}$$

- The second method used to compute the aerodynamic resistance r_{aa} is the method using the formula derived by Shuttleworth and Gurney (1990) as given by Equation 4.68, which is very similar to the Equation 4.45 for the calculation of the aerodynamic resistance between the soil surface and the canopy source height.

$$r_{aa} = \frac{1}{k\,u^*}\,ln\left[\frac{z_{ref} - displ}{h - displ}\right] + \frac{h}{n\,K_h}\left[\exp\left(n\left(1 - \frac{z_0 + displ}{h}\right)\right) - 1\right] \quad (4.68)$$

where all parameters and variables have already been described above.

In the rest of the study, only the resistance r_{aa} calculated from Equation 4.68 was used because this formulation gave the best results in the model parameterisation and comparison with fluxes measurement (see Chapter 5 for the model/data agreement).

4.3 Implementation in CenW_HH

4.3.1 Solving equations to close the surface energy balance

As we have seen, the modelling scheme proposed by Shuttleworth and Wallace (1985), described above, was designed to split the contributions from the soil and the vegetation layer above it. In all the equations derived to calculate fluxes, the temperatures of the different components of the ecosystem need to be calculated. Changes in temperatures are usually fast and even with a short time step of less than an hour temperature changes can have a significant feedback on energy fluxes such as net radiation, sensible heat, and evapotranspiration (Sellers et al., 1986). In the development of CenW_HH, two different approaches were used to calculate these temperatures with the same overall objective of closing the energy budgets at the soil surface (Equation 4.4), the litter layer (Equation 4.6), which is on top of the soil surface, and the vegetation cover (Equation 4.5).

The first method was used for the vegetation and used the Newton–Raphson algorithm (Anderson et al., 2000) to modify the temperature of the canopy (only one layer of vegetation is considered in the model) based on measured meteorological variables, stored water in the vegetation (intercepted rainfall and dew deposition) and the calculation of the fluxes as described in the previous sections of this chapter. For the first time step of a model run, vegetation temperature was initially set to be equal to air temperature. Energy fluxes were

then calculated based on this set of temperatures. If temperatures of any component (soil, vegetation and litter layer) were too high, net losses of energy would be calculated and the converse if set temperatures were too low. If such energy imbalances were found, temperatures would be adjusted and the calculations be repeated.

This procedure is iterative and calculations are only stopped when closure of the energy budget is achieved to within a defined precision (99.5 %), or when a specified number of iterations are reached (50 in the model). If energy closure could not be reached within those 50 iterations, a second method, as described below, is used. However, for all runs with CenW_HH for Scott farm, such an issue arose only three to five times per year, mostly during drought conditions. Under most circumstances, the algorithm usually reaches a solution after less than ten iterations.

The second method consisted of solving the paired differential equations of soil surface, litter layer, and vegetation temperatures. This method was used for the calculation of temperatures changes of the soil surface and the litter layers and of the vegetation canopy when the first method (Newton–Raphson) failed to converge on a solution. The use of this routine involves a reduction of the calculation time step to ensure the stability of the solution. This is achieved by recalculating at each time interval the thermal conductivities of the system components, assuming that climatic variables remain constant over the 30 minutes of the model time step and that the reactions are sufficiently fast so that the equilibrium is reached over this time span.

Thermal conductivities are calculated according to the formulation proposed by deVries (1963) as the sum of thermal conductivities of the different compounds of the material of interest.

Changes in soil temperature with depth are simulated in CenW_HH according to soil surface fluxes and the redistribution of heat between layers, assuming there is no transfer of heat beyond the deepest soil layer of the profile (see Equations 4.35 and 4.36).

Overall, the implementation of this procedure within the modelling framework was complex and time consuming but is functioning well and gave valuable results.

4.3.2 Simulation results and discussion

The modelled and observed energy and water fluxes are compared in Chapter 5, and this comparison will not be repeated here. However, as we have seen, CenW_HH adjusts vegetation, soil, and litter temperatures based on climatic conditions to close the energy balance of the system. Also, as stated in Sellers et al. (1986), temperature changes are fast and have important feedback effects on other processes and energy fluxes. In this section, therefore, the behaviour of simulated temperatures has been studied because they are important variables driving the behaviour of the overall model.

Figure 4.4a shows the diurnal variations of observed air temperature (T_{air}) and solar radiation ($SolRad$) and the modelled soil temperatures at 25 mm, 200 mm and 500 mm depth for the 01/01/2008 at Scott Farm, which was a summer day at the start of the observation period. Diurnal soil temperatures changes can be described as sinusoidal and it clearly shows that the amplitude of soil temperature is lower at depth and that the phase of the function is shifted toward the right side of the graph, e.g. maximum and minimum are reached later at greater depths.

The surface of the soil is highly affected by solar radiation (as we can observe in Figure 4.4a, the temperature at 25-mm depth falls during night time periods, reaching its minimum just before sunrise. As solar radiation increases over the course of the day, temperature also increases sharply as it depends on the amount of solar radiation received. The temperature reaches its maximum a few hours after solar noon, after which it falls again with decreasing solar radiation because of the soil thermal inertia.

Deeper in the soil profile, temperatures are more stable because heat transfer occurs through conduction, which reduces the amount of heat reaching the deepest soil layers. At 500 mm below the surface the temperature only varies a few tenths of a degree Celsius over one day (24 hours), whereas over the same

time period, the temperature at 25 mm depth varies between a minimum of 16.5 °C and a maximum of 29.7 °C.

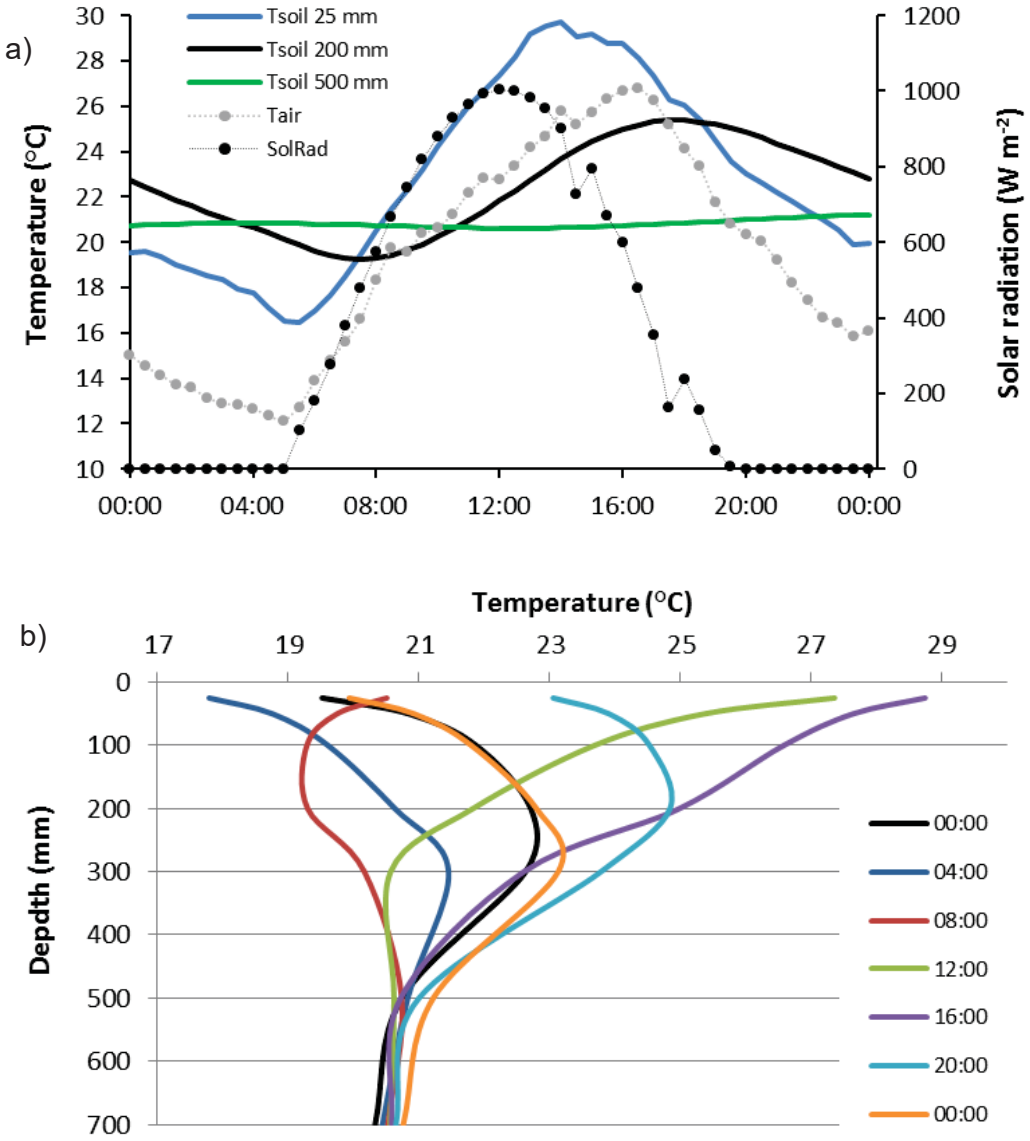

Figure 4.4: a) Diurnal variations of modelled soil temperatures at 25 mm, 200 mm and 500 mm depth along with observed (measured) air temperature and solar radiation. b) Modelled diurnal changes in soil temperature profile. Simulations and observations are for the 01/01/2008 at Scott farm as an illustrative example.

Figure 4.4b shows the temperatures profiles modelled by CenW_HH. The x-axis shows temperatures, and the y-axis shows soil depth (0 is the soil surface) and each coloured line represents the soil temperature profile at a given time of the day as shown in the figure. As seen in Figure 4.4a, diurnal temperature

variations are more important for the top soil layers than deeper in the soil. Between 12am and 4am (night time period), the top soil (<500 mm) is cooling and deepest soil layers (>500 mm) are still continuing to become slightly warmer because the previous day's heat is still slowly being conducted to depth in the soil. From sunrise onwards, the temperatures of shallow soil layers increase again. At 12pm, the top soil reaches 27.3 °C and more heat is transferred through the profile, which increases temperatures of soil layers at greater depths. At 4pm, while the first (top) layer of soil has already started to cool down (Fig. 4.4a) as less solar radiation is received, the temperature of deeper layers continues to increase as heat is transferred downwards. This time lag between the timings at which maximum temperatures were observed down the soil profile is caused by the soil thermal inertia. By 12am (orange line that corresponds to the temperature profile modelled 24 hours after the first plotted profile shown in black), the shape of the temperature profile is very similar to the one observed the night before (black line) with, however, a slight shift of all temperatures toward the right that corresponds to a longer-term general temperature increase across all soil layers, indicating that the soil is still warming up towards its overall summer maximum temperature.

Figure 4.5 shows long-term soil temperature variations. Figure 4.5a shows the temporal series of modelled soil temperatures at 25 mm and 700 mm over the 2 years of the study period (see Chapter 5 for more details on the experimental site and data). We can see the seasonal variations of modelled soil temperatures and once again the differences in variability with depth, which have been described above. During droughts (yellow boxes), the temperatures of the upper soil layers increased sharply. During the severe drought of 2008, the temperature of the 25 mm soil layer could reach temperatures above 50 °C.

This was principally due to high solar radiation in combination with the absence of cooling from transpiration because soil water reserves had been depleted. The heat capacity of a dryer soil is also much lower than that of a wet soil, so the same energy imbalance can lead to much larger temperature fluctuations. Soil temperatures could therefore reach much higher values during drought

periods than they could during wet periods with similar solar radiation. With cooling from transpiration, soil temperatures did not generally exceed 30 C.

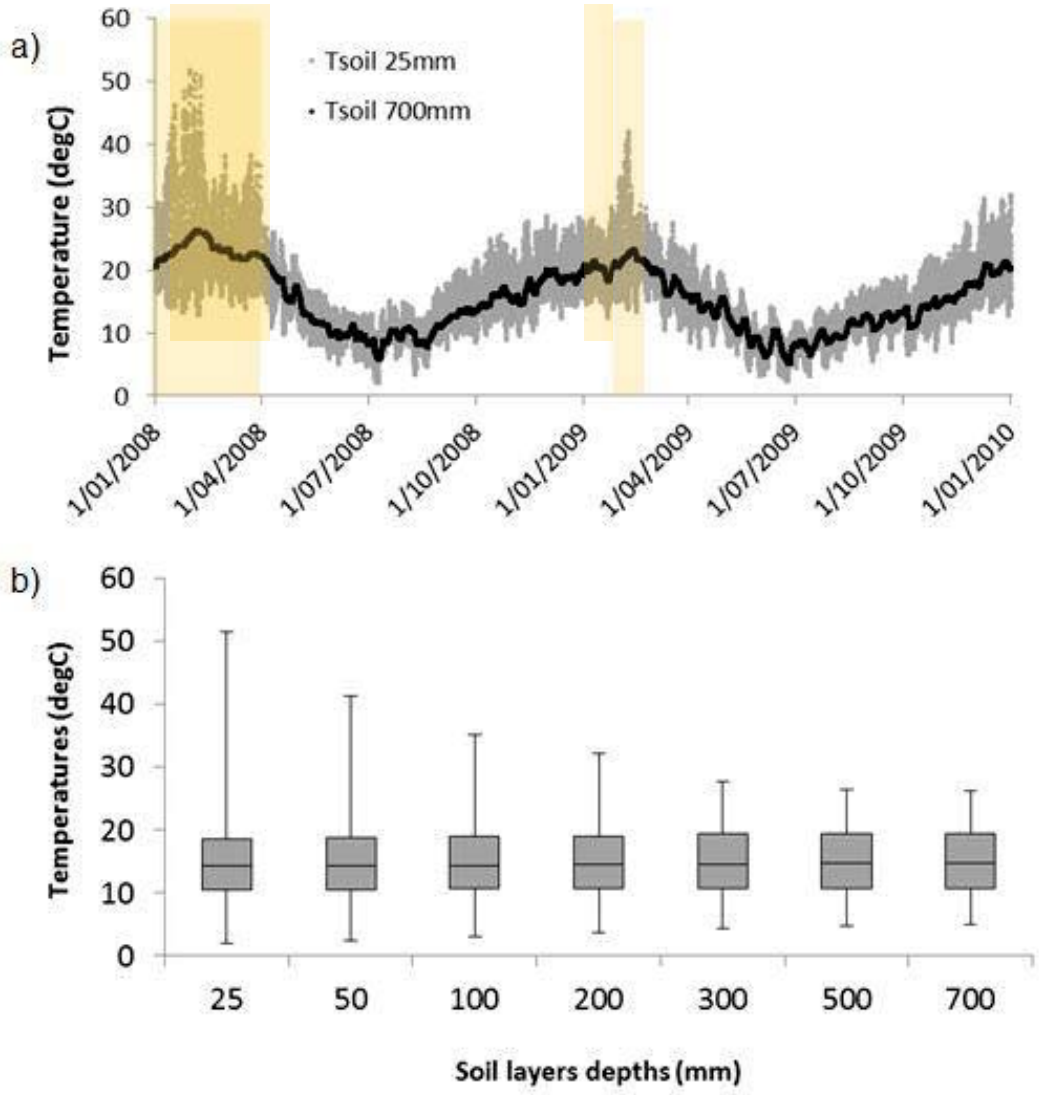

Figure 4.5: Long-term variations of soil temperatures. a) 2 years' time series of modelled soil temperatures for two depths (25 mm grey and 700 mm black), the shaded boxes correspond to drought periods. b) Box plots showing the annual variability of soil temperatures at different depths. Horizontal bar = median; upper and lower limits of box = 75 and 25 percentiles, respectively; upper and lower tails = maximum and minimum values, respectively.

Figure 4.5 b) shows box plots of modelled soil temperature variations over 2 years for different depths in the soil (given on the x-axis). The horizontal bars in the boxes give the median temperature at depth, the upper and lower sides of

the boxes give the 75 and 25 percentiles, respectively and the upper and lower tails provide the maximum and minimum values, respectively.

Changes in soil temperature are also affected by the soil cover, e.g. the amount of vegetation absorbing the solar radiation before it reaches the soil surface, the soil albedo that causes the reflection of solar radiation at the surface, and the soil composition and water content and evaporation as illustrated on Figure 4.5a, where a drastic increase of temperature is observed during drought periods (shaded boxes). In CenW_HH, half-hourly changes of the soil temperature profile are simulated and the modelled temperatures in each of the soil layers are used to simulate soil organic carbon decomposition in the different pools for each soil layers. This is also an important change in the model as microbes are considered to be much more active at higher temperatures.

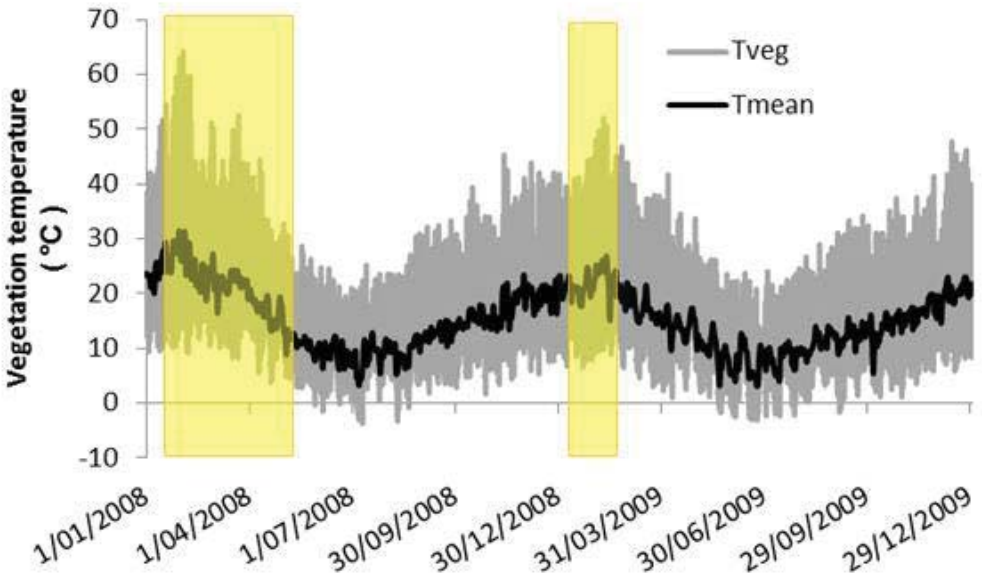

Figure 4.6: Time series of half hourly (T_{veg}) and daily averaged (T_{mean}) vegetation temperatures obtained from the modelling of one paddock at Scott Farm over the 2 years of eddy covariance measurement. The shaded boxes correspond to drought periods.

Vegetation temperature also depends on the upscaling scheme chosen to make the runs as stomatal conductance is at first calculated in the PS routines described in Chapter 3 and then used in the energy and water budget

procedure. If the big leaf scheme is used, the vegetation characteristics are chosen in such a way that the whole canopy is represented as a single leaf and only one temperature is modelled, which represents the temperature of all the leaves. The other upscaling scheme used in this study corresponds to the sun/shade model (dePury and Farquhar, 1997) which, as we have seen in Chapter 3, separate the contributions of the sunlit and shaded portions of the canopy. Also, as we have seen in this chapter, the energy budget and the temperature of a surface depends on the solar radiation impinging on it and so, if the sun/shade scheme is used, two temperatures are derived for each fraction of leaves and averaged according to their relative amount in each class. This is a simplification of what would actually happen in the real world as heat transfers between those two types of leaves is not taken into account in CenW_HH.

Diurnal variations of canopy temperature are important (Fig. 4.6) because the thermal capacity of leaves is small and so their temperatures could adapt fast to changes in climatic conditions (Sellers et al., 1986; LoSeen et al., 1997). Temperatures reach high values during drought periods because when water is limiting, stomata close, thus limiting or stopping the transpiration flux that under non-water limited conditions cools the leaves, and causes substantial increases in temperature.

Figure 4.7 shows the diurnal variations of solar radiation, air temperature, and the components of the energy budget, e.g. net radiation (R_n), soil heat flux (G), sensible heat flux (H) and evapotranspiration (LE) for 2 given days with contrasting water stress. Those 2 days were chosen so that climatic conditions experienced on both days were similar (Fig. 4.7a, b), and comparable amounts of vegetation were present on the paddock but with plants having access to different soil water contents, leading to different water limitation levels.

The 01/01/2009 corresponds to a summer day with high solar radiation and air temperature and with no water limitation (Fig. 4.7a). During night-time, net radiation was negative (R_n<0). This is a normal pattern because with no incoming solar radiation, the energy balance is essentially given by the loss of emitted longwave radiations (which is proportional to the fourth power of the absolute temperature). With overall energy loss, the soil heat flux must also be

negative (G<0), indicating a gradual soil cooling during the night. The soil surface is losing heat mainly through radiative transfer, thus reversing the temperature gradients that occur during the day. Sensible and latent heat fluxes are close to 0 under observed conditions on those specific nights. The 26/01/2008 also corresponds to a summer day with high solar radiation and air temperature but with plants suffering strong water stress (Fig. 4.7b, d).

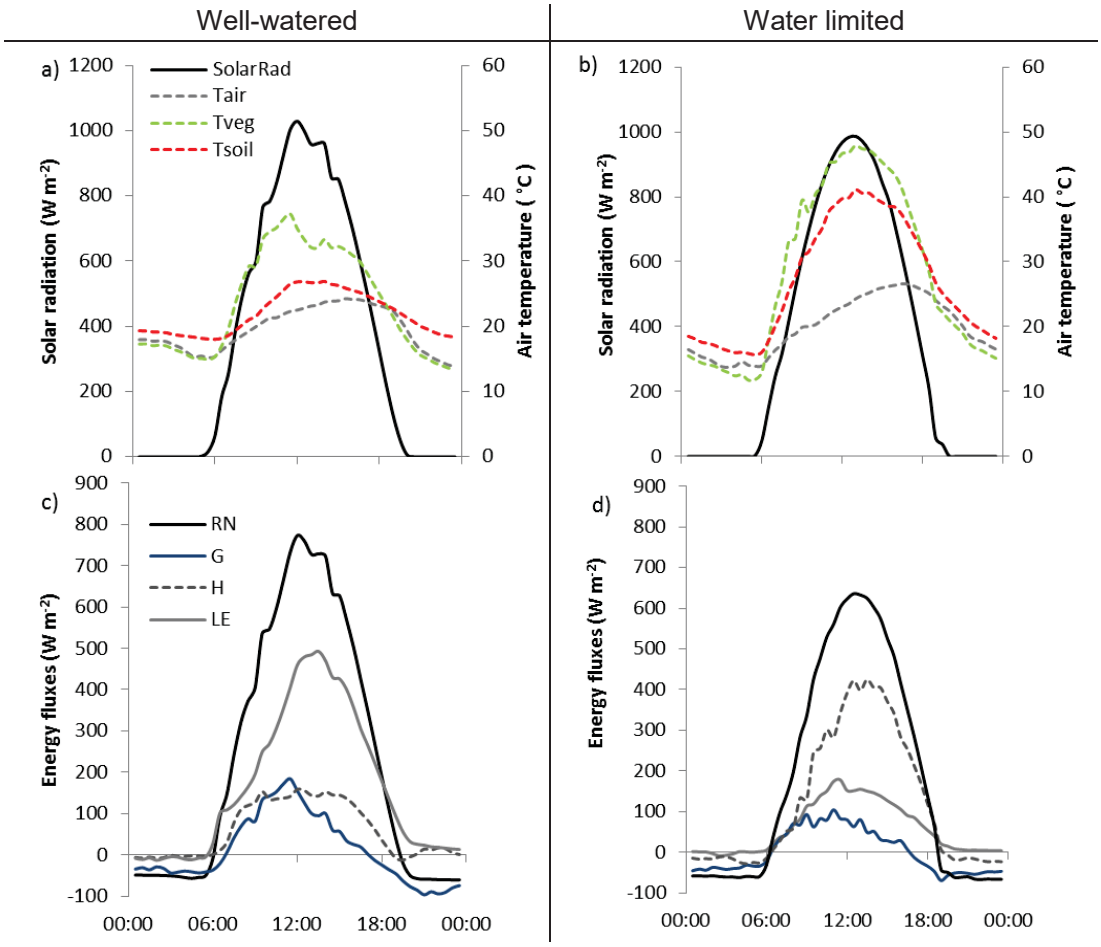

Figure 4.7: Diurnal variation of solar radiation and air, vegetation and top soil temperatures (a and b) and the components of the energy budget, net radiation, soil heat flux, sensible heat flux and evapotranspiration (c, d) for 2 summer days. The two plots on the left (a, c) are for the 01/01/2009, when there was no water limitation (before the summer drought), and the plots on the right (b, d) are for the 26/01/2009, in the middle of a summer drought when there was a strong limitation by water availability.

It is clear from the comparison of these 2 days (Fig. 4.7) that the availability of soil water is very important both for the surface energy budget and for the evolution of surface temperatures.

When water is not limiting (01/01/2009), the latent heat flux is about two to three times higher than the latent heat flux under water-stressed conditions (Fig. 4.7). Under well-watered conditions, the soil and vegetation reach maximum temperatures of 26 and 37 °C, respectively. In contrast, when the ecosystem experiences water stress, cooling through transpiration is limited, and the incoming energy needs to be dissipated through sensible heat (Fig. 4.7d) which causes an increase in surfaces temperatures (Fig. 4.7b), with the soil surface reaching 40 °C and the vegetation temperature approaching 50 °C.

These modelling results confirmed the strong influence of water limited conditions on the simulations of soil and vegetation temperatures as well as on carbon, water and energy fluxes and on vegetation growth and photosynthesising capacity. A good representation of the underlying processes affected by these conditions and a proper parameterisation of the CenW_HH ecosystem model are required to make proper runs (see Chapter 5 for the evaluation of the model).

4.4 Summary and Conclusions

This chapter presented mathematical relationships describing the energy and water budgets and some other modifications implemented in the newly developed half-hourly model designated as CenW_HH.

The Shuttleworth and Wallace (1985) modelling scheme was chosen and equations were modified to include a litter pool on top of the soil surface and a multilayer soil profile for heat and water transfers. This has made it possible to simulate fluxes mechanistically between the different components of the ecosystem and the atmosphere.

The net energy gain of the surface is the sum of absorbed solar (short-wave) radiation plus absorbed atmospheric longwave radiation. This energy gain must be balanced by the longwave radiation emitted from the surface, which is principally controlled by its temperature and losses as latent heat through evapotranspiration. Remaining energy imbalances can be dissipated through positive or negative sensible heat exchanges with the surrounding air and heat

fluxes into or out of the soil. Soils generally heat up during the day, absorbing excess energy, and cool during the night, releasing that stored energy again.

The sensible heat flux corresponds to the transport of heat by convection in the atmospheric boundary layer. The sensible heat flux is directly proportional to the temperature gradient between a surface and the surrounding air divided by a resistance term which depends on surface characteristics and wind speed.

The latent heat flux, or evapotranspiration, involves a transfer of mass (water vapour) and energy between the leaf and soil surface and the atmosphere. A considerable amount of energy is required to evaporate water. Calculations of latent energy are similar to sensible heat flux calculations except that they involve the gradient of vapour pressures instead of temperature.

Heat conduction is the transfer of heat by direct contact, unlike sensible heat flux, which is due to air movement. Heat conductance depends on the thermal conductivity of the object and of the gradient of temperature. Because the heat capacity of the canopy tends to be very small, the only significant heat conductance is the energy flux into or out of the soil.

The sets of equations derived for the soil, vegetation, and litter energy budgets are solved iteratively and/or with the use of a Newton–Raphson algorithm by changing the components' temperatures until the energy balance of the system is closed.

Soil temperature simulations show there is a strong diurnal variability in the response of soil surface temperature to radiative forcing. Drought periods cause a large increase in temperatures, mostly because evapotranspiration is reduced, or even stopped, which limits the dissipation of incoming energy by latent heat transfer. Soil layers deeper in the soil profile do not respond as strongly as the soil surface to climatic conditions, but longer-term seasonal changes are clearly visible. In the half-hourly ecosystem model, this procedure is coupled to the soil organic matter dynamics routine, which uses the modelled soil temperature and moisture profiles to drive the temperature and moisture response functions of SOC decomposition in the different soil layers.

Flux partitioning and energy budgets are thus strongly affected by water limitation and the temperatures dynamics of the different components of the ecosystem. Overall, the energy and water budget procedure as implemented in CenW_HH seems to respond properly to the different climatic conditions experienced at Scott Farm. Comparison of modelled energy and water fluxes and soil temperature with observations is studied in Chapter 5.

CHAPTER 5: CASE STUDY OF A DAIRY FARM IN THE WAIKATO REGION OF NEW ZEALAND

5.1 Introduction

The first part of this chapter (Section 5.2) gives a description of the study site where carbon balances studies were undertaken using EC measurements and the data used to parameterise the CenW_HH model. It also includes a brief description of modifications made to the original CenW model except for the carbon assimilation and energy budget procedures, which have been described in detail in the previous chapters. The second part of this chapter (Section 5.3) shows the model's ability to simulate observations at different temporal scales once CenW_HH had been fully parameterised. The last part (Section 5.4) compares gap filled and CenW_HH modelled NEP fluxes under climatic conditions under which it was impossible to obtain EC measurements.

5.2 Materials and methods

5.2.1 Description of the study site

Detailed descriptions of the experimental set up, measurement, data processing and site management have already been published (Mudge et al., 2011; Rutledge et al., 2014, 2015), and in the following, only specific details relevant for the present study have been repeated.

The experimental site was established on a DairyNZ experimental dairy farm located near Hamilton, Waikato, New Zealand at 37.46 °S 175.22 °E for a total duration of 4 years starting in January 2008. The available dataset consists of continuous, 30 minute averaged, eddy-covariance measurements of net carbon dioxide (*NEP*) and water vapour (*ET*) exchange. These data are complemented with conventional meteorological data (solar radiation, air temperature, relative humidity and wind speed and direction) and measurements of soil moisture and temperature at different soil depths.

There also were daily records of grazing and harvesting events, supplementary feeding and other major management interventions occurring on each individual paddock during the time span of the study. Over the first year of the study (2008), there were also weekly records of total above ground biomass

measurements for most of the paddocks based on calibrated visual assessment as described in Piggot (1989). Most of the farm and the soil surface and subsoil horizons within the flux footprint area are classified as Matangi silt loam which is an Orthic Gley Soil (Mudge et al., 2011).

At the beginning of the study, the grazing species were typical of a New Zealand pastoral system with a mixed sward of perennial ryegrass (*Lolium perenne*) and white clover (*Trifolium repens*) growing on the paddocks of the study area. It was assumed that all the paddocks had well established pastures at the beginning of the study. The overall farm stocking rate was about 3 cows ha^{-1} and cattle are allowed to graze, in small herds of 9–21 cows, all year round on individual 0.5 ha paddocks. Even though herd and paddock sizes were smaller than on a typical commercial dairy farm, the stocking rate and management practices were similar (Mudge et al., 2011).

The farm was managed by DairyNZ researchers and the Waikato University eddy-covariance measurement team had no control over farm operations. All the paddocks received between 150 and 200 kgN $ha^{-1}y^{-1}$, but there are no detailed records of the precise timing of fertiliser applications. In this study, the total amount of annual fertiliser applied to the paddocks were split into several applications of 35 kgN ha^{-1} with the assumption that fertiliser was applied to all paddocks at the same time. It was assumed that there were no fertiliser applications during the summer (December/February) and winter (June/August) months but –one application was assumed to be supplied in autumn (March/May) and all other applications supplied in spring (September/November) which corresponds to the time of the year with climatic conditions for maximum nutrient demand for plant growth while minimising losses of nitrogen (mainly through volatilisation and leaching).

As the farm does not have a typical layout but consists of small individually grazed paddocks placed around the tower (Fig. 5.1), the model runs needed to take this aspect into account. In most cases, grazing events were restricted to a single day, but sometimes they were spread across several consecutive days. Unfortunately, grazing records only indicated the theoretical presence of cattle on the different paddocks on given days but provided no information about the time at which cows were moved in and out of particular paddocks. The small

herd size and the rotational grazing of individual paddocks led to considerable heterogeneity within the flux footprint. However, the respiration of a relatively small number of cattle present on the different plots at a given time would not have dominated the underlying CO_2 fluxes as completely as it would have if one big herd had been grazing (Kirschbaum et al., 2015).

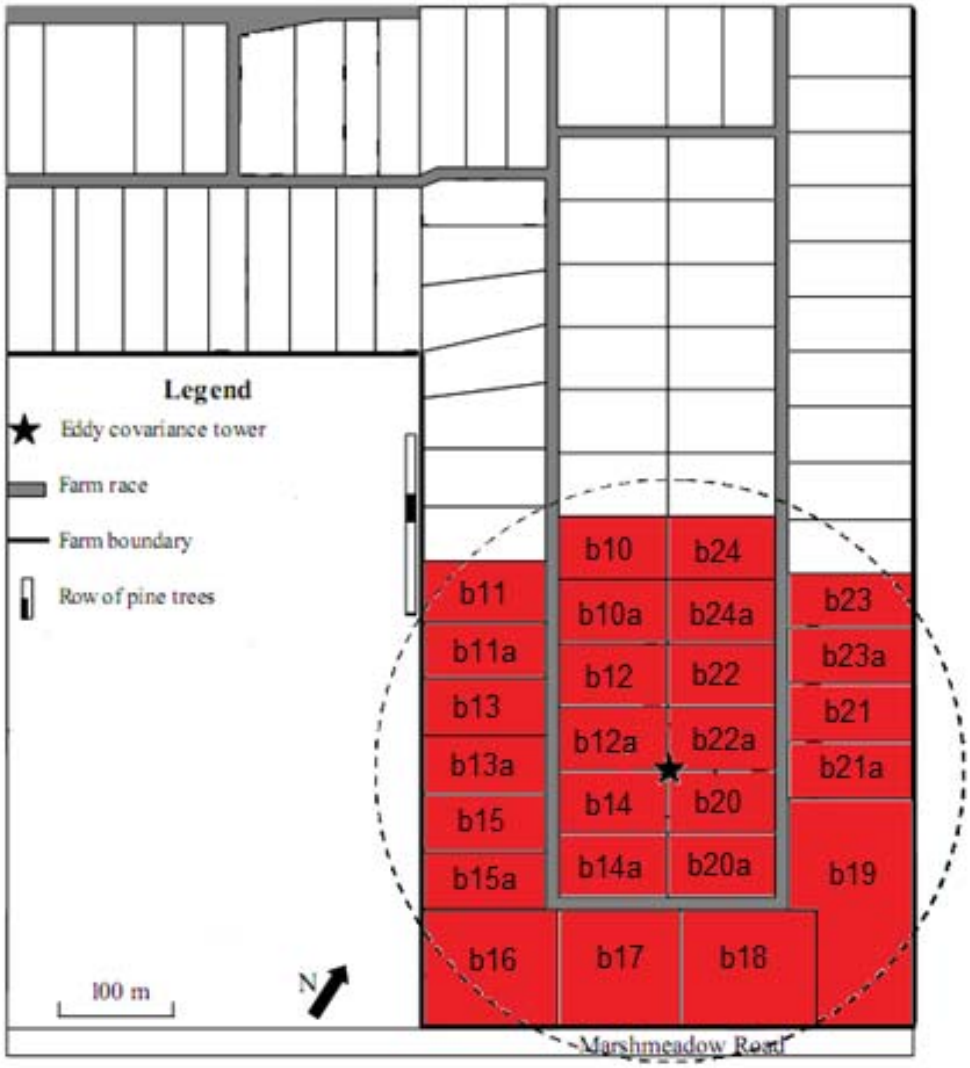

Figure 5.1: Scott Farm layout adapted from Mudge (2009). The paddocks coloured in red are those that were modelled individually.

Study of the footprint of EC measurements indicated that around 80% of the flux contribution came from 26 paddocks around the tower (red area in Fig. 5.1). Outside the farm boundaries, most of the land is also used for pastoral farming with the exceptions of a country road, 5 houses and a small area cultivated with

corn and ryegrass. Any fluxes coming from outside the farm borders were, therefore, thought to be similar to those coming from Scott farm (Mudge et al., 2011). To account for the fluxes from paddocks further away of the tower than the 26 paddocks individually modelled, and for which no information were available, an additional generic paddock was used, with grazing not restricted to distinct days, but assumed to occur continuously at a low rate.

The present work used only the 2008 and 2009 data for a well-established ryegrass/white clover pasture with the principal aim of the present work being the development and testing of an appropriate model and to test possible problems with the collection of EC data and standard gap-filling routines in this special ecosystem.

5.2.2 Data processing and data availability

CO_2 flux data were recorded as 30-minute averages of measurements made at 20 Hz. The availability and reliability of calculated fluxes was checked according to different criteria (see below) before being used. This work was carried out by the University of Waikato team ahead of this modelling study and detailed description of the flux processing has already been reported in Mudge et al. (2011), Kirschbaum et al. (2015), and Rutledge et al. (2015), so only the main issues relevant to the aims of the present study have been repeated here.

The quality of gas measurements was assessed in relation of the different criteria listed in Table 5.1.

Table 5.1: Criteria used to check the quality of exchange gas measurements as reported in Rutledge et al. (2015)

Causes of data rejection
Warnings from the IRGA or the sonic anemometer indicate a sensor failure
Unreliable readings from the LI-7500 (LI-COR Inc., Lincoln, NE, USA) CO_2 analyser as indicated by a deviation of the automated gain control (AGC) signal from the 'baseline', resulting, for example, from rain or fog
Fluxes above or below a filtering threshold ($\|NEE\| > 50$ μmol m^{-2} s^{-1})
Lack of stationarity in the high frequency CO_2 concentration time series

indicated by large standard deviation in CO_2 density (>15 mg m^{-3} during the day, and >30 mg m^{-3} at night)
Low friction velocity (< 0.11 m s^{-1})
Large deviation of calculated fluxes from the mean of computed values for corresponding times of day across a 20-day moving windows e.g. when fluxes exceeded a threshold number of standard deviations (night-time = 4, daytime = 3) from the mean flux.

These necessary data processing routines are used to assess the quality and reliability of the measurements by avoiding the inclusion of data that are apparently erroneous or at least unreliable. Exclusion of some data generate gaps in the dataset, however (Table 5.2).These gaps need to be filled to get daily mean carbon fluxes for comparison with modelled fluxes (with the daily version of CenW), or to get annual carbon balances at the farm scale.

Table 5.2: Summary of the availability of *NEP* data for the two years of the study at Scott Farm. The numbers of missing data represent the number of gaps during the period of time considered. The percentages of missing data are separated into three categories: 'Total' is the percentage for the entire set of data, while 'Night time' and 'Daytime' are the percentages of gaps occurring during the night and daylight periods, respectively

Year	Total number of missing data	Percentages of missing data		
		Total	Night time	Daytime
2008	10585	60.3	81.3	39.1
2009	10562	60.3	81.4	39.0
2 year average	10573.5	60.3	81.3	39.0

On average, about 60% of data were missing in the dataset for the two years of the study, mostly during night-time (81.3%), while daytime data could be obtained more reliably, with data missing for only 39% of the time. The difference in the gaps distribution between daylight and night-time hours is typical for EC studies and mainly caused by the smaller fluxes and higher atmospheric stability at night time.

This implied that any data summed to time periods longer than the initial 30-minutes measurements periods were highly dependent on the quality of the gap-filling techniques that were used. For the present work, the gap-filling and flux partitioning used an online procedure (www.bgc-jena.mpg.de/bgi/ index.php/ Services/ REddyProcWeb) described in Reichstein et al. (2005) whereby the filling of gaps was done according to an improved sliding window look-up table that used the co-variation of *NEP* with meteorological conditions and its temporal auto-correlation, e.g. *NEP* fluxes are looked-up for meteorological conditions of a fixed margin in the temporal vicinity of the gap to be filled (Moffat et al., 2007; Mudge et al., 2011). The Reichstein et al. (2005) routine could then be used to partition *NEP* fluxes between *GPP* and *ER* fluxes. For this partitioning phase, only actual measurements with good turbulence conditions were used. At first, the routine selected night-time *NEP* fluxes as in this case *ER* = *NEP* because at night *GPP* = 0. The dataset is then split into consecutive periods of several days (10 is the default value) and for each of them where more than six data points were available and a temperature range greater than 5 °C was found, the total ecosystem respiration rates were regressed against their corresponding soil temperature to determine the parameters of a Lloyd and Taylor (1994) equation type (Equation 5.1).

$$ER(T) = ER_{ref} e^{E_0\left(\frac{1}{T_{ref}-T_0} - \frac{1}{T-T_0}\right)} \quad (5.1)$$

where T_{ref} is the reference temperature which was fixed to 10 °C as in Lloyd and Taylor (1994), T_0 is a regression parameter which was set to –46.02 °C according to the original model, E_0 is the activation energy regression parameter, which was allowed to vary, and ER_{ref} is the ecosystem respiration at reference temperature, which was calculated within the Reichstein et al. (2005) routine. Once all parameters were determined for every half-hour, Equation 5.1 was then used to calculate both night-time and daytime half-hourly *ER* fluxes by extrapolating night-time respiration in the daylight hours according to the corresponding measured soil temperatures.

Finally, once *NEP* and *ER* fluxes were available for every half-hour of the measurement period, gross primary production was simply deduced as the

difference of net ecosystem productivity and total ecosystem respiration (*GPP* = *NEP* – *ER*).

In the context of the present work, gaps caused by the presence of grazing animals within the flux footprint were particularly problematic. In some cases, measured *NEP* fluxes might have been rejected by the filtering procedure simply because grazing animals were present within the footprint and respired carbon dioxide at high rate. The filtering procedure could have rejected these observed values simply because they deviated too much from calculated fluxes at corresponding times on other days. Gap-filled values would then have been used instead of the missing observations but the gap-filled data would not have corresponded to what actually happened at those times. These issues, together with their significance for total annual fluxes, are developed more fully in Chapter 6

Even if gap-filling algorithms are deemed reliable, because we don't have actual observations, it is not guaranteed that the conditions, under which gaps (missing or filtered out data) occurred, might not be systematically different from the conditions with reliable data and that the gap-filled method is not systematically wrong under those conditions. The model was parameterised only with the best quality effectively measured data because having used gap-filled fluxes might have led to a slightly different parameter set. More importantly, one goal of this thesis was to study the bias added to the dataset through the use of gap-filling technique which can only be achieved by running a model with the same time step as the sampling rate of the eddy covariance system (30 minutes at Scott Farm).

The selection of the observations to be used in the model parameterisation was made according to the criteria:

- Use only "actual" observations and discard all periods where gap-filled data would have to be used.
- Exclude all periods where fluxes were affected by grazing events occurring close to the tower, i.e. on the four paddocks directly surrounding the EC tower.

This data screening process aimed to use only the best quality and most reliable observations to limit errors in the model parameterisation. Removing unreliable data created new gaps in the dataset. There were, however, sufficiently large numbers of continuous good quality data segments to parameterise the CenW_HH model. Effects of having cattle in the footprint of the tower on the model data agreements of carbon fluxes were studied in detail in Chapter 6 of this study.

Meteorological measurements made at the study site were used as inputs for the model. They comprised global solar radiation, air temperature, relative humidity and wind velocity. It has been decided, as part of the model development plans, to keep the number of required meteorological inputs to as few as possible and to use only the most frequently measured and available observations to ensure that the model could be readily used for as many places as possible.

Meteorological measurements started only when EC fluxes started to be measured at the study site, but the model was run for four years before the studied period to ensure good initial conditions were reached at the beginning of the validation period (Kirschbaum et al., 2015). Daily weather data were available from a nearby weather station (6.4 km from the EC tower). They were corrected for any systematic climatic differences as described in Kirschbaum et al. (2015). 30-minute weather records were reconstructed from these daily weather data using simple equations (sinusoidal and linear equations) whose parameters were derived from observations made at Scott Farm in 2008 and 2009 and calculations of solar position characteristics modelled for every half hours according to Reda and Andreas (2003).

5.2.3 Other model modifications for half-hourly runs

The implementations of two central procedures in the model have been described in detail in Chapter 3 (carbon assimilation) and Chapter 4 (energy and water budgets). These new routines were specifically required to run the model at the intended 30 minute time step. However other procedures also needed to be adjusted to make proper model runs. In most cases, modifications of the model source code were managed with the aim to simulate half hourly

fluxes with the same model structure that is used for the daily version of the model, but simply with a reduced simulation time step. For many routines, this reduction of the simulation time step could be simply implemented by adjusting the values of the time dependent parameters to the new running time step.

The water contents of each soil layer were simulated every 30 minutes driven by the energy and water budget procedures to constrain SOM decomposition and carbon transfers between pools (with the same decay constants and the same interactions between the different pools that are used in the daily version of the model). The temperature profile within the different layers in the soil, together with their sub-diurnal variations, are now calculated in much greater detail than for the daily version of the model as described in Chapter 4.

The grazing procedure was slightly modified to ensure that biomass was evenly removed in the model throughout the day to approximate the grazing animals' continuous respiration and methane release during each half hour time step.

A few routines, however, could not be adjusted by a simple adjustment of the relevant time steps. One of those dealt with the uptake of nitrogen from the soil. The daily version of CenW made the simplifying assumption that equated the amount of N mineralised each day with that implicitly assumed to be present in a pool of mineral N. Appropriate model parameterisation then allowed sensible relationships to emerge between daily amounts of N being mineralised and quantities leached or taken up by plants.

However, that simplification could not be maintained when the calculation time step itself was allowed to change (such as between half-hourly and daily). It thus required an explicit modelling of nitrogen dynamics dependent on calculated soil nitrogen concentrations. A new nitrogen pool was therefore added to the model to simulate the nitrogen uptake by plants. The new formulation involves the calculation of the nitrogen concentrations in soil layers which are available for plant uptake and the use of Michaelis-Menten kinetics to simulate the nitrogen uptake by plants (York et al., 2016) at any specified time step (Equation 4.69). Calculation of plant nitrogen uptake rate depends of the amount of roots biomass in each soil layers (in kgC ha^{-1} per layer) with no

separation of available nitrogen into ammonium and nitrate ions. The nitrogen uptake per soil layer is calculated according to Equation 4.69.

$$I_n = \frac{I_{max}\,(C_l - C_{min})}{K_m + (C_l - C_{min})} \tag{4.69}$$

Where I_n is the root nitrogen uptake rate (gN kgC^{-1} s^{-1}) in the soil layer where C is the amount of carbon contained in the roots present in the considered soil layer, I_{max} is the maximum nitrogen uptake rate (gN kgC^{-1} s^{-1}), K_m is the Michaelis-Menten constant (gN L^{-1}) which represents the solution concentration at $0.5 * I_{max}$, C_l is the ion concentration in solution (gN L^{-1}) and C_{min} is a threshold ion concentration for which the nitrogen uptake (I_n) is zero (gN L^{-1}).

The overall plant nitrogen uptake rate is then calculated by summing over the uptake rates from all soil layers.

5.2.4 Model parameterisation and performances

5.2.4.1 *Overview*

The newly developed version of the CenW model, hereafter called CenW_HH, running with a half-hourly time step, and which has been described above, was parameterised and validated against EC and ancillary measurements made at Scott Farm using data from the first two years of the data acquisition period.

The optimisation of model parameters was achieved by selecting the set of parameters that minimised the residual sum of squares between eddy covariance measurements of carbon (NEP) and water vapour (LE) and their respective simulated values over the two years of the study period. Only actually measured thirty minute fluxes were used in this procedure. Gap-filled data were discarded from the original dataset to avoid possibly biasing the parameter fitting if systematic errors had been present in the gap-filled data. Because the presence of grazing animals within the flux footprint caused large negative carbon fluxes, data were also discarded if they corresponded to times when any of the 4 paddocks closest to the tower were grazed and within the footprint and so have affected, to some extent, carbon fluxes measured by the eddy-covariance tower (Kirschbaum et al., 2015). The apparent problems introduced through grazing on the inner four paddocks have been studied and

described separately and in detail in the next chapter (Chapter 6). Over the two years of the study, there were a large number of observations available which made it possible to be selective in the data that were used in the fitting routines.

Originally, the daily version of CenW was run in combination with an Excel spreadsheet for the parameter fitting routine. However because of the large size of the output file when the half-hourly version was used, a programme was written in R to read the output file, appropriately combine the fluxes from the 26 individually-modelled paddocks with the footprint model and calculate the residual sum of squares (see below).

5.2.4.2 *Description of the parameter fitting routine*

The automatic parameter fitting routine used in this study to optimise model performances against observations works by minimising the residual sum of squared differences between model estimates and measurement of selected variables.

The routine consists of three components: the first part consists of the normal CenW_HH calculation routines, the second part is the parameter optimisation procedure which is also running inside the CenW_HH ecosystem model and the third one is an external program written in R (R Core Team, 2016) that is used to calculate the sum of squared differences between observed and modelled variables. These routines in the different modules were designed to work together to optimise the parameter set (Fig. 5.2).

The parameter fitting process starts by simultaneously launching CenW_HH (Fig. 5.2) and running the R script. The R script reads the “Data files” and waits to get access to modelled variables. CenW_HH starts by running with an initial set of parameters. The user then selects a set of parameters to optimise and specifies a number of running conditions, such as a maximum number of iterations and allowable ranges within which selected parameters are allowed to be optimised. The model then reads the climate data in the “Weather data” file and makes a normal run and once it reaches the end of the running period, it writes a first text file containing the modelled variables (“Output Files”) and creates an empty second file (“Job Done”) to indicate to the R program that the model run has been completed and that the “Output file” is available.

The R program then loads the modelled variables and uses the footprint information to predict fluxes which should be similar to those measured by the EC system. Predicted fluxes are compared to their observed counterparts and the residual sum of squares of the differences between model predictions and observations are calculated. The value is then written to the “Residuals” text file.

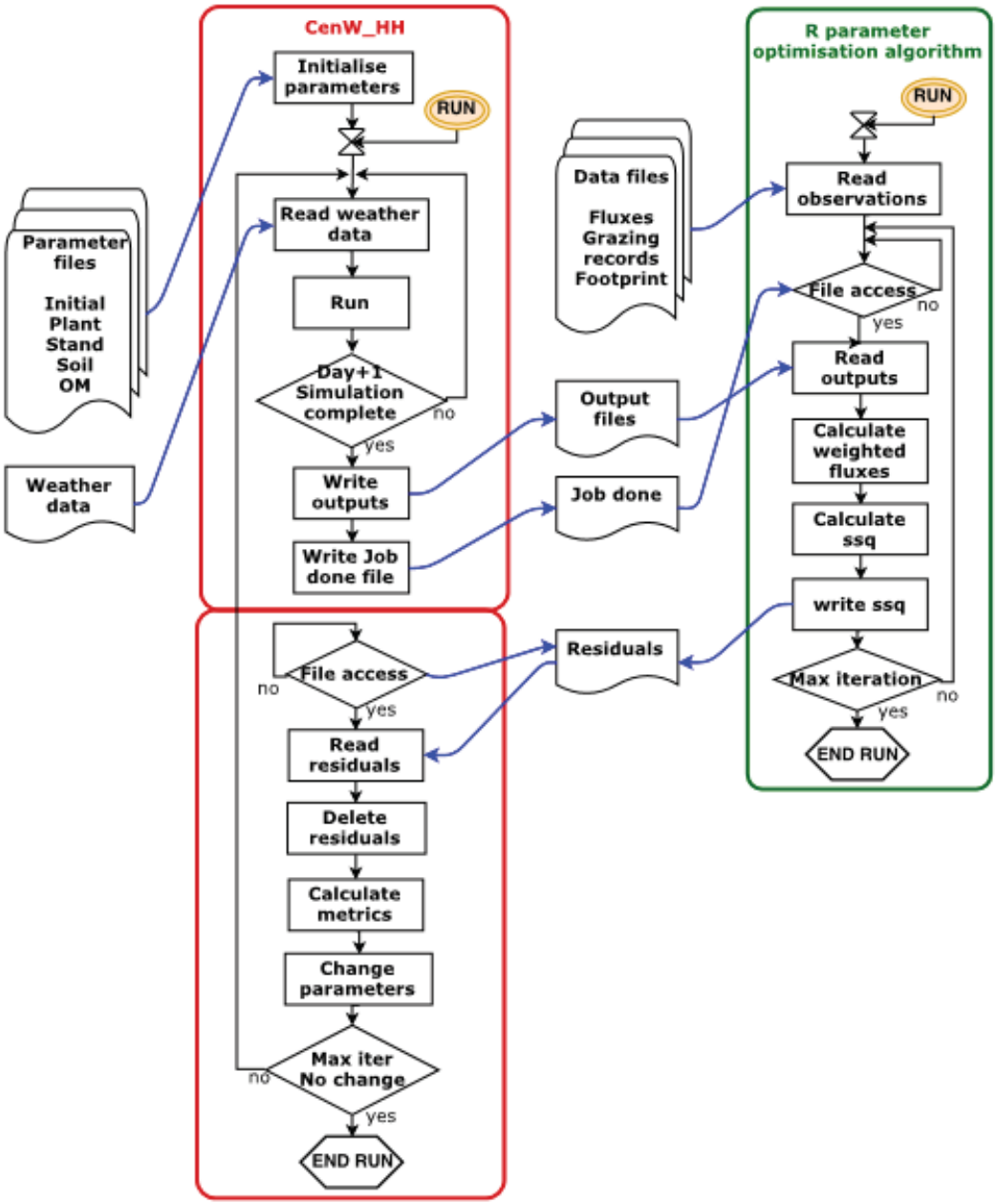

Figure 5.2: Schematic representation of the parameter fitting procedure used to optimise the CenW_HH parameters.

CenW_HH meanwhile is in waiting mode, but once the Residuals text file has been written, CenW_HH accesses it, reads the value written in it and uses it to calculate metrics to change the parameters values towards minimising the residual sums of squares. These processes are repeated iteratively until an optimal parameter set is found and changes of parameters no longer improve model simulations or until the maximum number of iterations is reached. When the optimal set of selected parameters is achieved, the user can choose either to save them in the “Parameter files” or not.

5.2.4.3 ***Statistical criteria to evaluate model performances***

Model performances were evaluated by comparing time series of measurements with their corresponding simulated values and by calculating different statistical indices which gave information on model/data agreement. The principal criterion used to assess model/data goodness of fit was the Nash-Sutcliffe efficiency (*NSE*) calculated from Equation (5.2).

$$NSE = 1 - \frac{\sum_{i=1}^{N}(O_i - S_i)^2}{\sum_{i=1}^{N}(O_i - \bar{O})^2} \tag{5.2}$$

Where O_i represents an observed variable measured at time (i), S_i is the corresponding modelled variable and $\bar{O}$ is used for the average of all observations.

NSE can range from −∞ to 1. An efficiency of 1 (*NSE* = 1) corresponds to a perfect match between modelled and observed data. An efficiency of 0 (*NSE* = 0) indicates that the model predictions are as accurate as the mean of the observed data, whereas an efficiency less than zero (*NSE*< 0) occurs when the observed mean is a better predictor than the model or, in other words, when the residual variance, which is described by the numerator of Equation (5.2), is larger than variance of the data (given by the denominator of Equation (5.2)). Essentially, the closer the model efficiency is to 1, the more accurate the model is. Also, *NSE* is sensitive to extreme values and might yield sub-optimal results when the dataset contains large outliers.

The second criterion is the root mean square error (*RMSE*) which measures how much error there is between modelled and observed datasets and which has been calculated as:

$$RMSE = \sqrt{\frac{1}{N}\sum_{i=1}^{N}(S_i - O_i)^2} \tag{5.3}$$

Where *N* is the number of data points.

The calculated *RMSE* values will have the same units as the selected variables, and so, it is not possible to directly compare *RMSE* values from variables with different units. This index has been widely used in modelling studies and small values of *RMSE* indicate better model predictions.

The mean bias error (*MBE*) was also used because it indicates the percentage of error of modelled data and it was calculated according to Equation (5.4)

$$MBE = \frac{1}{N}\sum_{i=1}^{N}(S_i - O_i) \tag{5.4}$$

Positive values of *MBE* indicate a model overestimation with respect to measured data, while negative values indicate a model underestimation.

The goodness of fit was studied graphically from scatter plots of observed variables against their modelled counterparts. Linear regression between simulations and observations were also used to evaluate model performance. The regression provides two pieces of information: 1) the slope of the linear least squares regression line, which indicates whether or not there is a bias, and 2) the coefficient of determination (R^2), which assesses the scatter, or how much of the variance between the two variables is explained by the linear regression.

The coefficient of determination is calculated by taking the square of the Pearson correlation coefficient (*r*) which is given by:

$$r = \frac{\sum_{i=1}^{N}(S_i - \bar{S})\,(O_i - \bar{O})}{\sqrt{\sum_{i=1}^{N}(S_i - \bar{S})^2 \sum_{i=1}^{N}(O_i - \bar{O})^2}} \quad (5.5)$$

The numerator corresponds to the covariance of the two variables and the denominator is the product of their standard deviation and so, Equation (5.5) gives information about the correlation between model simulations and observations. Values of *r* range between +1 for a perfect increasing linear relationship and -1 for a perfect decreasing relationship whereas a value of 0 indicates no linear relationship between observed and simulated variables.

Because the coefficient of determination is the square of the Pearson correlation coefficient, it takes values between 0 and 1.

The higher r^2 is the more confidence one can have in the derived linear equation. Statistically, the coefficient of determination represents the proportion of the total variation in the y variable that is explained by the regression equation. Even if r and r^2 have been widely used for the evaluation of models, these metrics are very sensitive to outliers (Legates and McCabe, 1999).

Overall, all the metrics presented above were used to determine to what extent the model simulations were representative of observations. In the model/data comparisons presented in the following section, the density of points was also used because the large numbers of points in the comparisons (35 040), over the 2 years of the study, were overlaying and because of the presence of some outliers, not representative of the overall goodness of fit of predicted and observed values.

5.3 Parameterisation and validation of the half hourly model

5.3.1 Effects of using the flux footprint on the modelling of fluxes

As described in Chapter 2, the eddy covariance technique uses a single point measurement above the ground to infer the fluxes coming from an upwind surface area.

Because of the Scott Farm layout and grazing management, it was not possible to simulate the whole farm (or paddocks on the area around the flux tower) as a whole because of the heterogeneities in pastures caused by the rotational grazing of the small 0.5 ha paddocks of the study site. The 26+1 paddocks surrounding the EC set up have been simulated independently based on the available information, such as farm grazing records which recorded grazing events that took place on each individual paddock on a daily basis as well as the amount of supplement feed brought to different paddocks to sustain animals' needs when pasture growth was insufficient. However, just simulating the exchange rates of individual paddocks was not sufficient for comparing measured and modelled *NEP* fluxes. It was also necessary to aggregate the individually simulated fluxes from the different paddocks into one flux comparable to the one effectively measured by the eddy covariance system.

Two options can be used to fulfil this goal and were tested in the following section: the first option is to simply take the average of the fluxes from the 27 individual paddocks (Equation 5.6) which will be called F_1.

$$F_1 = \sum_{i=1}^{27} \frac{1}{27} \, Flux_i \tag{5.6}$$

where F_1 is the resulting modelled flux and $Flux_i$ is the flux simulated for the i^{th} paddock, where *i* represents the index of each individual paddock.

The second tested option was to use a footprint model and weight the relative contribution of each individual paddock by the approximated source area of fluxes effectively measured by the eddy covariance system mounted on the tower. This flux is designated here as F_2.

$$F_2 = \sum_{i=1}^{27} RFP_i \; Flux_i \tag{5.7}$$

where RFP_i is the relative contribution of the i^{th} paddock so that the sum of all *RFP* is equal to 1.

The second method contains more information on the originating source of the overall flux at any given time but it also requires more information to be used in the model. Modelling the source area of measured fluxes requires

measurements of wind speed and direction for all half hourly periods over the time span of the study. As a consequence, the performance of CenW_HH partly depends on the accuracy and reliability of the footprint model (in this study, the Kormann and Meixner (2001) analytical footprint model).

It is important to note that the model was parameterised with the use of the detailed footprint contribution of each individual paddocks, and that for the comparison of the two methods described above, all simulated variables for the 27 paddocks were exactly the same with the only difference being their spatial integration.

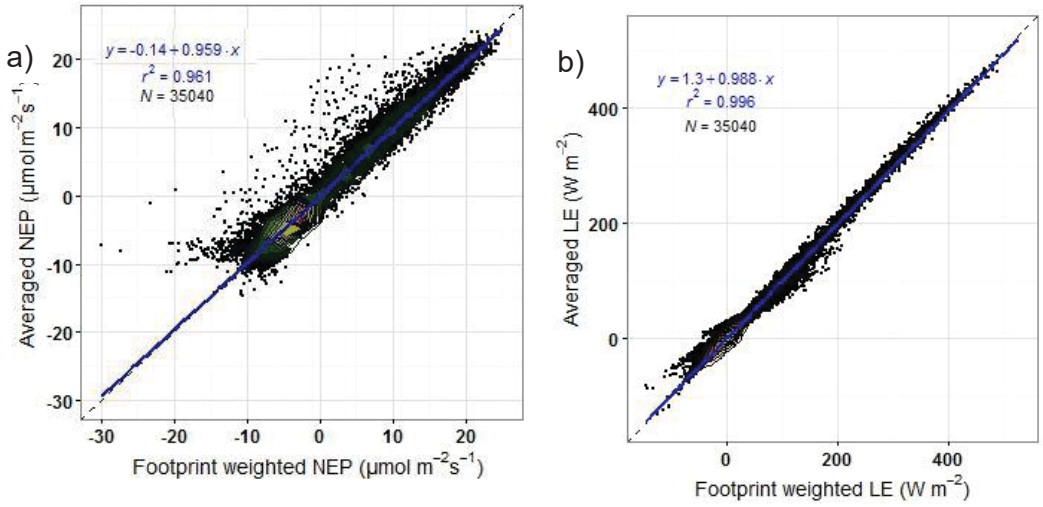

Figure 5.3: Direct comparison of modelled *NEP* a) and *LE* b) fluxes when the footprint information is used (x-axis) or when the modelled fluxes from each individual paddocks were averaged (y-axis).

For the purpose of this study, the complete dataset with 2 years of measured and gap-filled data (N=35 040) was used to compare observations and modelled fluxes either derived by taking the averaged contribution of all paddocks (“averaged fluxes”) or by using the footprint information (“footprint-weighted fluxes”) according to Equations 5.6 and Equations 5.7, respectively

Figure 5.3 shows the scatter plots of the direct comparison of the modelled net carbon flux a) and evapotranspiration rates b). The x-axis for both graphs corresponds to the footprint weighted fluxes and the y-axis to the averaged fluxes. Plots are interesting because they directly show the differences related to the choice of the spatial integration of fluxes.

The net carbon flux (*NEP*) appears to be more affected by the choice of the integration method compared to the latent heat flux (Fig. 5.3) as indicated by the points that deviate from the one to one line. In both cases, modelled evapotranspiration rates are very similar, which is indicated by the slope of the linear regression that is very close to 1 (0.998), an r^2 of 0.996 and a model efficiency of 0.996 (Table 5.3). *NEP* proved to be more sensitive to the choice of integration with a slope of 0.96 for the linear regression, an r^2 of 0.96 which is appreciably lower than for *LE* and a model efficiency of 0.96 (Table 5.3).

Table 5.3: Summary of statistical criteria used to evaluate the model performances with and without using footprint information for net ecosystem productivity (*NEP*), latent heat flux (*LE*) and sensible heat flux (*H*) over two years (N=35 040). a and b represent the coefficients of the linear regression between modelled and observed fluxes as shown in red on Figure 5.4 and which is given as y=ax+b (a is the slope and b is the intercept)

	Comparison of footprint weighted and averaged modelled fluxes			Statistics of the comparison of observations against model simulations					
				With footprint weighting			Average of all paddocks		
	NEP	LE	H	NEP	LE	H	NEP	LE	H
NSE	0.96	0.99	0.99	0.85	0.85	0.76	0.84	0.85	0.75
RMSE	1.40	6.13	3.57	3.01	34.31	28.38	3.01	33.92	29.14
MBE	0.16	-0.67	-0.21	17.10	-23.20	43.00	-16.1	-22.2	44.80
a	0.97	0.99	0.99	0.99	0.89	0.95	1.03	0.90	0.95
b	-0.14	1.30	0.41	-0.08	20.32	-4.31	0.07	19.32	-4.53
R^2	0.97	0.99	0.99	0.85	0.89	0.77	0.85	0.89	0.76

Graphically, the use of one or the other of these methods to spatially aggregate fluxes does not show any noticeable differences for the evapotranspiration flux (Fig. 5.4c, d) nor for the sensible heat flux (Fig. 5.4e, f). This is also confirmed by the goodness of fit criterion summarised in Table 5.3 which were not statistically different for the two tested methods.

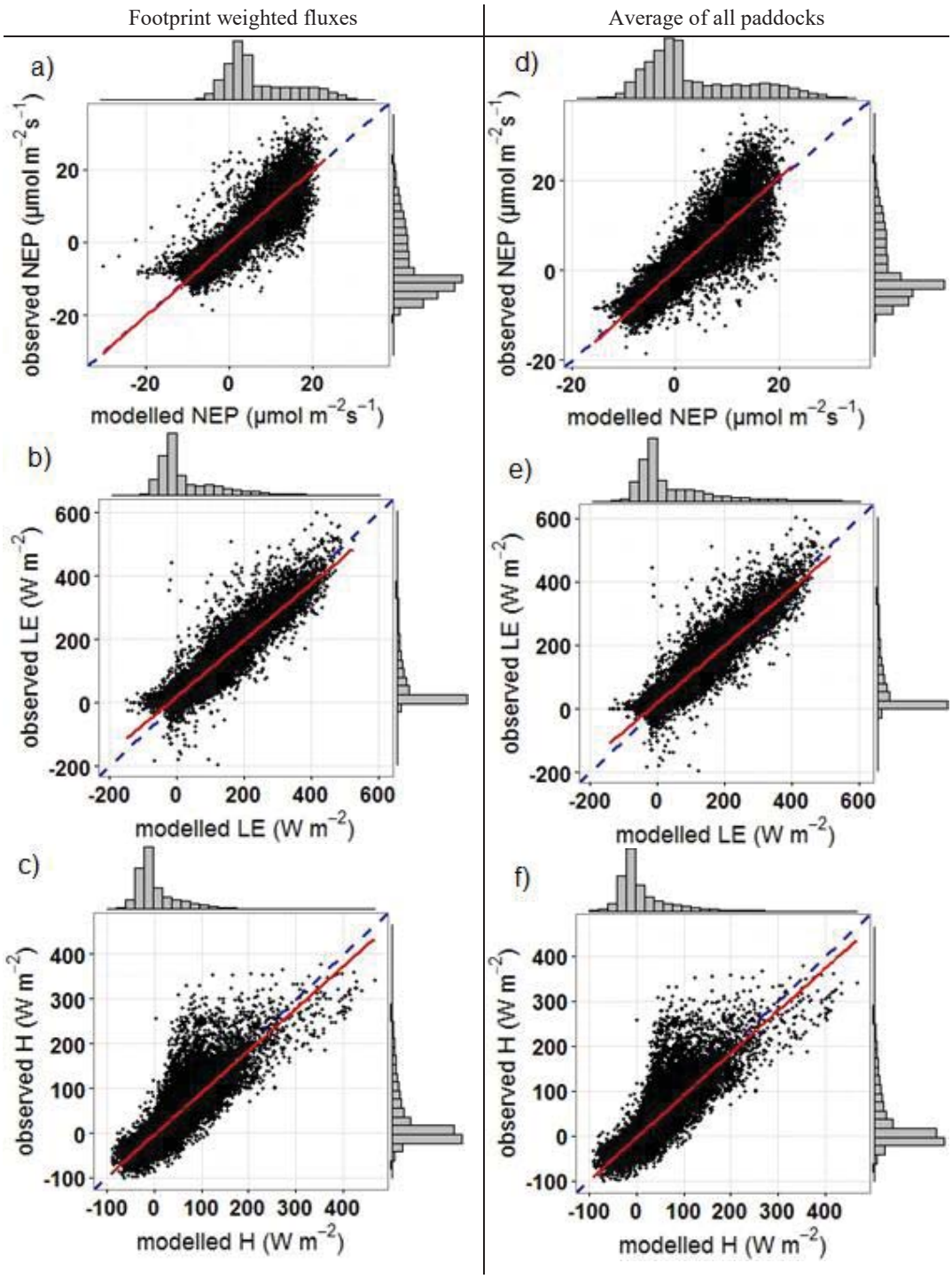

Figure 5.4: Effects of using footprint information on model/data agreements. Modelled fluxes (*NEP*, *LE* and *H*) presented on the left panels (a, b and c) were obtained by weighting each individual paddock contribution by the footprint information and panels on the right (d, e and f) were obtained by a simple averaging of the fluxes from all paddocks. The dashed blue line is the one to one line and the red line is the linear regression (equations of linear regressions and their respective coefficient of determination are given in Table 5.3).

However, like the observations made on Figure 5.3, differences were more pronounced for the carbon flux (*NEP*). It can be seen in Figure 5.4b, that most of the outlier points are on the left side of the graph on Figure 5.4a and correspond to underestimations of the half hourly modelled *NEP* fluxes, compared to observations closer to the one to one line. This tends to show a better model/data agreement for the "averaged fluxes" compared to "footprint weighted fluxes", which is, however, not confirmed by the overall model performances evaluated over the two years of the study period (Table 5.3).

The statistics reported in Table 5.3 for the evaluation of the effects of these two methods on *NEP* were very similar with a model efficiency of 0.85 when the footprint weighting is used compared to a model efficiency of 0.84 for the average of all paddocks. The biggest difference in the statistics used to evaluate model performances is found in the *MBE*; when the footprint information is used to aggregate the fluxes from the 27 individual paddocks, $MBE_{(NEP)}$ indicated an overestimation of the carbon flux by CenW_HH while the opposite was found when the average of the fluxes from all individual paddocks was used to simulate what is "seen" by the EC tower e.g. the model underestimated the observed half hourly *NEP* fluxes.

Not taking into account the footprint information smoothed the response of carbon fluxes during grazing events (Fig. 5.5).

Figure 5.5 shows that over the first night, the blue line was nearly constant, but slightly trending upwards because of decreasing night-time temperature causing a reduction of the respiration rate. Then from 6 am onwards, NEP drastically increases as it follows the daytime photosynthetic carbon uptake, with the few minor wiggles in the red line reflecting changes in radiation levels. In contrast, the green line slightly exceeded the blue line when the wind blew from a direction other than where the cows were grazing, but when the wind blew from the grazed paddocks, the net uptake rate was much lower with the weighted fluxes than with the averaged fluxes. Then from 16:00 onwards the cows were still there, but the wind consistently blew from a different direction, retaining a small signal from the grazing animals in the averaged fluxes but not showing up in the weighted fluxes.

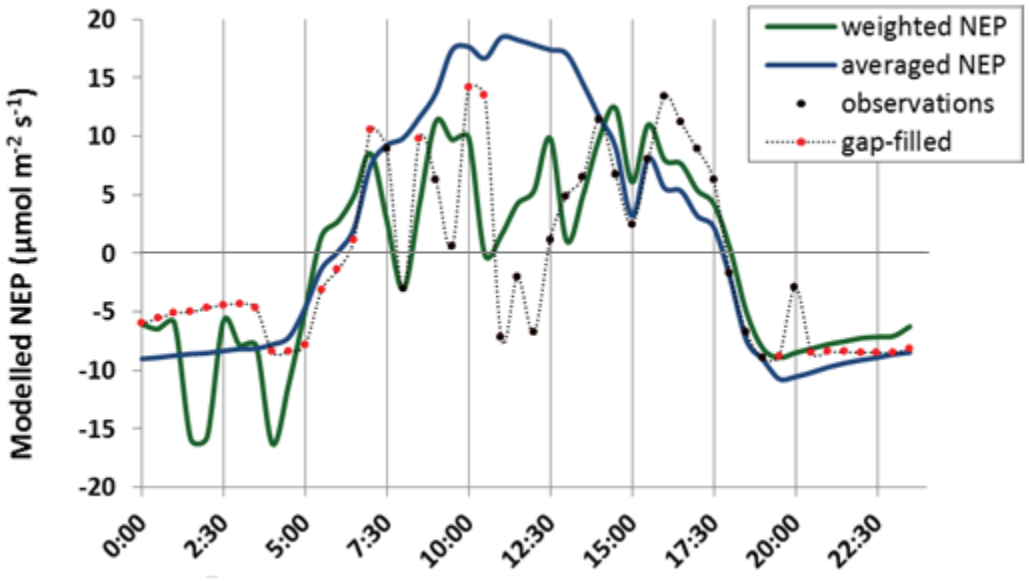

Figure 5.5: Time series of modelled half hourly NEP calculated as the average of all paddocks (blue), weighted by the flux footprint model (green) and observed (black dots) and gap-filled (red dots) NEP flux for a day where cattle were grazing paddocks within the EC tower footprint (17/12/2009).

Most of the differences between the two methods to spatially integrate contributions from different paddocks (Fig. 5.3) related to grazing events occurring on the mosaic of small paddocks around the tower (Fig. 5.5). This figure shows a time series of half hourly footprint-weighted NEP in green, averaged *NEP* (see definitions above) in blue and observed (black dots) and gap-filled (red dots) for the 17/12/2009. On this particular day, dairy cows were grazing paddocks within the flux footprint and because of their large respiratory losses of carbon, large drops in the net carbon flux seen by the tower were simulated by CenW_HH. Also, because the wind direction shifted between two measurement intervals, the footprint area moved accordingly and the contribution of the grazed paddocks was not constant over time. This is illustrated by the black line on Figure 5.5 and observed data.

Taking the average of all the simulated paddocks tends to cancel out the large respiratory losses of carbon from grazing animals (blue line on Fig. 5.5) which was also not accounted for in the gap-filled data (red dots on Fig. 5.5). In the rest of the study, the choice was made to use the footprint information to

spatially aggregate modelled fluxes as it is a more realistic way of accounting for the spatial and temporal variations of grazing animals' respiration.

Effects of grazing events on model/data agreements are studied in detail in Chapter 6 of this study.

5.3.2 Validation of the model with EC data

5.3.2.1 *Half hourly model/data comparison*

5.3.2.1.1 CO_2 fluxes

The overall aim of this section was to compare results obtained with the parameterised version of the CenW_HH model and half hourly observations of carbon dioxide fluxes (NEP, GPP and ER) measured by the eddy covariance system and gap filled using the Reichstein et al. (2005) flux partitioning algorithm over the first two years of the study (2008 and 2009).

Because the choice was made to use only the best quality measurements for the model parameterisation mainly to avoid adding any possible bias in the model parameter set, the 35 088 half hours of the measurement periods were reduced to 10 362 *NEP* observations e.g. after removing gap-filled data, and data affected by grazing animals in the footprint on the four inner paddocks around the EC tower. CenW_HH was explicitly parameterised over these 10 362 observations of net ecosystem productivity (*NEP*) as shown in Figure 5.6.

The slope of the linear regression is very close to one with a small intercept close to 0, and an r^2 of 0.819. A model efficiency (*NSE*) of 0.815 (Table 5.4) showed that the model was able to explain more than 80% of the variance in the data. It confirmed that the model was able to satisfactory simulate *NEP* fluxes measured at the Scott Farm study site.

The model was however unable to simulate very high rates of net carbon assimilation which were measured. In fact, CenW_HH could not model net C fluxes (*NEP*) higher than 20 $\mu molCO_2\ m^{-2}\ s^{-1}$, while observations indicated that the *NEP* flux could reach 30 $\mu molCO_2\ m^{-2}\ s^{-1}$. One possible explanation could be related to the fact that the model with the optimised parameter set simulates smaller maximum rates of gross carbon assimilation than the data suggest (Fig. 5.7a) and higher respiratory losses (Fig. 5.7b). Added together, they could have

limited modelled *NEP*, which would not reach the most extreme observed *NEP* values. Model parameters were set so that it was impossible to get unusually high values (parameters are bonded to keep a physical meaning and are set for the model to simulate the largest proportion of observed data); whereas observations are not constrained in that way, and occasionally high true rates will have combined with random upward scatter to give unrealistically high values.

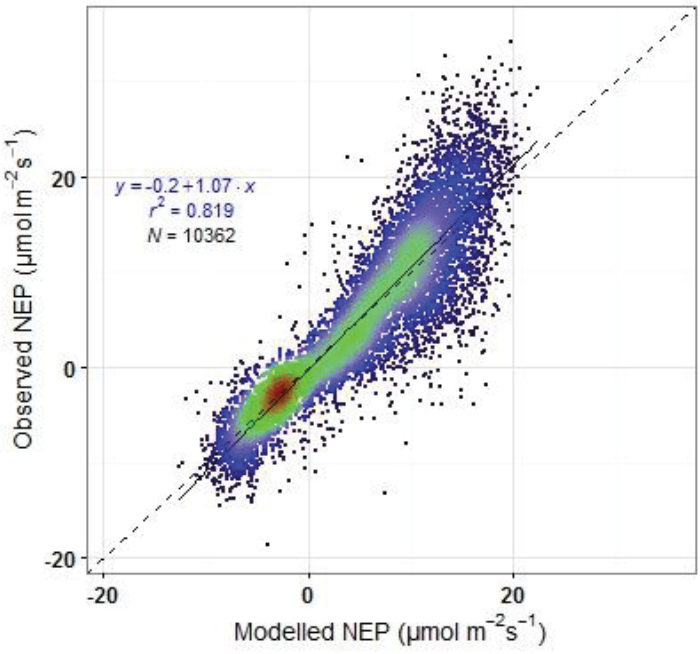

Figure 5.6: Scatter plots of observed against modelled by CenW_HH net carbon productivity (*NEP*). The dashed line is the 1:1 line, the blue line is the linear regression with the equation given on the figure with its r^2, N is the number of points on the graph and the colours were used to represent the density of points going from green for highest densities to brown for lower densities. The observed data exclude gap-filled points and cow-influenced points.

Also, as we can see from the density of points shown on Figure 5.6, most of the modelled and observed net ecosystem productivity agrees very well as they appeared to bunch around the one to one line and only a few numbers of points are responsible for the apparent large discrepancies at the highest *NEP* fluxes.

Components of the measured *NEP* flux (gross primary production and ecosystem respiration) were not used in the parameter optimisation of CenW_HH because, as explained above, those fluxes were not directly measured but derived from gap filling using the Reichstein et al. (2005)

algorithm. The aim was to avoid the inclusion of any possible systematic errors that could have been introduced through the use of gap filling models.

For the gross primary production (*GPP*), see Figure 5.7a, the agreement between CenW_HH modelled and Reichstein gap filled fluxes is, as for *NEP*, very good with a model efficiency of 0.746, a regression line very close to the one to one line and a coefficient of determination close to 0.75 (Table 5.4). As with *NEP*, CenW_HH was constrained to not reproduce the most extreme EC-derived carbon assimilation rates (*GPP* above 30 µmol m^{-2} s^{-1}). Some of these extreme observed values would have been due to random noise in the observations, and some of the extremely high values are matched by a similar number of observations much lower than the 1:1 line.

CenW_HH tended to slightly overestimate ecosystem respiration (*ER*) as indicated by the slope of the linear regression (0.836). We also observed more scatter than that found for *GPP* and *NEP* with a coefficient of determination of 0.728. The model simulated higher respiratory rates than derived by the Reichstein et al. (2005) gap-filling algorithm which corresponded to grazing events on some paddocks further away and within the footprint of the EC tower (see Chapter 6 for a detailed study on the effects of grazing events on model data agreement). These discrepancies could be related to the fact that the partitioning of observed *NEP* into *GPP* and *ER* is made according to the Reichstein et al. (2005) algorithm, which, in contrast to CenW_HH, does not use any information about grazing events occurring in the footprint area and so could not differentiate the pasture respiration rate (soil + vegetation) on one hand from grazing animals respiration on the other hand.

Overall, most of the points agreed very well as shown by the highest density of points around the one to one line which indicated that that the development and parameterisation of CenW_HH adequately simulated carbon fluxes observed at Scott Farm over the two years of the study period. Achieving such high agreement between observed and modelled carbon fluxes was only possible through the proper selection of the photosynthesis routine and modification of the running time steps of heterotrophic and autotrophic respiration simulation procedures and their parameters.

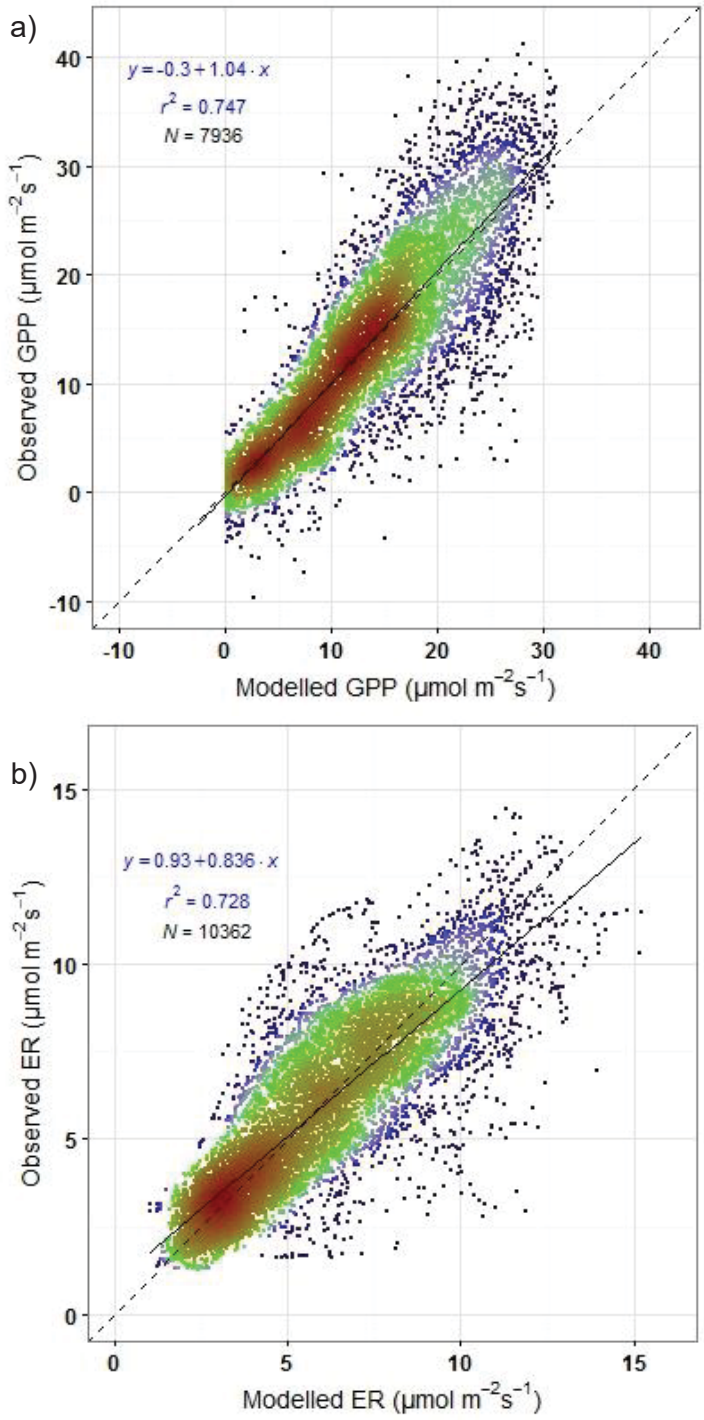

Figure 5.7: Scatter plots of EC-derived a) *GPP* and b) *ER*. (Both partitioned by the Reichstein et al. (2005) algorithm) against CenW_HH modelled GPP and ER. The dashed line is the 1:1 line, the blue line is the linear regression with equations given in the figure with their corresponding r^2, N is the number of points on each graph and the colours were used to represent the density of points going from red for highest to black for lowest densities.

As we have seen in this section, CenW_HH was able to achieve excellent agreement with the carbon fluxes observed (*NEP*) and partitioned (*GPP* and *ER*) at Scott Farm. There was no identified consistent bias across a wide range of values covering periods with diverse weather and soil moisture conditions and with pastures in various stages of regrowth after grazing. There remained a reasonable amount of scatter around modelled values which was largely attributable to random scatter in the observed fluxes and uncertainty in partitioned values. Errors in the footprint model would have contributed to remaining error by incorrectly attributing modelled fluxes to the wrong paddocks. Also, in this analysis, only fluxes affected by the presence of grazing animals from the four closest paddocks surrounding the EC tower were discarded but the grazing events occurring further away from the tower also affected the agreement between modelled and observed carbon fluxes.

A few specific remaining issues related to some slight underestimation of maximum photosynthetic carbon uptake rates and a small number of instances where large cattle respiration rates were modelled but not observed. These instances probably related to times when cows were not actually present despite records indicating that grazing took place, or when the footprint model might have incorrectly attributed fluxes to grazed paddocks when observed fluxes actually originated from non-grazed paddocks.

5.3.2.1.2 Evapotranspiration and sensible heat flux

In the previous section, modelled and observed carbon fluxes were compared. As we have seen, eddy covariance measurement systems also measure fluxes of sensible heat (*H*) and evapotranspiration (or latent energy, *LE*). Like carbon fluxes, latent energy and sensible heat fluxes were simulated for every individual paddock and weighted with the footprint model to get integrated fluxes at the tower that could be compared to observed fluxes, even if they appeared to be less sensitive to the choice of spatial integration than carbon fluxes (Section 5.3.1).

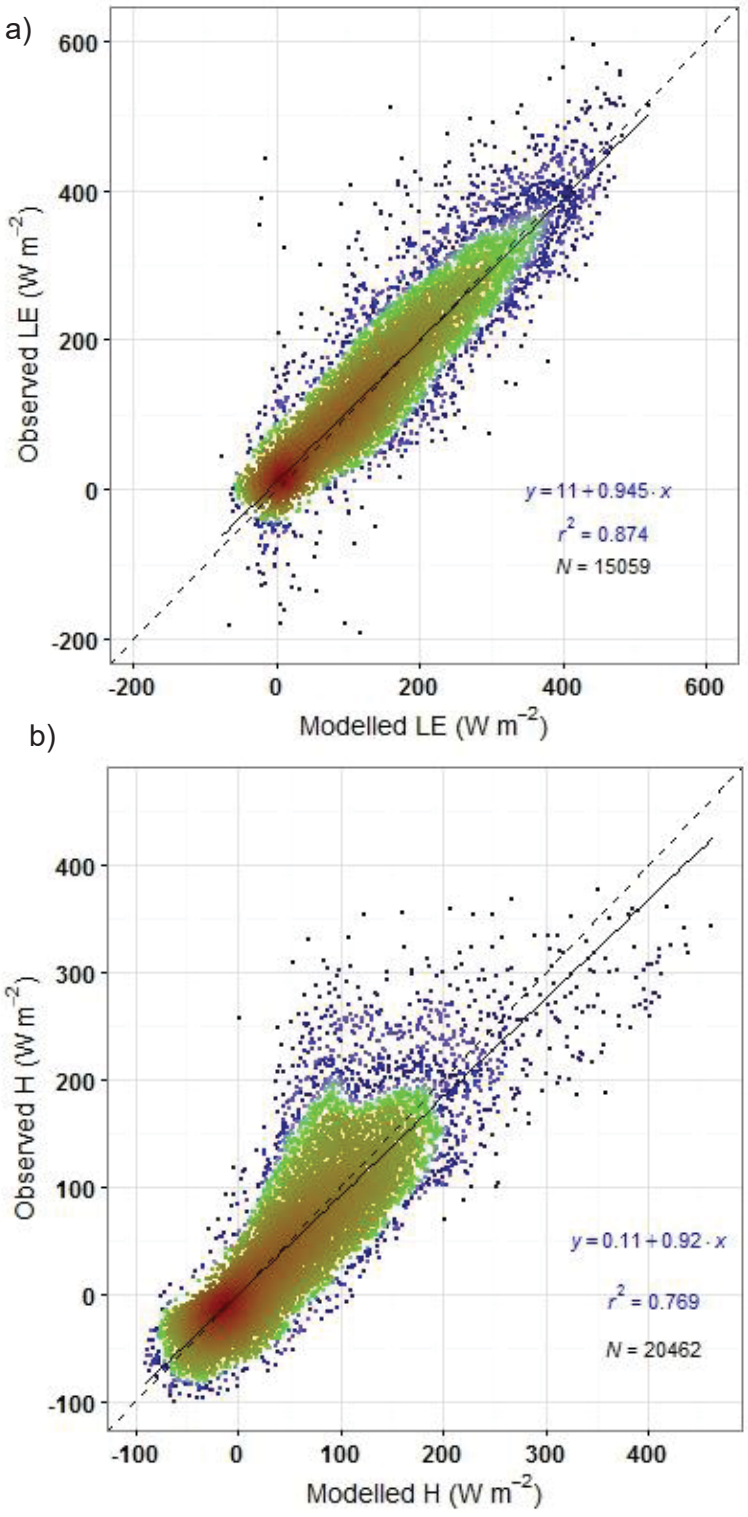

Figure 5.8: Scatter plots of observed against modelled fluxes of a) latent energy, or evapotranspiration and b) sensible heat, *H*.

Model/data agreement is very good for latent heat flux (Fig. 5.8 a). The model could explain about 87% of the variability in observations (NSE=0.869). The slope of the linear least square regression line is 0.945 which is reasonably close to 1 to warrant that there were no significant systematic differences between observed and modelled latent heat fluxes and the coefficient of determination of 0.874 (Table 5.4) showing a small scatter.

This is excellent agreement across a wide range of conditions, across seasonal variations, including a major and some minor drought periods, diurnal variations with daytime and night time data, including dew formation and shifts across different plant states with freshly grazed and fully regrown canopies. It shows that the modelling scheme developed and used in this study (see Chapter 4) is adequate for the simulation of the evapotranspiration rate measured over an intensive dairy farm.

To achieve such a good agreement between observed and modelled latent heat flux, the model needed to properly simulate the interactions between all parts of the ecosystem and their seasonal and short term variations driven by vegetation dynamics and response to climatic conditions at a sub-daily time step. In particular, the model responded quite well to drought conditions when no precipitation was received for an extended period and soil water availability for plant extraction and utilisation was greatly reduced. This caused stomatal closure to prevent ongoing or additional water losses through transpiration. In order to fully account for the effects of summer droughts it was also required that the photosynthetically active area was reduced otherwise the pattern of reduced water extraction during water limited periods could not be modelled adequately. This was consistent with the visual observations of senescent pasture during drought. In the model, under water limiting condition part of the green leaves die and their biomass is transferred to a dead foliage pool. It is controlled by the severity of the drought and by a parameter controlling the rate of desiccation of the vegetation.

The simulations of sensible heat flux did not agree with the observations as well as for evapotranspiration. Model efficiency for *H* was 0.762, showing that the model could explain about 76% of the variations of the observed *H* flux. The slope of linear regression (0.919) was slightly lower than 1, meaning that the

model showed a tendency to slightly overestimate the sensible heat flux, and the value of the coefficient of determination of the linear correlation was 0.769 indicating more scatter than for latent heat.

Overall, results from the model are satisfactory for the simulation of sensible heat flux and even better for evapotranspiration as shown by the high model efficiencies and r^2. These good agreements prove that the new routines implemented in CenW_HH to mechanistically model energy and water fluxes, coupled to the carbon assimilation procedure through stomatal conductance and growth, realistically and appropriately account for the drivers of evapotranspiration (soil evaporation and surface evaporation after rain and transpiration from the vegetation). Accurate modelling of latent heat flux is important over land ecosystems for hydrological and agronomic applications or to study the effects of climate and land use change on ecosystems and water resources and CenW_HH proved that it could be used adequately to study these issues.

5.3.2.1.3 Net radiation and soil temperature

Accurately modelling net radiation (*RN*) is important as it is the key driver of the energy budget at the surface. As presented in detail in Chapter 4, *RN* is the difference between short wave radiation received in solar radiation and reflected by surfaces that depend on soil and vegetation albedos and incoming and outgoing long-wave radiations, which are function of surface temperature and emissivities. It also represents the radiative driver of latent energy and sensible heat fluxes with surface temperature as an emergent property of the modelled ecosystem. Accurate modelling of the soil temperature profile is also important in CenW_HH. Not only does it influence the surface energy exchange, but modelled temperatures of each soil layer are also an important modifier of the soil heterotrophic respiration through organic matter decomposition.

Unlike fluxes, measured with the EC system, which were studied above, observed net radiation and soil temperature are not spatial measurements. These two variables were measured locally and depend on local biotic and abiotic conditions. Sensors were installed in one of the four closest paddocks

from the eddy covariance tower (paddock b22a on Fig. 5.1) and so no spatial integration was needed for the comparison with modelled variables.

In this section, modelled variables were simply retrieved from the simulation of this specific paddock and directly compared to observations. The soil temperature was measured at 0.05 m depth and compared with the modelled temperature of the soil layer corresponding to this depth.

Figure 5.9 shows the comparisons of modelled (x-axis) versus observed (y-axis) net radiation (*RN*) on panel a) and 5 cm depth soil temperature on panel b). The dashed line is the 1:1 line (perfect agreement between model and observations).

The model was able to explain about 94% and 92% of the variance in observed net radiation and soil temperature, respectively (Table 5.4) as indicated by the model efficiencies. The modelling of net radiation and soil temperature is implemented in the energy and water budget procedure which was described in Chapter 4. The slope of the least square linear regression line shows that the model tends to overestimate net radiation (*RN*) introducing a systematic error of about 10% (Fig. 5.9a). CenW_HH modelled more negative *RN* during night time, when the observations reach zero, CenW_HH seems to model fluxes of about -70 W m^{-2} and most extreme modelled values go up to ~ -150 W m^{-2} whereas observations do not seem to exceed -100 W m^{-2}. Because *RN* was measured by a radiometer, systematic errors in measurement are unlikely and so, CenW_HH was certainly overestimating night time fluxes by assuming too much energy storage caused by errors in the simulation of the emissivities, albedos or temperatures of the different parts of the system (soil, litter and vegetation). Daytime fluxes (*RN* > 0) were very close to the one to one line as indicated by the density colouring on Figure 5.9a). Night time values would have forced the high (35 W m^{-2}) intercept, which, in turn, would have forced the slope of less than 1. However, model efficiency and coefficient of determination are high and according to the density of points (Fig. 5.9a), there is good agreement between modelled and observed net radiation with the large majority of points bouncing around the 1:1 line.

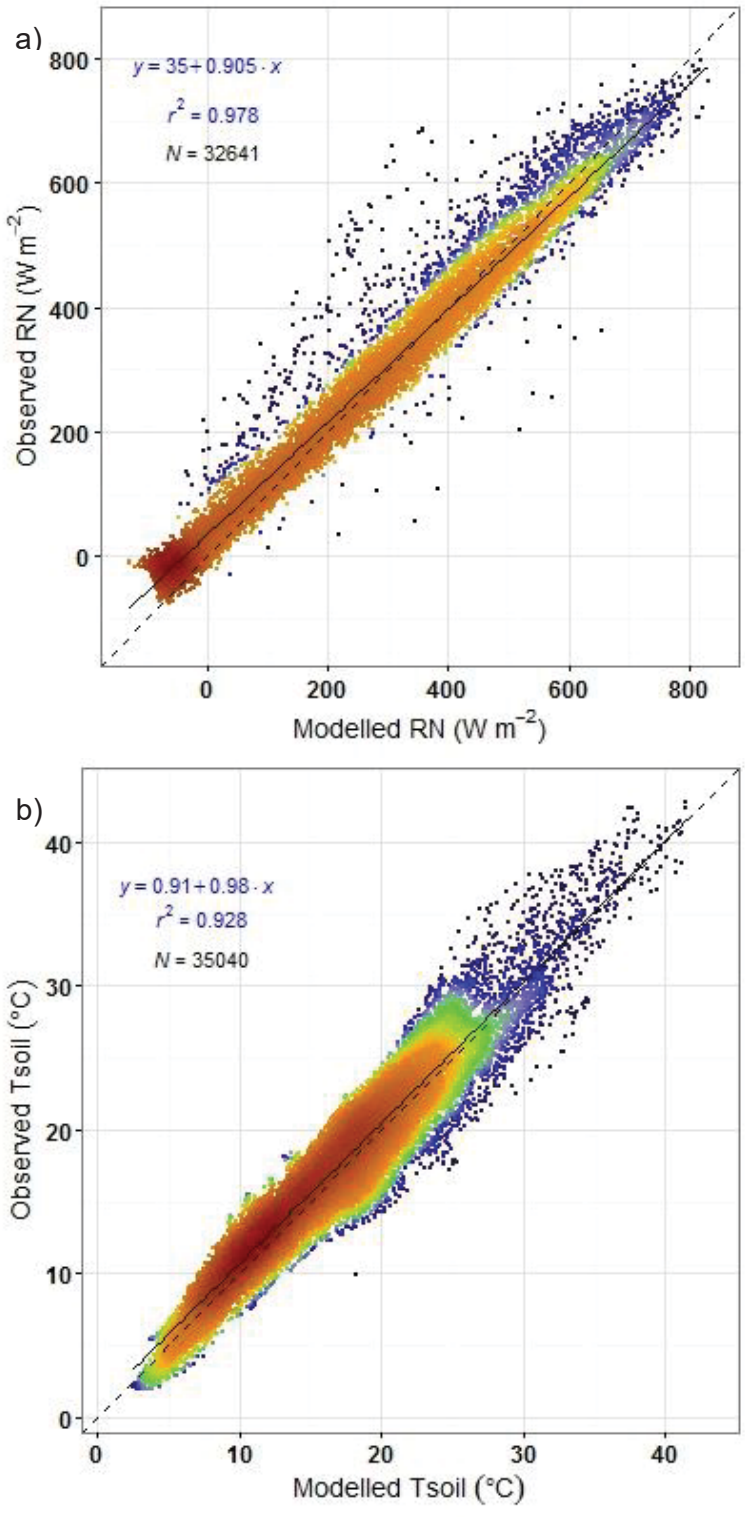

Figure 5.9: Observed half hourly *RN* plotted against modelled *RN* (a) and observed half hourly 5 cm soil temperature plotted against modelled 5 cm soil temperature (b). On panel a) only best quality measurements were selected whereas on panel b) measurements over the total length of the study were used.

Soil temperature modelling depends on several factors in the model. At first, it is driven by the amount of available energy at the soil level and secondly by the amounts of water and organic matter in the different soil layers that affect their thermal properties. The slope of the linear regression and coefficient were 0.98 and 0.93, respectively showing a very good agreement between observation and simulation, which is also confirmed by the high model efficiency of 0.92 (Table 5.4) and the high density of points around the one to one line, indicating that the different process included in CenW_HH were adequate for the modelling of this system as most of the trends were well reproduced.

Table 5.4: Summary of half hourly statistics used to evaluate model performances in the simulation of fluxes of carbon, water and energy observed at Scott farm over two years of measurement. NSE, RMSE, MBE and R^2 were defined in the text above and a and b represents respectively the slope and intercept of the linear regression line between modelled (x-axis) and observed (y-axis) variables.

	NEP ($\mu mol\ m^{-2}\ s^{-1}$)	*GPP* ($\mu mol\ m^{-2}\ s^{-1}$)	*ER* ($\mu mol\ m^{-2}\ s^{-1}$)	*LE* ($W\ m^{-2}$)	*H* ($W\ m^{-2}$)	*RN* ($W\ m^{-2}$)	*Tsoil* (°C)
NSE	0.815	0.746	0.700	0.869	0.762	0.938	0.919
RMSE	3.723	4.433	1.374	38.268	32.681	41.982	1.719
MBE	-0.123	-0.186	-0.013	-5.525	2.241	-28.567	-0.610
a	1.067	1.038	0.836	0.945	0.919	0.909	0.981
b	-0.198	-0.301	0.930	11.002	0.112	35.001	0.908
R^2	0.819	0.747	0.728	0.874	0.769	0.978	0.928

Overall, the model does a good job in modelling 30 minute carbon, energy and water fluxes as well as net radiation and soil temperature at 5 cm depth when compared to observations. The good model/data agreement obtained for the simulation of these variables shows that once parameterised, the model is able to run properly on this challenging dataset, and that most of the processes are correctly included and modelled in CenW_HH.

5.3.2.2 ***Patterns observed with longer averaging time steps***

5.3.2.2.1 Daily and weekly model/data agreements

Unlike for the study of half hourly fluxes presented above, the complete dataset (actual observations + gap filled data) was used in this section of the study to

compare data amalgamated into daily and weekly averages. However, the same parameterisation of the model was used as in the previous section. That means that the model was parameterised based only on comparison with the best observations e.g. by removing from the analysis gap-filled data and fluxes affected by the presence of grazing animals in the four closest paddocks from the EC tower. Half hourly output variables, which were presented in the above section, were summed/averaged over 24 hours (from midnight to midnight the next day) to obtain daily values. Weekly averaged variables were then derived from measurements and simulations obtained over corresponding 7-day periods. Units of the fluxes were converted to be more appropriate for a longer time scale. The carbon fluxes (*NEP*, *GPP* and *ER*) are now given in kgC ha^{-1} d^{-1}, energy fluxes (*RN* and *H*) in MJ ha^{-1} d^{-1} and water fluxes (*LE*) in mmH_2O d^{-1}. Statistics used to evaluate the ability of the model to reproduce daily observations have been reported in Table 5.5 and Figure 5.10 shows the scatter plots between CenW_HH modelled (x-axis) and observed (y-axis) of *GPP* a), *ER* b), *NEP* c), *LE* d), *RN* e) and *Tsoil* f). On each panel, daily and weekly averaged fluxes were plotted with small black circles and red up-arrows, respectively.

Daily and weekly model/data agreements of *GPP* are very good as shown on Figure 5.10a) where most of the points lie around the one to one line and as indicated by the good statistics reported in Table 5.5. Slopes of the daily and weekly regression lines were very close to 1 and large coefficients of determination and model efficiencies confirmed that modelled photosynthesis rates agreed very well with Reichstein “gap filled” *GPP* and so, it was not possible to identify any significant systematic differences between the two modelled carbon assimilation rates.

The daily *ER* agreement (Fig. 5.10b) appeared to be weaker but this is explained by the fact that CenW_HH modelled much higher respiratory fluxes during grazing events than what the data (observed and gap-filled fluxes) suggested. However, grazing animals’ respiration is not accounted for in the Reichstein gap-filling algorithm and so high carbon efflux values would have been missed in the data. Weekly averaging fluxes improved the agreement between CenW_HH ecosystem respiration estimates and data because with

fluctuations of the flux footprint and the rotational grazing of the different paddocks, large respiratory losses from grazing animals were averaged out. Except for differences caused by the large respiratory fluxes due to the presence of grazing animals within the flux footprint that affected only a small number of days, most of the daily ER fluxes showed a very good agreement as they lie around the one to one line with not much scatter.

Daily *NEP* agreement was found to be weaker than for *GPP* and *ER* (Fig. 5.10c). Large disagreements were found when the presence of grazing animals affected data and simulated fluxes. In those circumstances, daily averaged CenW_HH fluxes were very negative but daily *NEP* data were positive as respiratory C losses from grazing animals were not accounted for. However fluxes highly affected by the presence of grazing cattle represent only a minority of days and the large majority of points presented better agreements.

Figure 5.10d) shows the scatter plot of daily and weekly modelled *LE* against observed *LE* fluxes. Coefficients of determination were high (above 0.9) also, CenW_HH appeared to slightly but systematically overestimate *LE* (points above the one to one line) which was not reflected in half-hourly fluxes (Fig. 5.8a). CenW_HH also modelled more negative daily fluxes while data were always positive or very close to zero. This could be explained by CenW_HH modelling dew formation during wet and steady nights, where half-hourly LE fluxes were negative followed by days with heavy cloud cover so that there is not even enough energy to evaporate the night's dew while the gap-filling procedure does not include such detailed feature and uses available information from times with good climatic for the eddy-covariance technique to be used and which not reflect the specific conditions at the study site.

Daily and weekly net radiations (Fig. 5.10e) were above the one to one line, indicating that daily and weekly *RN* fluxes modelled by CenW_HH were lower than observations. This is caused by the fact that modelled night time *RN* was systematically more negative than observations as shown on Figure 5.9a) and even if daytime fluxes agreed well, summing over daily and weekly periods reduced the inferred fluxes and the agreement.

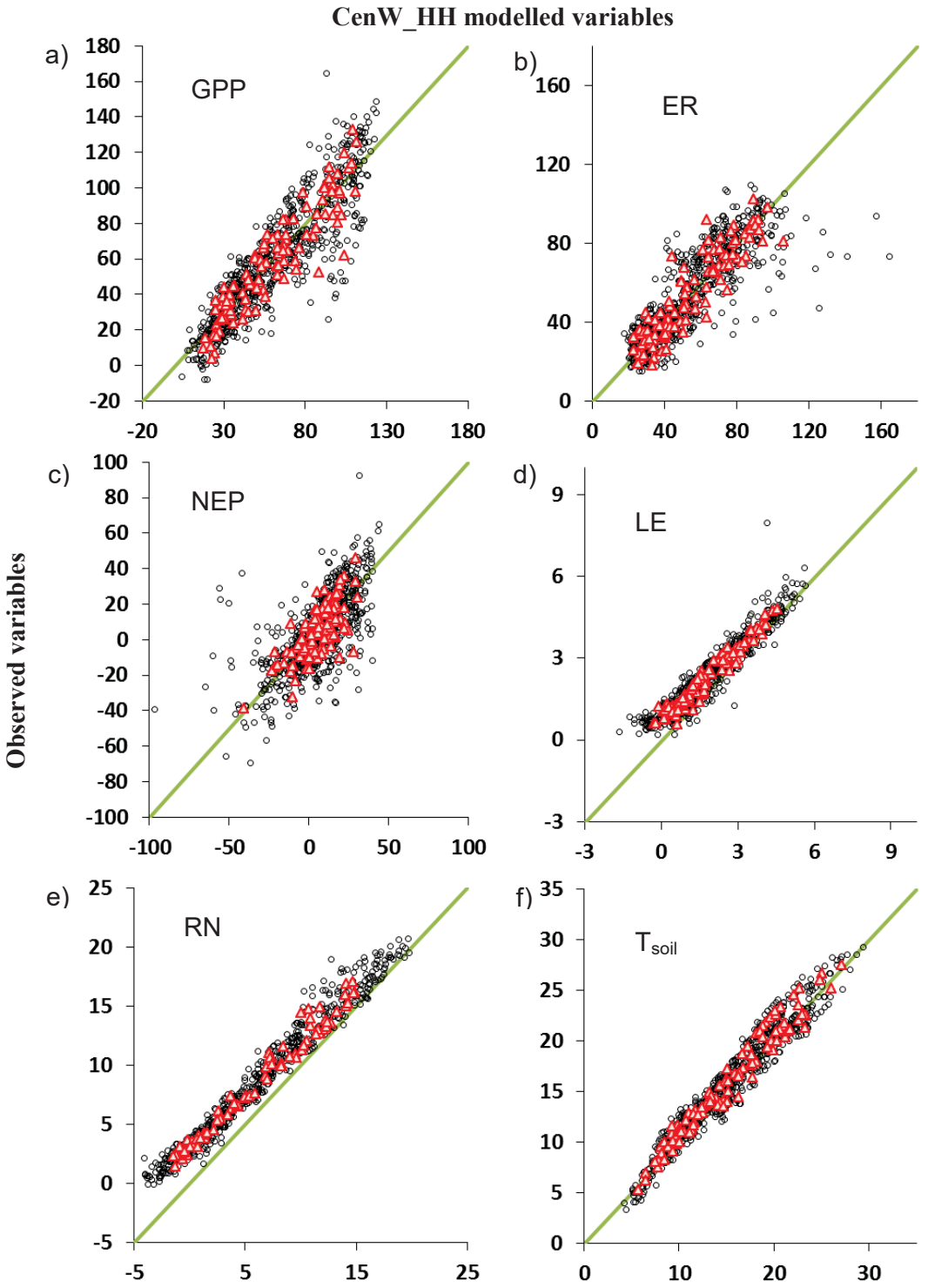

Figure 5.10: Comparisons of daily (black circles) and weekly (red up arrows) averaged CenW_HH modelled variables and EC observed variables. *GPP* a), *ER* b), *NEP* c), *LE* d), *RN* e) and *Tsoil* f).

Figure 5.10d) shows the comparison of modelled and observed daily and weekly soil temperature (*Tsoil*) at 5 cm depth. Both daily and weekly averages

showed very good agreements with no identifiable systematic differences and increasing the averaging period reduced the scatter, improving the fit between observed and modelled soil temperature and the evaluation statistics.

Slopes of linear regressions were above 0.8 for all the variables except for daily *NEP* which had a slope of 0.786 signalling that CenW_HH was modelling daily *NEP* flux about 20% higher than observations. To derive daily and weekly fluxes from half-hourly observations, it was necessary to use gap-filled data and so, any lack of agreement could be due to measurement problems, and certainly could be related to problems in the gap-filling routine. CenW_HH should be a better predictor than the Reichstein et al. (2005) gap filling algorithm principally because grazing animals respiration has been included in a more physically realistic way.

Table 5.5: Daily and weekly model efficiencies (NSE), linear regression equation (lm) and coefficient of determination (r^2). For the linear regression equations, the x-axis was used for modelled and the y-axis for observed variables

	NSE		lm		r^2	
	Daily	Weekly	Daily	Weekly	Daily	Weekly
GPP	0.794	0.851	$y = -1.466 + 1.002x$	$y = -1.390 + 1.001x$	0.797	0.853
ER	0.673	0.832	$y = 9.130 + 0.820x$	$y = 2.283 + 0.948x$	0.707	0.838
NEP	0.445	0.514	$y = 0.458 + 0.786x$	$y = 0.002 + 0.869x$	0.477	0.521
LE	0.724	0.705	$y = 0.758 + 0.856x$	$y = 0.747 + 0.860x$	0.908	0.949
RN	0.887	0.884	$y = 3.133 + 0.888x$	$y = 3.080 + 0.888x$	0.971	0.979
Tsoil	0.938	0.953	$y = 0.799 + 0.987x$	$y = 0.775 + 0.989x$	0.945	0.958

Usually, increasing the averaging time window e.g. going from daily to weekly fluxes, improved the model/data agreement because increasing the time averaging period cancels out the scatter in observations which is not reproducible by the model.

For all the variables studied but *NEP*, the model was able to explain more than 80% of the variability found in observations (Table 5.5). The lowest coefficient of determination was found for *NEP* with daily and weekly values of only about 0.5. This might have been caused by the inclusion of gap filled data or *NEP*

fluxes observations affected by the presence of grazing animals which can potentially causes large discrepancies between model estimates and observations (see Section 5.7 and Chapter 6).

Compared to results reported for Scott Farm using the daily version of the model (CenW version 4.1) model/data agreement for daily fluxes obtained in this study are slightly lower for *NEP* and *LE*. For these two fluxes, Kirschbaum et al. (2015) reported model efficiencies of 0.56 and 0.54 for daily and weekly *NEP* respectively while in this study model efficiencies were only of 0.445 and 0.514. These large differences could be explained by the fact that in Kirschbaum et al. (2005) days where fluxes were affected by the presence of cattle within the four closest paddocks from the tower were discarded from the analysis but not in this study. Lowest model efficiencies were also found for daily and weekly evapotranspiration rates with daily and weekly NSE (model efficiency) of 0.724 and 0.705 respectively in this study compared to 0.91 and 0.96 in Kirschbaum et al. (2015). Model efficiencies calculated in Kirschbaum et al. (2015) for evapotranspiration fluxes were impressively high. Half-hourly model efficiencies were much higher (0.87) as reported in Table 5.4, however this could have been boosted by the large diurnal variation, which disappears when one integrates values to longer-term means. Also, CenW_HH forces the energy balance to be closed at each time step of the model runs (half-hourly) and allow dew deposition (mainly during night time periods) both affecting modelled latent heat fluxes.

5.3.2.2.2 Modelled and observed monthly carbon fluxes

Figure 5.11 shows modelled and observed monthly carbon fluxes from Scott Farm that have been calculated as the sum of half-hourly modelled and observed fluxes. Similar to daily fluxes in the above section, monthly fluxes were calculated by including gap-filled data and fluxes affected by the presence of grazing animals within the vicinity of the tower were not removed from the analysis.

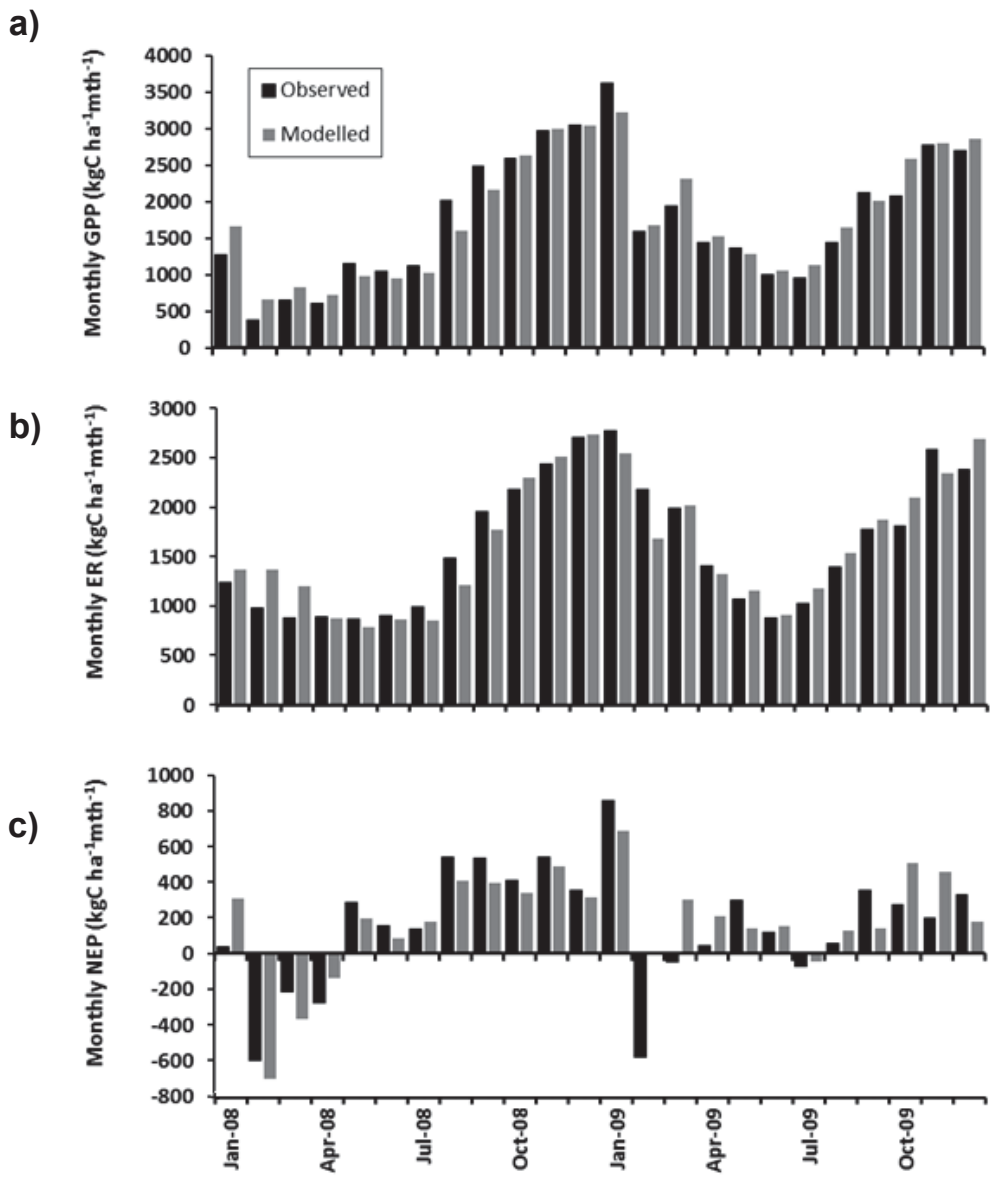

Figure 5.11: Monthly observed and modelled carbon fluxes, *GPP* a), *ER* b) and *NEP* c). Observed data are shown with black bars and modelled data with grey bars.

In summer 2008, a very severe drought strongly affected C fluxes from January to 14 April when drought was broken with substantial rainfall (83 mm over two days). This drought was qualified as a 1 in 100 year event (Mudge et al., 2011). *GPP* was sharply reduced as the soil dried out while respiration was less affected by these water limited conditions, and therefore the site lost carbon to the atmosphere. Other studies (Ciais et al., 2005; Ammann et al., 2007; Schwalm et al., 2010) also found that water limitations had a stronger effect on *GPP* (plant photosynthesis) than on respiration rates.

CenW_HH, as a process based model, simulates ecosystem respiration as the sum of plant autotrophic and soil heterotrophic respiration rates driven by biophysical factors and respiration from grazing animals based on grazing event records and amount of ingested vegetation. In contrast, the Reichstein et al. (2005) gap filling algorithm modelled ER as a function of soil temperature derived from actual night time NEP observations over a moving time window. The latter could not differentiate plant, soil and grazing animal respiration rates.

GPP simulations reproduced the observed patterns over 2 years (Fig. 5.11a), including the depression over the initial drought period, followed by the recovery after the rains resumed. Rates remained subdued over the winter months because of low temperature and radiation levels. Photosynthesis rates then increased with the onset of warmer conditions to reach maximal values in summer before they were reduced again by a minor summer drought in February 2009. Rates remained subdued after that because of reducing temperature and radiation through the autumn months. The winter and spring pattern in 2009 was similar to that in 2008, but did not reached the same high values because of lower temperatures. CenW_HH largely followed these trends, thus indicating an appropriate dependence on internal factors such as leaf area and extent of nutrient limitation, bioclimatic factors and the response to drought conditions.

CenW_HH ecosystem respiration simulations largely followed the variations in the observed data and predicted the absolute magnitude of respiratory change over the study period (Fig. 5.11b). Unlike the Reichstein model that is “governed” by being reparameterised every fortnight, CenW is parameterised only at the beginning of the run and then runs without any feedbacks from observations as to whether results are reasonable. Daily rainfall record input into CenW_HH allowed the model to simulate the drought effect on GPP and NEP with remarkable accuracy.

In CenW_HH, *NEP* fluxes were not directly modelled but resulted from the difference between *GPP* and *ER*. Over the two years studied here, modelled NEP flux followed very similar patterns to those shown in observations. The model reproduced the general trends in the observations particularly well including the net carbon losses over the summer 2008 drought period but not

that of the small drought in 2009. This could be due to the fact that in 2009 the drought was less pronounced than in 2008 and the model with its parameterisation could not deal with both drought periods without causing big discrepancies in one period or the other.

During the 2008 drought period, CenW_HH tended to simulate higher respiration rates than the observations suggested (Fig. 5.11b) and modelled *GPP* was also higher than the observed one (Fig. 5.11a). Both modelled and observed *NEP* fluxes were negative during the extended drought period indicating a net loss of carbon from the ecosystem to the atmosphere, CenW_HH slightly overestimated the carbon losses compared to observations (Fig. 5.11c). This dry summer was followed by a typical wet winter with lower solar radiation and temperatures during which both carbon assimilation and respiration rates remained quite low, and the site became a small sink for CO_2 until the beginning of August 2008. Modelled and observed fluxes agreed well over this period. With the onset of warmer weather after August 2008, *GPP* and *ER* increased steadily until the beginning of November. CenW_HH reproduced the observed *GPP* very accurately over these three months but showed a tendency to underestimate *ER* which is even clearer when looking at *NEP* fluxes (Fig. 5.11c). As a result, over this period, the model indicated that Scott Farm was a weaker CO_2 sink than reflected in the observations.

From November 2008 until February 2009, carbon assimilation and respiration rates were nearly constant and at their maximum because of good climatic conditions and no drought periods. Between mid-January to mid-February, water limitations started to develop but they were not as strong as in the 2008 drought. The pasture on some paddocks within the EC footprint were also sprayed with herbicide and were re-sown (Mudge et al., 2011), reducing the amount of photosynthesising biomass present on these paddocks. These conditions affected both *GPP* and *ER*, but it reduced modelled *ER* to a greater extent than was apparent in the observations (Fig. 5.11b). Good agreement between modelled and observed carbon fluxes in the 2008 drought, confirming the good sensitivity of the model to water limited conditions. Agreements were poorer in the 2009 drought because CenW_HH was not re-parameterised just to fit the 2009 observations measured over the drought period which was

shorter and not as strong as in the first year. It was also possible that after pasture renewal, the model underestimated the amounts of standing root biomass or its rate of decomposition. Once roots are dead, CenW_HH assumes that they start to decompose at a prescribed rate, but it is possible that they decomposed even faster than modelled, maybe because their lignin content is lower or nitrogen concentration higher than modelled. No ancillary measurements were available to further support what might have happened on those specific plots.

In March 2009, *NEP* model/data agreement was poor; observations showed that paddocks were losing a small amount of C as indicated by the slightly negative *NEP* while CenW_HH modelled *NEP* was positive (Fig. 5.11c). For this month, both modelled and observed *ER* fluxes were of the same magnitude (Fig. 5.11b) and the observed discrepancy mostly came from the carbon assimilation rate, which was higher for the model than for the measurements (Fig. 5.11a). Until July 2009, Scott Farm was a sink of CO_2 but then both *NEP* rates (modelled and observed) indicated that the site became a net source of CO_2 to the atmosphere (Fig. 5.11c). According to Mudge et al. (2011), this was likely due to colder than usual winter climatic conditions and grazing management practices which reduced the carbon assimilation rate. From then and until the end of 2009, the site remained a net sink of carbon and over this period, CenW_HH showed a tendency to slightly overestimate *GPP* and *ER*.

Overall, monthly carbon fluxes showed that the two years were quite different in terms of carbon fluxes dynamics (Fig. 5.11). Generally, modelled and observed fluxes agreed well with the biggest discrepancies observed during drought periods. The CenW_HH model managed to reproduce the variations in observed monthly carbon fluxes dynamics.

5.3.2.2.3 Annual and cumulative carbon fluxes

Figure 5.12 shows the annual cumulative modelled (lines) and observed (dashed lines) carbon fluxes *GPP* a), *ER* b) and *NEP* c) for the two years of the study. For this graph, both the trends and signs of cumulative fluxes are important as positive values indicate that the study site acted as a sink of carbon and negative values shows that it was a source of carbon to the

atmosphere. Positive trends indicate that more carbon is fixed over a particular period (removed from the atmosphere) and negative trends signal net carbon losses.

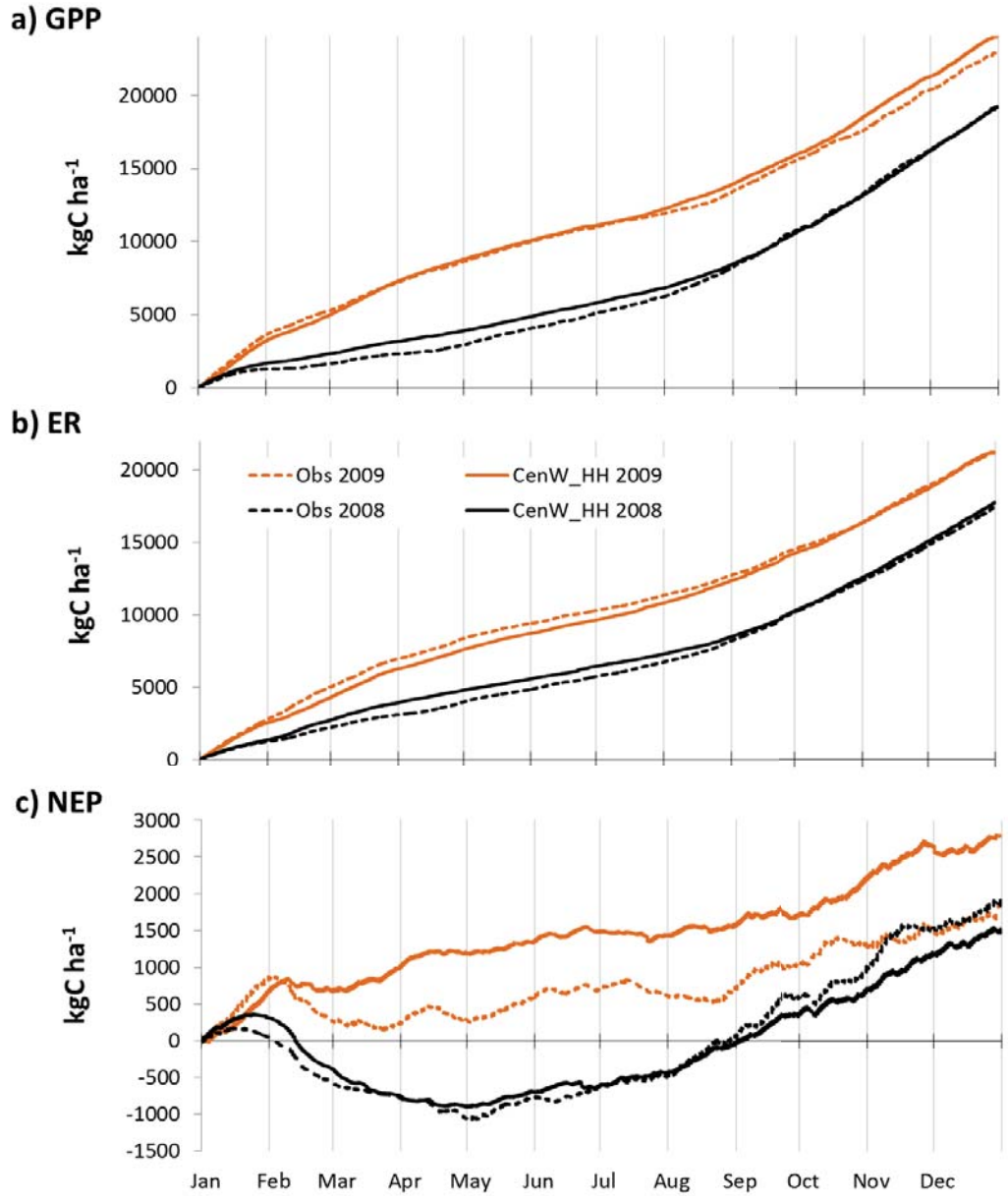

Figure 5.12: Cumulative observed and modelled a) gross primary production (*GPP*), b) ecosystem respiration (*ER*) and c) net ecosystem productivity (*NEP*) for 2008 (black) and 2009 (orange). Dashed lines are used for observations and continuous lines for modelled carbon fluxes.

A striking aspect of the cumulative carbon fluxes (Fig. 5.12) are the large differences between years.

Figure 5.12 highlighted that modelled and observed *ER* and *GPP* largely followed similar patterns, e.g. 1) a sharp increase over summer unless there is drought, 2) more moderate increases over winter and 3) sharper increases over spring and into summer. Patterns for modelled and observed are very similar, except for a few periods, with the lines running parallel for most of the other times. Modelled and observed cumulative *NEP* also showed very similar trends as lines on Figure 5.12 c) were mostly parallel. However, short periods of discrepancies caused offsets, like a short period of underestimating gains in spring 2008 caused an overall underestimate of 2008 carbon gain, and in 2009, it was mainly the Feb-Mar period, where the reduced down-turn was not sufficiently replicated by the model, that caused most of the discrepancy that was carried through until the end of 2009.

In CenW_HH, functional connections between variables, such as the fact that *ER* depends on *GPP*, with most of *ER* coming from recently fixed *GPP* through autotrophic (maintenance + growth respiration). For example, an overestimate of *GPP*, in the first year (Fig. 5.12a), inevitably leads to an overestimate in *ER*. Because they are linked through a conservation of (C) mass, such a discrepancy cannot be overcome by adjusting any parameters of the model.

As we have seen in the previous sections, a severe drought at the beginning of 2008 (until mid-April) caused large losses of carbon to the atmosphere. At the beginning of the drought, in January 2008, CenW_HH overestimated *GPP* while *ER* was consistent with observations, and as a result, the cumulative difference in *NEP* reached ~ 300 kgC ha^{-1} by the end of this month. From there and until the return of substantial rainfall in mid-April 2008 which marked the end of the period with water limited conditions, cumulative curves (Fig. 5.12) show that both modelled *GPP* and *ER* were higher than their EC derived counterparts (upward trend) which led to a reduction of the cumulative error in *NEP* that is almost zero in mid-April. From May and until the end of 2008, the study site acted as a net carbon sink as indicated by the steady upward trend of both modelled and observed cumulative *NEP* fluxes.

During the whole first year (2008), cumulative *NEP* flux dynamics (Fig. 5.12a) were very similar which indicated that the model was able to properly account for most of the processes and their responses to climatic conditions involved in

driving the observed behaviour of the *NEP* fluxes. CenW_HH overestimated *NEP* fluxes in November as indicated by the deviation of the two curves at this time. At the end of 2008, there was a difference of 400 kgC ha^{-1} between modelled (black line) and observed (dashed black line) cumulative *NEP* curves.

In summer 2009, as in 2008, the study site experienced water limited conditions, which is not unusual in the Waikato. However, this drought period was not as long and severe than in the previous year which has been qualified as a 1 in 100 year drought and which was followed by a cooler than usual winter that strongly affected carbon fluxes (Mudge et al., 2011). Water limitations started slightly later than in 2008 as indicated by the orange dashed line on Figure 5.12a) and which lasted only until about late March, thus for around 7 weeks. Over this period, observed cumulative *NEP* flux (orange dashed line) showed that Scott Farm was a net source of CO_2 whereas, over the same time period, modelled cumulative *NEP* flux (orange line) indicated that the pasture was approximately CO_2 neutral and that paddocks started to gain carbon sooner than observations suggested. At the end of the seven weeks, the two curves had already strongly deviated with a difference of 600 kgC ha^{-1}. From there, the modelled and observed cumulative *NEP* are similar but the offset remains with the two curves following the same pattern so that by the end of 2009, CenW_HH has overestimated the net carbon flux by 967 kgC ha^{-1}, mostly due to the offset caused by the drought.

Overall, the cumulative *NEP* fluxes for the two years of the study show very different patterns (Fig. 5.12) mostly caused by the large carbon losses occurring during the severe drought in 2008 that was not present in 2009. Also, modelled and observed cumulative *GPP*, *ER* and *NEP* followed, most of the time, very similar trends.

Now that it has been shown that the carbon fluxes modelled with the parameterised version of the CenW_HH model agreed well with Scott Farm observations, in the next section of this chapter, the model/data agreement has been tested with gap filled observations under different climatic conditions.

5.4 Comparison of NEP estimates from the Reichstein et al. (2005) gap filling algorithm and the CenW_HH model.

5.4.1 Introduction

The previous chapters have demonstrated that EC data have a great potential for the study of GHG emissions from pastoral systems in New Zealand. However, the parameterisation of mechanistic ecosystem models to simulate observations requires the availability of detailed management records (grazing events, harvests, cultivation or fertiliser applications). They need to be comprehensive and detailed enough to match the time step of the model to provide critical information about management events that can have over-riding effects on ecosystem carbon fluxes. The accuracy and reliability of mechanistic models like CenW_HH is closely related to the quality of the data used to parameterise it.

A great advantage of eddy covariance measurement systems is that environmental input data and resultant gas exchange rates are taken continuously over long time periods (multiple years). These observations thus provide information over diverse and representative climatic and land management conditions. Regional and global networks like OzFlux or FLUXNET (see Chapter 2), largely developed over the past three decades, are in charge of homogenising datasets, and building up databases of EC measurements of water, gas (CO_2, CH_4 or N_2O) and energy exchanges between surface and the atmosphere made over different land cover types (forest, grasslands, crops, etc.). These quality controlled data sets are then made available to the research community for further analysis. They are of particular interest for global change studies, for example, where the upscaling of local measurements to regional, continental and global scales is important for improving models, and for our general understanding of the carbon cycle and its effects on the climate.

However, in such long time series there are inevitably missing values caused by instrument failure or maintenance operations and unsuitable climatic conditions for EC measurement such as precipitation, fog, dew deposition, or inappropriate turbulence conditions. Those gaps in the dataset are potentially problematic for researchers and are not avoidable. A critical and indispensable step for the temporal integration of CO_2 fluxes and other quantities to daily or longer scales is the filling of those missing values through the “gap filling” process (Falge et al., 2001b).

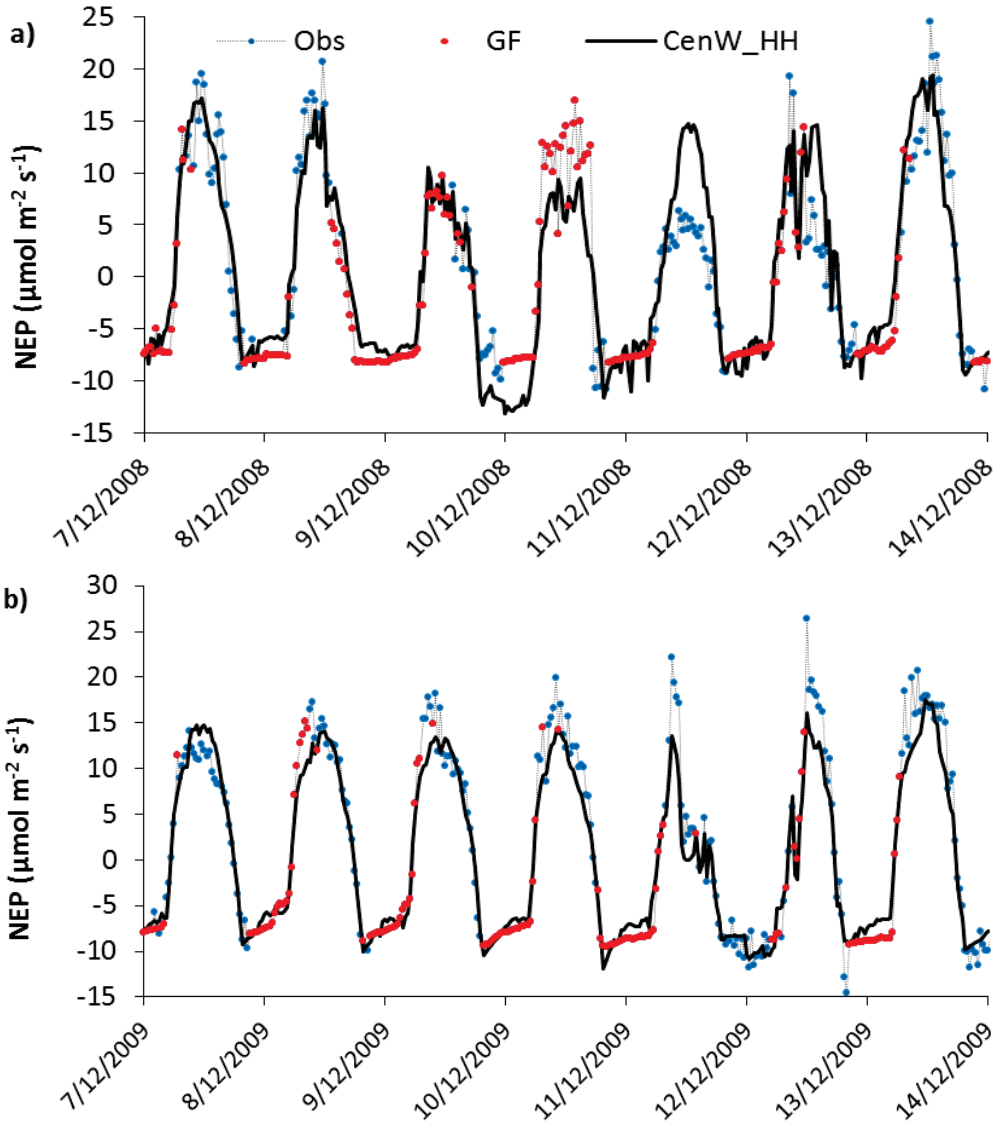

Figure 5.13: Time series of half-hourly net carbon productivity (*NEP*) over 7 days in 2008 a) and 2009 b). Blue dots are used for actual observations, red dots for Reichstein gap-filled data and the black line for CenW_HH modelled fluxes.

Several gap filling methods exist and can be used by researchers to generate complete time series of EC measurement (Falge et al., 2001a; Moffat et al., 2007). However, there are several sources of uncertainties in annual carbon budgets of land surfaces related to the distribution and size of those gaps and there is no general consensus on the best procedure to be used on every study site.

Figure 5.13 shows time series of observed, gap-filled and CenW_HH modelled NEP fluxes over a 7 day period in December 2008 (Fig. 5.13a) and the same period in 2009 (Fig. 5.13b). It highlights the strong day to day and inter-annual temporal variations of the NEP flux. Most of half-hourly observed and gap-filled data agreed well with CenW_HH estimates. The big majority of the night time fluxes over these two time periods were gap-filled (red dots). Trends in the observed NEP time series were reasonably well reproduced by CenW_HH. Ecosystem respirations rates agreed well and showed the same patterns e.g. higher respiration at the beginning of the night followed by a reduction throughout the night driven by the decline of the temperature. No grazing events happened over the week in 2009 and fluxes agreed well, in contrast of 2008 where a grazing event was recorded in the footprint on the 10th of December. For this day, CenW_HH modelled higher respiration rate affecting both nigh-time and daytime fluxes that, in this case, were gap-filled. The Reichstein et al. (2005) gap-filling algorithm did not have information nor took into account the respiratory losses from grazing animals in the footprint area. Accordingly the resulting gap-filled fluxes were higher than those modelled by the more complex CenW_HH model that specifically used the grazing records and footprint information.

Falge et al. (2001b) reported that the number of gaps in a selection of eddy covariance sites ranged between 10% and 60%, with an average of 35% of missing data for typical years. Our study site (Scott Farm), had an average of 60.3% of gaps (Table 5.2) which placed it on the upper limit of the data coverage reported in previous studies and made the construction of annual carbon budgets highly dependent on the accuracy and reliability of gap filled flux values. At Scott farm, more than 81% of the gaps occurred during night time (Table 5.2) and were mostly due to site characteristics such as low wind

velocity and turbulence during night time hours as well as high humidity rate that caused the formation of dew which affected sensors readings.

Also, because the number of gaps in EC data time series is generally important, gap filling methods received substantial attention and it is important that they contribute little bias to annual sums of net ecosystem fluxes (Moffat et al., 2007; Carvalhais et al., 2009). However, it was shown by Kirschbaum et al. (2007) that gaps are typically not randomly distributed, as may be the case with gaps associated with rainfall events. If there are no observations under these particular kinds of conditions, there would be no good basis for a simple gap-filling routine to fill the gaps. The routine could only be guided by observations under conditions that are different from those for which the missing numbers are to be provided, and that could potentially lead to biases in the gap-filling procedure (Kirschbaum et al., 2007).

In this section, the newly developed version of the CenW model running at a half-hourly time step (CenW_HH) was used, after its parameterisation with best-quality measurements (see above), to compare its simulated results with the much simpler, but widely used gap filling algorithm (Reichstein et al., 2005). The overall aim was to identify and quantify any systematic errors or biases in carbon fluxes estimates under some specific climatic conditions that may lead to gaps in eddy covariance measurements.

The Reichstein et al. (2005) gap-filling and partitioning algorithm is essentially a fitting tool to incrementally fit a very simple model to the data one step at a time. So, it has no parameters for generic plant responses to temperature, water stress, nitrogen concentration or anything else. It just looks at the fluxes over a short time interval and fits parameters to describe the information over that time interval. Its strength is its frequent re-parameterisation and thus an adjustment to emerging system responses to changing environmental conditions. Its weakness is the limited amount of information it uses. Its total reliance on observations before and after the gap that needs to fill becomes a problem if the conditions during the gap are very different from the conditions before and after the gap. This is a major problem when grazing occurs, but could be less problematic with other changes such as short periods of precipitation.

CenW is a fundamentally different model. Its parameterisation is equally sensitive to the observations over the whole two year period, and it relies on the correct incorporation of physiological processes to model the changing exchange rates over time. But its reliance on the use of physiological processes then also gives it a better ability to extrapolate fluxes into periods for which no observations are available, and the explicit incorporation of extraneous information, such as grazing times, gives it a better opportunity to model fluxes during these events.

5.4.2 Materials and methods

The parameterised CenW_HH ecosystem model (see above) was used in this part of the study. It was run at a half-hourly time step to match the sampling interval of the eddy covariance system to allow a direct comparison between half hourly estimates of *NEP* from CenW_HH and those from the simpler and widely used Reichstein et al. (2005) gap filling algorithm.

From the Scott Farm dataset described above, only periods with missing carbon fluxes and without grazing events in the four closest paddocks surrounding the flux tower were specifically selected. Chapter 6 gives a detailed analysis of periods when grazing on the inner paddocks played an important role. As described before (Table 5.2), over the 2-year study period, approximately 60% of data were missing, which represented 21 147 individual data points out of a total of 35 088 observations periods. When acquisition periods affected by grazing animals were excluded from the analysis (see Chapter 6 for more details), the total number of gap filled observations was reduced to 18 376 still constituting about 87% of all gap filled data.

Different factors caused gaps in the dataset. Equipment maintenance or failure was responsible for only 1% (N = 350) of the missing observations (Mudge et al., 2011). Some specific meteorological conditions are not suitable for making measurements with the EC technique. At Scott Farm, an open path IRGA was used and during rain, frost and fog, water drops between or on the open path windows can affect IRGA readings as indicated by the automatic gain control (AGC) signal. Periods affected by these conditions were very prevalent at Scott Farm and affected readings at 49% (N = 17 193) of all half hourly periods

(Mudge et al., 2011). These periods were further classified as being linked either to rainfall or fog or dew based on rainfall readings at the time.

Low turbulence conditions, usually characterised by the friction velocity (u*) and mostly related to night time conditions are also not suitable for good quality flux measurements (Papale et al., 2006) and are usually filtered out by applying a u* threshold. With a u* threshold set to 0.11 m s^{-1}, Mudge et al. (2011) found that low turbulence conditions affected 37% (N = 12 983) of all half hourly sampling periods. These gaps are particularly important as they can lead to systematic underestimation of nocturnal respiratory fluxes under low turbulence conditions and can strongly influence the sink/source status of the ecosystem (Moncrieff et al., 1996; van Gorsel et al., 2007, 2008). Overall, gaps from the three different sources overlapped 28.4% of the time (Mudge et al., 2011).

When multiple causes of gaps overlapped, the corresponding data taken during this time periods were excluded from the following analysis. The aim was to use only data gaps where the cause of data rejection could be clearly identified. Gaps due to instrument failure were not specifically analysed in this study because in this case, sensors dysfunctions were not related to any particular climatic conditions that might have biased the dataset through the gap filling method and only represented a very small proportion of the total number of gaps encountered in the dataset.

5.4.3 Results and discussion

Figure 5.14 shows the comparison of half-hourly modelled by CenW_HH and gap-filled by the Reichstein et al. (2005) algorithm *NEP* fluxes obtained under different climatic conditions. When all net carbon fluxes from the two models are compared (Fig. 5.14a), the agreement between them is very good as indicated by the r^2 of 0.89 and the slope of the linear least square regression line of 0.99. This is also confirmed by the statistics reported in Table 5.6. The 18 376 points corresponding to all half-hourly gap filled data compared to their CenW_HH estimates gave a model efficiency of 0.88, a RMSE of 1.96 µmol m^{-2} s^{-1} and a MBE of 0.45.

NEP gaps due to low turbulence conditions (u* < 0.11 m s^{-1}), filled by the Reichstein et al. (2005) algorithm and modelled by the CenW_HH model also

agreed well (Fig. 5.14b). Most of these gaps occurred at night time as indicated by the highest density of negative points shown on Figure 5.14b). Under these climatic conditions, CenW_HH tended to simulate slightly lower positive flux values and some higher night time fluxes (more negative). This could be due to the explicit grazing from even the outer paddocks missing from the Reichstein gap-filled data, leading to negative intercepts and underestimates of night-time fluxes in Reichstein gap filled data. Also, under stable conditions the footprint model is not as reliable as in more developed turbulence conditions which also could have added bias by indicating that fluxes originated from the wrong surface area.

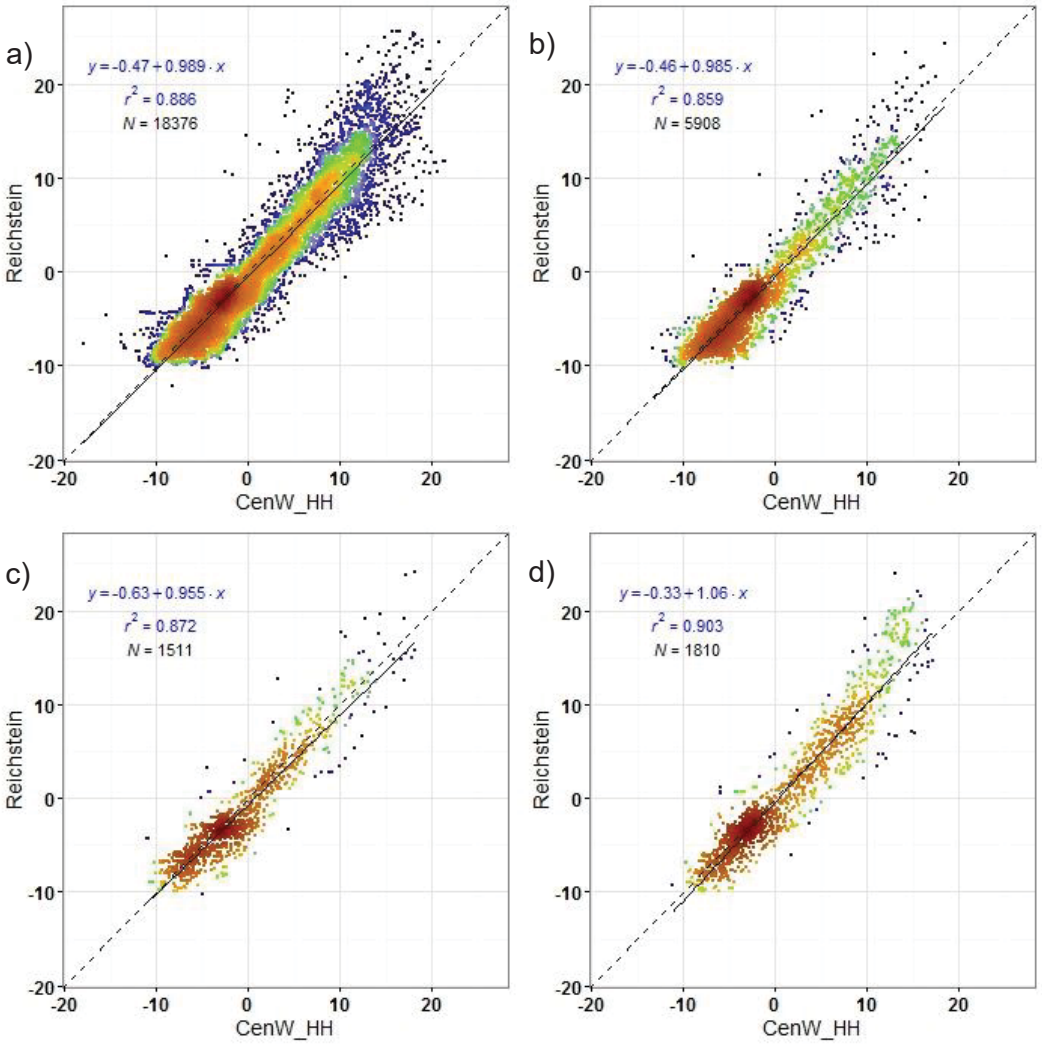

Figure 5.14: Comparisons of Reichstein gap filled (y axis) and CenW_HH modelled (x axis) *NEP* fluxes under different climatic conditions: a) all gap filled fluxes, b) u*<0.11 m s^{-1}, c) rainfall, and d) fog or dew deposition. All fluxes are given in units of µmol m^{-2} s^{-1}.

Rainfall caused 1511 gaps in half-hourly *NEP* measurement periods in the Scott Farm dataset. Agreement between those gap filled fluxes and simulations from the CenW_HH model was also very good (Fig. 5.14c; Table 5.6), with a slope for the linear regression between the two modelled NEP estimates of 0.96, a coefficient of determination of 0.87, a model efficiency of 0.86 and a mean bias error of 0.55 which indicates slightly higher *NEP* estimates by CenW_HH than by the Reichstein model. However the value of MBE is small and it is not possible to identify any significant systematic bias between CenW_HH and Reichstein modelled *NEP* fluxes under rainy conditions.

Table 5.6: Summary of half hourly statistics used to evaluate Reichstein/CenW_HH agreements in the simulation of net fluxes of carbon at Scott farm over two years of measurement. NSE, RMSE, MBE and r^2 were defined in the text above, N is the number of data points in each categories and a is the slope of the least square regression line.

	N	a	r^2	NSE	RMSE	MBE
All GF	18376	0.99	0.89	0.88	1.96	0.45
Rain	1511	0.95	0.87	0.86	1.85	0.55
Fog	1810	1.06	0.90	0.87	2.02	0.35
U*	5908	0.98	0.82	0.81	1.85	0.49

The last climatic condition selected to be studied in this section is referred to "dew and fog" and corresponds to measurement periods where the IRGA readings have been affected by the presence of water (indicated by the AGC signal from the IRGA) but when the rain gauge did not recorded any rainfall water. A total of 1810 half hourly measurements were affected by that condition (Fig. 5.14d; Table 5.6). As for other climatic conditions discussed above, CenW_HH simulations and Reichstein gap filled data agree very well under foggy conditions with an r^2 of 0.90, a slope 1.06, indicating that CenW_HH tended to simulate slightly higher *NEPs* under these weather conditions, and a NSE of 0.87 and a RMSE of 1.85. Differences between the two were attributed to the fact that CenW_HH specifically modelled NEP fluxes under those climatic conditions while the Reichstein algorithm extrapolated from non-dewey conditions to those with dew that were not representative of what actually happened.

Overall, there was close agreement between half-hourly Reichstein gap filled and CenW_HH modelled *NEP* fluxes whatever the climatic conditions responsible of the gap in the dataset with model efficiencies (NSE) of 0.81 for low turbulence conditions, 0.86 for rainfall and 0.87 for fog or dew and with a maximum value of 0.88 for all gap filled data (Table 5.6). With the results obtained in this section, it was not possible to identify any climatic conditions responsible for adding significant bias in the dataset during the gap filling of missing *NEP* data. CenW_HH relies on physiological modelling to simulate fluxes, but it is also handicapped by a lack of high quality, relevant observations to be parameterised accordingly to these specific conditions. Also, any explanation for the small differences in fluxes and bias are of only limited relevance with slopes of linear regressions that are not significantly different from 1 and the small number points involved.

5.5 Summary and conclusion

This section focussed on the evaluation of the newly developed version of the CenW ecosystem model running at a half hourly time step (CenW_HH, which has been described in detail in Chapters 3 and 4). The model was compared against eddy covariance observations made in 2008 and 2009 at Scott Farm (an intensive dairy farm in the Waikato).

Using the footprint information (including adjacent paddocks and grazing events) had a strong effect on carbon fluxes (Fig. 5.3a, 5.4a and d and Table 5.3) as it accounted for the respiratory losses from grazing animals within the sampling area of the EC tower and the state of vegetation after grazing events but has only a slight effect on water fluxes (Fig. 5.3b, 5.4b and e and Table 5.3).

Half hourly model data agreement:

After its parameterisation, the modelled fluxes were compared with the underlying observations, using only actual observation and excluding poor-quality data (i.e. gap-filled data) and observations affected by the presence of grazing animals within the vicinity of the EC tower.

Model efficiencies were high for half hourly carbon fluxes, with values of NSE of 0.81, 0.75 and 0.70 for *NEP*, *GPP* and *ER*, respectively, showing a very good agreement between modelled and observed C fluxes. Good agreements were also found for latent and sensible heat fluxes, net radiation and soil temperature with model efficiencies of 0.87, 0.76, 0.94 and 0.92, respectively, showing that CenW_HH was able to predict the great majority of the fluxes and their temporal variability reasonably well (Table 5.4).

Very high rates of net carbon assimilation were not simulated by the model (Fig. 5.6 and 5.7) as CenW_HH used an optimised parameter set constrained to smaller maximum rates of carbon assimilation and higher respiratory losses than the data suggested, which when added together could have limited the model to reach the most extreme observed *NEP* values. Grazing events on some paddocks further away and within the footprint of the EC tower caused CenW_HH to model some higher respiratory rates than those derived by the Reichstein et al. (2005) algorithm. These discrepancies could be explained by the fact that the partitioning of *NEP* into *GPP* and *ER* from the Reichstein et al. (2005) algorithm, in contrast to CenW_HH, does not use any information about grazing events occurring in the footprint area and so could not differentiate the pasture respiration rate (soil + vegetation) on one hand from grazing animals respiration on the other hand. Remaining errors were probably related to times when cows were not actually present despite records indicating that grazing took place, or when the footprint model might have incorrectly attributed fluxes to grazed paddocks when observed fluxes actually originated from non-grazed paddocks. Overall, achieving such high agreements between observed and modelled carbon fluxes was only possible through the way in which the photosynthesis routine and the heterotrophic and autotrophic respiration were coded and parametrised to match the shorter time steps.

The excellent agreement for LE and H (Fig. 5.8 and Table 5.4) span across a wide range of conditions driven by seasonal variations, including a major and some minor drought periods, diurnal variations with daytime and night time data, including dew formation and shifts across different plant states with freshly grazed and fully regrown canopies. Also, to achieve such a good agreement between observed and modelled latent heat flux, the model needed to properly

include interactions between all part of the ecosystem and their seasonal and short term variations driven by vegetation dynamics and response to climatic conditions at a sub-daily time step. In particular, the model responded quite well to drought conditions when no precipitation was received for an extended period and soil water availability for plant extraction and utilisation was greatly reduced. This caused stomatal closure to prevent ongoing or additional water losses through transpiration and in order to fully account for the effects of summer droughts it was also required that the photosynthetically active area was reduced otherwise the pattern of reduced water extraction during water limited periods could not be modelled adequately. Overall, it showed that the energy and water modelling scheme developed and used in this study is adequate for the simulation of evapotranspiration and sensible heat rates measured over the intensive dairy farm.

Daily and weekly agreements:

Increasing the averaging time window e.g. going from daily to weekly fluxes, improved the model/data agreement because increasing the time averaging period cancelled out the scatter in observations which were not predicted by the model. To derive daily and weekly fluxes from half-hourly observations, it was compulsory to use gap-filled data and so, the lack of agreement could be due to model or measurement problems, and certainly could be related to problems in the gap-filling routine. Also, in principle CenW_HH should be a better predictor than the Reichstein et al. (2005) gap filling algorithm principally because grazing animals' respiration has been included in a more physically realistic way.

Apparently, daily and weekly summed carbon and water fluxes were less well modelled than those obtained with the daily version of the CenW model as reported in Kirschbaum et al. (2015) as indicated by the lowest model efficiencies calculated in this study (Table 5.5). However, in Kirschbaum et al. (2015), fluxes affected by the presence of grazing animals within the EC footprint were discarded from the analysis which is not the case in this study. As those fluxes were large outliers, the goodness of fit would have been reduced.

Monthly carbon fluxes agreements:

On a monthly time scale, modelled fluxes agree well with observations except during the 2008 drought where *ER* and *GPP* were overestimated by CenW_HH, and in February 2009 where ER_{CenW_HH} was about 600 kgC ha^{-1} lower than $ER_{observation}$. Overall, monthly carbon fluxes showed that the two years were quite different in terms of carbon flux dynamics and that generally, modelled and observed fluxes agreed well (Fig. 5.11). The biggest discrepancies were observed during drought periods but overall the CenW_HH model managed to predict well the trends in observed monthly carbon fluxes dynamics.

Annual carbon fluxes agreements:

Modelled and observed *ER* and *GPP* largely followed similar patterns (Fig. 5.12):

- sharp increases over summer unless there is drought
- more moderate increases over winter
- sharper increases over spring and into summer.

However, short periods of discrepancies in GPP and ER caused offsets, like a short period of carbon gain was underestimated in spring 2008, which caused an overall underestimation of 2008 carbon gain. In 2009, it was mainly the Feb-Mar period, where the reduced down-turn was not accurately predicted by the model, this caused most of the discrepancy that was carried through until the end of 2009.

In the process based CenW_HH model, variables are intrinsically linked, such as the fact that *ER* depends on *GPP*, with most of *ER* coming from recently fixed *GPP* through autotrophic (maintenance + growth) respiration. Hence, an overestimate of *GPP*, in the first year, almost inevitably must lead to an overestimate in *ER*. As carbon fluxes are linked through a conservation of (C) mass, that discrepancy cannot be overcome by adjusting any parameters of the model.

Overall, annual model/data agreement of carbon fluxes different for the two years of the study. In 2008, the annual net ecosystem productivity was underestimated by 397 kgC ha^{-1} by CenW_HH but overestimated by about 1000 kgC ha^{-1} in 2009. Overall, CenW_HH was able to accurately simulate carbon and water fluxes observed half hourly with however a difference of about

600 kgC ha^{-1} between modelled and observed *NEP* fluxes at the end of the two years.

Modelled vs gap-filled net ecosystem productivity:

Finally, CenW_HH was used with the aim to test the reliability of the Reichstein et al. (2002) gap filling algorithm under different climatic conditions that are unsuitable for eddy covariance data acquisition and which caused gaps in the dataset. This included removing data affected by the presence of grazing animals on the four inner paddocks and within the footprint of the EC tower. Three categories of *NEP* gaps were evaluated against model simulations based on the observed climate at Scott farm.

All half hourly gap filled *NEP* fluxes agree well with their CenW_HH modelled counterparts as indicated by the high model efficiency of 0.88, which is higher than the reported model efficiency reported for all actual observations (Fig. 5.14 and Table 5.6). This could be explained by the fact that the gap-filling model is essentially a smooth line fitted through observations, as a consequence, it should give much the same values as the observation minus the scatter in the observations although plus any systematic deviations between observations and the Reichstein model. Under all selected climatic conditions, model/data (gap filled only) agreement was also very good as indicated by model efficiencies always higher than 0.8.

Gaps caused by low turbulence conditions ($u^*<0.11$ m s^{-1}) were modelled by CenW_HH with a NSE of 0.81 (Fig. 5.14 and Table 5.6). Most of these gaps occurred at night time and the model tended to simulate slightly lower positive flux values and some higher night time fluxes. This could be due to the explicit grazing from even the outer paddocks missing from the Reichstein gap-filled data, leading to negative intercepts and underestimates of night-time fluxes in Reichstein and to problems with the footprint model.

CenW_HH modelled gaps due to rainfall with a NSE of 0.86 and gaps from foggy conditions with a model efficiency of 0.87 (Fig. 5.14 and Table 5.6). Differences between modelled and gap-filled fluxes were attributed to the fact that CenW_HH specifically modelled NEP under those climatic conditions while

the Reichstein algorithm extrapolated from “good” climatic conditions to those causing gaps that were not representative of what actually happened.

Overall agreements between Reichstein et al. (2002) algorithm and CenW_HH were quite good and there were only small systematic biases when fluxes affected by the presence of grazing were removed from the analysis.

CHAPTER 6: EFFECTS OF CATTLE RESPIRATION ON CARBON FLUXES MEASURED BY EDDY COVARIANCE

6.1 Introduction

Land use and associated management practices can strongly affect ecosystem nutrient, carbon, and water cycling through changes in plant photosynthesis, respiration, and energy partitioning. Grazing, the most important farm management practice for managed grassland ecosystems in New Zealand, also has important effects on carbon fluxes and the energy balance of pasture systems under intensive dairying. Knowledge of the responses of carbon fluxes to grazing is essential for developing sustainable management plans, coping with consequences of climate change, mitigating its effects and maintaining or improving soil carbon stocks.

Historically grazed pastures received much less attention than other biomes from eddy covariance researchers but the number of flux measurement sites has increased over the recent years (see Chapter 2.1). Soussana et al. (2010) hypothesised that grazed pasture ecosystems might have a great potential for carbon storage and be an option for mitigating part of the GHG budget of the agricultural sector. However, the findings of the recent modelling study by Kirschbaum et al. (2017), which tested several scenarios to increase soil carbon storage under dairying, did not identify such potential mostly because of trade-offs between milk production and transfer of carbon to the soil.

Most EC studies (e.g. Allard et al.,2007) carried out over pastoral ecosystems were conducted without the presence of grazing animals and did not try to differentiate cows respiration rate from the base rate of respiration of the soil and the vegetation, hereafter called “pasture respiration”.[1]

Jerome et al. (2014) was the first study to report on the effects of grazing animals on pasture net ecosystem exchange (NEE) measurements from eddy covariance. They showed that the presence of livestock in the flux footprint has several effects on fluxes measured by eddy covariance techniques. The direct effect on data, which is the one we are interested in, is the respiratory losses of

[1] Pasture respiration=sum of soil heterotrophic respiration and above and below ground plant autotrophic respiration rates. This is different from ER because it does not include cattle respiration.

carbon occurring during grazing events, where cows eat the standing vegetation and respire around 50% of it. The second effect (which is not studied here) is the reduction of the above-ground amount of photosynthesising vegetation that follows the grazing event and so reduces the subsequent stand carbon assimilation rate.

In another recent study, the presence of dairy cows within the footprint area was also recognised to be important in terms of CO_2 flux estimates (Kirschbaum et al., 2015). It was also acknowledged that capturing carbon dioxide losses from dairy cows with eddy covariance instruments depends heavily on the footprint of the tower (mostly driven by wind speed and direction and tower and vegetation height) and the location of grazing animals at any given time. CO_2 fluxes measured during cattle grazing events tend to occur at higher rates than natural carbon losses from pasture respiration, and therefore if grazing fluxes are missed or discarded due to filtering procedures it could lead to bias in CO_2 flux estimates (Kirschbaum et al., 2015). This last study has also stressed that careful thought needs to be given to the best approach to account for animal respiration under different grazing systems, with coupled EC measurements and modelling being one promising option to explore further (Kirschbaum et al., 2015).

The overall aim of this section was to better understand the direct effects of grazing dairy cow respiration both on half- hourly EC measurements and on annual estimates of NEP and NECB (net ecosystem carbon balance).

Annual NEP is not sufficient to determine the carbon sink/source status of the farm (study area) but all other carbon transfers (e.g. pasture utilised, milk and meat removed and dung and urine distribution) need to be accounted for in order to determine a proper NECB of highly managed pasture systems (Skinner, 2008). Studies of managed temperate grasslands' carbon balances have found contrasting results. It was reported that the ecosystem could either act as a carbon sink (Allard et al., 2007; Mudge et al., 2011; Rutledge et al., 2015), a source (Skinner, 2008) or be carbon neutral (Prescher et al., 2010). NEP is a very important term in the calculation of NECB and is the result of the difference between two large carbon fluxes, e.g. carbon assimilation (GPP) and

ecosystem respiration (ER). Bias in one of these two fluxes could lead to a shift in the carbon balance of the studied ecosystem from being a sink of carbon to a source of carbon (Felber et al., 2016).

Felber et al. (2016) used two different ways of processing EC data to study the effect of cow respiration on annual and shorter time scale NEP fluxes. This study may well be the first – and only – publication that looked particularly at how to deal with the presence of grazing animals in the footprint of the tower and their effect on carbon flux measurement, processing, gap filling, and partitioning. One of their key findings was that traditional gap filling and partitioning algorithms gave reliable results at annual time step but for shorter time scale (daily, monthly), uncertainties were more important mostly because of the severe variability of the presence of cows in the footprint, which cancel out for longer periods because of the combination of rotational grazing and footprint distribution (Felber et al., 2016).

In the following study, the effects of cow respiration on eddy covariance measurements of carbon flux were studied to find if the incomplete capture of cow respiration during grazing events could have biased the dataset and to what extent it affected the carbon budget of the studied dairy farm.

This effect could have influence at different levels and could make it harder for modellers either to achieve good model performances or to rely on model parameters and, even more importantly, might lead to an overestimation of annual carbon budgets of intensively managed grasslands.

6.2 Materials and methods

6.2.1 Study site and management practices

Data used in this chapter were measured in 2008 and 2009 at Scott Farm, a DairyNZ experimental dairy farm located in the Waikato region of New Zealand. The study site, available data, and other relevant information have already been described in the sections 5.1 and 5.2 of this thesis and only some important and/or additional information are repeated below.

The farm layout (Fig. 5.1) is not typical for New Zealand dairy farms as it consists of a mosaic of small 0.5-ha paddocks, as shown on the schematic representation of Scott Farm in Figure 6.1. The farm map and EC tower location schematic panels proved to be very useful to analyse the responses of both modelled and observed fluxes measured by the EC system. The location of the eddy covariance tower is indicated by the green circle, and each cell represents one of the 26 paddocks around the tower, which were simulated individually (the generic paddock used for flux coming from outside farm boundaries is not shown).

Schematic panels (Fig. 6.1) were used to display information at time steps ranging from 30 minutes to an average of 2 years, depending on what kind of analysis was performed. Such figures proved to be particularly useful in this section because they display the originating surface area of the measured flux and show whether or not fluxes were affected by cattle respiration and to what extent. Shading (clear through yellow to red) was used to represent the intensity of the emissions contribution.

Figure 6.1a shows the 2-year averaged relative contribution of individual paddocks to the overall measured CO_2 fluxes, derived from the half hourly Kormann and Meixner (2001) footprint algorithm. Numbers represent the 2-year averaged relative contribution of the paddocks (e.g. they represent the average source area of the measured fluxes over the time span of the study given in %). That means, for example, that on average, 14.24% of fluxes measured at the tower originated from the paddock located just to the top left of the tower. About 77.4% of the fluxes should come from the 26 paddocks shown on Figure 6.1, the remaining percentage originating from paddocks further away from the tower and outside the study site boundaries. The figure also shows that around 50% of the fluxes came from the 4 inner paddocks and the contribution of the others ranged between 0.5 and 3.2%, showing the importance of the 4 inner paddocks to the overall flux seen by the EC system.

Figure 6.1b shows the maximum half-hourly contribution of each individual paddock to the overall measured fluxes over the 2 years of the study. The maximum contributions were found for the four closest paddocks to the EC

tower with values ranging from 89.6 to 96.5% while the contributions from other paddocks were much lower, ranging from a minimum of 4.5% to a maximum of 33.8%.

Figure 6.1a and 6.1b clearly indicate that the contribution of the four inner paddocks, to the overall measured fluxes was very important compared with the contribution of paddocks further away from the tower.

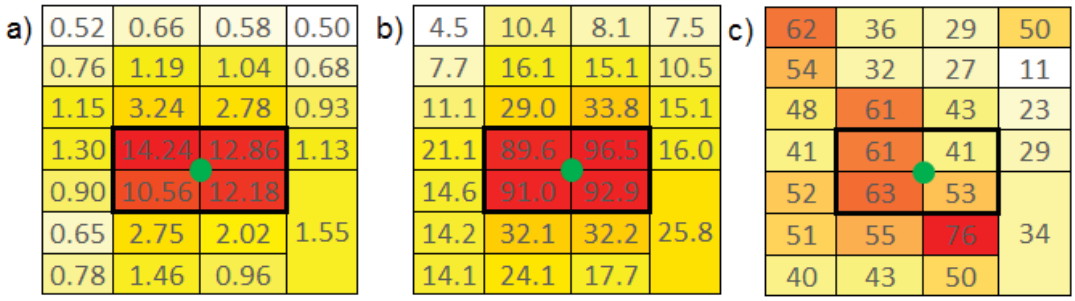

Figure 6.1: Schematic representation of Scott Farm. Each cell represent a 0.5-ha paddock, the green circle indicates the position of the EC tower and the black circled area determines the 4 inner paddocks around the tower. a) Shows the average relative contribution of each paddock over 2 years; b) shows each paddock's maximum half-hourly contribution to the observed flux over 2 years; and c) shows the number of days paddocks were grazed over 2 years. The colours scale from white for the lowest values to red for the highest.

Figure 6.1c presents the number of days paddocks were grazed by cattle over the two years of measurements made at Scott Farm. Daily records of grazing events were used to run the model, to account for the total number of grazing events recorded to have occurred on each individual paddocks. Over the 2 years of the experiment, the grazing management of each small 0.5-ha paddock was very different (Figure 6.1c). The presence of grazing cattle on the different paddocks was very uneven and, according to grazing records, ranged from 11 days for the "less grazed paddock" to 76 days for the paddock with the most recorded grazing days.

Grazing events that sometimes spread over several consecutive days were assumed to result from a smaller herd grazing. Grazing restricted to single days was assumed to result from a larger herd consuming all available standing vegetation in a single day, with commensurately larger respiration flux.

Footprint analysis indicated that the paddocks' relative contribution to the observed fluxes was very variable at daily and shorter time scales, which was mostly driven by shifts in wind speed and direction (not shown). For most half-hourly sampling intervals, only some of the paddocks contributed to the observed fluxes; the others made no contribution at all.

Farm grazing management records combined with the paddocks relative contribution have shown that dairy cows were present in at least one of the 4 inner paddocks during 192 days over the total 731 days of the study, which is about 26% of the total measurement period. When combined with the flux footprint, it appears that animals grazing on the 4 inner paddocks affected measurements during about 14% of all half hourly periods; 18% in 2008 and 10% in 2009. This highlighted the importance of the footprint information combining the records of animals' positions because the drop from 26% to 14% was entirely due to grazing events not being captured by the EC tower due to wind coming from another direction than across the grazed paddocks.

6.2.2 Modelling approach

Model runs used the newly developed version of the CenW model (CenW_HH) running at a half-hourly time step, which is the same as the time step of measured EC data. The details of the model have been described in Chapters 3 and 4, with the best set of parameters resulting from the parameterisation and validation part of the study described in Chapter 5.3. CenW_HH has been used because it explicitly simulates grazing animals' respiratory losses of carbon and can be used to illustrate the differences between simulated, measured and gap filled NEP fluxes.

The model was run independently for each individual paddock according to their specific management practices, e.g. daily records of grazing events and harvests and with meteorological inputs measured at the EC tower, which included solar radiation, air temperature, relative humidity, rainfall, and wind speed.

Modelled fluxes resulting from CenW_HH runs for each of the 27 individual paddocks were then weighted by their corresponding half-hourly paddock

relative contribution as described above from the footprint analysis in order to retrieve those fluxes that should have been measured at the tower.

6.2.3 NEP data and NECB calculation

NEP data from the eddy covariance tower had been filtered, corrected, gap-filled, and partitioned beforehand by the University of Waikato team using state of the art procedures (Mudge et al., 2011; Rutledge et al., 2015). Gap filling and flux partitioning algorithms used in this study were described by Reichstein et al. (2005). At first, the gap-filling algorithm was used to fill gaps in the dataset caused by the processing of the raw data or instrument failure (see section 5.2). The procedure works by using both the covariation of the fluxes with meteorological variables and the auto-correlation of fluxes (Reichstein et al., 2005). Practically, the algorithm uses a look-up table built over a centred, time-varying moving window and uses the average of actual fluxes measured under similar climatic conditions (solar radiation, temperature, and vapour pressure deficit) to calculate the missing values. The size of the window starts at 7 days and can reach 140 days if not enough data have been measured under similar conditions over the shorter time window. See the original Reichstein et al. (2005) publication for more detailed information about the gap-filling algorithm.

Once all gaps in the dataset have been filled, the flux partitioning routine separates the net ecosystem productivity (NEP) into its two components: ecosystem respiration (ER) and gross primary production (GPP). This is done by first deriving from measurements a short-term temperature sensitivity term that is used in a Lloyd and Taylor equation (Lloyd and Taylor, 1994) to extrapolate ER from night-time measurements to the daytime.

The Reichstein et al. (2005) gap filling method has been widely used to process eddy covariance data (Fluxnet) and was shown to give reliable estimates of NEP if the vegetation cover is homogenous (Stoy et al., 2006; Moffat et al., 2007). However with the special layout of the dairy farm studied here, which consists of a mosaic of small paddocks rotationally grazed by small herds and managed independently, the ability of this algorithm to give reliable fluxes might have been affected by the originating footprint area of the observed flux and

cows position. This is principally caused by the fact that these routines (gap filling and partitioning) were not designed to take account of the presence of grazing animals within the flux footprint and their large respiration fluxes; these are not linked to bioclimatic drivers but only to farm management decisions.

NEP is a very important term in the calculation of the farm carbon budget and incorrect estimates of this term in the calculation of the net ecosystem carbon balance (NECB) could lead to very different results on the carbon balance of the system, which could either be carbon neutral (NECB = 0), a source, e.g. loosing carbon to the atmosphere (NECB < 0), or a sink of carbon (NECB > 0). The latter is the most beneficial because in this last condition the $C0_2$ is removed from the atmosphere.

The NECB was calculated by using a modified equation from Chapin et al. (2006) as it was used in Rutledge et al. (2015).

$$NECB = NEP + F_{feed} + F_{effluent} - F_{product} - F_{harvest} - F_{methane} - F_{dung} - F_{resp} - F_{leach} \quad (6.1)$$

Where NEP is the net ecosystem production, F_{feed} is the C content of the feed imported from outside boundaries, $F_{effluent}$ is the amount of C contained in effluent applied to paddocks, $F_{product}$ represents the carbon exported as milk or meat products, $F_{harvest}$ is the C exported from the farm as silage, $F_{methane}$ is the amount of C lost to the atmosphere through enteric fermentation (CH_4) from cows and deposited dung, F_{dung} is the C lost from dung deposited on farm races and in the milking shed, F_{resp} represents the carbon dioxide lost through respiration by cows while in the milking shed and F_{leach} is the loss of dissolved organic and inorganic carbon through water drainage.

In this section, the same terminology was used for all the terms described above as in Rutledge et al. (2015). More explicitly, all the terms at the right of NEP in Equation 6.1 were referred to as "non-CO_2-C fluxes" and when used, their values will come directly from Rutledge et al. (2015) and were not recalculated specifically for the purposes of this study.

6.2.4 Selection of period of interest

In order to better understand how grazing would affect short-term (half-hourly) carbon flux and to quantify its effects on cumulative annual NEP and NECB, periods when cow respiration should have affected NEP fluxes measured by EC were specifically selected. The selection of these fluxes is based on farm records to determine which paddocks were grazed by cows on particular days, and on the flux footprint analysis (Kormann and Meixner, 2001) which gave the relative contribution of each individual paddock to the overall flux for every half-hour during the time span of the study (2 years starting in 2008).

Because of the unusual farm layout and grazing management practices implemented at Scott Farm, flux measurement periods affected by the presence of grazing animals in the footprint would have concerned a large proportion of the dataset (38%). Also, a large number of those selected points (affected by cattle respiration) were likely to account for only a few percent of the overall flux at the tower location, making it hard to distinguish any signal from the background variability of the carbon flux.

Instead, the choice was made to restrict the study to grazing events recorded on the four inner paddocks around the EC tower and when the relative paddocks contribution indicated that part of the measured flux should originate from one of them. This choice seemed to be valid for the purpose of the study as these 4 paddocks were well representative of the grazing regime used on the farm (Fig. 6.1c) and were also contributing the most to the observed flux (Fig. 6.1a, b).

The “weighted cattle respiration” used in the graphs shown below corresponds to these conditions and is calculated according to Equation 6.2.

$$weighted\ cattle\ respiration = \sum_{i=1}^{4} RelContrib_i \times CattleResp_i \tag{6.2}$$

where *i* is the index of one of the four inner paddocks considered, $RelContrib_i$ is the relative contribution of the ith paddock to the overall flux based on the

footprint analysis and $CattleResp_i$ is the modelled cattle respiration rate occurring during the grazing event on paddock number *i*.

6.3 Results and discussion

6.3.1 Analysis of half hourly NEP fluxes during grazing events.

The selection of periods where C flux was affected by cattle respiration was done by using the combination of farm management records (to get the position of animals on the farm on a given day) and the footprint model (to select periods where cows were in the footprint) as described in the section 6.2.4. This selection process revealed that 4331 measurement periods (half hours) should have been affected by the carbon flux from cattle respiration on the four inner paddocks.

Figure 6.2 and most of the figures used to illustrate this chapter are similar and illustrate how cattle respiration during grazing events in the four paddocks directly surrounding the EC tower affects the model/data agreement. Plotting information in this way provides important insights because it directly shows the differences between modelled and observed NEP fluxes (errors between model and observations) as a function of the supposed influence of grazing cattle, which is given by the modelled cattle respiration rates on each individual paddock weighted by the paddock contribution to the overall flux from footprint information.

On the y-axis the differences between observed and modelled NEP fluxes have been calculated and plotted against, on the x-axis, cattle's respiration rates from the 4 paddocks surrounding the EC tower. These fluxes were individually modelled according to the grazing routine implemented in CenW_HH and weighted by the relative contribution of each individual paddocks from the footprint analysis in order to retrieve the flux actually measured by the EC system.

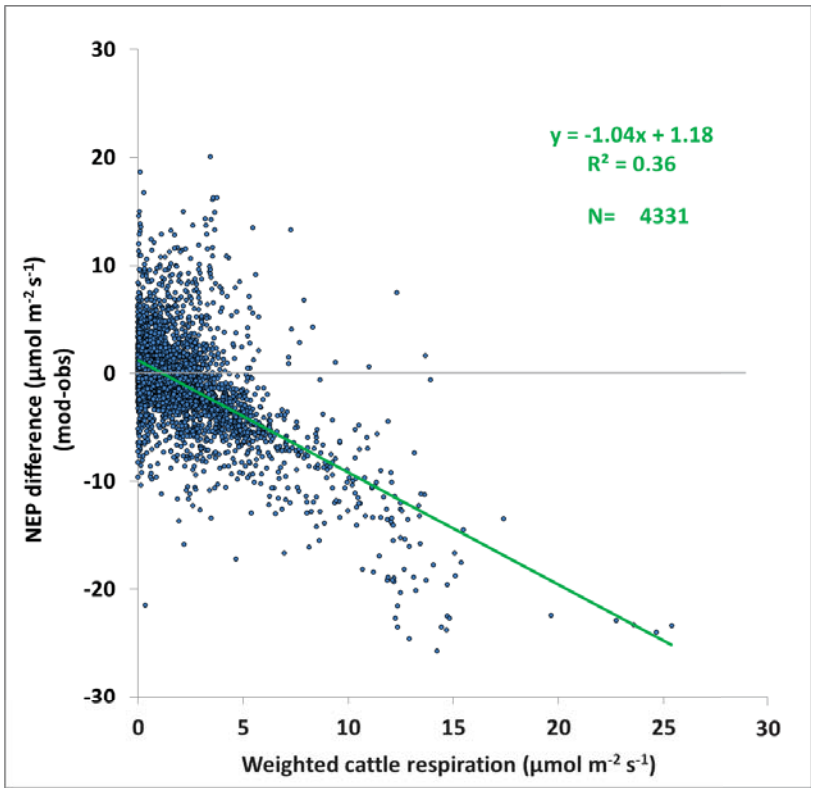

Figure 6.2: Effects of cattle respiration on the difference between modelled and observed half hourly NEP fluxes over two years. Y-axis gives the bias between modelled (CenW_HH) and observed NEP fluxes during grazing events as a function of the grazing animals' respiratory fluxes from the four closest paddocks to the tower for two years of measurements (Equation 6.2). The analysis used only periods when cattle were present in the flux footprint and on one of the four inner paddocks. Observed data include both actually measured and gap-filled data, and modelled cattle respiration was calculated from the modelled flux from each paddock multiplied by each paddock's relative contribution to the flux observed at the tower.

We can see from Figure 6.2 that the discrepancies between modelled and observed NEP fluxes increased as a quasi-linear function of grazing cattle respiration on the inner paddocks. If there had been no problems in the data capture and processing, the differences between modelled and observed NEP fluxes should have been independent from cattle respiration on the inner paddocks. The fitted regression line had a slope close to –1, which indicated that fluxes originating from cattle respiration from the inner paddocks were completely missed from the fluxes observed at the tower, which explained about 36% of the variance of NEP differences between model and data. It seems unequivocal from this relationship (Fig. 6.2) that the presence of grazing cattle

within the footprint of the EC tower had a strong effect on the model/data agreement. To test its significance, a two-tailed Students t-test was used to test the null hypothesis. e.g. there is no difference in model/data agreement between a subsample containing NEP fluxes affected by cattle and another one made of the rest of the dataset. The test was highly significant (p<0.001) and the Null hypothesis was rejected.

The hypothesis that the agreement between observed and gap filled NEP fluxes was affected by the presence of grazing cattle appears to be valid. Because of the strong relationship found in Figure 6.2, the importance of these missed carbon fluxes should have an important impact on annual NEP and NECB and was tested in the following.

Once this relationship had been found, it became necessary to understand why such a strong relationship existed and what was controlling it. First, the sub-dataset of fluxes affected by the presence of dairy cows shown on Figure 6.2 was separated by year (Fig. 6.3).

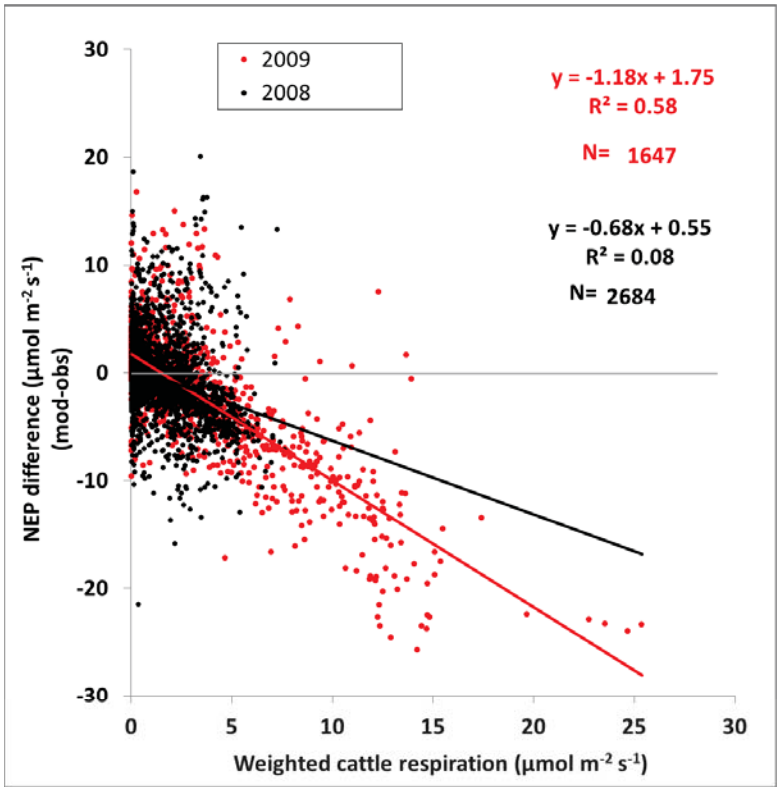

Figure 6.3: Effects of cattle respiration on half hourly differences between modelled and observed NEP fluxes for two consecutive years (2008=black and 2009=red).

In Figure 6.3 we can see that the weighted contribution of cattle respiration was often much higher in 2009 than in 2008. In 2008, the relationship between modelled and NEP data differences and the weighted cattle respiration was weaker than for 2009, as indicated by the slopes of the linear relationships. Also, because of the very low r^2 in 2008 (0.08) it was not possible to get any certainty in this derived relationship. In contrast, in 2009, when there was more intensive grazing, a stronger relationship was found that tends to confirm that the presence of dairy cattle in the flux footprint affected EC measurements.

By looking at the overall effect of the presence of grazing animals within the footprint of the flux measurement described by Figure 6.2, a relationship was found, and by separating the NEP differences by years it was shown that observations taken during 2009 (red dots on Figure 6.3) controlled much of the two year relationship. The linear regression for 2009, with a slope of –1 indicates a strong relationship between the differences in modelled and observed NEP fluxes and the presence of grazing cattle within the footprint. With a coefficient of determination of 0.58, the relationship appears to be more significant than was found for 2008.

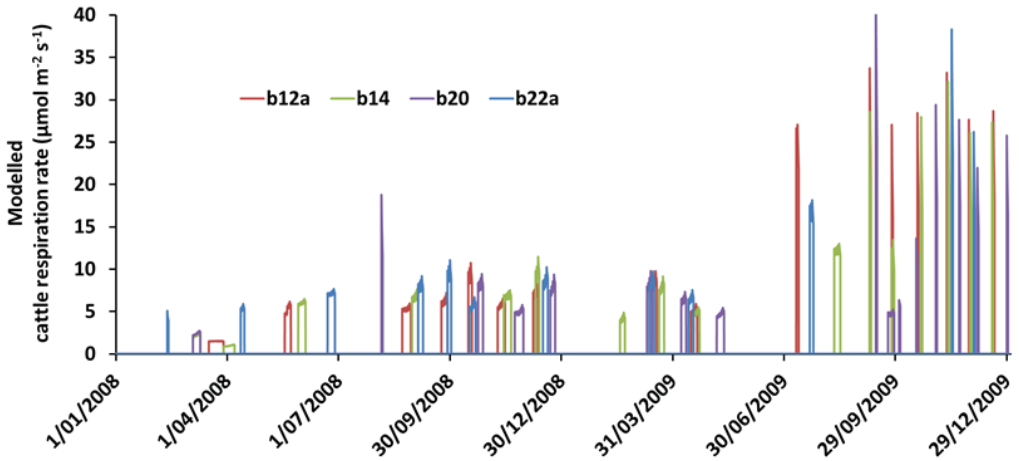

Figure 6.4: Half-hourly modelled cattle respiration rates from the 4 paddocks directly surrounding the EC tower at Scott Farm for 2008 and 2009. The different colours are used to represent the animal respiration rate for each of the four individual paddocks directly surrounding the EC tower.

The dissimilarities between the two years (Fig. 6.3) could be well explained by differences in grazing regimes between the two years (Fig. 6.4 and Rutledge et

al., 2015). Over approximately the first three quarters of the study, grazing events on the various paddocks were mostly spread over several consecutive days and involved lower stocking densities. In contrast, for the last quarter of the study period, from August 2009, most grazing events were constrained to single days because larger herds were used for grazing on each individual paddock. As we can see from Figure 6.4, this change in grazing management caused cattle respiration rates from each of the paddocks to be larger (about twice) and so gives a higher relative contribution of dairy cows' respiration to NEP fluxes and a smaller number of time periods affected by the presence of livestock in the footprint of the tower (2684 in 2008 and 1647 in 2009 as seen in Figure 6.3).

When larger herds were grazing the same surface area over a shorter time period, the cattle respiratory rate from each paddock would be expected to be higher. Under such conditions, the measured NEP flux was then more likely to reach the flux rejection threshold used in the processing of EC data (see section 5.2), which would have added non-random gaps in the dataset to cause the non-capture of large carbon losses. These gaps were non-randomly distributed in the dataset because they corresponded to specific conditions, e.g. grazing events.

By looking separately at how grazing animals' respiration affects the differences between modelled and observed net ecosystem productivity fluxes for 2 years with contrasting grazing management (Fig. 6.3), it became clear that the discrepancies between modelled and observed fluxes increased with grazing intensity.

6.3.2 Effect of dairy cattle respiration on the difference between modelled, observed and gap filled fluxes during night time

In this section, no separation between years was used; the data plotted on Figure 6.5 corresponded to a subset of the total measurement period where cows were present in one of the four paddocks directly surrounding the EC tower and in its footprint. Here, only the 2603 data points corresponding to night-time periods (PPFD<10 μmol m^{-2} s^{-1}) were selected out of the 4331 data

points shown on Figure 6.2. As shown in Figure 6.5, the 306 actual measurements were plotted on panel a) and the 2297 gap filled ones on panel b). There are many more points in the gap filled data set than observed ones, which is normal, because of the high percentage of gaps in the dataset during night time (81.3 % see Table 5.2 in Paragraph 5.2). However, it was not obvious why there were many more gap-filled data than observed ones. First, night time climatic conditions are usually more stable than during daytime and so unfavourable for EC measurements. Second, even if climatic conditions were adequate for measurement, during nights, there is no carbon assimilation (positive fluxes) but only pasture respiration (negative flux) and when adding the large respiration from animals to the base rate, it was more likely to be rejected by the fluxes quality control procedures described in section 5.2 and in Rutledge et al. (2015).

Both of the graphs presented in Figure 6.5 depict a strong influence of cattle respiration on the differences between modelled and observed NEP. The slope of the linear regression is very close to –1 in both cases but the coefficient of determination for the relationship concerning gap-filled data is about twice the R^2 of the actual observations, 0.68 and 0.37 respectively.

Actual observations (Fig. 6.5 a) were measured almost exclusively during times when the “weighted cattle respiration” was very low, e.g. less than or equal to 5 µmol m^{-2} s^{-1}, with only three observations measured when cattle respiration was higher. These three points also presented the worst model/data agreement corresponding to an overestimation of the modelled ecosystem respiration rate in this particular case. Gap-filled data (Fig. 6.5 b) correspond to periods of measurement that were more strongly affected by the respiration rate of grazing cattle with values of “weighted cattle respiration” up to 25 µmol m^{-2} s^{-1} and more points above 5 µmol m^{-2} s^{-1} compared with observations.

During nights, NEP fluxes represent ER (negative flux) because there is no carbon assimilation through photosynthesis. The negative slope of the relationship between the difference (simulation – observation) of net ecosystem productivity and the weighted cattle respiration tends to indicate that both gap filled and real fluxes were systematically underestimated during grazing events.

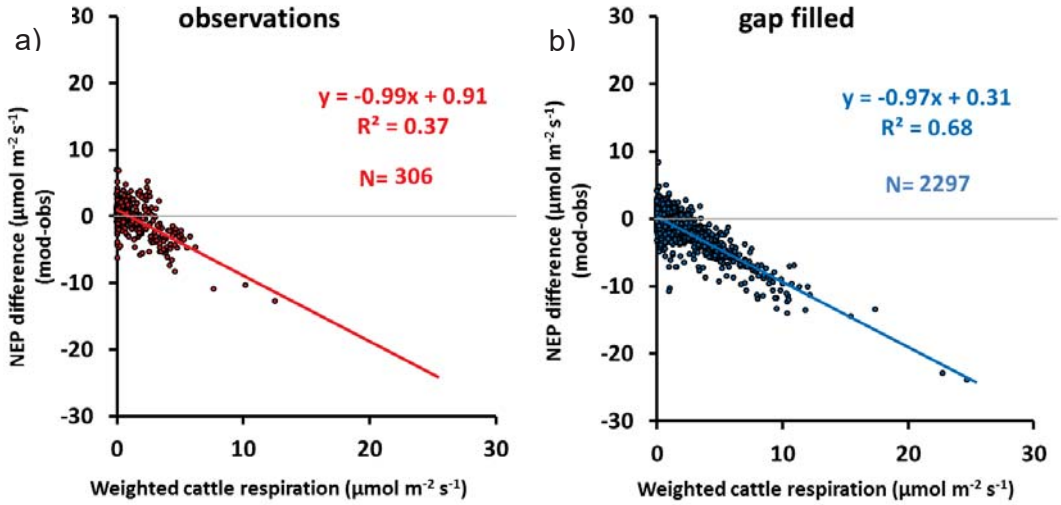

Figure 6.5: Effects of cattle respiration on half-hourly differences between modelled and observed NEP fluxes during night time (PPFD<10 µmol m^{-2} s^{-1}) for the 2 years of the study with a separation between real observations (a) and gap filled observations (b).

In fact, getting such a relationship makes sense for gap-filled NEP data, mainly because gap-filling procedures do not account for all the grazing events in the footprint and their large respiratory losses of carbon. Observed NEP fluxes affected by large cattle respiratory flux might have been excluded from the original dataset when the flux quality control procedures used two of the criterion as indicated in Rutledge et al. (2015). These criteria included: (1) flux values exceeding a threshold number of standard deviations (night-time=4, daytime=3) from the mean flux computed for the appropriate time of the day over a 20-day moving windows and (2) out-of-range flux values (|NEP| > 50 µmol m^{-2} s^{-1}). This could, to some extent, help explain the high number of gaps in the final dataset. Those gaps were then filled according to "modelled" values calculated from the Reichstein et al. (2005) gap-filling and fluxes-partitioning algorithm. This procedure uses actual observations, e.g. mostly C flux measurements slightly or not affected by cattle respiration, to fill gaps caused by the rejection of large carbon fluxes made of the contributions of the pasture and grazing cattle respiration rates. However, unlike pasture respiration, cattle respiration is not driven by bioclimatic factors and so it is not possible for the gap-filling procedure, which is based on a look up table of observed fluxes measured under similar climatic conditions, to be used.

To a smaller extent, this also resulted from the large number of night-time gaps in the dataset and size of the averaging windows used to fill the gaps by the Reichstein et al. (2005) algorithm, which could spread over conditions where no grazers have affected the ecosystem respiration rate (Felber et al., 2016).

In contrast, finding an equally strong relationship for the data measured during night time (Fig. 6.5 a) was, at first, surprising. All these observations were not used to parameterise the model because they were classified as affected by grazing animals' respiration and excluded from the parameterisation set. However, because these were real measurements and the parameterised version of CenW had been used to simulate NEP, the hypothesis was that both modelled and observed data should have correctly captured at least some of the cattle respiration and if so, the relationship between the model/data difference and cattle respiration should have been absent, or at least weaker than for the gap filled data. Actual data were therefore studied in more detail in section 6.3.4, after daytime flux patterns are considered in section 6.3.3.

From this study of the difference between half-hourly carbon fluxes measured and modelled during grazing events at night time, it is clear that grazing management and how the EC data are processed are important factors to consider. Traditional gap-filling procedures, like the Reichstein et al. (2005) algorithm used in this study, do not include information about the presence of dairy cows within the footprint and, as shown in Figure 6.5a, the discrepancies between modelled and observed NEP are important and systematic under this circumstances. Not taking into account cattle respiration to fill gaps in the dataset could cause an overestimation of the ecosystem respiration rate and bias the dataset.

6.3.3 Effect of grazing cattle respiration on the difference of modelled, observed and gap filled fluxes during daytime

Figure 6.6 shows a subset of the total measurement period where cows were present in one of the four paddocks directly surrounding the EC tower and in its footprint. In this case, 2319 data corresponding to daytime periods (PPFD≥10 µmol m^{-2} s^{-1}) were selected for analysis out of the 4331 shown in Figure 6.2.

Over the 2319 selected periods spreading over 2 years of data acquisition, 1312 were real measurements and have been plotted on Figure 6.6a, and 1007 involved gaps that have been filled and were displayed on Figure 6.6b. The numbers/quantity of observed and gap-filled NEP data were more even during daytime than night time, primarily because there is a smaller percentage of gaps (39.0 % see Table 5.2 in section 5.2).

In the case of daytime conditions, NEP is the resulting flux from the difference between carbon assimilation rate through photosynthesis and the sum of all respiratory losses (soil + vegetation + grazing animals).

For the same analysis for night-time conditions (Chapter 6.3.2) there was a strong relationship between the difference of modelled and observed NEP fluxes and cattle respiration for both measured (Fig. 6.6a) and gap-filled (Fig. 6.6b) observations. The linear regressions had similar slopes of about –1 for both of the sub-datasets, once again indicating a very strong relationship between model/data errors and cattle respiration. The coefficient of determination is lower for actual observations (0.19) than for the gap-filled data (0.46), which indicates that there is more scatter around the linear regression line due to normal random variations in modelled and observed NEP fluxes (caused by both modelling and measurement errors) and that the relationship is not as strong for actual measurement as it is for gap-filled observations.

With a r^2 of 0.19, the relationship regarding daytime model/observations differences during grazing events (Fig. 6.6a) is not reliable. It is also interesting to notice that the “Weighted cattle respiration” flux for observations is slightly lower than for gap filled values certainly because large respiratory fluxes from grazing cattle were more likely to be rejected by the quality control procedures for flux and were not accounted for by smaller gap filled fluxes. This is illustrated by larger discrepancies between model estimates and data when grazing elevated the contribution from cattle respiration (Fig. 6.6b).

The relationship between the differences of modelled and gap-filled daytime NEP and the weighted cattle respiration shows that the incomplete capture of this extra carbon loss in gap-filled data caused an increasing discrepancy

between modelled and observed data, and this would have biased the dataset and leads to an overestimation of NEP during daytime periods (inferring more photosynthesis and less respiration).

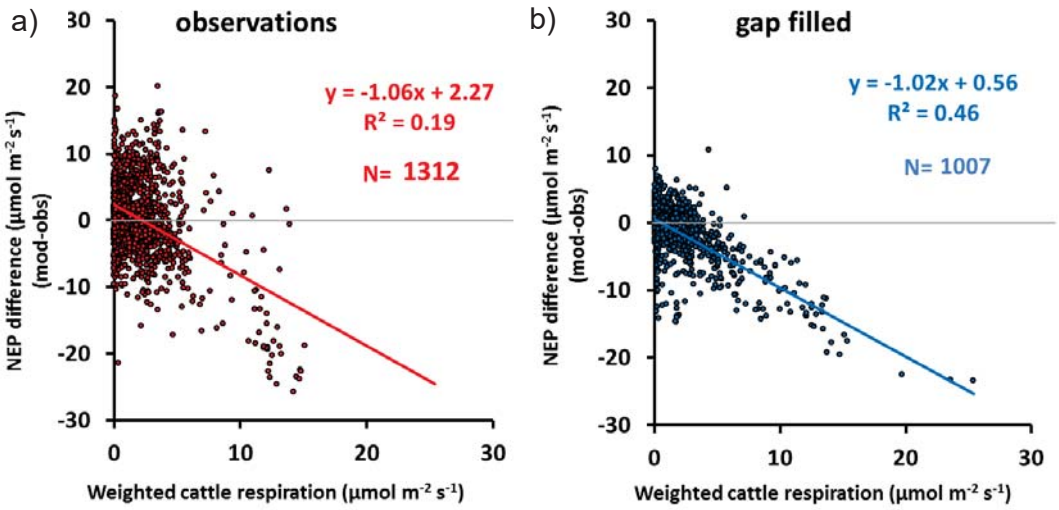

Figure 6.6: Effects of cattle respiration on half-hourly differences between modelled and observed NEP fluxes during day time (PPFD>10 µmol m^{-2} s^{-1}) for the 2 years of the study with a separation between real observations (a) and gap filled observations (b).

Actual observations (night-Section 6.3.2 and daytime Section 6.3.3) had not been expected to give the stronger relationship with modelled data. The data are studied in more detail below (see section 6.3.4).

6.3.4 Re-analysis of actual observation/model agreement affected by the presence of livestock

As discussed in the previous sections of this chapter, it makes sense to get a slope of –1 for gap filled data (Figs. 6.5b, 6.6b) because the Reichstein et al. (2005) gap filling and flux partitioning algorithm used in the study did not use any information about the large contribution and presence of respiring cattle to provide the missing flux values. This caused an underestimation of the carbon respiratory losses when grazing events occurred in the flux footprint. Also, the bias that it could have added to the dataset might have been accentuated by the fact that measurement periods affected to a large extent by the large flux coming from the respiration of grazing animals were likely to be systemically removed from the dataset by the quality control procedures.

It was even more surprising to get a linear relationship with a slope of –1 for actual observations (Figs. 6.5a, 6.6a) because, as they were actually measured by the EC system and not rejected by the flux quality checks, they should have contained some contribution of animals' respiratory losses of carbon which should have been reproduced by the model. However, having such a strong relationship could indicate either 1) an error in the originating area of the flux (no contribution from grazed paddocks) in this case the model simulates correctly all fluxes from each individual paddocks but the footprint used for the spatial integration was not correct, 2) a too large modelled animal respiration rate that could have reduced the modelled NEP flux but which was not as strong in the field, and 3) erroneous or not precise enough records of grazing events occurring on the different paddocks.

We focussed this part of the study on actual NEP measurements made during data acquisition periods which should have been affected by the presence of dairy cows during night time (Fig. 6.10a) and during daytime (Fig. 6.10b), which were based on the same data subsets as the ones shown in sections 6.3.2 and 6.3.3. The overall aim was to identify the possible causes leading to such an unexpected relationship between NEP differences and the weighted cattle respiration rate for actual observations.

We specifically selected points that were likely to drive the relationship between model/data agreement and the large contribution from cattle respiration on the four inner paddocks. This was done by ranking the points presented on the scatter plots of Figures 6.5a and 6.6a based on the combination of two criteria: 1) periods with the largest divergence of modelled and observed NEP fluxes, and 2) points with the largest contribution from grazing cattle.

As Figure 6.7 shows, excluding points from the sub-datasets has a strong effect on the coefficients of the linear regression (slope and R^2) for both night time (Fig. 6.7a) and daytime (Fig. 6.7b) conditions. The general trends, for night time periods, for the slope of the linear regression and for its corresponding coefficient of determination are a reduction from around –1 to –0.3 and from 0.35 to less than 0.03 respectively. The same trends are also observed for

daytime conditions with slopes reducing from –1 to –0.4 and r^2 from 0.2 to less than 0.03.

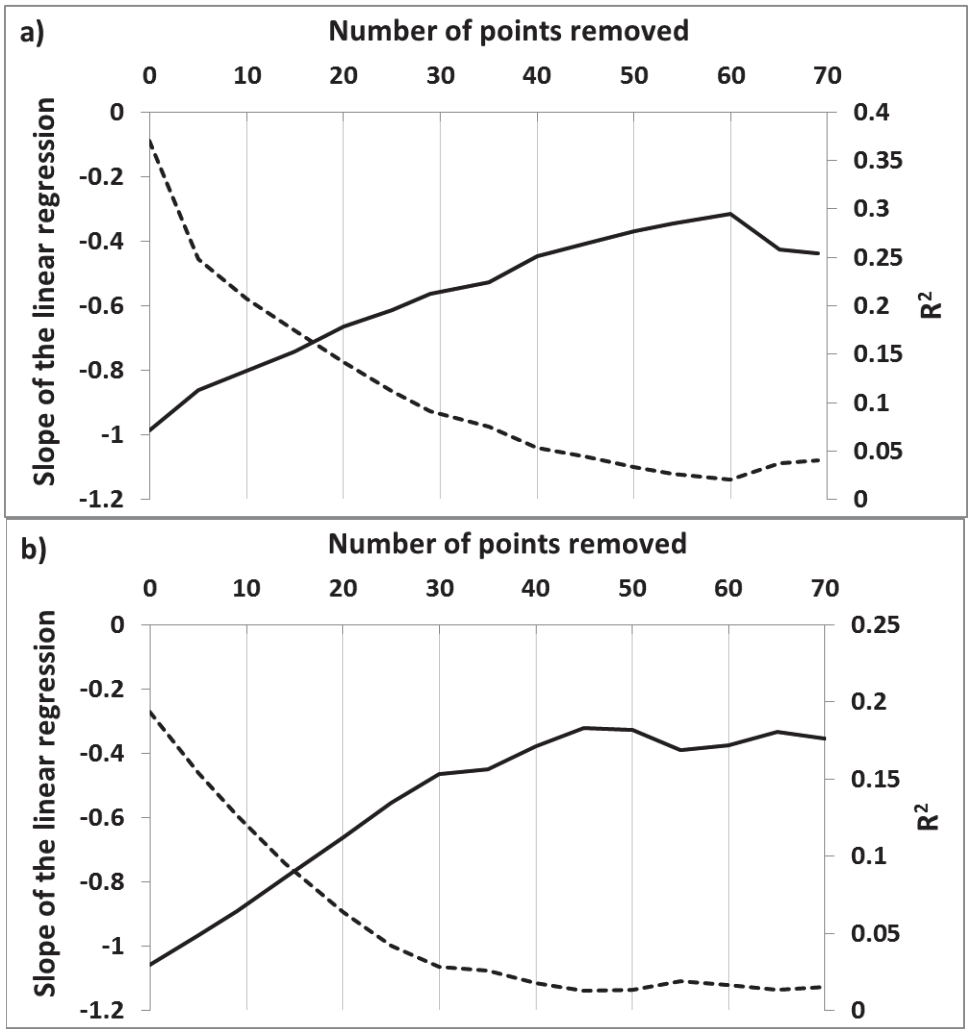

Figure 6.7: Effects of removing the points with the largest divergence between modelled and observed NEP fluxes with the largest contribution from grazed paddocks on the slope (line) and R^2 coefficients of the linear regressions for night time (a) and daytime (b).

A threshold corresponding to the exclusion of the 40 points with the higher ranks based on the conditions given above (shown in green in Fig. 6.10) was arbitrary chosen as it allowed a significant reduction of the values of the regression parameters while keeping a significant number of observations in the study. The temporal analysis of the repartitioning of these 80 points (40 for night time and 40 for daytime measurement conditions) showed that all the points coloured in green have the largest differences between observed NEP fluxes

and CenW_HH simulations. Most of them corresponded to periods of consecutive hours on given days spread over the 2 years of the study period. For illustrative purpose, points measured on the 18/12/2009 were selected to be studied in detail in the following.

Figure 6.8, which is presented below, shows the time series of half-hourly observed, gap-filled and modelled NEP fluxes for 5 consecutive days in December 2009 (14–18 December) with their corresponding daily averaged paddock contribution and the daily records of cows' positions. This period was selected to illustrate the study and get a better understanding of measurement conditions encountered at the farm and their effects on carbon fluxes. During these 5 days, most of night time fluxes were missing, as were the gap-filled (red dots) fluxes. In contrast, most of daytime conditions were favourable to eddy covariance measurements and most of the fluxes were actual observations (Fig. 6.8). On 14 December 2009, no grazing events were recorded in the 26 paddocks and most of the C flux originated from the closest paddocks to the tower. As we can observe, both NEP fluxes modelled, observed, and gap filled, agreed very well.

On the second day (15 December), cows were brought in to graze a paddock outside the four inner ones. Over this day, the contribution of the grazed paddock to the overall measured NEP flux was low, e.g. only a small fraction of the C flux originating from the grazed paddock is effectively measured by the EC system, and here again, the model/data agreement was very good.

On the third day (16 December), grazing animals were moved to the next paddock, also not one of the four inner paddocks, to be grazed. This time period corresponded to the intensive grazing management where paddocks were grazed with larger herds and for shorter time. The footprint indicated a very small contribution from the grazed paddock and again there was very good agreement between CenW simulations and both observed and gap-filled NEP fluxes.

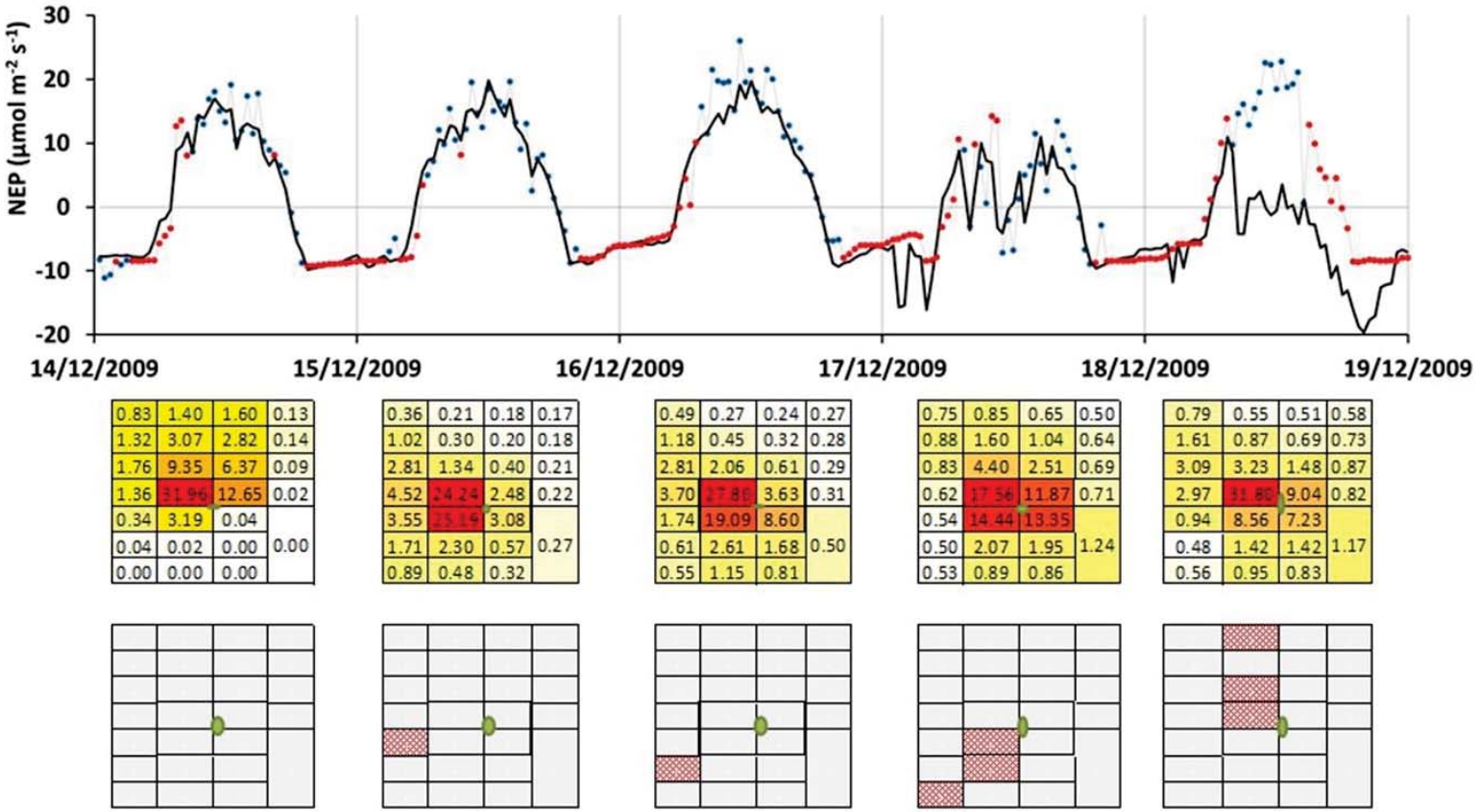

Figure 6.8: Time series of observed (blue dots), gap filled (red dots) and modelled (black continuous line) NEP over 5 consecutive days with their corresponding daily averaged footprints (the sum of the percentage in the boxes do not add to 100% because the contributions from outside the 26 paddocks is not shown) and the location of paddocks being grazed on that day according to farm management records (shaded boxes).

On the fourth day (17 December), 3 paddocks out of 26 were grazed, including a significant representation of one the four just surrounding the tower. Data for this day illustrate well the conditions highlighted by the analysis in this chapter, e.g. measured NEP flux influenced by the presence of grazing cattle on the inner paddock. The footprint analysis shows there were some shifts in the wind direction during the day, as illustrated by the nearly equal relative contribution of the four inner paddocks. The overall model/data agreement is very good under these sampling conditions. It shows some periods indicating that both model and observations agreed well and were able to capture the reduction of NEP due to the extra respiratory flux from cattle. At times the footprint indicated a substantial contribution from the grazed paddock, which was captured by the model (decreases in modelled NEP) but was not in the data as they corresponded to gap-filled observations.

On the fifth and last day of this period (18 December), grazing records indicated that all three herds were moved to other paddocks, always within the boundaries of the 26 paddocks around the tower determining the study area. Over that day, there should have been a large contribution from the grazed paddock to the measured NEP flux as indicated by the footprint and grazing records. However, actual observations gave no indications of any significant grazing cattle respiratory fluxes, and large discrepancies between modelled and observed NEP occurred, e.g. large differences between modelled and observed (blue dots) NEP.

To further understand the causes for such large discrepancies between the model and the data, this last day was studied in more detail in the following (Fig. 6.9). During the first 4 days, there was good agreement between the model simulations and observations of the carbon flux with or without the presence of grazing animals within the footprint before, but on the last day of the selected period, there were large discrepancies.

Figure 6.9a shows in detail observed (blue dots), gap-filled (red dots) and modelled (black line) NEP fluxes obtained for 18 December 2009, the small scheme on the top right gave the position of the cows, which was recorded for this day, and different background colours were used to differentiate six periods

(P1 – P6) where measurement conditions were different. In addition, Figure 6.9b shows the averaged relative paddocks contribution to the measured NEP flux for those six periods. The average is made over the time span of the period of interest.

The first period (P1) corresponds to a night time (NEP=ER) period where the wind was mostly blowing from the other side of the grazed paddocks. This caused the non-capture of the grazing event in measurements, therefore gap-filled data were introduced and model simulations agree with the gap-filled data in this period. Some wind shift during the period caused a reduction of the modelled NEP as indicated by the sudden drops in the modelled flux, which were not seen in the observation because data have been gap filled and, as discussed previously, the Reichstein et al. (2005) gap-filling procedure cannot deal with fluxes from grazing animals.

P2 was an early morning period that went from 6 am (sunrise) to 7.30 am. All measurement corresponded to gap-filled fluxes with the wind, as for P1, coming from the direction of un-grazed paddocks and so the respiration of the cows would have affected neither data nor simulations – again, gap-filled and modelled NEP fluxes agree well. In the very stable atmospheric conditions that were not favourable for EC measurements there are also some missing footprint observations, which were replaced by the average contribution of all the 27 paddocks.

P3 was more problematic and the one in which we are more particularly interested in this section of the study. This time period corresponds to daytime conditions and all data were actual observations. A complete shift in the wind direction occurred compared with the previous period (P2) and over the entire period, therefore more than half the measured NEP flux should have come from the grazed inner paddock (Fig. 6.9b). However, there were large discrepancies between modelled and observed carbon fluxes, with observations indicating fluxes about 20 μmol m^{-2} s^{-1} higher than the modelled fluxes. These data points were some that differed most from modelled fluxes over the 2 years and after model parameterisation.

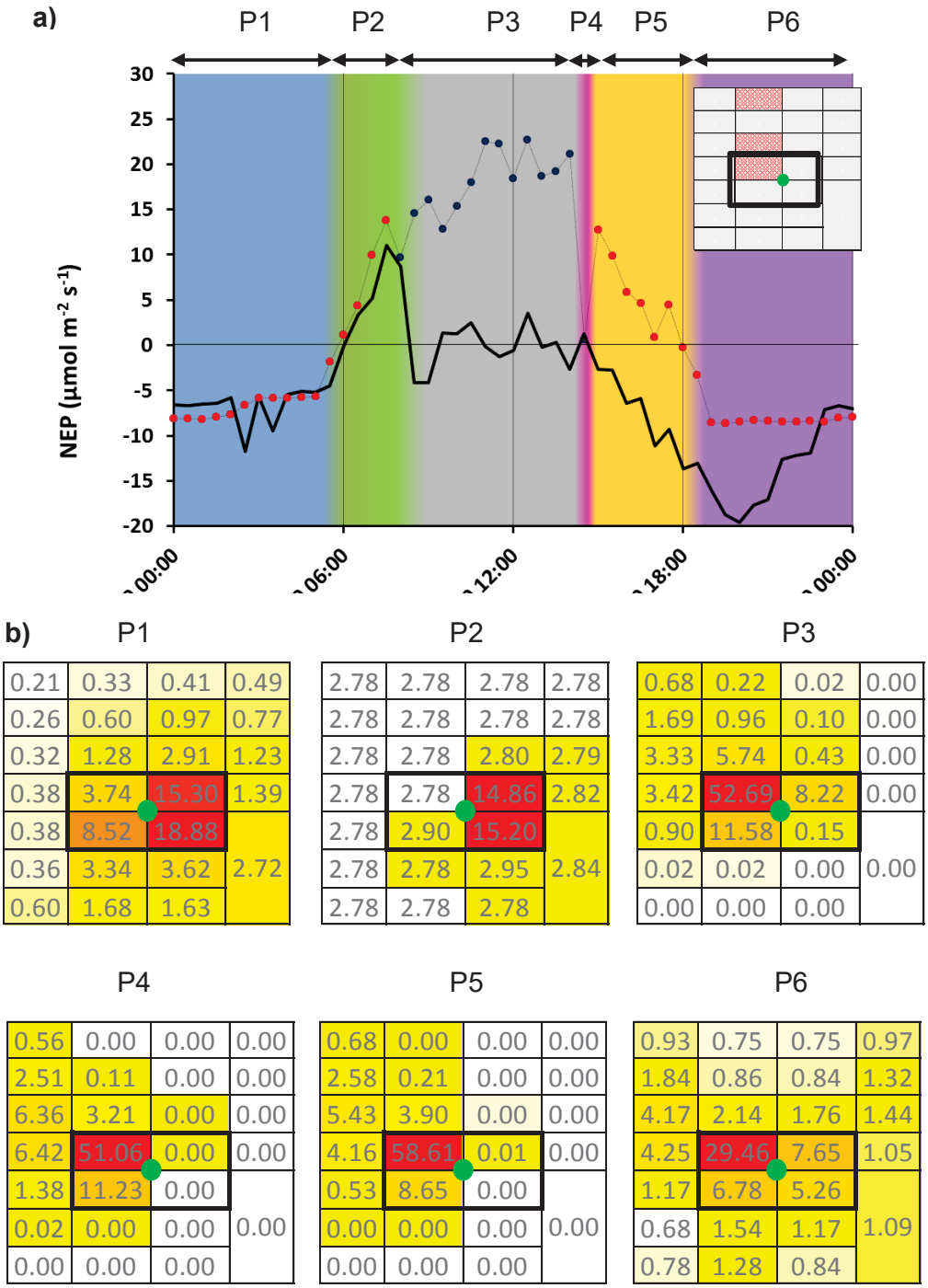

Figure 6.9: a) Observed (blue dots), gap-filled (red dots) and modelled (black line) NEP for different periods of the day (18/12/2009), the recorded cows position (top right insert), and six periods with different measurements conditions described in the text. b) Modelled footprint contribution of the surface area to the measured fluxes averaged over the time span of the different periods.

Different reasons could potentially explain these differences between modelled and observed NEP data: 1) errors in the footprint model, which is, however, unlikely because the estimate of the footprint area worked fine for the previous days; 2) errors in CenW simulations, which is also unlikely to have badly modelled cattle respiration by such a significant amount; 3) errors in NEP data, which are also not likely in this case because all NEP fluxes correspond to actual observations that passed the quality checks and as indicated by the excellent agreement found on preceding days; 4) insufficient information in the grazing records. This last reason appears to be the most valid explanation as even if the recorded paddock was effectively grazed no information was available on the precise timing of cattle movement on the farm or on the number of dairy cows in each of the small herds grazing the different paddocks.

P4 consisted of only a single half-hour observation, which was also measured during daytime with a very similar footprint distribution to P3 (Fig. 6.9b) but in this case the model/data agreement was very good, which indicated that cows were, at this time, effectively grazing the recorded paddock as indicated by the close to zero NEP flux and the important respiratory flux modelled by CenW_HH (not shown). The most valid explanation for the large variance between modelled and observed values is that this measurement corresponded to the actual timing at which the cows were moved onto the paddock recorded as being grazed on that day.

The next period (P5) consisted in measurement taken in the afternoon and until sunset. Data acquisition conditions were good and the contribution from the grazed paddock was the largest for this day, with more than 58%. However, measurements did not pass the quality check procedures and data were excluded from observations and were gap-filled. For this period, the most convincing hypothesis was that cows were grazing the recorded paddock and that the measured flux was largely affected by the animals' respiration, which caused the rejection of the data. The modelled/gap-filled NEP differences were important because while the CenW_HH takes into account the respiration from grazing animals, the Reichstein et al. (2005) gap-filling algorithm does not, which caused an overestimation of the carbon assimilation by the ecosystem.

P6 (the last period) was a night time period and all measurements were gap-filled. During the first hours of the night, the footprint indicated that the carbon flux was coming from the grazed paddocks and again the model/data agreement was poor. Later, the wind direction shifted and most of the flux came from un-grazed paddocks, which reduced the differences between modelled and gap filled carbon flux.

The detailed analysis of the data for these periods increased the understanding of the conditions responsible for the largest discrepancies between modelled and observed NEP fluxes during data acquisition periods affected by grazing cattle respiration.

Data points plotted on Figures 6.10a and 6.10b were actual observations. The observations should have captured cattle respiratory losses during some of the grazing events. As we have seen in the previous sections, actual measurements do not show a relationship as strong as the one derived for gap filled data both during nights and days. There were also fewer points strongly affected by grazing animals' respiration.

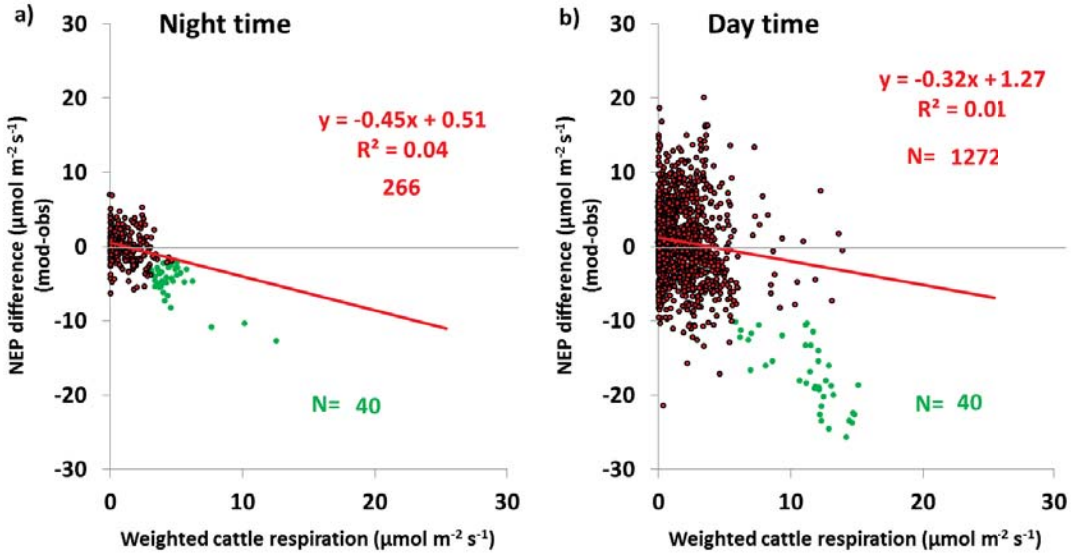

Figure 6.10: Re-analysis of the effects of grazing animals' respiration on half-hourly differences between modelled and observed NEP fluxes during night time (left) and day time (right) for the 2 years of the study. Green dots represent identified periods where cattle position was not precise enough and were excluded from the subsets.

By removing from the graph those points (around 40 for each case), a new relationship was derived. As indicated by the slopes of the linear regressions, the effect of cattle respiration on NEP model/data difference has been weakened with slopes of only –0.45 and –0.33 and R^2 of 0.04 and 0.01 for nights and daytime respectively. Because of the very low coefficients of determination it is possible to determine that there is a lot of scatter caused by random errors in CenW_HH, measurement and footprint model but not systematic errors related to the non-capture of grazing animals' respiration in actual NEP observations.

This part of the study seems to indicate that the records of positions and timing of movements of cattle on the farm were not detailed enough. It concerns especially the timing and time spent in the milking shed and the records of cows' movements between paddocks within a given day. These cattle movements on the farm include the effective length of grazing events on each individual paddocks, which is usually driven by seasons and amount of grass available to feed the variable cow feed demand (i.e. period of lactation). Cow movements and grazing intervals will reflect the interaction of feed supply and demand: when there is insufficient standing grass in the paddock to support feed demand, cows will graze for short intervals; conversely, when pasture covers are high two periods of grazing may be required to eat the supply. The herd may be returned to the paddock to finish the grazing for a few hours before being moved to another paddock. Because farm records do not contain this important information, CenW_HH is unable to simulate accurate NEP estimates.

6.3.5 Effect of cattle respiration on cumulative NEP observed and modelled over 2 years.

Previous sections highlighted the biases between modelled and observed half-hourly NEP fluxes when grazing cattle were present in the footprint of the EC tower and have shown that large discrepancies existed for both night time and daytime gap-filled fluxes.

In this section, the magnitude of the difference between using a conventional gap-filling method (grazing animal respiration excluded) and the detailed modelling scheme (grazing animal respiration included) is quantified.

To study the effect of using incorrect estimates of gap-filled net ecosystem productivity fluxes during grazing events, two datasets have been used. Both datasets used the same data when actual measurements had been available, but they differed in the handling of data gaps. For the first dataset, the Reichstein et al. (2005) algorithm was used to fill all the gaps present in the data set, which is the traditional technique ("Reichstein gap filled" in Figure 6.11) and was used by Rutledge et al. (2015). The second dataset is similar to the first dataset except that all gap-filled fluxes influenced by the respiration of dairy cows on the four inner paddocks were replaced by the modelled NEP coming from CenW_HH ("CenW gap filled" on Fig. 6.11).

Differences between using traditional gap-filling techniques (which do not include the contribution of grazing animals in the respiratory fluxes) and the use of detailed farm modelling (CenW_HH) combined with footprint information are shown in Figure 6.11.

The two lines start to deviate just after the beginning of the first grazing season in March 2008. We also observe that the difference between the 2 lines remained the same as long as the grazing regime remained similar (until August 2009), but differences became even more pronounced (dashed line on Fig. 6.11) with the use of the more intensive grazing management that was implemented at the end of 2009.

After 2 years, we can see from the data plotted on Figure 6.11 that the cumulative carbon uptake at Scott farm was positive. Calculations had shown that 3732 kgC ha^{-1} have been fixed at Scott Farm after 2 years if we choose to use the traditional gap filling routine, but only 2971 kgC ha^{-1} have been fixed when the second approach was used. The 760 kgC ha^{-1} difference indicates the quantitative importance of specifically taking into account cattle respiration when filling half-hourly NEP gaps.

Rutledge et al. (2015) estimated the net ecosystem carbon budget (NECB) of Scott Farm for 2008 and 2009 by taking into account all carbon imports and exports and found that after these 2 years (Table 6.1) the study site was a net carbon sink with a NECB of 1285 ± 1064 kgC ha^{-1}.

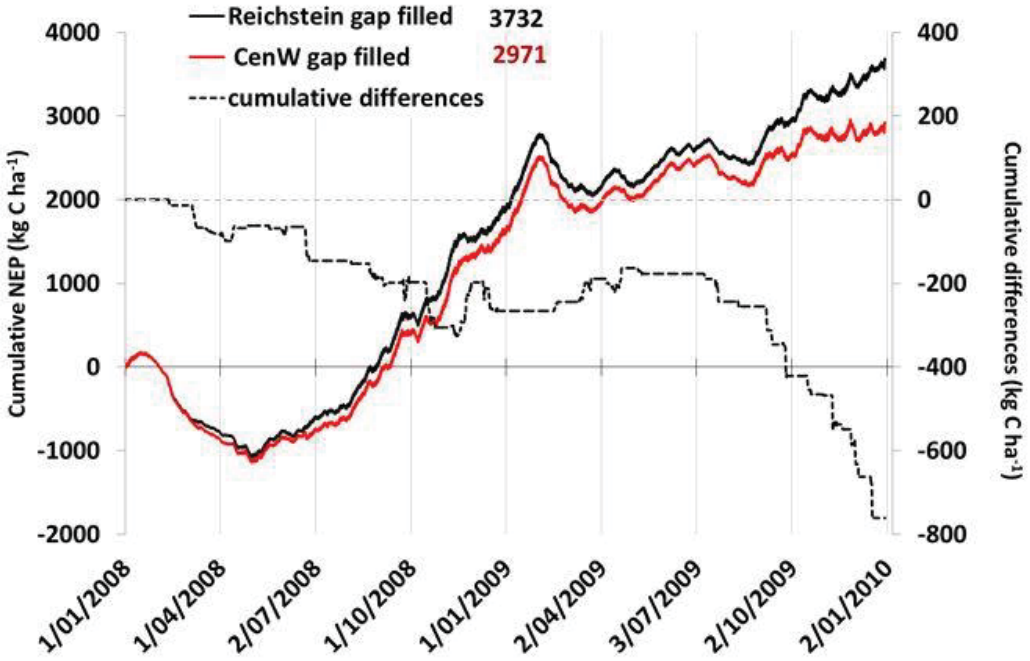

Figure 6.11: Cumulative NEP over the 2 years of EC measurement for the original data set in which gaps were filled with the conventional Reichstein et al. (2005) gap-filling algorithm (black) and data where modelled NEP flux values (with CenW_HH) were used to fill the gaps affected by the presence of livestock on the four inner paddocks (red). The dashed line represents the cumulative differences between the two gap filling procedures (CenW gap-filled – Reichstein gap-filled).

In 2008, the difference in NEP between the two gap-filling strategies was 262 kgC ha^{-1} y^{-1} and was even larger in 2009, with 500 kgC ha^{-1} y^{-1}. As indicated above, those differences were only caused by taking into account the contribution of grazing animals' respiration in the gap filling of NEP flux and this finding highlighted the importance of the carbon respiratory losses during grazing events. In both years of the study, NEP was the predominant net carbon input into the ecosystem and the inclusion of cattle respiration in the gap filled fluxes caused a reduction of 262 and 500 kgC ha^{-1} y^{-1} for 2008 and 2009 respectively. Accounting for cattle respiration therefore has a very significant effect on the total carbon budget of the study site. NECB was reduced by 31%

in 2008 and by 113% in 2009, turning this year from a calculated sink into a carbon source.

An extra NECB of 762 kgC ha^{-1} appears to have been found in this study, caused by the missing estimates of hourly grazing animal respiratory C losses in gap-filled data. If the same error estimates on "non-CO_2-C fluxes" as used in Rutledge et al. (2015) are considered, then it is not possible to conclude with any confidence that the study site was a net C sink. The newly derived NECB is now equal to 523 ± 1064 kgC ha^{-1} and because of the large error intervals associated with non-CO_2-C fluxes, Scott Farm could either be a source, neutral or a sink of carbon.

Table 6.1: Components and uncertainties of annual carbon balance (NECB) for Scott Farm (2008-2009). All data were extracted from Rutledge et al. (2015) except "NEP CenW gap filled" and "NECB CenW" which were recalculated for this study by replacing all gap filled NEP data affected by cattle respiration by their CenW modelled counterparts. All components of the carbon balance were expressed in kgC ha^{-1} y^{-1} except for the Sum which is the sum over the two years of the study and was given in kgC ha^{-1}

C flux	2008	2009	Sum
NEP Reichstein gap filled	1895 ± 542	1837 ± 466	3732 ± 1008
NEP CenW gap filled	1633	1338	2971
F_{feed}	202 ± 47	252 ± 59	454 ± 106
$F_{effluent}$	0	0	0
$F_{product}$ (milk)	659 ± 99	768 ± 154	1427 ± 253
$F_{harvest}$	128 ± 18	296 ± 42	424 ± 60
$F_{methane}$	174 ± 35	205 ± 41	379 ± 76
F_{dung}	146 ± 37	198 ± 50	344 ± 87
F_{resp}	92 ± 29	124 ± 40	216 ± 69
F_{leach}	55 ± 55	55 ± 55	110 ± 110
NECB Reichstein	843 ± 559	442 ± 505	1285 ± 1064
NECB CenW	581 ± 559	-58 ±505	523 ± 1064

This finding is certainly important for the carbon budget of Scott Farm but it is also highly relevant for other studies measuring the carbon budget of intensively grazed dairy pasture. Modifications of the farm carbon budget by taking into

account the extra respiratory losses of CO_2 from cattle during grazing events appeared to be important for Scott Farm. The recent study of an intensive dairy pasture in Switzerland from Felber et al. (2016) also found significant differences in annual carbon fluxes estimates when the contribution of grazing animals was or was not taken into account. This Swiss study took place on a similar pasture type to the one encountered at Scott Farm (grass/clover mix), on rotationally grazed 0.6-ha paddocks with an effective stocking rate of 5.6 cows/ha, which is higher than the 3 cows/ha at Scott Farm. Felber et al. (2016) estimated that the respiration of cows was responsible of a reduction of 180 gC m^{-2} yr^{-1} (1800 kgC ha^{-1} yr^{-1}) of the annual NEP. This is higher than that found in this study of Scott Farm and should be largely correlated to differences in farm management practices, soil properties and climate.

It would be good practice for the study of grazed grasslands with eddy covariance systems to ensure the position of cattle is as accurate as possible through GPS collars on cows, digital cameras or farm records to account for the respiration of animals from within the flux footprint. These periods should be processed separately in order to reach better flux estimates and possibly reconcile carbon budgets derived from EC measurements and soil sampling studies (Skinner and Dell, 2015).

6.4 General discussion

This chapter highlighted the importance of cattle respiration on NEP fluxes measured by eddy covariance. As shown, having good records of animal position is critical for examining processes at short time steps, e.g. hourly and daily, or to parameterise models. It is even more important if the data are to be used to predict long-term carbon budgets and changes in soil carbon stocks or the climate change mitigation potential of grasslands because, as this study shows, once errors were introduced in measurement (at an half hourly time step) they would not cancel out or disappear from the dataset.

The Scott Farm dataset does not contain the required information on animal location that is needed to properly understand what really happened during

grazing events, using positioning devices like GPS or pictures might have helped to determine the real impact of animal respiration on measurements (Felber et al., 2015, 2016).

A detailed, process-based ecosystem model (CenW_HH) running at a half-hourly time step (same as EC measurements) was able to simulate management practices (especially grazing events) from farm records and therefore study and quantify the long-term effects of cattle respiration on NEP fluxes and carbon budget of the dairy farm. This study would not have been possible without using such a detailed model, mostly because the design of the original study was not aimed to specifically investigate the effects of grazing animals respiratory carbon losses on farm carbon budget as it was studied in this section. In another study where the farm layout was similar to Scott Farm, Felber et al. (2016) used the number of cows present in the footprint based on footprint analysis and GPS devices to estimate cattle respiration and get different estimates of C fluxes by either using or not using cows' respiration. While Hunt et al. (2016), Skinner (2008), and Skinner and Dell (2015) excluded periods from their datasets that were affected by the presence of animals in the footprint, and the effect of cattle was taken into account only in the annual budget through the amount of grass removed during grazing events (see publications for details). The farm layout in those studies was more typical, with larger herds and paddocks and, as reported by Hunt et al. (2016), the presence of cows in the vicinity of the tower only affected about 3% of the measurement periods during the year of the study.

The small paddocks (and relatively small herd sizes) at Scott Farm meant that fluxes from cattle respiration would not have dominated overall fluxes as much as they would have if only one large herd had been grazing larger paddocks, but it made it easier to capture the animals' respiratory losses. In more traditional intensive dairy farms in New Zealand, in which larger herds graze larger areas over a short time period (Hunt et al., 2016), the effects of animal respiration on NEP measurement should be similar to observations for the end of the second year (2009) at Scott Farm. It should give larger respiration contributions from higher grazing numbers/ha but with fewer measurement

periods affected by the presence of grazing cattle in the footprint. This hypothesis will need to be tested in future modelling studies of more conventional dairy farms with precise recordings of animals' positions.

The presence of cows in the flux footprint of the EC tower and the timing of grazing are important. If there are data gaps at times with large animal respiratory losses and gaps are filled based on observations without grazer respiration, resultant net fluxes could be substantially overestimated. The opposite is also true, and if data affected by livestock respiration (high respiration rate) are used to fill gaps for periods without grazing dairy cows, the resulting NEP flux would be underestimated. These problems would also not be overcome even if data were averaged over 7 days before and after any gaps.

Intensively grazed grasslands with small paddocks, like Scott Farm, are particularly hard to study with eddy covariance because the flux footprint can be spread over several paddocks at any given time, and there are likely to be different stages of vegetation recovery after grazing. The spatial distribution of small herds around the EC tower made it nearly impossible to remove periods where grazing animals were present in the footprint area (Mudge et al., 2011; Felber et al., 2016). The Reichstein et al. (2005) gap-filling algorithm does not explicitly consider the presence of grazing cattle in the calculation of missing fluxes, which can lead to unreliable flux estimates during grazing events. This proved to be important in annual carbon budget of grazed grasslands.

The advantage of using CenW-HH to fill data gaps comes through its implicit modelling of each of the paddock individually with the simulation of dairy cows' respiration flux. It also modifies the vegetation cover and consequent gas exchange rates following each grazing event. The use of the footprint models makes it possible to incorporate that spatial heterogeneity of flux sources. The fact that the model is mechanistic (process based) also makes it possible to look at specific issues related to grazed pasture. The model could also be used to simulate carbon and water fluxes, energy partitioning, soil water, temperatures, and organic matter behaviour not only for Scott Farm but also for other farming systems as long as sufficient information is available to run and parameterise it.

The main drawbacks are that the model is complex, uses a high number of parameters that need to be calibrated, has to deal with paddock management practices, and needs to run with the same time step as the dataset (typically 30 minutes). It is also necessary to accurately record animal positions and weight the contribution of cattle respiration through estimates of the footprint area.

This study also confirmed that it was better to use only actual observations to parameterise the model and not the complete data set with gap-filled data.

The main issue with the study presented here is the still insufficient information about cattle position and farm management. The daily records available to run the model properly at a half-hourly time step and achieve high model efficiency were not sufficiently detailed. Missing information is mostly related to cattle movements on the farm and corresponds to:

- number, timing and length of milking events for every day
- timing of the beginning and end of grazing events within give days for each paddocks

The more information available on cattle position, the more likely the model/data agreement would be high for measured data and the more realistic for gap-filled data (using a detailed modelling approach).

6.5 Conclusion

It is clear from the results shown in this chapter that the respiratory flux caused by the presence of large grazing animals in the footprint of the eddy covariance tower is a problem that needs to be addressed in EC studies of intensive dairy farms.

The present work is the first modelling study using a half-hourly time step that looked specifically at the effects of cattle respiration on NEP measurements with eddy covariance system made over a long measurement period. This study has shown the importance of taking this extra respiratory C loss into account both in terms of model/data agreement and, more importantly, to derive the NECB of the farm.

Most of model/data discrepancies occurred during periods with missing observations (gaps in NEP measurements). Gap-filled data gave erroneous estimates for grazing days because the gap-filling procedure was parameterised from observations with days without grazing events in the footprint and therefore did not include the large respiratory losses from cattle respiration.

Observed data also posed problems. However, it appeared that these problems were less pronounced than those in the gap-filled data because they have no direct effects on the annual carbon balance; however, they added bias in model carbon fluxes estimates, reducing the model efficiency and possibly the set of optimised parameters. Those issues might have been related to insufficient precision on the position of cattle in the different paddocks for which only daily records were available, errors in the footprint model, or errors in the management records if there was a mismatch between recorded and actual cattle locations on specific days. With the detailed analysis of modelled and observed carbon fluxes, it has been possible to identify clearly those periods when more precise records of animals position on the farm were needed to achieve a better simulation of the fluxes. The missing information consisted of the timing and duration of the times cows spent in the milking shed, the effective length of grazing events on each individual paddock, and the time at which dairy cows were moved to and from the different paddocks.

Problems were more pronounced for night time observations, probably because there were more data gaps to be filled, because of more optimal/appropriate turbulence conditions at day time and because large respiratory carbon losses from grazing cattle were balanced by photosynthetic carbon uptake so that net fluxes were more likely to remain within the observations window of the eddy-flux system. At night time, the two respiratory fluxes (base ecosystem respiration and animal respiration) added together were more likely to reach the data rejection threshold.

There were differences between years because of differences in grazing practices, with smaller herds grazing in 2008, which caused smaller respiration spikes than in 2009, when larger herds grazed paddocks for shorter duration

but more intensively. Bigger problems were therefore encountered with the 2009 data.

Overall, the non-capture of cattle respiratory losses from grazing events was estimated to have amounted to non-recorded respiratory losses from gap-filled periods alone of 262 kgC ha^{-1} $y^{-1}$and 500 kgC ha^{-1} y^{-1} in 2008 and 2009 respectively, which has serious consequences on the estimated overall carbon status of the farm. Taking into account these additional carbon losses in annual NEP calculations (as in "NEP CenW gap filled") reduced the inferred NECB by 31% in 2008 and around 113% in 2009. Rutledge et al. (2015) had concluded that over the 2 years of the study period, Scott Farm had a significant positive carbon balance, e.g. was storing carbon. However, if one considers the NEP bias described here, the carbon status of the farm became more neutral and, within the overall uncertainty of the various terms, the farm could either be a source or a sink. This uncertainty is mostly related to error bounds for non CO_2-C carbon fluxes.

The non-capture of grazing losses is thus a quantitatively serious issue that must be addressed for eddy covariance studies in grazed pastures. One approach is to omit periods when grazing elements are within the vicinity of the tower (Hunt et al., 2016). However, this approach was not an option at Scott Farm because of the use of a mosaic of small mini-paddocks so that some grazing animals were within the footprint area of the tower on most days, even in paddocks further away from the tower, and because of uncertainties in farm records of grazing events (Mudge et al., 2011). It should also be possible to estimate the respiration rate of cattle based on the feed ingested or according to the weight of animals and add it to the NEP flux from the pasture alone (Felber et al., 2016)

An alternative approach, which is the one used here and which gave important insights on the carbon budget of a grazed pasture, is the use of a more sophisticated model, like CenW_HH, to fill in data gaps affected by animals' respiration. Importantly, information about grazing events would need to be explicitly provided as input information to the model runs.

Overall, this study of NEP fluxes measured during grazing events in the footprint of eddy covariance tower proved that the respiratory flux from grazing cattle are likely to be unaccounted for or partly missed, causing a significant bias in the dataset, especially for gap-filled fluxes, leading to an overestimation of the carbon budget of the farm.

CHAPTER 7: CONCLUSION AND PERSPECTIVES

7.1 Summary and conclusion

The overall aim of my PhD was to study carbon dioxide and water vapour fluxes measured continuously at a half-hourly time step over 2 consecutive years (2008–2009) by an eddy-covariance tower located on an intensive dairy farm in the Waikato region of New Zealand.

To achieve this goal, the CenW ecosystem model was modified according to equations presented in Chapters 3 and 4 to make it run at a half-hourly time step corresponding to the sampling interval of the EC system. Different instantaneous leaf photosynthesis routines and integration schemes from the leaf level to the canopy scale have been implemented and tested in CenW_HH (Chapter 3), and the best results were achieved by using the Thornley (2002) photosynthesis routine. With this configuration of the model, there was an overall good correspondence between observed and modelled carbon assimilation rates (GPP) as indicated by a high model efficiency of 0.89 with, however, an apparent under-estimation of the highest fluxes.

To properly simulate water and carbon fluxes with the same time steps as EC data, thus allowing their direct comparison, it was necessary to develop and include new energy and water budget routines in the original daily version of the ecosystem model. The Shuttleworth and Wallace (1985) modelling scheme was chosen and equations were modified to include a litter layer on top of the soil surface and a multilayer soil profile for heat and water transfers.

Soil temperatures simulations highlighted the strong diurnal variability of the response of soil surface temperature to radiative forcing and that drought periods caused an important increase of temperatures, mostly because evapotranspiration rate is reduced, or even stopped, which limits the dissipation of incoming energy by latent heat transfer. Deeper soil layers were not as strongly affected by climate conditions as the soil surface, but longer-term seasonal changes are clearly visible. Flux partitioning and energy budgets are thus strongly affected by water limitation and the temperature dynamics of the different components of the ecosystem. Overall, the energy and water budget procedure as implemented in CenW_HH seemed to respond properly to

changes and variations of climatic conditions experienced at Scott Farm over the measurement period.

After model parameterisation, high model efficiencies were found for half-hourly carbon fluxes, with values of 0.81, 0.75, and 0.70 for NEP, GPP, and ER respectively, showing a very good agreement between modelled and observed C fluxes. Discrepancies between modelled and observed carbon fluxes were attributed to: 1) model parameters that make it impossible to simulate unusually high values while observations are not constrained in that way, and occasionally high true rates will have combined with random upward scatter to give high values not matched by simulations; 2) higher respiratory losses due to grazing events on some paddocks further away and within the footprint of the EC tower that caused CenW_HH to model some higher respiratory rates than those derived by the Reichstein et al. (2005) algorithm; 3) errors in grazing records or in the footprint model. Good agreements were also reported for latent and sensible heat fluxes, net radiation, and soil temperature with model efficiencies of 0.87, 0.76, 0.94, and 0.92 for LE, H, R_n, and T_s respectively. These results showing that the model properly included interactions between all parts of the ecosystem and their seasonal and short-term variations driven by vegetation dynamics and response to climatic conditions at a sub-daily time step. The model responded quite well to drought conditions through stomatal closure to prevent ongoing or additional water losses through transpiration and the reduction of the plant living area to reduce water extraction.

Overall, achieving such high agreements between observed and modelled half-hourly fluxes was only possible through proper selection and implementation of the photosynthesis and energy and water budget routines and modifications of the running time steps of heterotrophic and autotrophic respiration simulation procedures and the overall parameterisation of CenW_HH.

Daily and weekly summed carbon and water fluxes were less well modelled than those obtained with the daily version of the CenW model that were reported in Kirschbaum et al. (2015), as indicated by the lower model efficiencies calculated in this study. The lack of agreement could be due to model or measurement problems, and certainly could be related to problems in

the gap-filling routine. Also, in principle, CenW_HH should be a better predictor than the Reichstein et al. (2005) gap-filling algorithm principally because grazing animals' respiration has been included in a more meaningful way. However, fluxes affected by the presence of grazing animals within the EC footprint were discarded from the analysis in Kirschbaum et al. (2015), which was not the case in this study because those fluxes were large outliers, the statistics would have been reduced.

On a monthly time scale, modelled fluxes agree well with observations but drought periods also strongly affected the capacity of CenW_HH to reproduce observations. During the 2008 drought ER and GPP were overestimated by CenW_HH, and in February 2009 ER_{CenW_HH} was about 600 kgC ha^{-1} lower than $ER_{observation}$. Overall, monthly carbon fluxes showed that the 2 years were quite different in terms of carbon fluxes dynamics and that modelled and observed fluxes generally agreed well.

On an annual time scale, modelled and EC-derived *ER* and *GPP* largely followed similar general patterns, for example, a sharp increase over summer unless there was a drought, more moderate increases over winter, and a sharper increase over spring and into summer. Model/data agreements of cumulative net carbon flux are contrasted for the 2 years of the study. In 2008, the annual net ecosystem productivity was underestimated by 397 kgC ha^{-1} by CenW_HH but overestimated by about 1000 kgC ha^{-1} in 2009 but overall, CenW_HH was able accurately to simulate half hourly observed carbon and water fluxes but with a difference of about 600 kgC ha^{-1} between modelled and observed NEP fluxes at the end of the 2 years. In the process-based CenW_HH model, variables are intrinsically linked, for example, *ER* depends on *GPP*, with most of *ER* coming from recently fixed *GPP* through autotrophic (maintenance + growth respiration). Hence, an overestimate of *GPP*, as over the first year, almost inevitably leads to an overestimate in *ER*; and because carbon fluxes are linked through a conservation of C mass, that discrepancy cannot be overcome by adjusting any parameters of the model.

Once CenW_HH was parameterised and the good agreements between simulations and observations were verified, the model was used to test the

reliability of the Reichstein et al. (2002) gap-filling algorithm under the different climatic conditions that caused gaps in the dataset. Low turbulence conditions ($u^*<0.11$ m s^{-1}) were modelled by CenW_HH with a NSE of 0.81. Most of these gaps occurred during night-time and the model tended to simulate slightly lower positive flux values and some higher night-time fluxes, which was explained by the fact that the explicit grazing respiration from even the outer paddocks were missing in the Reichstein gap-filled data, leading to negative intercepts and underestimates of night-time fluxes in Reichstein and to problems with the footprint model, which is not very reliable under low turbulence. NEP gap-filled fluxes due to rainfall were modelled by CenW_HH with a NSE of 0.86 and gap-filled data from foggy conditions with a model efficiency of 0.87. Differences between modelled and gap-filled fluxes were attributed to the fact that CenW_HH specifically modelled NEP under those climatic conditions, while the Reichstein algorithm extrapolates from “good” climatic conditions to those causing gaps that were not sufficiently representative of what actually happened.

The half-hourly version CenW developed in this study also helped identify weaknesses of EC data and their processing when sampling periods were affected by the presence of grazing animals in the flux footprint. To the best of my knowledge, this was the first modelling study that looked specifically at the effects of cattle respiration on long-term eddy covariance NEP measurements. The importance of taking this extra respiratory C loss into account was highlighted both in terms of model/data agreement and, of more importance, to derive the NECB of the farm.

Gap-filled data gave erroneous estimates for grazing days because the gap-filling procedure was parameterised from observations with days without grazing events in the footprint and therefore did not include the large respiratory losses from cattle respiration causing most of the observed discrepancies between simulations and data.

Differences between actual observations and simulations were less pronounced than those encountered for the gap-filled ones because they have no direct effects on the annual carbon balance. They did, however, add bias to model

carbon fluxes estimates, reducing the model efficiency and possibly biasing the set of optimised parameters. The detailed analysis of modelled and observed carbon fluxes showed that more precise records of animals position on the farm on some periods were needed to achieve a better simulation of the fluxes.

Night-time observations proved to be the more problematic, probably because more data gaps needed to be filled. Also, during nights, base ecosystem respiration and animal respiration added together were more likely to reach the data rejection threshold, as compared with day time, where more optimal/appropriate turbulence conditions are encountered and large respiratory carbon losses from grazing cattle were balanced by photosynthetic carbon uptake so that net fluxes were more likely to remain within the observations window of the eddy-flux system. The biggest differences were encountered with the 2009 data and were related to changes in grazing practices with smaller herds grazing in 2008, which caused smaller respiration spikes than in 2009, when larger herds grazed paddocks for shorter duration but more intensively. The non-capture of cattle respiration during grazing events was estimated to have amounted to non-recorded respiratory losses from gap-filled periods alone of 262 kgC ha^{-1} y^{-1} and 500 kgC ha^{-1} y^{-1} in 2008 and 2009, respectively. By taking into account these additional carbon losses in annual NEP calculations, the inferred NECB was reduced by 31% in 2008 and by around 113% in 2009, which had important effects on the carbon status of the farm.

The study of NEP fluxes measured during grazing events in the footprint of the eddy covariance tower proved that grazing cattle respiration was not likely to be accounted for or partly missed, which caused a significant bias in the dataset, especially for gap-filled fluxes, and led to an overestimation of the farm carbon budget.

7.2 Perspectives for future researches

The model was successfully tested over a challenging dataset and proved that good agreements between modelled and observed water and carbon fluxes were possible after a rigorous parameterisation of the model. However, as

CenW_HH has only been tested and validated on a single study site and with only one dataset, it would be necessary to test it on multiple datasets and locations to fully validate it and reach a better understanding of parameters uncertainties and variabilities.

Currently, the model could only be applied to pastoral systems as it has only been developed to run on this ecosystem type. Further development of the model equations is still possible if the model needs to be applied to other ecosystems. These modifications and runs on other systems would be required to achieve global-scale estimates of carbon, energy, and water fluxes.

Mechanistic are particularly adapted for testing scenarios (Cuddington et al. 2013). Also, as a process-based model, e.g. based on the theoretical understanding of ecological processes, CenW_HH is highly valuable for testing scenarios. Interesting scenarios could be related to modifications of farming practices in order to identify which practices could be implemented to store more carbon in the soil or to better understand how climate change would affect ecosystems in the long term.

REFERENCES

Abberton M, Conant R, Batello C (2010). Grassland carbon sequestration: management, policy and economics. *Proceedings of the Workshop on the role of grassland carbon sequestration in the mitigation of climate change, Integrated Crop Management.*

Adams B, White A, Lenton TM (2004). An analysis of some diverse approaches to modelling terrestrial net primary productivity. *Ecological Modelling*, *177*, 353-391.

Agren GI, Bosatta E (1996). Quality: A bridge fbetween theory and experiment in soil organic matter studies. *Oikos*, 76, 522-528.

Allard V, Soussana JF, Falcimagne R, Berbigier P, Bonnefond JM, Ceschia E, D'Hour P, Henault C, Laville P, Martin C, Pinares-Patino C (2007). The role of grazing management for the net biome productivity and greenhouse gas budget (CO_2, N_2O and CH_4) of semi-natural grassland. *Agriculture Ecosystems & Environment, 121*, 47-58.

Allen DE, Pringle MJ, Page KL, Dalal RC (2010). A review of sampling designs for the measurement of soil organic carbon in Australian grazing lands. *Rangeland Journal*, 32, 227-246.

Ammann C, Flechard CR, Leifeld J, Neftel A, Fuhrer J (2007). The carbon budget of newly established temperate grassland depends on management intensity. Agriculture Ecosystems & Environment, 121, 5-20.

Amthor JS (1994). Scaling CO_2 photosynthesis relationships from the leaf to the canopy. *Photosynthesis Research*, 39, 321-350.

Amundson R. (2001). The carbon budget in soils. *Annual Review of Earth and Planetary Sciences*, 29, 535-562.

Anadranistakis M, Liakatas A, Kerkides P, Rizos S, Gavanosis J, Poulovassilis A (2000). Crop water requirements model tested for crops grown in Greece. Agricultural Water Management, 45, 297-316.

Anderson MC, Norman JM, Meyers TP, Diak GR (2000). An analytical model for estimating canopy transpiration and carbon assimilation fluxes based on canopy light-use efficiency. *Agricultural and Forest Meteorology*, 101, 265-289.

Anten NPR, Hirose T (2003). Shoot structure, leaf physiology, and daily carbon gain of plant species in a tallgrass meadow. *Ecology*, 84, 955-968.

Aubinet M, Grelle A, Ibrom A, Rannik U, Moncrieff J, Foken T, Kowalski AS, Martin PH, Berbigier P, Bernhofer C, Clement R, Elbers J, Granier A, Grunwald T, Morgenstern K, Pilegaard K, Rebmann C, Snijders W, Valentini R, Vesala T (2000). Estimates of the annual net carbon and water exchange of forests: The EUROFLUX methodology. *Advances in Ecological Research*, 30, 113-175.

Aubinet M, Vesala T, Papale D (2012). *Eddy Covariance - A Practical Guide to Measurement and Data Analysis*, Springer, Dordrecht Heidelberg London New York.

Badger MR, Andrews TJ (1974). Effects of CO_2, O_2 and temperature on a high-affinity form of Ribulose Diphosphate Carboxylase-Oxygenase from spinach. *Biochemical and Biophysical Research Communications*, 60, 204-210.

Baldocchi DD, Wilson KB (2001). Modeling CO_2 and water vapor exchange of a temperate broadleaved forest across hourly to decadal time scales. *Ecological Modelling*, 142, 155-184.

Baldocchi DD (2003). Assessing the eddy covariance technique for evaluating carbon dioxide exchange rates of ecosystems: past, present and future. Global Change Biology, 9, 479-492.

Baldocchi DD, Hicks BB, Meyers TP (1988). Measuring biosphere-atmosphere exchanges of biologically related gases with micrometeorological methods. *Ecology*, 69, 1331-1340.

Baldocchi DD, Verma SB, Rosenberg NJ (1981). Mass and energy exchanges of a soybean canopy under various environmental regimes. *Agronomy Journal*, 73, 706-710.

Ball JT, Woodrow I, Berry J (1987). A model predicting stomatal conductance and its contribution to the control of photosynthesis under different environmental conditions. In: Biggins, J. (ed.) *Progress in Photosynthesis Research*, 5, 221-224. Springer Netherlands.

Berg P, Roy H, Janssen F, Meyer V, Jorgensen BB, Huttel M, de Beer D (2003). Oxygen uptake by aquatic sediments measured with a novel non-invasive eddy correlation technique. Marine Ecology Process Series, 261, 75-83.

Bernacchi CJ, Bagley JE, Serbin SP, Ruiz-Vera UM, Rosenthal DM, Vanloocke A (2013). Modelling C_3 photosynthesis from the chloroplast to the ecosystem. *Plant Cell and Environment*, 36, 1641-1657.

Bernacchi CJ, Pimentel C, Long SP (2003). In vivo temperature response functions of parameters required to model RuBP-limited photosynthesis. *Plant Cell and Environment*, 26, 1419-1430.

Bernacchi CJ, Rosenthal DM, Pimentel C, Long SP, Farquhar GD (2009). Modeling the Temperature Dependence of C_3 Photosynthesis. *Photosynthesis in silico*, 231-246. Springer Science.

Bernacchi CJ, Singsaas EL, Pimentel C, Portis AR, Long SP (2001). Improved temperature response functions for models of Rubisco-limited photosynthesis. *Plant Cell and Environment*, 24, 253-259.

Bhandral R (2005). Nitrous oxide emission from soil under pasture as affected by grazing and effluent irrigation. Doctor of Philosophy, Massey University, Palmerston North, New Zealand.

Bhumralkar CM (1975). Numerical experiments on computation of ground surface-temperature in an atmospheric general circulation model. *Journal of Applied Meteorology*, 14, 1246-1258.

Bodin P, Franklin O (2012). Efficient modeling of sun/shade canopy radiation dynamics explicitly accounting for scattering. *Geoscientific Model Development*, 5, 535-541.

Bonan GB, Oleson KW, Fisher RA, Lasslop G, Reichstein M (2012). Reconciling leaf physiological traits and canopy flux data: Use of the TRY and FLUXNET databases in the Community Land Model version 4. *Journal of Geophysical Research-Biogeosciences*, 117.

Bosatta E, Agren GI (1985). Theoretical-analysis of decomposition of heterogeneous substrates. *Soil Biology & Biochemistry*, 17, 601-610.

Bosatta E, Agren GI (2003). Exact solutions to the continuous-quality equation for soil organic matter turnover. *Journal of Theoretical Biology*, 224, 97-105.

Brisson N, Itier B, L'Hotel JC, Lorendeau JY (1998). Parameterisation of the Shuttleworth-Wallace model to estimate daily maximum transpiration for use in crop models. *Ecological Modelling*, 107, 159-169.

Brooks A, Farquhar GD (1985). Effect of temperature on the CO_2/O_2 specificity of Ribulose-1,5-Bisphosphate Carboxylase Oxygenase and the rate of respiration in the light - Estimates from gas-exchange measurements on spinach. *Planta*, 165, 397-406.

Brutsaert W (1984). *Evaporation into the atmosphere: Theory, history and applications.*, Kluwer Publishers.

Burba G (2013). *Eddy covariance method for scientific, industrial, agricultural, and regulatory applications: A field book on measuring ecosystem gas exchange and areal emission rates*. LI-COR Biosciences, Lincoln, NE, USA.

Caldwell MM, Meister HP, Tenhunen JD, Lange OL (1986). Canopy structure, light microclimate and leaf gas exchange of *Quercus coccifera L*. in a Portuguese macchia: Measurements in different canopy layers and simulations with a canopy model. *Trees-Structure and Function*, 1, 25-41.

Camillo PJ, Gurney RJ (1986). A resistance parameter for bare-soil evaporation models. *Soil Science*, 141, 95-105.

Cammalleri C, Agnese C, Ciraolo G, Minacapilli M, Provenzano G, Rallo G (2010). Actual evapotranspiration assessment by means of a coupled energy/hydrologic balance model: Validation over an olive grove by means of scintillometry and measurements of soil water contents. *Journal of Hydrology*, 392, 70-82.

Cammalleri C, Anderson MC, Ciraolo G, D'urso G, Kustas WP, La Loggia G, Minacapilli M (2010b). The impact of in-canopy wind profile formulations on heat flux estimation in an open orchard using the remote sensing-based two-source model. *Hydrology and Earth System Sciences*, 14, 2643-2659.

Campbell GS, Norman JM (1998). *An introduction to environmental biophysics*.

Carvahais N, Reichstein M, Jung M, Lasslop G, Papale D (2009). Considerations on eddy-covariance data from fluxnet in model-data fusion and data-assimilation. ECMWF/GLASS Workshop on Land Surface *Modelling*, 9-12 November 2009.

Chapin FS, Woodwell GM, Randerson JT, Rastetter EB, Lovett GM, Baldocchi DD, Clark DA, Harmon ME, Schimel DS, Valentini R, Wirth C, Aber JD, Cole JJ, Goulden ML, Harden JW, Heimann M, Howarth RW, Matson PA, Mcguire AD, Melillo JM, Mooney HA, Neff JC, Houghton RA, Pace ML, Ryan MG, Running SW, Sala OE, Schlesinger WH, Schulze ED (2006). Reconciling carbon-cycle concepts, terminology, and methods. *Ecosystems*, 9, 1041-1050.

Chen JM, Liu J, Cihlar J, Goulden ML (1999). Daily canopy photosynthesis model through temporal and spatial scaling for remote sensing applications. *Ecological Modelling*, 124, 99-119.

Choudhury BJ, Monteith JL (1988). A 4-layer model for the heat-budget of homogeneous land surfaces. *Quarterly Journal of the Royal Meteorological Society*, 114, 373-398.

Ciais P, Reichstein M, Viovy N, Granier A, Ogee J, Allard V, Aubinet M, Buchmann N, Bernhofer C, Carrara A, Chevallier F, De Noblet N, Friend AD, Friedlingstein P, Grunwald T, Heinesch B, Keronen P, Knohl A, Krinner G, Loustau D, Manca G, Matteucci G, Miglietta F, Ourcival JM, Papale D, Pilegaard K, Rambal S, Seufert G, Soussana JF, Sanz MJ, Schulze ED, Vesala T, Valentini R (2005). Europe-wide reduction in primary productivity caused by the heat and drought in 2003. *Nature,* 437, 529-533.

Ciais P, Sabine C, Bala G, Bopp L, Brovkin V, Canadell J, Chhabra A, Defries R, Galloway J, Heimann M, Jones C, Le Quéré C, Myneni RB, Piao S, Thornton P (2013). Carbon And Other Biogeochemical Cycles. In: Stocker, TF, Qin, D, Plattner, G-K, Tignor, M, Allen, SK, Boschung, J, Nauels, A, Xia, Y, Bex, V, Midgley, PM (2013). *Climate Change 2013: The Physical Science Basis*. Contribution of Working Group I to the Fifth Assessment Report of the Intergovernmental Panel on Climate Change. Cambridge, United Kingdom and New York, NY, USA: Cambridge University Press.

Ciais P, Wattenbach M, Vuichard N, Smith P, Piao SL, Don A, Luyssaert S, Janssens IA, Bondeau A, Dechow R, Leip A, Smith PC, Beer C, Van Der Werf GR, Gervois S, Van Oost K, Tomelleri E, Freibauer A, Schulze ED, Team CS (2010). The European carbon balance. Part 2: croplands. *Global Change Biology*, 16, 1409-1428.

Clark DB, Mercado LM, Sitch S, Jones CD, Gedney N, Best MJ, Pryor M, Rooney GG, Essery RLH, Blyth E, Boucher O, Harding RJ, Huntingford C, Cox PM (2011). The Joint UK Land Environment Simulator (JULES), model description - Part 2: Carbon fluxes and vegetation dynamics. *Geoscientific Model Development*, 4, 701-722.

Collalti A, Marconi S, Ibrom A, Trotta C, Anav A, D'andrea E, Matteucci G, Montagnani L, Gielen B, Mammarella I, Grunwald T, Knohl A, Berninger F, Zhao Y, Valentini R, Santini M (2016). Validation of 3D-CMCC Forest Ecosystem Model (v.5.1) against eddy covariance data for 10 European forest sites. *Geoscientific Model Development*, 9, 479-504.

Collatz GJ, Ball JT, Grivet C, Berry JA (1991). Physiological and environmental regulation of stomatal conductance, photosynthesis and transpiration - a model that includes a laminar boundary layer. *Agricultural and Forest Meteorology*, 54, 107-136.

Conant RT, Easter M, Paustian K, Swan A, Williams S (2007). Impacts of periodic tillage on soil C stocks: A synthesis. *Soil & Tillage Research*, 95, 1-10.

Conant RT, Paustian K, Elliott ET (2001). Grassland management and conversion into grassland: Effects on soil carbon. *Ecological Applications*, 11, 343-355.

Conant RT, Ryan MG, Agren GI, Birge HE, Davidson EA, Eliasson PE, Evans SE, Frey SD, Giardina CP, Hopkins FM, Hyvonen R, Kirschbaum MUF, Lavallee JM, Leifeld J, Parton WJ, Steinweg JM, Wallenstein MD, Wetterstedt JAM, Bradford MA (2011). Temperature and soil organic matter decomposition rates - synthesis of current knowledge and a way forward. *Global Change Biology*, 17, 3392-3404.

Crous KY, Osvaldsson A, Ellsworth DS (2015). Is phosphorus limiting in a mature *Eucalyptus* woodland? Phosphorus fertilisation stimulates stem growth. *Plant and Soil*, 391, 293-305.

Dai YJ, Dickinson RE, Wang YP (2004). A two-big-leaf model for canopy temperature, photosynthesis, and stomatal conductance. *Journal of Climate*, 17, 2281-2299.

DairyNZ (2014). *New Zealand Dairy Statistics 2013-14*.

Deardorff JW (1978). Efficient prediction of ground surface-temperature and moisture, with inclusion of a layer of vegetation. Journal of Geophysical *Research-Oceans and Atmospheres*, 83, 1889-1903.

Depury DGG, Farquhar GD (1997). Simple scaling of photosynthesis from leaves to canopies without the errors of big-leaf models. *Plant Cell and Environment*, 20, 537-557.

Dietze MC (2014). Gaps in knowledge and data driving uncertainty in models of photosynthesis. *Photosynthesis Research*, 119, 3-14.

Ding RS, Kang SZ, Du TS, Hao XM, Zhang YQ (2014). Scaling up stomatal conductance from leaf to canopy using a dual-leaf model for estimating crop evapotranspiration. *Plos One, 9(4)*.

Dufrene E, Davi H, Francois C, Le Maire G, Le Dantec V, Granier A (2005). Modelling carbon and water cycles in a beech forest Part I: Model description and uncertainty analysis on modelled NEE. *Ecological Modelling*, 185, 407-436.

Duncan WG, Loomis RS, Williams WA, Hanau R (1967). A model for simulating photosynthesis in plant communities. *Hilgardia*, 38, 181-205.

El-Masri B, Barman R, Meiyappan P, Song Y, Liang M, Jain AK (2013). Carbon dynamics in the Amazonian Basin: Integration of eddy covariance and ecophysiological data with a land surface model. *Agricultural and Forest Meteorology*, 182, 156-167.

Embarcadero. Delphi XE. (2010). Embarcadero Technologies, San Francisco, CA, USA.

Evans JR, Terashima I (1987). Effects of nitrogen nutrition on electron transport components and photosynthesis in spinach. *Australian Journal of Plant Physiology*, 14, 59-68.

Evans JR (1989). Photosynthesis and nitrogen relationships in leaves of C_3 plants. *Oecologia*, 78, 9-19.

Falge E, Baldocchi D, Olson R, Anthoni P, Aubinet M, Bernhofer C, Burba G, Ceulemans R, Clement R, Dolman H, Granier A, Gross P, Grunwald T, Hollinger D, Jensen NO, Katul G, Keronen P, Kowalski A, Lai CT, Law BE, Meyers T, Moncrieff H, Moors E, Munger JW, Pilegaard K, Rannik U, Rebmann C, Suyker A, Tenhunen J, Tu K, Verma S, Vesala T, Wilson K, Wofsy S (2001). Gap filling strategies for defensible annual sums of net ecosystem exchange. *Agricultural and Forest Meteorology*, 107, 43-69.

Farahani HJ, Ahuja LR (1996). Evapotranspiration modeling of partial canopy/residue-covered fields. *Transactions of the American Society of Agricultural and Biological Engineers*, 39, 2051-2064.

Farahani HJ, Bausch WC (1995). Performance of evapotranspiration models for maize - bare soil to closed canopy. Transactions of the American Society of *Agricultural and Biological Engineers*, 38, 1049-1059.

Farquhar GD, Caemmerer SV, Berry JA (1980). A biochemical model of photosynthetic CO_2 assimilation in leaves of C_3 species. *Planta*, 149, 78-90.

Felber R, Munger A, Neftel A, Ammann C (2015). Eddy covariance methane flux measurements over a grazed pasture: effect of cows as moving point sources. *Biogeosciences*, 12, 3925-3940.

Felber R, Neftel A, Ammann C (2016). Discerning the cows from the pasture: Quantifying and partitioning the NEE of a grazed pasture using animal position data. *Agricultural and Forest Meteorology*, 216, 37-47.

Fen Shu S (1982). *Moisture and heat transport in a soil layer forced by atmospheric conditions*. M.Sc. thesis, University of Connecticut, Conn.

Finnigan JJ, Clement R, Malhi Y, Leuning R, Cleugh HA (2003). A re-evaluation of long-term flux measurement techniques - Part I: Averaging and coordinate rotation. *Boundary-Layer Meteorology, 107*, 1-48.

Fischer EM, Seneviratne SI, Luthi D, Schar C (2007). Contribution of land-atmosphere coupling to recent European summer heat waves. *Geophysical Research Letters*, 34(6).

Friend AD (1995). PGEN - An integrated model of leaf photosynthesis, transpiration, and conductance. *Ecological Modelling*, 77, 233-255.

Garratt JR (1975). Limitations of the Eddy-correlation technique for the determination of turbulent fluxes near the surface. *Boundary-Layer Meteorology*, 8, 255-259.

Gentine P, Entekhabi D, Chehbouni A, Boulet G, Duchemin B (2007). Analysis of evaporative fraction diurnal behaviour. *Agricultural and Forest Meteorology*, 143, 13-29.

Gifford RM (1995). Whole plant respiration and photosynthesis of wheat under increased CO_2 concentration and temperature: Long-term vs short-term distinctions for modelling. *Global Change Biology*, 1, 385-396.

Goudriaan J (1986). A simple and fast numerical-method for the computation of daily totals of crop photosynthesis. *Agricultural and Forest Meteorology*, 38, 249-254.

Grace PR, Post WM, Hennessy K (2006). The potential impact of climate change on Australia's soil organic carbon resources. *BioMed Central Ltd [Online]*.

Harley PC, Loreto F, Dimarco G, Sharkey TD (1992). Theoretical considerations when estimating the mesophyll conductance to CO_2 flux by analysis of the response of photosynthesis to CO_2. *Plant Physiology*, 98, 1429-1436.

Harley PC, Thomas RB, Reynolds JF, Strain BR (1992). Modeling photosynthesis of cotton grown in elevated CO_2. *Plant Cell and Environment*, 15, 271-282.

Herrero J, Polo MJ (2012). Parameterization of atmospheric longwave emissivity in a mountainous site for all sky conditions. *Hydrology and Earth System Sciences,* 16, 3139-3147.

Hikosaka K, Ishikawa K, Borjigidai A, Muller O, Onoda Y (2006). Temperature acclimation of photosynthesis: mechanisms involved in the changes in temperature dependence of photosynthetic rate. *Journal of Experimental Botany*, 57, 291-302.

Hirose T, Werger MJA (1987). Maximizing daily canopy photosynthesis with respect to the leaf nitrogen allocation pattern in the canopy. *Oecologia*, 72, 520-526.

Hunt JE, Laubach J, Barthel M, Fraser A, Phillips RL (2016). Carbon budgets for an irrigated intensively grazed dairy pasture and an unirrigated winter-grazed pasture. *Biogeosciences*, 13, 2927-2944.

Ingwersen J, Steffens K, Hogy P, Warrach-sagi K, Zhunusbayeva D, Poltoradnev M, Gabler R, Wizemann HD, Fangmeier A, Wulfmeyer V, Streck T (2011). Comparison of NOAH simulations with eddy covariance and soil water measurements at a winter wheat stand. *Agricultural and Forest Meteorology*, 151, 345-355.

IPCC (2007). *Climate change 2007: The Physical Science Basis*. Contribution of working group I to the fourth assessment report of the Intergovernmental Panel on Climate Change. In: Solomon, S., D. Qin, M. Manning, Z. Chen, M. Marquis, K.B. Averyt, M. Tignor And H.L. Miller (ed.). Cambridge, United Kingdom and New York, NY, USA.

IPCC (2014). *Climate Change 2014: Synthesis Report*. Contribution of Working Groups I, II and III to the Fifth Assessment Report of the Intergovernmental Panel on Climate Change. Core writing team, RK, Pachauri, LA, Meyer (eds). IPCC, Geneva, Switzerland. 151p.

Jackman RH (1964). Accumulation of organic matter in some New Zealand soils under permanent pasture. *New Zealand Journal of Agricultural Research*, 7, 472-479.

Jerome E, Beckers Y, Bodson B, Heinesch B, Moureaux C, Aubinet M (2014). Impact of grazing on carbon dioxide exchanges in an intensively managed Belgian grassland. *Agriculture Ecosystems & Environment*, 194, 7-16.

Joffre R, Agren GI, Gillon D, Bosatta E (2001). Organic matter quality in ecological studies: theory meets experiment. *Oikos*, 93, 451-458.

Johnson IR, Thornley JHM, Frantz JM, Bugbee B (2010). A model of canopy photosynthesis incorporating protein distribution through the canopy and its acclimation to light, temperature and CO_2. *Annals of Botany*, 106, 735-749.

Kaimal JC, Finnigan JJ (1994). *Atmospheric boundary layer flows-Their structure and measurement*. Oxford University Press. 304p.

Kaiser WM (1987) Effects of water deficit on photosynthetic capacity. *Physiologia plantarum*, 71, 142-149.

Kato T, Kimura R, Kamichika M (2004). Estimation of evapotranspiration, transpiration ratio and water-use efficiency from a sparse canopy using a compartment model. *Agricultural Water Management*, 65, 173-191.

Kattge J, Knorr W (2007). Temperature acclimation in a biochemical model of photosynthesis: a reanalysis of data from 36 species. Pl*ant Cell and Environment*, 30, 1176-1190.

Kattge J, Knorr W, Raddatz T, Wirth C (2009). Quantifying photosynthetic capacity and its relationship to leaf nitrogen content for global-scale terrestrial biosphere models. *Global Change Biology*, 15, 976-991.

Kell DB (2011). Breeding crop plants with deep roots: their role in sustainable carbon, nutrient and water sequestration. *Annals of Botany*, 108, 407-418.

Killham K (1994). *Soil ecology*. Cambridge University Press. Cambridge. 242 p.

Kim SH, Lieth JH (2003). A coupled model of photosynthesis, stomatal conductance and transpiration for a rose leaf (*Rosa hybrida* L.). *Annals of Botany*, 91, 771-781.

Kirschbaum MUF, Farquhar GD (1984). Temperature dependence of whole leaf photosynthesis in *Eucalyptus pauciflora* Sieb. Ex Spreng. *Australian Journal of Plant Physiology*, 11, 519-538.

Kirschbaum MUF, Paul KI (2002). Modelling C and N dynamics in forest soils with a modified version of the CENTURY model. *Soil Biology & Biochemistry*, 34, 341-354.

Kirschbaum MUF, Watt MS (2011). Use of a process-based model to describe spatial variation in *Pinus radiata* productivity in New Zealand. *Forest Ecology and Management*, 262, 1008-1019.

Kirschbaum MUF (1994). The sensitivity of C_3 photosynthesis to increasing CO_2 concentration - A theoretical analysis of its dependence on temperature and background CO_2 concentration. *Plant Cell and Environment*, 17, 747-754.

Kirschbaum MUF (1999a). CenW, a forest growth model with linked carbon, energy, nutrient and water cycles. *Ecological Modelling*, 118, 17-59.

Kirschbaum MUF (1999b). Modelling forest growth and carbon storage in response to increasing CO_2 and temperature. *Tellus Series B-Chemical and Physical Meteorology*, 51, 871-888.

Kirschbaum MUF (2000). CenW: a generic forest growth model. *New Zealand Journal of Forestry*, 45, 15-19.

Kirschbaum MUF, Keith H, Leuning R, Cleugh HA, Jacobsen KL, Van Gorsel E, Raison RJ (2007). Modelling net ecosystem carbon and water exchange of a temperate *Eucalyptus delegatensis* forest using multiple constraints. *Agricultural and Forest Meteorology*, 145, 48-68.

Kirschbaum MUF, Rutledge S, Kuijper IA, Mudge PL, Puche N, Wall AM, Roach CG, Schipper LA, Campbell DI (2015). Modelling carbon and water exchange of a grazed pasture in New Zealand constrained by eddy covariance measurements. *Science of the Total Environment*, 512, 273-286.

Kirschbaum MUF, Schipper LA, Mudge PL, Rutledge S, Puche NJB, Campbell DI (2017). The trade-offs between milk production and soil organic carbon storage in dairy systems under different management and environmental factors. *Science of the Total Environment*, 577, 61-72.

Kirschbaum MUF, Simioni G, Medlyn BE, McMurtrie RE (2003). On the importance of including soil nutrient feedback effects for predicting ecosystem carbon exchange. *Functional Plant Biology*, 30, 223-237.

Knorr W, Kattge J (2005). Inversion of terrestrial ecosystem model parameter values against eddy covariance measurements by Monte Carlo sampling. *Global Change Biology*, 11, 1333-1351.

Kondo J, Saigusa N, Sato T 1990. A parameterization of evaporation from bare soil surfaces. Journal of Applied Meteorology, 29, 385-389.

Koopmans D, Berg P (2015). Stream oxygen flux and metabolism determined with the open water and eddy correlation techniques. *Limnology and Oceanography*. 60, 1344-1355.

Kormann R, Meixner FX (2001). An analytical footprint model for non-neutral stratification. *Boundary-Layer Meteorology*, 99, 207-224.

Kramer K, Leinonen I, Bartelink HH, Berbigier P, Borghetti M, Bernhofer C, Cienciala E, Dolman AJ, Froer O, Gracia CA, Granier A, Grunwald T, Hari P, Jans W, Kellomaki S, Loustau D, Magnani F, Markkanen T, Matteucci G, Mohren GMJ, Moors E, Nissinen A, Peltola H, Sabate S, Sanchez A, Sontag M, Valentini R, Vesala T (2002). Evaluation of six process-based forest growth models using eddy-covariance measurements of CO_2 and H_2O fluxes at six forest sites in Europe. *Global Change Biology*, 8, 213-230.

Kuddington K, Fortin M-J, Gerber LR, Hastings A, Liebhold A, O'Connor M, Ray C (2013). Process-based models are required to manage ecological systems in a changing world. *Ecosphere*, 4*,* 20.

Kustas WP, Zhan X, Schmugge TJ (1998). Combining optical and microwave remote sensing for mapping energy fluxes in a semiarid watershed. *Remote Sensing of Environment*, 64, 116-131.

Le Quéré C, Peters GP, Andres RJ, Andrew RM, Boden TA, Ciais P, Friedlingstein P, Houghton RA, Marland G, Moriarty R, Sitch S, Tans P, Arneth A, Arvanitis A, Bakker DCE, Bopp L, Canadell JG, Chini LP, Doney SC, Harper A, Harris I, House JI, Jain AK, Jones SD, Kato E, Keeling RF, Klein Goldewijk K, Körtzinger A, Koven C, Lefèvre N, Maignan F, Omar A, Ono T, Park GH, Pfeil B, Poulter B, Raupach MR, Regnier P, Rödenbeck C, Saito S, Schwinger J, Segschneider J, Stocker BD, Takahashi T, Tilbrook B, Van Heuven S, Viovy N, Wanninkhof R, Wiltshire A, Zaehle S (2014). Global carbon budget 2013. *Earth System Science Data*, 6, 235-263.

Ledgard SF, Schils R, Eriksen J, Luo J (2009). Environmental impacts of grazed clover/grass pastures. *Irish Journal of Agricultural and Food Research*, 48, 209-226.

Legates DR, McCabe GJ (1999). Evaluating the use of "goodness-of-fit" measures in hydrologic and hydroclimatic model validation. *Water Resources Research*, 35, 233-241.

Leuning R (1997). Scaling to a common temperature improves the correlation between the photosynthesis parameters J_{max} and V_{cmax}. *Journal of Experimental Botany*, 48, 345-347.

Leuning R, Dunin FX, Wang YP (1998). A two-leaf model for canopy conductance, photosynthesis and partitioning of available energy. II. Comparison with measurements. *Agricultural and Forest Meteorology*, 91, 113-125.

Leuning R, Kelliher FM, Depury D, Schulze ED (1995). Leaf nitrogen, photosynthesis, conductance and transpiration: scaling from leaves to canopies. *Plant Cell and Environment*, 18, 1183-1200

Liang H, HU KL, Batchelor WD, Qi ZM, Li BG (2016). An integrated soil-crop system model for water and nitrogen management in North China. *Scientific Reports*, 6, 25755.

Litton CM, Raich JW, Ryan MG (2007). Carbon allocation in forest ecosystems. *Global Change Biology*, 13, 2089-2109.

Liu SG, Bliss N, Sundquist E, Huntington TG (2003). Modeling carbon dynamics in vegetation and soil under the impact of soil erosion and deposition. *Global Biogeochemical Cycles*, 17(2).

Lloyd J, Taylor JA (1994). On the temperature-dependence of soil respiration. *Functional Ecology*, 8, 315-323.

Lloyd J, Grace J, Miranda AC, Meir P, Wong SC, Miranda BS, Wright IR, Gash JHC, Mcintyre J (1995). A simple calibrated model of Amazon rain-forest productivity based on leaf biochemical-properties. *Plant Cell and Environment*, 18, 1129-1145.

Long SP, Baker NR, Raines CA (1993). Analysing the responses of photosynthetic CO_2 assimilation to long-term elevation of atmospheric CO_2 concentration. *Vegetatio*, 104, 33-45.

Loseen D, Chehbouni A, Njoku E, Saatchi S, Mougin E, Monteny G (1997). An approach to couple vegetation functioning and soil-vegetation-atmosphere-transfer models for semiarid grasslands during the HAPEX-Sahel experiment. *Agricultural and Forest Meteorology*, 83, 49-74.

Lund MR, Soegaard H (2003). Modelling of evaporation in a sparse millet crop using a two-source model including sensible heat advection within the canopy. *Journal of Hydrology*, 280, 124-144.

Luyssaert S, Inglima I, Jung M, Richardson AD, Reichstein M, Papale D, Piao SL, Schulzes ED, Wingate L, Matteucci G, Aragao L, Aubinet M, Beers C, Bernhofer C, Black KG, Bonal D, Bonnefond JM, Chambers J, Ciais P, Cook B, Davis KJ, Dolman AJ, Gielen B, Goulden M, Grace J, Granier A, Grelle A, Griffis T, Grunwald T, Guidolotti G, Hanson PJ, Harding R, Hollinger DY, Hutyra LR, Kolar P, Kruijt B, Kutsch W, Lagergren F, Laurila T, Law BE, Le Maire G, Lindroth A, Loustau D, Malhi Y, Mateus J, Migliavacca M, Misson L, Montagnani L, Moncrieff J, Moors E, Munger JW, Nikinmaa E, Ollinger SV, Pita G, Rebmann C, Roupsard O, Saigusa N, Sanz MJ, Seufert G, Sierra C, Smith ML, Tang J, Valentini R, Vesala T, Janssens IA (2007a). CO_2 balance of boreal, temperate, and tropical forests derived from a global database. *Global Change Biology*, 13, 2509-2537.

Luyssaert S, Janssens IA, Sulkava M, Papale D, Dolman AJ, Reichstein M, Hollmen J, Martin JG, Suni T, Vesala T, Loustau D, Law BE, Moors EJ (2007b). Photosynthesis drives anomalies in net carbon-exchange of pine forests at different latitudes. *Global Change Biology,* 13, 2110-2127.

Mahrt L, Ek M (1984). The influence of atmospheric stability on potential evaporation. *Journal of Climate and Applied Meteorology*, 23, 222-234.

Manzoni S, Porporato A (2009). Soil carbon and nitrogen mineralization: Theory and models across scales. *Soil Biology & Biochemistry*, 41, 1355-1379.

Medlyn BE, Dreyer E, Ellsworth D, Forstreuter M, Harley PC, Kirschbaum MUF, Le Roux X, Montpied P, Strassemeyer J, Walcroft A, Wang K, Loustau D (2002a). Temperature response of parameters of a biochemically based model of photosynthesis. II. A review of experimental data. *Plant Cell and Environment*, 25, 1167-1179.

Medlyn BE, Loustau D, Delzon S (2002b). Temperature response of parameters of a biochemically based model of photosynthesis. I. Seasonal changes in mature maritime pine (*Pinus pinaster Ait*.). *Plant Cell and Environment*, 25, 1155-1165.

Medlyn, BE, Robinson, AP, Clement, R, Mcmurtrie, RE (2005). On the validation of models of forest CO_2 exchange using eddy covariance data: some perils and pitfalls. *Tree Physiology*, 25, 839-857.

MFE (2014). *New Zealand's Greenhouse Gas Inventory 1990 – 2012*. Ministry for the Environment, Wellington, New Zealand. Available online at: http://www.mfe.govt.nz/sites/default/files/media/Climate%20Change/ghg-inventory-1990-2012.pdf.

MFE (2015). Ministry for the Environment & Statistics New Zealand (2015). New Zealand's Environmental Reporting Series: *Environment Aotearoa 2015*. Available from www.mfe.govt.nz and www.stats.govt.nz.

Minasny B, Malone BP, McBratney AB, Angers DA, Arrouays D, Chambers A, Chaplot V, Chen Z-S, Cheng K, Das BS, Field DJ, Gimona A, Hedley CB, Hong SY, Mandal B, Marchant BP, Martin M, McConkey BG, Mulder VL, O'Rourke S, Richer-de-Forges AC, Odeh I, Padarian J, Paustian K, Pan G, Poggio L, Savin I, Stolbovoy V, Stockmann U, Sulaeman Y, Tsui C-C, Vågen T-G, van Wesemael B, Winowiecki L (2017, 15 April). Soil carbon 4 per mille. *Geoderma*, 292, 59-86, ISSN 0016-7061, (http://www.sciencedirect.com/science/article/pii/S0016706117300095)

Mo XG, Liu SX (2001). Simulating evapotranspiration and photosynthesis of winter wheat over the growing season. *Agricultural and Forest Meteorology*, 109, 203-222.

Moffat AM, Papale D, Reichstein M, Hollinger DY, Richardson AD, Barr AG, Beckstein C, Braswell BH, Churkina G, Desai AR, Falge E, Gove JH, Heimann M, Hui D, Jarvis AJ, Kattge J, Noormets A, Stauch VJ (2007). Comprehensive comparison of gap-filling techniques for eddy covariance net carbon fluxes. Agricultural and Forest Meteorology, 147, 209-232.

Monteith JL (1965). Light distribution and photosynthesis in field crops. *Annals of Botany*, 29(1), 17-37.

Monteith JL, Unsworth M (1973). *Principles of environmental physics*. *Academic Press*. 4th edition. 422 p.

Mudge PL, Wallace DF, Rutledge S, Campbell DI, Schipper LA, Hosking CL (2011). Carbon balance of an intensively grazed temperate pasture in two climatically contrasting years. Agriculture *Ecosystems & Environment*, 144, 271-280.

Noilhan J, Planton S (1989). A simple parameterization of land surface processes for meteorological models. *Monthly Weather Review*, 117, 536-549.

Norman JM, Kustas WP, Humes KS (1995). Source approach for estimating soil and vegetation energy fluxes in observations of directional radiometric surface-temperature. *Agricultural and Forest Meteorology*, 77, 263-293.

Odhiambo LO, Irmak S (2011). Performance of extended Shuttleworth-Wallace model for estimating and partitioning of evapotranspiration in a partial residue-covered subsurface drip-irrigated soybean field. *Transactions of the American Society of Agricultural and Biological Engineers*, 54, 915-930.

Pal P, Clough TJ, Kelliher FM, Van Koten C, Sherlock RR (2012). Intensive cattle grazing affects pasture litter-fall: an unrecognized nitrous oxide source. *Journal of Environmental Quality*, 41, 444-448.

Parton WJ, Schimel DS, Cole CV, Ojima DS (1987). Analysis of factors controlling soil organic matter levels in great plains grasslands. Soil Science *Society of America Journal*, 51, 1173-1179.

Piggot GJ (1989). A comparison of 4 methods for estimating herbage yield of temperate dairy pastures. *New Zealand Journal of Agricultural Research*, 32, 121-123.

Post J, Krysanova V, Suckow F, Mirschel W, Rogasik J, Merbach I (2007). Integrated eco-hydrological modelling of soil organic matter dynamics for the assessment of environmental change impacts in meso- to macro-scale river basins. *Ecological Modelling*, 206, 93-109.

Powlson DS, Whitmore AP, Goulding KWT (2011). Soil carbon sequestration to mitigate climate change: a critical re-examination to identify the true and the false. *European Journal of Soil Science*, 62, 42-55.

Prescher AK, Grunwald T, Bernhofer C (2010). Land use regulates carbon budgets in eastern Germany: From NEE to NBP. *Agricultural and Forest Meteorology*, 150, 1016-1025.

R CORE TEAM (2016). *R: A Language and Environment for Statistical Computing*. R Foundation for Statistical Computing.

Randall DA, Dazlich DA, Zhang C, Denning AS, Sellers PJ, Tucker CJ, Bounoua L, Los SO, Justice CO, Fung I (1996). A revised land surface parameterization (SiB2) for GCMs .3. The greening of the Colorado State University general circulation model. *Journal of Climate*, 9, 738-763.

Rantakari M, Lehtonen A, Linkosalo T, Tuomi M, Tamminen P, Heikkinen J, Liski J, Makipaa R, Ilvesniemi H, Sievanen R (2012). The Yasso07 soil carbon model - Testing against repeated soil carbon inventory. *Forest Ecology and Management*, 286, 137-147.

Reda I, Andreas A (2003). Solar position algorithm for solar radiation applications. NREL report No. TP-560-34302. 55 pp. Revised January 2008.

Reichstein M, Falge E, Baldocchi D, Papale D, Aubinet M, Berbigier P, Bernhofer C, Buchmann N, Gilmanov T, Granier A, Grunwald T, Havrankova K, Ilvesniemi H, Janous D, Knohl A, Laurila T, Lohila A, Loustau D, Matteucci G, Meyers T, Miglietta F, Ourcival JM, Pumpanen J, Rambal S, Rotenberg E, Sanz M, Tenhunen J, Seufert G, Vaccari F, Vesala T, Yakir D, Valentini R (2005). On the separation of net ecosystem exchange into assimilation and ecosystem respiration: review and improved algorithm. *Global Change Biology,* 11, 1424-1439.

Reynolds JF, Chen JL, Harley PC, Hilbert DW, Dougherty RL, Tenhunen JD (1992). Modeling the effects of elevated CO_2 on plants - Extrapolating leaf response to a canopy. *Agricultural and Forest Meteorology*, 61, 69-94.

Reynolds O (1894). On the Dynamical Theory of Incompressible Viscous Fluids and the Determination of the Criterion. Pro*ceedings of the Royal Society of London*, 56, 40-45.

Robert M (1997). Degradation of soil quality: Risks for human health and environment. *Bulletin De L Academie Nationale De Medecine*, 181, 21-42.

Running SW, Coughlan JC (1988). A general model of forest ecosystem processes for regional applications .1. Hydrologic balance, canopy gas exchange and primary production processes. *Ecological Modelling*, 42, 125-154.

Running SW, Gower ST (1991). FOREST-BGC, A general model of forest ecosystem processes for regional applications. 2. Dynamic carbon allocation and nitrogen budgets. *Tree Physiology*, 9, 147-160.

Rutledge S, Mudge PL, Campbell DI, Woodward SL, Goodrich JP, Wall AM, Kirschbaum MUF, Schipper LA (2015). Carbon balance of an intensively grazed temperate dairy pasture over four years. *Agriculture Ecosystems & Environment*, 206, 10-20.

Rutledge S, Mudge PL, Wallace DF, Campbell DI, Woodward SL, Wall AM, Schipper LA (2014). CO_2 emissions following cultivation of a temperate permanent pasture. *Agriculture Ecosystems & Environment*, 184, 21-33.

Salinger MJ (2007). Agriculture's influence on climate during the Holocene. *Agricultural and Forest Meteorology*, 142, 96-102.

Sands PJ (1995a). Modeling canopy production .1. Optimal distribution of photosynthetic resources. *Australian Journal of Plant Physiology*, 22, 593-601.

Sands PJ (1995b). Modeling canopy production .2. From single leaf photosynthetic parameters to daily canopy photosynthesis. *Australian Journal of Plant Physiology*, 22, 603-614.

Santaren D, Peylin P, Viovy N, Ciais P (2007). Optimizing a process-based ecosystem model with eddy-covariance flux measurements: A pine forest in southern France. *Global Biogeochemical Cycles*, 21.

Schipper LA, Parfitt RL, Fraser S, Littler RA, Baisden WT, Ross C (2014). Soil order and grazing management effects on changes in soil C and N in New Zealand pastures. *Agriculture Ecosystems & Environment*, 184, 67-75.

Schipper LA, Parfitt RL, Ross C, Baisden WT, Claydon JJ, Fraser S (2010). Gains and losses in C and N stocks of New Zealand pasture soils depend on land use. *Agriculture Ecosystems & Environment*, 139, 611-617.

Schmid HP (2002). Footprint modeling for vegetation atmosphere exchange studies: a review and perspective. *Agricultural and Forest Meteorology*, 113, 159-183.

Schwalm CR, Williams CA, Schaefer K, Arneth A, Bonal D, Buchmann N, Chen JQ, Law BE, Lindroth A, Luyssaert S, Reichstein M, Richardson AD (2010). Assimilation exceeds respiration sensitivity to drought: A FLUXNET synthesis. *Global Change Biology*, 16, 657-670.

Sellers PJ (1985). Canopy reflectance, photosynthesis and transpiration. *International Journal of Remote Sensing*, 6, 1335-1372.

Sellers PJ, Heiser MD, Hall FG (1992). Relations between surface conductance and spectral vegetation indexes at intermediate (100 m^2 to 15 km^2) length scales. *Journal of Geophysical Research-Atmospheres*, 97, 19033-19059.

Sellers PJ, Mintz Y, Sud YC, Dalcher A (1986). A simple biosphere model (Sib) for use within general circulation models. *Journal of the Atmospheric Sciences*, 43, 505-531.

Sellers PJ, Randall DA, Collatz GJ, Berry JA, Field CB, Dazlich DA, Zhang C, Collelo GD, Bounoua L (1996). A revised land surface parameterization (SiB2) for atmospheric GCMs .1. Model formulation. *Journal of Climate*, 9, 676-705.

Sharkey TD, Stitt M, Heineke D, Gerhardt R, Raschke K, Heldt HW (1986). Limitation of photosynthesis by carbon metabolism .2. O_2 insensitive CO_2 uptake results from limitation of Triose Phosphate Utilization. *Plant Physiology*, 81, 1123-1129.

Shuttleworth WJ, Gurney RJ (1990). The theoretical relationship between foliage temperature and canopy resistance in sparse crops. *Quarterly Journal of the Royal Meteorological Society*, 116, 497-519.

Shuttleworth WJ, Wallace JS (1985). Evaporation from sparse crops - an energy combination theory. *Quarterly Journal of the Royal Meteorological Society*, 111, 839-855.

Six J, Ogle SM, Breidt FJ, Conant RT, Mosier AR, Paustian K (2004). The potential to mitigate global warming with no-tillage management is only realized when practised in the long term. *Global Change Biology*, 10, 155-160.

Skinner RH, Dell CJ (2015). Comparing pasture C sequestration estimates from eddy covariance and soil cores. *Agriculture Ecosystems & Environment*, 199, 52-57.

Skinner RH (2008). High biomass removal limits carbon sequestration potential of mature temperate pastures. *Journal of Environmental Quality*, 37, 1319-1326.

Smith NG, Dukes JS (2013). Plant respiration and photosynthesis in global scale models: incorporating acclimation to temperature and CO_2. *Global Change Biology*, 19, 45-63.

Smith P, Lanigan G, Kutsch WL, Buchmann N, Eugster W, Aubinet M, Ceschia E, Beziat P, Yeluripati JB, Osborne B, Moors EJ, Brut A, Wattenbach M, Saunders M, Jones M (2010). Measurements necessary for assessing the net ecosystem carbon budget of croplands. *Agriculture Ecosystems & Environment*, 139, 302-315.

Smith REH, Allen CD, Charlton MN (2004). Dissolved organic matter and ultraviolet radiation penetration in the Laurentian Great Lakes and tributary waters. *Journal of Great Lakes Research*, 30, 367-380.

Solomon Z, Olsson M, Masresha F (2007). Growth, gas exchange, chlorophyll a fluorescence, biomass accumulation and partitioning in droughted and irrigated plants of two enset (*Ensete ventricosum Welw. Cheesman*) clones. *Journal of Agronomy*, 6, 499-508.

Soussana JF, Tallec T, Blanfort V (2010). Mitigating the greenhouse gas balance of ruminant production systems through carbon sequestration in grasslands. *Animal*, 4, 334-350.

Steinfeld H, Gerber P, Wassenaar T, Castel V, Rosales M, De Haan C (2006). Livestock's long shadow: environmental issues and options. *Food And Agriculture Organization Of The United Nations.*

Stoy PC, Katul GG, Siqueira MBS, Juang JY, Novick KA, Uebelherr JM, Oren R (2006). An evaluation of models for partitioning eddy covariance-measured net

ecosystem exchange into photosynthesis and respiration. *Agricultural and Forest Meteorology*, 141, 2-18.

Swinbank WC (1951). The measurement of vertical transfer of heat and water vapor by eddies in the lower atmosphere. *Journal of Meteorology*, 8, 135-145.

Taconet O, Bernard R, Vidalmadjar D (1986). Evapotranspiration over an agricultural region using a surface flux temperature model based on NOAA-AVHRR data. *Journal of Climate and Applied Meteorology*, 25, 284-307.

Tate KR, Giltrap DJ, Claydon JJ, Newsome PF, Atkinson IAE, Taylor MD, Lee R (1997). Organic carbon stocks in New Zealand's terrestrial ecosystems. *Journal of the Royal Society of New Zealand*, 27, 315-335.

Tate KR, Wilde RH, Giltrap DJ, Baisden WT, Saggar S, Trustrum NA, Scott NA, Barton JR (2005). Soil organic carbon stocks and flows in New Zealand: System development, measurement and modelling. *Canadian Journal of Soil Science*, 85, 481-489.

Taylor KE (2001). Summarizing multiple aspects of model performance in a single diagram. *Journal of Geophysical Research-Atmospheres*, 106, 7183-7192.

Thomas SM, Ledgard SF, Francis GS (2005). Improving estimates of nitrate leaching for quantifying New Zealand's indirect nitrous oxide emissions. *Nutrient Cycling in Agroecosystems*, 73, 213-226.

Thornley JHM, Cannell MGR (1997). Temperate grassland responses to climate change: An analysis using the Hurley pasture model. *Annals of Botany*, 80, 205-221.

Thornley JHM (1998). Dynamic model of leaf photosynthesis with acclimation to light and nitrogen. *Annals of Botany*, 81, 421-430.

Thornley JHM (2002). Instantaneous canopy photosynthesis: Analytical expressions for sun and shade leaves based on exponential light decay down the canopy and an acclimated non-rectangular hyperbola for leaf photosynthesis. *Annals of Botany*, 89, 451-458.

Vandegriend AA, Owe M (1994). Bare soil surface-resistance to evaporation by vapor diffusion under semiarid conditions. *Water Resources Research*, 30, 181-188.

van Gorsel E, Leuning R, Cleugh HA, Keith H, Suni T (2007). Nocturnal carbon efflux: Reconciliation of eddy covariance and chamber measurements using an alternative to the u*-threshold filtering technique. *Tellus B,* 59, 1–7.

van Gorsel E, Leuning R, Cleugh HA, Keith H, Kirschbaum MUF, Suni T. (2008). Estimating net ecosystem exchange in moderately complex topography. *Agricultural and Forest Meteorology*, 148, 1174-1180.

Verbeeck H, Peylin P, Bacour C, Bonal D, Steppe K, Ciais P (2011). Seasonal patterns of CO2 fluxes in Amazon forests: Fusion of eddy covariance data and the ORCHIDEE model. *Journal of Geophysical Research: Biogeosciences*, 116, G02018.

Verhoeven AS, Demmigadams B, Adams WW (1997). Enhanced employment of the xanthophyll cycle and thermal energy dissipation in spinach exposed to high light and N stress. *Plant Physiology*, 113, 817-824.

Vesala T, Kljun N, Rannik U, Rinne J, Sogachev A, Markkanen T, Sabelfeld K, Foken T, Leclerc MY (2008). Flux and concentration footprint modelling: State of the art. *Environmental Pollution*, 152, 653-666.

Von Caemmerer S (2000). *Biochemical models of leaf photosynthesis*. Collingwood, Victoria: CSIRO Publishing.

Walker AP, Beckerman AP, GU LH, Kattge J, Cernusak LA, Domingues TF, Scales JC, Wohlfahrt G, Wullschleger SD, Woodward FI (2014). The relationship of leaf photosynthetic traits - V_{cmax} and J_{max} - to leaf nitrogen, leaf phosphorus, and specific leaf area: a meta-analysis and modeling study. *Ecology and Evolution*, 4, 3218-3235.

Wang YP, Baldocchi D, Leuning RAY, Falge EVA, Vesala T (2007). Estimating parameters in a land-surface model by applying nonlinear inversion to eddy covariance flux measurements from eight Fluxnet sites. *Global Change Biology*, 13, 652-670.

Wang X, Cheng G, Li X, Lu L, Ma M, Su P, Zhu G, Tan J (2015). A comparison of two photosynthesis parameterization schemes for an alpine meadow site on the Qinghai-Tibetan Plateau. *Theoretical and Applied Climatology*, 1-14.

Wang YP, Leuning R (1998). A two-leaf model for canopy conductance, photosynthesis and partitioning of available energy I: Model description and comparison with a multi-layered model. *Agricultural and Forest Meteorology*, 91, 89-111.

Webb EK, Pearman GI, Leuning R (1980). Correction of flux measurements for density effects due to heat and water-vapor transfer. *Quarterly Journal of the Royal Meteorological Society*, 106, 85-100.

Whitehead D, Teskey RO (1995). Dynamic-response of stomata to changing irradiance in Loblolly-pine (*Pinus taeda* L.). *Tree Physiology*, 15, 245-251.

Will RE, Teskey RO (1999). Influence of rate of change in stomatal conductance to fluctuating irradiance on estimates of daily water use by *Pinus taeda* leaves. *Tree Physiology*, 19, 761-765.

Wilson K, Goldstein A, Falge E, Aubinet M, Baldocchi D, Berbigier P, Bernhofer C, Ceulemans R, Dolman H, Field C, Grelle A, Ibrom A, Law BE, Kowalski A, Meyers T, Moncrieff J, Monson R, Oechel W, Tenhunen J, Valentini R, Verma S (2002). Energy balance closure at FLUXNET sites. *Agricultural and Forest Meteorology*, 113, 223-243.

Wilson TB, Meyers TP, Kochendorfer J, Anderson MC, Heuer M (2012). The effect of soil surface litter residue on energy and carbon fluxes in a deciduous forest. *Agricultural and Forest Meteorology*, 161, 134-147.

Wofsy SC, Goulden ML, Munger JW, Fan SM, Bakwin PS, Daube BC, Bassow SL, Bazzaz FA (1993). Net exchange of CO_2 in a midlatitude forest. *Science*, 260, 1314-1317.

Woods DB, Turner NC (1971). Stomatal response to changing light by 4 tree species of varying shade tolerance. *New Phytologist*, 70, 77-84.

Wullschleger SD (1993). Biochemical limitations to carbon assimilation in C_3 plants - A retrospective analysis of the A/C_i curves from 109 species. *Journal of Experimental Botany*, 44, 907-920.

York LM, Silberbush M, Lynch JP (2016). Spatiotemporal variation of nitrate uptake kinetics within the maize (*Zea mays L*.) root system is associated with greater nitrate uptake and interactions with architectural phenes. *Journal of Experimental Botany*, 67, 3763-3775.

Yuan WP, Liu S, Zhou GS, Zhou GY, Tieszen LL, Baldocchi D, Bernhofer C, Gholz H, Goldstein AH, Goulden ML, Hollinger DY, Hu Y, Law BE, Stoy PC, Vesala T, Wofsy SC (2007). Deriving a light use efficiency model from eddy covariance flux data for predicting daily gross primary production across biomes. *Agricultural and Forest Meteorology*, 143, 189-207.

Zeeman MJ, Hiller R, Gilgen AK, Michna P, Pluss P, Buchmann N, Eugster W (2010). Management and climate impacts on net CO_2 fluxes and carbon budgets of three grasslands along an elevational gradient in Switzerland. *Agricultural and Forest Meteorology*, 150, 519-530.

Zhang BZ, Liu Y, Xu D, Cai JB, Li FS (2011). Evapotranspiraton estimation based on scaling up from leaf stomatal conductance to canopy conductance. *Agricultural and Forest Meteorology*, 151, 1086-1095.

Zhang LX, Hu ZM, Fan JW, Zhou DC, Tang FP (2014). A meta-analysis of the canopy light extinction coefficient in terrestrial ecosystems. *Frontiers of Earth Science*, 8, 599-609.

Zheng Y, Zhao Z, Zhou JJ, Zhou H (2012). Evaluations of different leaf and canopy photosynthesis models: A case study with black locust (*Robinia pseudoacacia*) plantations on a loess plateau. *Pakistan Journal of Botany*, 44, 531-539.